http://waikato.researchgateway.ac.nz/

Research Commons at the University of Waikato

Copyright Statement:

The digital copy of this thesis is protected by the Copyright Act 1994 (New Zealand).

The thesis may be consulted by you, provided you comply with the provisions of the Act and the following conditions of use:

- Any use you make of these documents or images must be for research or private study purposes only, and you may not make them available to any other person.
- Authors control the copyright of their thesis. You will recognise the author's right to be identified as the author of the thesis, and due acknowledgement will be made to the author where appropriate.
- You will obtain the author's permission before publishing any material from the thesis.

Geodesic Geometry of Black Holes

A thesis

submitted in partial fulfilment

of the requirements for the Degree

of

Doctor of Philosophy

at the

University of Waikato

by

Gabriela Slezáková

The
University
of Waikato
Te Whare Wānanga
o Waikato

University of Waikato

2006

Abstract

The study of geodesics is of intrinsic significance in the study of the geometry of space-time. In this thesis null, space-like and time-like geodesics are studied in the case of the space-times of Schwarzschild, Reissner-Nordström and Kerr black holes. These space-times have been investigated with varying degrees of thoroughness in many articles and some books. However, there are some significant gaps in these treatments and the central aim of this thesis is to fill these gaps where necessary. Moreover, the following topics are covered for the first time.

1. In Chapter 4 a thorough treatment of the space-like geodesics of the Schwarzschild solutions has been given. These geodesics are the trajectories of Tachyons (faster than light particles) and are treated in a complete manner. This has been done by obtaining exact solutions and solving them numerically.

2. In Part II all solutions for geodesics for a Reissner-Nordström black hole have been given in complete detail, i.e. time-like, null and space-like geodesics and orbit of a charged particle.

3. In Chapter 14 all solutions for geodesics in the equatorial plane of a Kerr black hole have been given in complete detail, i.e. time-like, null and space-like geodesics.

4. The study of special types of non-equatorial geodesics for a Kerr black hole have been given in complete detail, i.e. time-like (Chapter 17), null (Chapter 15) and space-like (Chapter 16). This has been done in order to distinguish the qualitatively different types of solutions.

Calculation of the explicit formulas, which describe these geodesics, as well as numerically computed diagrams representing the geodesics have been incorporated in these studies. The following subjects have been also treated:

5. Solutions for the geodesics in Reissner-Nordström black holes with $|Q_*| \geq M$, which are black holes with one ($|Q_*| = M$) or no horizon ($|Q_*| > M$) (Chapter 8).

6. Solutions of geodesics in extreme and fast Kerr black holes, i.e. black holes with $a = M$ (extreme) and $a > M$ (fast). As in the case of $|Q_*| > M$, fast black holes have naked singularities (Chapter 14).

7. Some general observations about orbit types of the Kerr black holes regarding relationships between parameters such as angular momentum, energy, Carter constant and mass and angular momentum of black holes (Chapter 13).

8. Some corrections to errors found in the literature.

While it has not been possible to cover all different cases which occur for possible relations amongst the parameters specifying a general black hole, interesting geodesics have, however, been studied and a more thorough presentation of the properties of geodesics has now been given.

Acknowledgements

I would like to present my deepest gratitude to:

My supervisors from the University of Waikato, NZ - Prof. Ernest Kalnins, for his many suggestions and constant support during my study in New Zealand, and Prof. Ian Craig, for his comments and suggestions.

Prof. Jan Horský and Dr. Zdeněk Kopecký, supervisors of my MSc. thesis, from the Masaryk University, CZ. What I learnt from them helped me in my study here.

And all others who taught me mathematics and physics.

All authors of the papers and books whose names are in the reference section. Each of them taught me something.

My husband for his support, help, comments and many hours spent fixing my computer.

My parents who supported me through my studies.

God who provided me with the resources that I use to understand a minute part of the complexities of His creation.

Contents

List of Figures

CD content

The content of the attached CD is listed in the `read_me.txt` file on the CD.

This is the content of that file:

```
PhD Thesis
Geodesic Geometry of Black Holes
Gabriela Slezakova
The University of Waikato
30 April 2006
email: gsle@i4free.co.nz
Description of the files in the CD
======= folder <code> ==================
There is the omputer code for generating the figures used in the thesis,
written in Maple ver. 6 and Matlab ver. 12 languages.
Listings of all codes are printed in Appendix A.
Functionality of the different programs are clear from
name of the containing folder
Appendix A describes which figure is created from which program.
========================================
======= folder <Thesis> ================
There is a file in this folder that is called (thesis.tex)
and three other folders (each of them have many files).
This (thesis.tex) is the main file, that calls
```

all other files of the root of this folder

and files inside the sub-folders of this folder.

This folder structure is used for the latex.

Also there is another file that is called (thesis.ps)

which is a stand alone file that is in post script format

and contains all of the thesis.

==========

======= folder <gsview_installer> =======

In this folder there are two installers.

Install both of them. Than you have gsview.

Gsview can be used to read postscript files.

==========

Chapter 1

Introduction

1.1 Gravitational collapse

A star is a self-gravitating collection of atoms supported by thermal pressure. Eventually, fusion at the core must stop, after which the star cools and contracts. For $M < 1.4M_{\odot} = M_{\mathrm{C}}$ (Chandrasekhar limit) (adopted from [42, chapter 1], but [31, chapter 24] gives the value 1.2 solar masses), the star is supported by electron degeneracy pressure, and ends as a white dwarf.

For $M > M_{\mathrm{C}}$ the star must continue to contract until nucleon-nucleon repulsion halts the implosion. The result is a neutron star ($M_{\mathrm{max}} \sim 3M_{\odot}$), unless the core's mass is so great, that gravity overcomes neutron-degeneracy pressure and pulls the star on in to form a black hole. The original analysis of the collapse of a star with uniform density and zero pressure was given by Oppenheimer and Snyder in 1939.

1.2 Black holes

1.2.1 Theoretical history

The idea of a dark star has its origins with John Mitchell [15] who presented this concept to the Royal Society in 1783. By using Newton's theory of gravitation with his corpuscular theory of light, he found that for a star of the same density as the Sun, the escape velocity would be the speed of light if the star had a radius $R = 486R_{\odot}$ and mass $M = 1.2 \times 10^8 M_{\odot}$. The French mathematician and philosopher Pierre Simon Laplace also independently published the idea of such a star. These objects were at the time not believed to exist.

In 1915, Einstein presented his theory of General Relativity. His theory was widely accepted once it was established that it explained the precession of Mercury's orbit, and predicted the bending of starlight by the Sun. One of the first solutions to Einstein's equations in a vacuum was determined by Karl Schwarzschild. This was a spherically symmetric exact solution. It has a special property of having a so called Schwarzschild Radius $r = 2M$ which is the radius below which the gravitational attraction between the particles of a body must cause it to undergo irreversible gravitational collapse. The Schwarzschild solution represents the empty space-time external to a spherically symmetric object. It has a singularity at $r = 0$ where r is the natural radial coordinate.

In the 1920's to the 1960's there was considerable development of the theory of General Relativity as it related to the idea of black holes (see [7] or summary in [37]). Subsequent to the measurement of the bending of light by the expedition led by Sir Arthur Eddington there was much research into the theory of Einstein. In his book "The Internal Constitution of Stars" Eddington maintained that all stars ended their life cycle by collapsing into white dwarfs. After applying quantum physics and Relativity to Eddington's calcu-

lations, astrophysicist S. Chandrasekhar showed that only stars of mass below a certain limit could become white dwarfs. This mass is known as the Chandrasekhar limit. This notion was not accepted by Eddington and was the cause of dispute for some time thereafter. In fact if the mass of a star is more than $1.2M_{\odot}$ then the star cannot stabilize and further collapse is inevitable. Indeed, Baade and Zwicky predicted that further collapse strips atoms of their electrons resulting in the idea of a neutron star. These stars have enormous densities.

The first idea of a black hole occurs in the work of Oppenheimer and Snyder who calculated that if a star has sufficient mass it must collapse and cut itself off from communication with the rest of the universe. Not even neutron degeneracy pressure, which gives rise to neutron stars, can stop the collapse. It was realised that for the Schwarzschild radius $r = 2M$ the Schwarzschild solution was not singular but that if the mass was contained inside this "horizon" boundary no light could escape. If the Schwarzschild radius was contained inside the star then this was not relevant.

On physical grounds it is expected that black holes should rotate and have a oblate "shape" which requires different solutions to the equations of General Relativity other than that of Schwarzschild. The unique solution which has all the correct properties was obtained by Roy Kerr [30]. It is a so called Petrov Type D solution. The metric is readily interpretable when written in terms of the so called Boyer-Lindquist coordinates. The geodesics of this metric can be explicitly calculated because of the existence of the fourth constant of the motion in addition to the Lie symmetries that are known to be present which correspond to time translation and axial symmetry.This space-time has been well studied with one principal result being that a collapsing star loses all its individual characteristics and its final state is determined by mass and angular momentum only. Therefore, the final state is determined by a Kerr metric with

these parameters.

1.2.2 Observational history

It was not until in 1963 when Maarten Schmidt [35] discovered extremely luminous distant objects called quasars that the existence of black holes was generally acknowledged. Their enormous energy output from small volumes of space suggested that they were powered by accretion of matter onto very massive black holes residing in galactic nuclei. From observations in the 1980's of motions of stars around the galactic center, it is now believed that such supermassive black holes (SMBHs) with masses in the range 10^6 to 10^{10} solar masses exist in the center of most galaxies ([26, 16, 32]). [14] argue that SMBHs may be of pregalactic origin. If that is true primordial black holes would be the centers for growing protogalaxies.

The first observational evidence for the existence of a stellar massive black hole was given in the early 70's by the observations of the binary X-ray source Cygnus X-1 ([20, 38, 9]). Today, there are about 20 stellar mass black hole candidates that range in mass from 3 to 15 solar masses
([13, 29]). Additionally, there is some evidence for intermediate-mass black holes, (those with masses of a few thousand times of the Sun.) ([21])

The big boost for black hole research came when the Hubble Space Telescope (HST) was launched (1994). Over the last decade the combination of HST and ground-based data has led to the measurement of the black-hole masses of some 40 inactive galaxies in the nearby Universe and the last few years has also seen a new industry emerge in estimating the black-hole masses of active galaxies ([33]).

1.3 Outline of thesis

It is known (e.g. [42] or [31]) that gravitational collapse in a general relativity context ultimately leads to the formation of a black hole where the external solution is characterized by the generalized Kerr-Newman four parameter family of vacuum solutions. The parameters that specify this family are identified with the *mass*, the *angular momentum*, the *electric charge,* and the *magnetic charge*. This thesis considers only the cases of zero magnetic charge. The derivation of these metrics is given in Appendix B and in greater detail in [7].

One of the best ways to grasp the essence of the geometry of a space-time is to study geodesics. They are the analogues of straight lines in curved space geometries, and they are second in importance only to curvature. A curve λ on M is a geodesic if its tangent vector, after parallel propagation, remains a multiple of itself. There are two types of geodesics described by freely falling particles, *time-like* and *null*. If they have non-zero positive rest-mass they are time-like and if they are massless they are called null. *Space-like* geodesics can be perceived as trajectories of particles faster than light (tachyons) [17]. Geodesic motion is interesting in an astrophysical context as many astrophysical models assume that in-falling matter moves along time-like geodesics, and because radiation propagates to a distant observer along null geodesics (as long as the wavelength is small compared to the radius of the black hole) [9], [10].

Geodesics are examined in many papers (for a list see e.g. [37]), but many solutions are omitted, usually because they lack clear physical significance (e.g. space-like geodesics or naked singularities). The intention of this thesis is to "fill these gaps", and as a result, give a comprehensive study of the geodesics of black holes.

In the first part of the thesis solutions are given for geodesic orbits in a black hole characterized only by mass (Schwarzschild). Radial orbits (null,

time-like and space-like) are depicted (schematically only) in [31, Chapter 31]. General space-like orbits are discussed and numerically obtained trajectories shown in [27]. In this thesis analytical solutions of general space-like orbits are presented (refer to Abstract–section 1).

The chapters dealing with time-like and null geodesics are based on exhaustive discussion in [7, chapter 3]. The complete analytical solution for τ and t coordinates of general orbits are added to that. These were generated by Maple software and then manually simplified. Time-like and null orbits are also discussed in [22] and [12], who restricts the analysis to the time-like circular geodesics. [31, Chapter 25] describe qualitative features of orbits of particles with zero or finite mass.

The second part of the thesis examines geodesics of a charged black hole (Reissner-Nordström–refer to Abstract–section 2). Time-like circular orbits for a naked singularity ($|Q_*| > M$, where Q_* is charge of the black holes) are discussed by [28]. [7, chapter 5] examines null and time-like radial and circular orbits of black holes with $|Q_*| < M$. In this thesis [7, chapter 5] is extended by solving equations of motion for general time-like and null orbits. The space-like orbits and black holes with $|Q_*| \geq M$ are included (refer to Abstract–section 5). The solution for $t = t(\tau)$ in Schwarzschild space-time for general geodesics did not bring any new features compared to solutions for $t = t(\tau)$ for the space-like radial geodesics, therefore, we do not present explicit formulas in this case (that is why there are not large formulas in chapters after Schwarzschild space-time). Motion of charged particles is mentioned briefly.

In the third part geodesics of rotating black holes are discussed. General features are thoroughly examined in [34, chapter 4]. Discussion of general features of the time-like and the null geodesics can be found in [7, chapter 7] and [39]. There is a small discussion of general null geodesics by [2], but his emphasis is on equatorial geodesics. Equatorial geodesics of a black hole with

$1.088M > a > M$ are investigated by [19]. Null geodesics in the equatorial plane are used in [11] to study the black hole as a gravitational mirror. Null geodesics of naked singularity are covered by [5]. An account of null geodesics for the range $0 \leq a^2 \leq M^2$ is given in [24]. General time-like geodesics appear in [43] with emphasis on the bound geodesics; time-like geodesic of naked singularity appear in [18]; [6] are interested in geodesics in the naked singularity which (do not) violate causality; [45] uses numerical methods to obtain criteria for the existence of bound particle orbits. The space-like orbits in the equatorial plane are added, and time-like and null geodesics where analytical solutions are not given are completed in the form of elliptic integrals (refer to Abstract–section 3). We do not restrict ourselves with the condition $a^2 \leq M^2$. Finally we give several examples of orbits out of the equatorial plane (refer to Abstract–section 4).

Throughout the thesis $c = G = 1$, where c is velocity of light in vacuum and G the gravitational constant. Metrics with the signature $(+, -, -, -)$ are used. Unless stated otherwise, we assume that E and M are positive.

For easy orientation the original work of this thesis is printed blue.

Part I

Geodesics in Schwarzschild space-time

Chapter 2

Introduction to geodesics in the Schwarzschild space-time

In this part of the thesis we will give solutions for geodesic orbits in the Schwarzschild space-time (black hole characterized only by mass M), which is space-time with an event horizon at $r = 2M$. Solutions for time-like and null geodesics (except for solution for τ and t coordinates of non-radial geodesics) are based on (and in greater detail explained in) [7, Sections 19 and 20], while space-like geodesics (sometimes associated with tachyons) are new.

[27] claim there exist repulsive space-like orbits. Our analysis in chapter 4 shows that because of restrictions which have to be made on parameters E, L, and M, there are only attractive space-like orbits in the Schwarzschild space-time.

Pictures of geodesics in this part were generated by MATLAB (for source codes see appendix A.1) from differential equations.

Chapter 3

The null geodesics in the Schwarzschild space-time

For the Schwarzschild space-time, the Lagrangian is

$$\mathcal{L} = \frac{1}{2}\left[\left(1-\frac{2M}{r}\right)\dot{t}^2 - \frac{\dot{r}^2}{1-2M/r} - r^2\dot{\theta}^2 - (r^2\sin^2\theta)\dot{\varphi}^2\right], \tag{3.1}$$

where dot denotes differentiation with respect to τ. The corresponding canonical momenta are

$$\begin{aligned} p_t &= \frac{\partial\mathcal{L}}{\partial\dot{t}} = \left(1-\frac{2M}{r}\right)\dot{t}\,, \quad p_\varphi = -\frac{\partial\mathcal{L}}{\partial\dot{\varphi}} = (r\sin\theta)^2\dot{\varphi}\,, \\ p_r &= -\frac{\partial\mathcal{L}}{\partial\dot{r}} = \left(1-\frac{2M}{r}\right)^{-1}\dot{r} \quad \text{and} \quad p_\theta = -\frac{\partial\mathcal{L}}{\partial\dot{\theta}} = r^2\dot{\theta}\,. \end{aligned} \tag{3.2}$$

By rescaling the affine parameter τ, we can arrange that the Lagrangian has the value 0 for null geodesics which describe the motion of massless freely falling particles.

Further integrals of the motion are

$$p_t = \left(1-\frac{2M}{r}\right)\frac{\mathrm{d}t}{\mathrm{d}\tau} = \text{constant} = E \quad \text{(say)} \tag{3.3}$$

and

$$p_\varphi = r^2\sin^2\theta\,\frac{\mathrm{d}\varphi}{\mathrm{d}\tau} = \text{constant}\,, \tag{3.4}$$

where E is the 'kinetic energy' as we can see from equation (3.6). Moreover, since a geodesic is described in an invariant plane ($\theta = \pi/2$), equation (3.4) gives

$$p_\varphi = r^2 \frac{\mathrm{d}\varphi}{\mathrm{d}\tau} = \text{constant} = L \quad \text{(say)}, \tag{3.5}$$

where L represents angular momentum about an axis normal to the invariant plane.

The constancy of the Lagrangian for null geodesics with equations (3.3) and (3.5) gives

$$\left(\frac{\mathrm{d}r}{\mathrm{d}\tau}\right)^2 + \left(1 - \frac{2M}{r}\right)\frac{L^2}{r^2} = E^2 \,. \tag{3.6}$$

From the integral of the motion follows

$$\frac{\mathrm{d}\varphi}{\mathrm{d}\tau} = \frac{L}{r^2} \,. \tag{3.7}$$

By regarding r as a function of φ and substituting r with $u = r^{-1}$ as the independent variable, equation

$$\left(\frac{\mathrm{d}u}{\mathrm{d}\varphi}\right)^2 = 2Mu^3 - u^2 + \frac{1}{D^2} = \mathrm{f}(u) \qquad \text{(say)} \,, \tag{3.8}$$

is obtained, where

$$D = L/E \tag{3.9}$$

represents the impact parameter. This equation must be considered together with (3.3) and (3.7).

3.1 The radial geodesics

The relevant equations are

$$\frac{\mathrm{d}r}{\mathrm{d}\tau} = \pm E \tag{3.10}$$

because $\mathrm{d}\varphi/\mathrm{d}\tau = 0$, and so $L = 0$. Then from (3.3), after integration,

$$t = \pm r_* + \text{constant}_\pm \,, \tag{3.11}$$

where

$$r_* = r + 2M \ln\left(\frac{r}{2M} - 1\right) . \tag{3.12}$$

Equation (3.11) must be compared with the equation

$$r = \pm E\tau + \text{constant}_\pm \tag{3.13}$$

which relates r to the proper time τ. From equations (3.11) and (3.13) it is evident that while the radial geodesic crosses the horizon in its own proper time, it takes an infinite coordinate-time to reach the horizon.

3.2 The unbound orbits

The different cases that must be distinguished are related to the location of the roots of the cubic equation

$$\mathrm{f}(u) = 2Mu^3 - u^2 + \frac{1}{D^2} = 0 . \tag{3.14}$$

The sum and the product of the roots u_1, u_2, and u_3 of this equation are given by

$$u_1 + u_2 + u_3 = \frac{1}{2M} \qquad \text{and} \qquad u_1 u_2 u_3 = -\frac{1}{2MD^2} . \tag{3.15}$$

The equation $\mathrm{f}(u) = 0$ must allow a negative real root; and the two remaining roots may either be real (distinct or coincident) or be a complex-conjugate pair. The three cases are distinguished in fig. 3.1.

- Case (α): For every pair of values E and L, which permits three real roots $u_1 < 0 < u_2 < u_3$, there exists two distinct orbits limited, respectively, to the intervals $0 < u \leq u_2$ and $u \geq u_3$, i.e. orbits of the first kind and orbits of the second kind. The orbits of the first kind are the analogues of Newtonian hyperbolae, while the orbits of the second kind are unique to Einsteinian gravity.

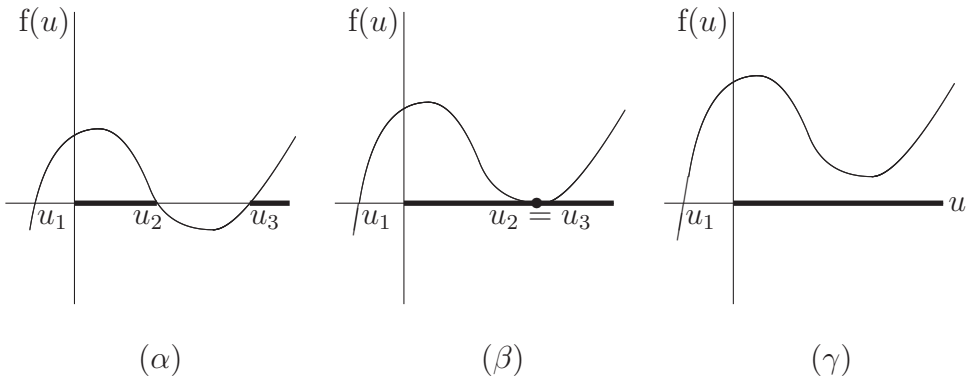

Figure 3.1: The disposition of the roots of a cubic $f(u) = 0$.

- Case (β): The two kinds of orbits coalesce as they asymptotically approach a common circle by spiralling round it from opposite sides an infinite number of times.

- Case (γ): These orbits are most conveniently parameterized by imaginary eccentricity. They are similar to the radial geodesics in view of the fact that they start from infinity and end in the singularity.

3.2.1 The geodesics of the first kind

First the case when all the roots of the cubic equation $f(u) = 0$ are real and the two positive roots are distinct will be looked at. Let the roots be

$$u_1 = \frac{P - 2M - Q}{4MP} \; (< 0)\,, \quad u_2 = \frac{1}{P}\,, \quad \text{and} \quad u_3 = \frac{P - 2M + Q}{4MP}\,, \tag{3.16}$$

where P denotes the perihelion distance and Q is a constant to be soon specified. The sum of the roots has been arranged to be equal to $\frac{1}{2M}$ as required by equation (3.15). The arrangement of the roots, $u_1 < u_2 < u_3$, demands that

$$Q + P - 6M > 0\,. \tag{3.17}$$

Next, with u_1, u_2, and u_3 as specified in equation (3.16), and the expression (3.14), we obtain the relations

$$Q^2 = (P - 2M)(P + 6M) \tag{3.18}$$

and

$$D^2 = \frac{P^3}{P - 2M}\,. \tag{3.19}$$

The relation (3.18) and the inequality (3.17) give

$$P > 3M\,. \tag{3.20}$$

Additionally, from equation (3.19), the inequality

$$D > 3M\sqrt{3} = D_{\rm c} \qquad \text{(say)} \tag{3.21}$$

can be obtained. Hence, the orbits in question lay entirely outside the circle $r = 3M$, and have impact parameters bigger than the critical value.

By a substitution

$$u - \frac{1}{P} = -\frac{Q - P + 6M}{8MP}(1 + \cos\chi)\,, \tag{3.22}$$

or, equivalently,

$$u + \frac{Q - P + 2M}{4MP} = \frac{Q - P + 6M}{8MP}(1 - \cos\chi)\,, \tag{3.23}$$

it can be determined that

$$\begin{aligned} u = \frac{1}{P} \qquad &\text{when} \qquad \chi = \pi\,, \qquad\qquad\qquad\qquad\qquad\qquad \text{and} \\ u = 0 \text{ and } r \to \infty \text{ when} \quad &\sin^2\frac{\chi}{2} = \frac{Q - P + 2M}{Q - P + 6M} = \sin^2\frac{\chi_\infty}{2} \quad \text{(say)}\,. \end{aligned} \tag{3.24}$$

The substitutions (3.22) and (3.23) also reduce equation (3.8) to

$$\left(\frac{{\rm d}\chi}{{\rm d}\varphi}\right)^2 = \frac{Q}{P}\left(1 - k^2\sin^2\frac{\chi}{2}\right)\,, \tag{3.25}$$

where

$$k^2 = \frac{Q - P + 6M}{2Q}\,, \tag{3.26}$$

and Q, P are defined in (3.18) and (3.19) respectively. The solution for φ than can be represented by the Jacobian elliptic integral in the form

$$\varphi = 2[{\rm K}(k) - {\rm F}(\chi/2, k)]\sqrt{\frac{P}{Q}}\,, \tag{3.27}$$

where the origin of φ has been chosen at the perihelion passage when $\chi = \pi$ (see equations (3.24)).

The critical orbits

The conditions for occurrence of two coincident roots can be described as follows. The derivative of equation (3.14) allows $u = (3M)^{-1}$ as a root; and if

$$D = 3M\sqrt{3}\,, \tag{3.28}$$

$u = (3M)^{-1}$ will be a double root of equation (3.14). From the equation (3.15), f$(u) = 0$ can be found. The full equation, suitable for this case,

$$\left(\frac{\mathrm{d}u}{\mathrm{d}\varphi}\right)^2 = 2M\left(u + \frac{1}{6M}\right)\left(u - \frac{1}{3M}\right)^2 \tag{3.29}$$

is satisfied by the substitution

$$u = -\frac{1}{6M} + \frac{1}{2M}\tanh^2\frac{\varphi - \varphi_0}{2}\,, \tag{3.30}$$

where φ_0 is a constant of integration. For φ_0 such that

$$\tanh^2\frac{\varphi_0}{2} = \frac{1}{3}\,, \tag{3.31}$$

it can be inferred that

$$u = 0 \qquad \text{and} \qquad r \to \infty \qquad \text{when} \qquad \varphi = 0\,. \tag{3.32}$$

In addition it can be observed that

$$u = \frac{1}{3M} \qquad \text{when} \qquad \varphi \to \infty\,. \tag{3.33}$$

So, a null geodesic, which comes from infinity with an impact parameter $D = 3M\sqrt{3}$, asymptotically approaches the circle of radius $3M$ (unstable circular orbit), by spiralling around it.

3.2.2 The geodesics of the second kind

In this section, in place of (3.22), the substitution

$$u = \frac{1}{P} + \frac{Q + P - 6M}{4MP}\sec^2\frac{\chi}{2} \tag{3.34}$$

is made to obtain the null geodesics, whose ranges are $u_3 \leq u < \infty$. This reduces equation (3.8) to the same form (3.25) with the same value of k^2. We may now write (cf. equation (3.27))

$$\varphi = 2\,\mathrm{F}(\chi/2, k)\sqrt{\frac{P}{Q}}\,, \tag{3.35}$$

where the origin of φ is now at aphelion passage. An example of general null geodesics of the first and second kind is in figure 3.2.

The critical orbits

With the orbit (3.30), there must be an associated orbit of the second kind, which starts at the singularity and, from the opposite side, asymptotically approaches the same circle at $r = 3M$, by spiralling around it. Such an orbit can be obtained by the substitution

$$u = \frac{1}{3M} + \frac{1}{2M}\tan^2\frac{\xi}{2} \tag{3.36}$$

in the same equation (3.29). Inserting the appropriate solution in equation (3.36), we obtain

$$u = \frac{1}{3M} + \frac{2\mathrm{e}^{\varphi}}{M\left(\mathrm{e}^{\varphi} - 1\right)^2}\,. \tag{3.37}$$

Along this orbit

$$\begin{gathered} u \to \infty \qquad \text{and} \qquad r \to 0 \qquad \text{when} \qquad \varphi \to 0 \\ \text{and} \\ u \to (3M)^{-1} \qquad \text{as} \qquad \varphi \to \infty\,. \end{gathered} \tag{3.38}$$

The orbit approaches the circle at $\frac{1}{3M}$, asymptotically, by spiraling around it an infinite number of times (cf. section 3.2.1). There is one important difference from the behavior of the orbits of the first kind: the circle at $\frac{1}{3M}$ is the perihelion for the orbits of the first kind, whereas it is the aphelion for the orbits of the second kind (see figure 3.3).

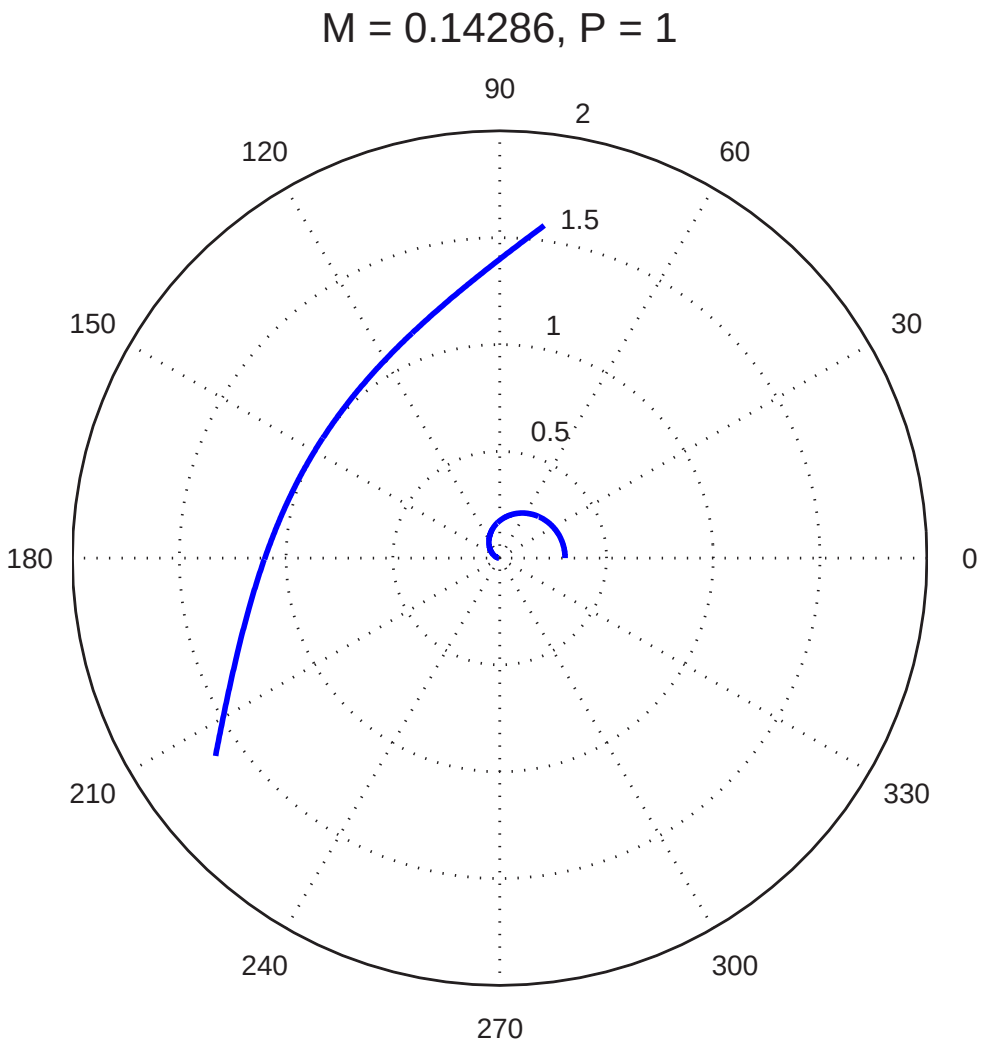

Figure 3.2: Orbits of the first and the second kind with $P = 1$. The orbit of the first kind arrives from infinity, and after reaching the perihelion, goes again to infinity. Orbit of the second, starting from a certain distance from the black hole (aphelion), falls into the singularity. ($M = 1/7$ in the scale along the coordinate axes).

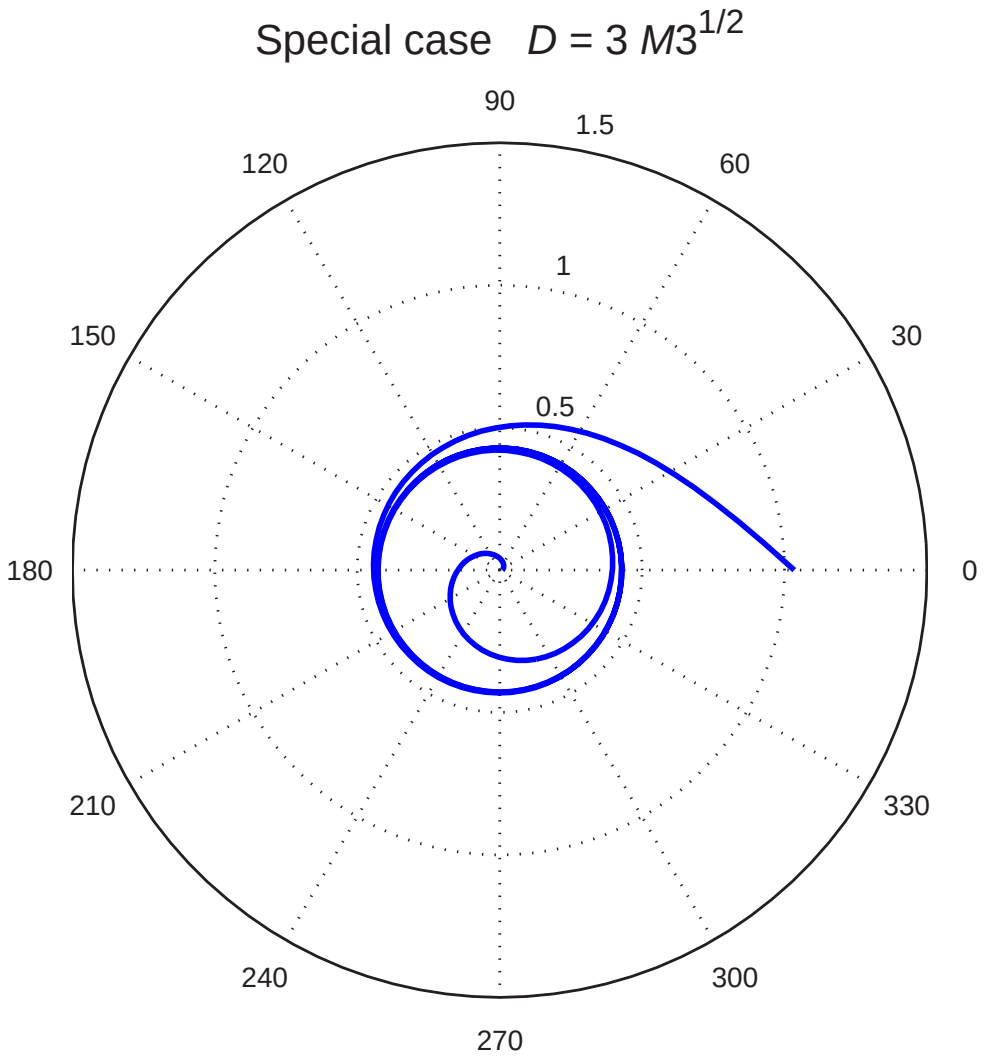

Figure 3.3: An example of the orbits of the orbits of the first kind, that starts from infinity, and the second kind, that starts from a certain distance from the black hole (radius of the unstable circular orbit) and falls into the singularity. The two orbits coalesce ($D = 3M\sqrt{3}$). ($M = 1/7$ in the scale along the coordinate axes.)

3.2.3 The orbits with imaginary eccentricities

To conclude this chapter, the orbits when the equation $\mathrm{f}(u) = 0$ has a pair of complex-conjugate roots, besides a negative real root, will be regarded. The roots shall be expressed in terms of an imaginary eccentricity $\mathrm{i}e$ ($e > 0$)

$$u_1 = \frac{1}{2M} - \frac{2}{l}\,, \quad u_2 = \frac{1+\mathrm{i}e}{l}\,, \quad \text{and} \quad u_3 = \frac{1-\mathrm{i}e}{l}\,, \tag{3.39}$$

where latus rectum, l, is some positive constant and the eccentricity e is more than 1. These orbits have an impact parameter less than the orbits studied in sections 3.2.1 and 3.2.2.

Now, parameters e^2 and μ are no longer independent but related: $\mathrm{e}^2 = 3 - \mu^{-1}$. With the assumption (3.39) regarding the roots of $\mathrm{f}(u) = 0$, the equation to be looked at is

$$\left(\frac{\mathrm{d}u}{\mathrm{d}\varphi}\right)^2 = 2M\left(u - \frac{1}{2M} + \frac{2}{l}\right)\left[\left(u - \frac{1}{l}\right)^2 + \frac{e^2}{l^2}\right] \tag{3.40}$$

and the substitution is

$$u \;= \frac{1}{l}\left(1 + e\tan\frac{\xi}{2}\right)\,. \tag{3.41}$$

The range of ξ must be terminated at ξ_∞ where

$$\begin{aligned} &\tan\frac{\xi_\infty}{2} = -e^{-1}\,, \\ &\text{or,} \\ &\sin\frac{\xi_\infty}{2} = -\frac{1}{\sqrt{1+e^2}} \quad \text{and} \quad \cos\frac{\xi_\infty}{2} = \frac{e}{\sqrt{1+e^2}}\,. \end{aligned} \tag{3.42}$$

For, when $\xi = \xi_\infty$, u becomes zero and when $\xi < \xi_\infty$, u becomes negative.

With the substitution (3.41), equation (3.40) reduces to

$$\frac{\mathrm{d}\xi}{\mathrm{d}\varphi} = \pm\sqrt{2[6\mu - 1 + 2\mu e\sin\xi + (6\mu - 1)\cos\xi]}\,. \tag{3.43}$$

The solution for φ can be expressed in terms of Jacobian elliptic integral

$$\pm\varphi = \frac{1}{\sqrt{\triangle}}\int^{\psi} \frac{\mathrm{d}\gamma}{\sqrt{1 - k^2\sin^2\gamma}}\,, \tag{3.44}$$

where

$$\triangle = \sqrt{(6\mu-1)^2+4\mu^2e^2}\,, \tag{3.45}$$

$$k^2 = \frac{\triangle+6\mu-1}{2\triangle}\,, \tag{3.46}$$

and

$$\sin^2\psi = \frac{\triangle+6\mu-1-2\left[2\mu e\sin\frac{\xi}{2}+(6\mu-1)\cos\frac{\xi}{2}\right]\cos\frac{\xi}{2}}{\triangle+6\mu-1}\,. \tag{3.47}$$

The solution for φ can be written as

$$\varphi = \frac{\mathrm{K}(k)-\mathrm{F}(\psi,k)}{\sqrt{\triangle}}\,. \tag{3.48}$$

In particular, as the orbit goes off to infinity,

$$\varphi_\infty = \frac{\mathrm{K}(k)-\mathrm{F}(\psi_\infty,k)}{\sqrt{\triangle}} \tag{3.49}$$

where ψ_∞ is given by

$$\sin^2\psi_\infty = \frac{\triangle+1}{\triangle+6\mu-1}\,. \tag{3.50}$$

Chapter 4

The space-like geodesics in the Schwarzschild space-time

The constancy of the Lagrangian with equations (3.3) and (3.5) gives

$$\frac{E^2}{1-2M/r} - \frac{\dot{r}^2}{1-2M/r} - \frac{L^2}{r^2} = 2\mathcal{L} = -1\,. \tag{4.1}$$

This can be rewritten in the form

$$\left(\frac{\mathrm{d}r}{\mathrm{d}\tau}\right)^2 + \left(1-\frac{2M}{r}\right)\left(\frac{L^2}{r^2}-1\right) = E^2\,. \tag{4.2}$$

By considering r as a function of φ, we obtain equation

$$\left(\frac{\mathrm{d}r}{\mathrm{d}\varphi}\right)^2 = \left(E^2+1\right)\frac{r^4}{L^2} - \frac{2Mr^3}{L^2} - r^2 + 2Mr\,. \tag{4.3}$$

Letting

$$u \;= r^{-1}\,, \tag{4.4}$$

we obtain the basic equation of the problem (cf. equation (3.8)):

$$\left(\frac{\mathrm{d}u}{\mathrm{d}\varphi}\right)^2 = 2Mu^3 - u^2 - \frac{2M}{L^2}u + \frac{E^2+1}{L^2}\,. \tag{4.5}$$

The solution can be completed by direct quadratures of the equations

$$\frac{\mathrm{d}\tau}{\mathrm{d}\varphi} = \frac{1}{Lu^2} \qquad \text{and} \qquad \frac{\mathrm{d}t}{\mathrm{d}\varphi} = \frac{E}{Lu^2(1-2Mu)}\,. \tag{4.6}$$

We observe that in contrast to the earlier definition (3.14), f(u), as now defined, has a linear term in u; and, as in the case of null geodesics, the constant term is always positive.

4.1 The radial geodesics

The radial geodesics have zero angular momentum. The equations governing these geodesics are

$$\left(\frac{\mathrm{d}r}{\mathrm{d}\tau}\right)^2 = \left(E^2+1\right) - \frac{2M}{r} \qquad \text{and} \qquad \frac{\mathrm{d}t}{\mathrm{d}\tau} = \frac{E}{1-2M/r}\,. \tag{4.7}$$

We shall consider trajectories of particles which start from rest at some finite distance r_i and fall towards the center. The starting distance is related to the constant E by

$$r_{\mathrm{i}} = \frac{2M}{E^2+1}\,. \tag{4.8}$$

As we can see, r_{i} cannot be bigger than $2M$. (The space-like radial geodesics always "start" under the horizon.)

The equations of motion are most conveniently integrated in terms of a variable η where

$$r = r_{\mathrm{i}}\cosh^2\frac{\eta}{2}\,. \tag{4.9}$$

Clearly when $\eta = 0$ then $r = r_{\mathrm{i}}$; and the value of η when r crosses the horizon at $r = 2M$ is

$$\eta_{\mathrm{H}} = 2\,\mathrm{arcsinh}E\,. \tag{4.10}$$

Since for $r = 0$

$$\eta_0 = 2\,\mathrm{i}\pi \tag{4.11}$$

is not real, radial space-like geodesics do not reach the singularity.

In terms of η, the equations to be integrated are

$$\left(\frac{\mathrm{d}r}{\mathrm{d}\tau}\right)^2 = \left(E^2+1\right)\tanh^2\frac{\eta}{2} \quad \text{and} \quad \frac{\mathrm{d}t}{\mathrm{d}\tau} = \frac{E\cosh^2\frac{\eta}{2}}{\cosh^2\frac{\eta}{2}-\cosh^2\frac{\eta_{\mathrm{H}}}{2}}\,, \tag{4.12}$$

together with

$$\frac{\mathrm{d}r}{\mathrm{d}\eta} = r_{\mathrm{i}} \sinh\frac{\eta}{2}\cosh\frac{\eta}{2}\,. \tag{4.13}$$

To have τ positive with η positive,

$$\frac{\mathrm{d}r}{\mathrm{d}\tau} = \left(1+E^2\right)^{1/2}\tanh\frac{\eta}{2} = \left(\frac{2M}{r_i}\right)^{1/2}\tanh\frac{\eta}{2}\,. \tag{4.14}$$

From equations (4.13) and (4.14), we now obtain

$$\frac{\mathrm{d}\tau}{\mathrm{d}\eta} = \left(\frac{r_{\mathrm{i}}^3}{2M}\right)^{1/2}\cosh^2\frac{\eta}{2} = (1+\cosh\eta)\sqrt{\frac{r_{\mathrm{i}}^3}{8M}}\,. \tag{4.15}$$

Therefore,

$$\tau = (\eta+\sinh\eta)\sqrt{\frac{r_{\mathrm{i}}^3}{8M}}\,, \tag{4.16}$$

where we have assumed that $\tau = 0$ at starting point $\eta = 0$. From equation (4.16) it follows that the particle crosses the horizon at finite arc lenght,

$$\tau_{\mathrm{H}} = (\sinh\eta_{\mathrm{H}}+\eta_{\mathrm{H}})\sqrt{\frac{r_{\mathrm{i}}^3}{8M}}\,. \tag{4.17}$$

The equation to be integrated to obtain t is

$$\frac{\mathrm{d}t}{\mathrm{d}\eta} = E\frac{\cosh^4\frac{\eta}{2}}{\cosh^2\frac{\eta}{2}-\cosh^2\frac{\eta_{\mathrm{H}}}{2}}\sqrt{\frac{r_{\mathrm{i}}^3}{2M}}\,. \tag{4.18}$$

On integration, this equation gives

$$t = E\left(\frac{r_{\mathrm{i}}^3}{2M}\right)^{1/2}\left[\frac{1}{2}(\eta+\sinh\eta)+\left(1+E^2\right)\eta\right] - 4M\,\mathrm{arctanh}\frac{\tanh\frac{\eta}{2}}{\tanh\frac{\eta_{\mathrm{H}}}{2}}\,. \tag{4.19}$$

According to this equation,

$$t\to-\infty \quad \text{as} \quad \eta\to\eta_{\mathrm{H}}-0\,. \tag{4.20}$$

Solutions (4.16) and (4.19) are illustrated in fig. 4.1. Because the space-like geodesics do not relate to any known physical object, the interpretation of this section is not clear. One might speculate that while the arc lenght of a tachyon increases, its coordinate time decreases, thus the particle moves backward in time. Also from the equation (4.8) that r_i is never 0 unless $M = 0$, therefore radially moving tachyon does not reach singularity.

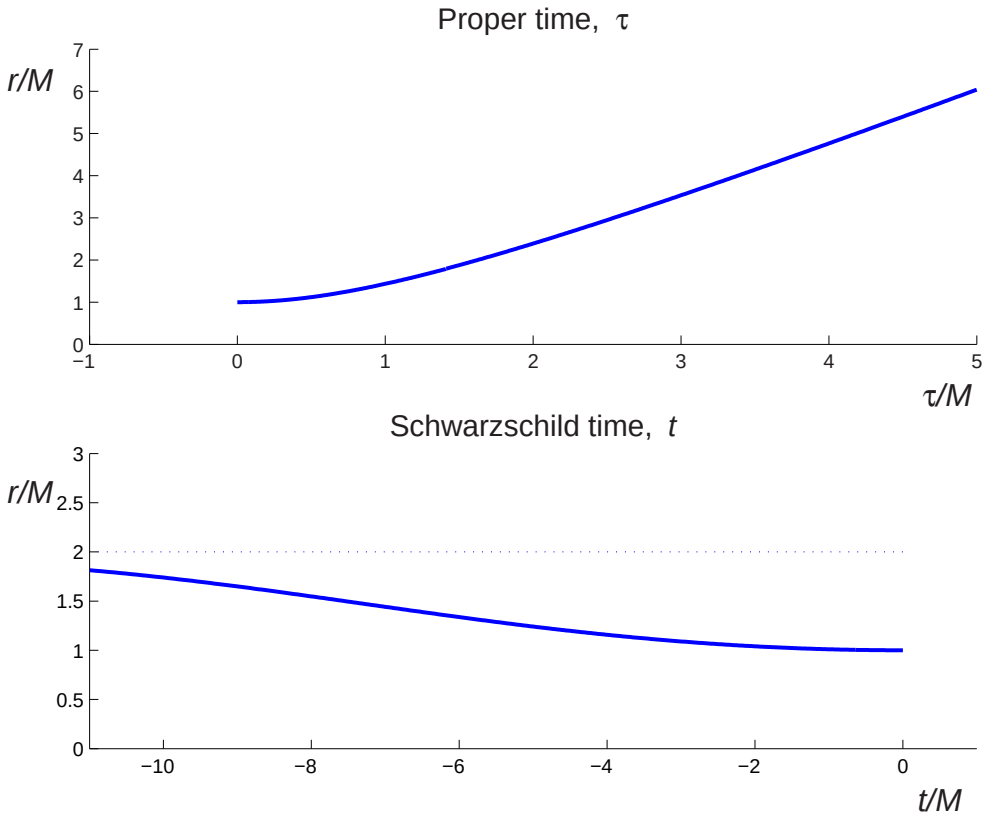

Figure 4.1: Proper time (τ) and coordinate time (t) along a space-like radial geodesic; initial condition is $r_{\rm i} = M$.

4.2 The unbound orbits

These orbits are governed by the equation

$$\left(\frac{\mathrm{d}u}{\mathrm{d}\varphi}\right)^2 = \mathrm{f}(u)\,, \tag{4.21}$$

where

$$\mathrm{f}(u) = 2Mu^3 - u^2 - \frac{2M}{L^2}u + \frac{E^2+1}{L^2}\,. \tag{4.22}$$

Letting u_1, u_2, and u_3 denote the roots of the cubic equation $\mathrm{f}(u) = 0$, we have

$$u_1 u_2 u_3 = -\frac{E^2+1}{2ML^2} \tag{4.23}$$

and

$$u_1 + u_2 + u_3 = \frac{1}{2M}\,. \tag{4.24}$$

Since $-(E^2+1) < 0$, the equation $\mathrm{f}(u) = 0$ must always allow a negative real root. From (4.24) it follows that we cannot have all roots negative.

The different cases that must be distinguished are, therefore, essentially the same as those for the null geodesics. There are no bound orbits in case of space-like geodesics!

The different cases we have distinguished can also be inferred by interpreting

$$\mathcal{V} = \left(1 - \frac{2M}{r}\right)\left(\frac{L^2}{r^2} - 1\right) \tag{4.25}$$

as 'potential energy' (see equation (4.2)). (In fig. 4.2 there are displayed some examples of potential energy.) The unstable orbits correspond to maximum potential.

4.2.1 Orbits of the first kind

Orbits of the first kind occur in cases (α), and (β); and we shall write the real roots of equation $\mathrm{f}(u) = 0$ as

$$u_1 = -\frac{1}{l}(e-1)\,,\ u_2 = \frac{1}{l}(e+1)\,,\ \text{and}\ u_3 = \frac{1}{2M} - \frac{2}{l}\,. \tag{4.26}$$

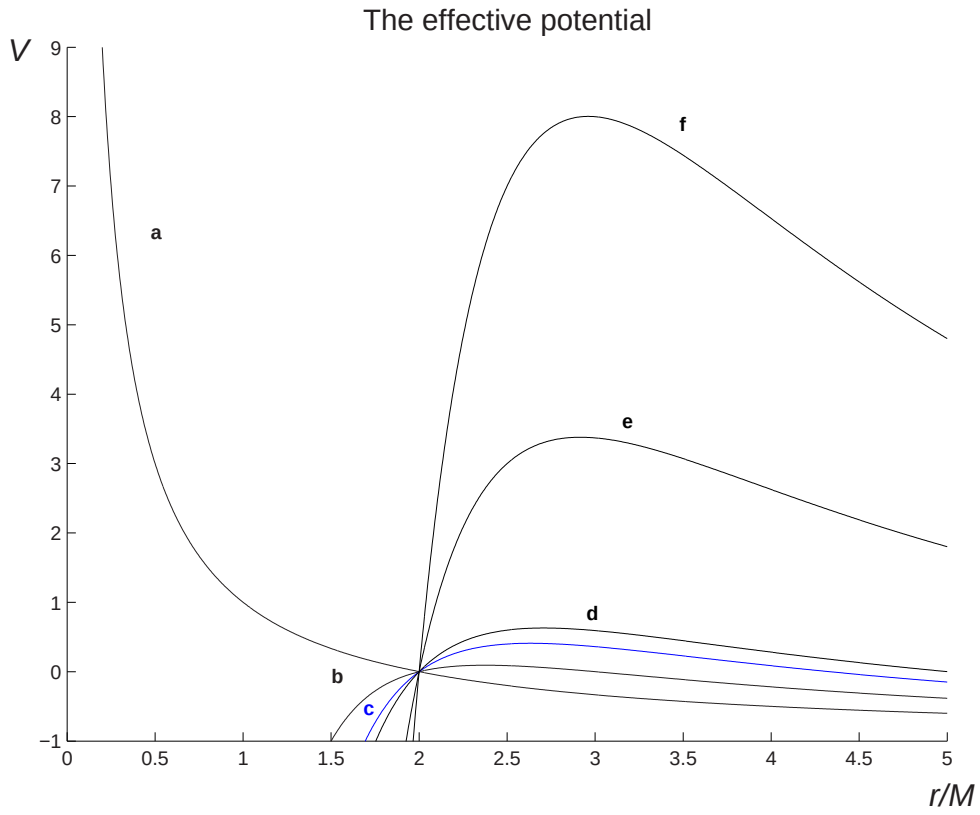

Figure 4.2: The effective potential appropriate for space-like trajectory (comp. equation (4.25)). L/M is a) 0, b) 3, c) 4.33, d) 5, e) 10, f) 15.

To be in conformity with ordering, $u_1 < u_2 \leq u_3$, we must require

$$l \geq 2M(e+3)\,. \tag{4.27}$$

Defining

$$\mu = \frac{M}{l} \tag{4.28}$$

we have the important inequality

$$\mu \leq \frac{1}{2(e+3)} \tag{4.29}$$

or

$$1 - 6\mu - 2\mu e \geq 0\,. \tag{4.30}$$

The condition, that

$$\mathrm{f}(u) = 2M\left(u + \frac{e-1}{l}\right)\left(u - \frac{e+1}{l}\right)\left(u - \frac{1}{2M} + \frac{2}{l}\right) \tag{4.31}$$

agrees with its definition (4.22), yields relations,

$$\frac{M}{L^2} = \frac{1}{l^2}\left[M\left(3+e^2\right) - l\right] \quad \text{and} \quad \frac{E^2+1}{L^2} = \frac{1}{l^3}(4M-l)\left(1-e^2\right)\,, \tag{4.32}$$

or, in terms of μ,

$$\frac{1}{L^2} = \frac{1}{lM}\left[\mu\left(3+e^2\right) - 1\right] \quad \text{and} \quad \frac{E^2+1}{L^2} = \frac{1}{l^2}(4\mu-1)\left(1-e^2\right)\,. \tag{4.33}$$

We write, since $e^2 > 1$,

$$\frac{1}{L^2} = \frac{1}{lM}\left[\mu\left(3+e^2\right) - 1\right] \quad \text{and} \quad \frac{E^2+1}{L^2} = \frac{1}{l^2}(1-4\mu)\left(e^2-1\right)\,. \tag{4.34}$$

Since $L^2 > 0$ and $E^2 + 1 > 0$

$$\mu\left(3+e^2\right) - 1 > 0\,, \tag{4.35}$$

and

$$\mu < \frac{1}{4}\,. \tag{4.36}$$

The allowed range of μ and e, according to (4.30) and (4.35), can be seen in

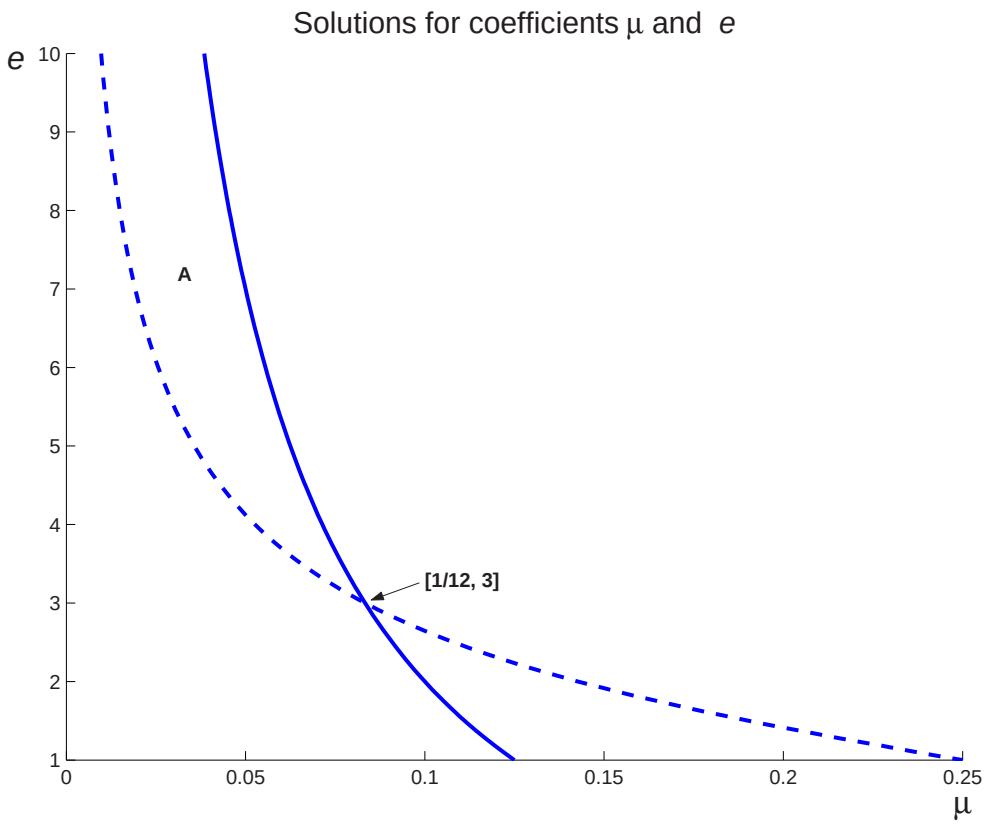

Figure 4.3: Area marked **A** designates where allowed pairs of e and μ lie.

fig. 4.3.

An alternative expression for E^2 may be noted here:

$$\frac{E^2}{L^2} = -\frac{1}{lM}(2\mu e - 2\mu + 1)(2\mu e + 2\mu - 1)\,. \tag{4.37}$$

We shall make a substitution

$$u \;= \frac{1}{l}(1 + e\cos\chi)\,. \tag{4.38}$$

Since $e > 1$,

$$u \;= 0 \quad \text{when} \quad \chi = \arccos\left(-e^{-1}\right) = \chi_\infty \qquad (\text{say})\,. \tag{4.39}$$

But the perihelion passage still occurs when $\chi = 0$. The allowed range of χ is, therefore,

$$0 \le \chi < \chi_\infty = \arccos\left(-e^{-1}\right)\,. \tag{4.40}$$

The substitution (4.38) reduces equation (4.21) to the simple form

$$\left(\frac{\mathrm{d}\chi}{\mathrm{d}\varphi}\right)^2 = 1 - 2\mu(3 + e\cos\chi) = 1 - 6\mu + 2\mu e - 4\mu e\cos^2\frac{\chi}{2}\,, \tag{4.41}$$

or, alternatively,

$$\pm\frac{\mathrm{d}\chi}{\mathrm{d}\varphi} = (1 - 6\mu + 2\mu e)^{1/2}\left(1 - k^2\cos^2\frac{\chi}{2}\right)^{1/2}\,, \tag{4.42}$$

where

$$k^2 = \frac{4\mu e}{1 - 6\mu + 2\mu e}\,. \tag{4.43}$$

The inequality (4.29) guarantees that

$$k^2 \le 1 \quad \text{and} \quad 1 - 6\mu + 2\mu e > 0\,. \tag{4.44}$$

It is now apparent that the solution for φ can be expressed in terms of the Jacobian elliptic integral

$$\mathrm{F}(\psi, k) = \int_0^\psi \frac{\mathrm{d}\gamma}{\sqrt{1 - k^2\sin^2\gamma}}\,, \tag{4.45}$$

where

$$\psi = \frac{1}{2}(\pi - \chi)\,. \tag{4.46}$$

Thus, keeping in mind restriction in the range of χ, we may now write the solution for φ in the form

$$\varphi = \frac{2}{\sqrt{1-6\mu+2\mu e}}\left[\mathrm{K}(k) - \mathrm{F}\left(\frac{\pi}{2} - \frac{\chi}{2}, k\right)\right]\,, \tag{4.47}$$

where $\mathrm{K}(k)$ denotes the complete elliptic integral,

$$\mathrm{K}(k) = \int_0^{\pi/2} \frac{\mathrm{d}\gamma}{\sqrt{1-k^2\sin^2\gamma}}\,. \tag{4.48}$$

In writing the solution for φ in the form (4.47), we have taken the origin of φ at the perihelion passage where $\chi = 0$. The trajectory goes off to infinity, asymptotically, along the direction

$$\varphi = \varphi_\infty = \frac{2}{\sqrt{1-6\mu+2\mu e}}\left[\mathrm{K}(k) - \mathrm{F}(\psi_\infty, k)\right] \quad \left(\psi_\infty = \frac{1}{2}\arccos\left(e^{-1}\right)\right)\,. \tag{4.49}$$

The solution can be now completed by direct integration of the equation (4.6) for t and τ. Thus,

$$\tau = \frac{1}{L}\int \frac{\mathrm{d}\varphi}{u^2} = \frac{1}{L}\int \frac{\mathrm{d}\varphi}{\mathrm{d}\chi}\frac{\mathrm{d}\chi}{u^2}\,, \tag{4.50}$$

and

$$t = \frac{E}{L}\int \frac{\mathrm{d}\varphi}{\mathrm{d}\chi}\frac{\mathrm{d}\chi}{u^2(1-2Mu)}\,. \tag{4.51}$$

By making use of equations (4.33), (4.37), (4.38), and (4.42), we obtain

$$\begin{aligned}\tau = -\frac{l}{(e^2-1)\left[k^2(e-1)-2e\right]\sqrt{\mu}}\Bigg\{&\frac{2e^2\sin\chi\sqrt{1-k^2+k^2\sin^2\frac{\chi}{2}}}{2e\sin^2\frac{\chi}{2}-e-1}+\\ &+2e\,\mathrm{E}\left(\frac{\pi}{2}-\frac{\chi}{2},k\right)+\mathrm{F}\left(\frac{\pi}{2}-\frac{\chi}{2},k\right)+\\ &+\Pi\left(\frac{\pi}{2}-\frac{\chi}{2},\frac{2e}{e-1},k\right)\left[k^2(e+3)-\frac{4e}{e-1}\right]\Bigg\}\sqrt{\frac{\mu(3+e^2)-1}{1-2\mu(3-e)}}\end{aligned} \tag{4.52}$$

and

$$t = -\frac{2e^2 \sin\chi}{(e^2-1)\left(1-e+2e\cos^2\frac{\chi}{2}\right)\left[k^2(e-1)-2e^2\right]}\cdot$$
$$\cdot\sqrt{\frac{(1-2\mu+2\mu e)(1-2\mu-2\mu e)\left(1-k^2\cos^2\frac{\chi}{2}\right)}{\mu(1-6\mu+2\mu e)}}+$$
$$+\frac{-8\Pi\left(\frac{\pi}{2}-\frac{\chi}{2},\frac{4\mu e}{1-2\mu+2\mu e},k\right)}{(e-1)(e^2-1)\left(1-e+2e\cos^2\frac{\chi}{2}\right)\left[k^2(e-1)-2e^2\right]}\Big\{(e-1)\big[2e(e+$$
$$+1)\left(e^2k^2-ek^2-k^2-2e^2+2e\right)\cos^2\frac{\chi}{2}+k^2\left(e^2+1\right)^2+$$
$$+2e^2\left(1-k^2e^2\right)\big]-2ek^2(e+1)\left[(e-1)\left(1+e\cos^2\frac{\chi}{2}\right)-e^2\right]\Big\}\cdot$$
$$\cdot\sqrt{\frac{\mu^3(1-2\mu-2\mu e)}{(2\mu e-2\mu+1)(1-6\mu+2\mu e)}}-\Pi\left(\frac{\pi}{2}-\frac{\chi}{2},\frac{2e}{e-1},k\right)\cdot$$
$$\cdot\frac{\{(e^2-1)[k^2(1-4\mu e+4\mu)+8\mu e]+2k^2(e-1)-4e\}}{(e-1)^2\left[k^2(e-1)-2e^2\right]}\cdot$$
$$\cdot\sqrt{\frac{(1-2\mu+2\mu e)(1-2\mu-2\mu e)}{\mu(1-6\mu+2\mu e)}}+$$
$$+\frac{-\mathrm{F}\left(\frac{\pi}{2}-\frac{\chi}{2},k\right)\left[k^2(e-1)-2e\right]}{(e^2-1)[k^2(e-1)-2e^2]}\sqrt{\frac{(1-2\mu+2\mu e)(1-2\mu-2\mu e)}{\mu(1-6\mu+2\mu e)}}+$$
$$+\frac{-2e\,\mathrm{E}\left(\frac{\pi}{2}-\frac{\chi}{2},k\right)}{(e^2-1)[k^2(e-1)-2e^2]}\sqrt{\frac{(1-2\mu+2\mu e)(1-2\mu-2\mu e)}{\mu(1-6\mu+2\mu e)}}\,, \quad (4.53)$$

where

$$\mathrm{E}(\psi,k)=\int_0^\psi\sqrt{\frac{1-k^2\gamma^2}{1-\gamma^2}}\mathrm{d}\gamma \quad (4.54)$$

and

$$\Pi(\psi,\alpha^2,k)=\int_0^\psi\frac{\mathrm{d}\gamma}{(1-\alpha^2t^2)\sqrt{(1-t^2)(1-k^2t^2)}} \quad (4.55)$$

are elliptic integrals.

The case $2\mu(3+e)=1$

In this case, the perihelion distance, r_p, is given by

$$r_\mathrm{p}=\frac{l}{1+e}=2M\frac{3+e}{1+e}\,. \quad (4.56)$$

For these orbits

$$\frac{L^2}{M^2} = \frac{4(3+e)^2}{(e-3)(e+1)} \qquad \text{and} \qquad E^2 + 1 = \frac{e^2-1}{e^2-9}\,. \tag{4.57}$$

According to the allowed range of e (see fig. 4.3), the corresponding perihelion-distances must be

$$2M < r_{\rm p} < 3M\,. \tag{4.58}$$

It is convenient to go back to the equation (4.41); it gives

$$\left(\frac{\mathrm{d}\chi}{\mathrm{d}\varphi}\right)^2 = 4\mu e \sin^2\frac{\chi}{2} \qquad \text{or} \qquad \frac{\mathrm{d}\chi}{\mathrm{d}\varphi} = -2\,(\mu e)^{1/2}\sin\frac{\chi}{2}\,, \tag{4.59}$$

where the negative sign has been chosen so that φ may increase when χ decreases. The required solution of equation (4.59) is

$$\varphi = -\frac{1}{\sqrt{\mu e}}\ln\tan\frac{\chi}{4}\,. \tag{4.60}$$

The asymptotic direction is

$$\varphi_\infty = -\frac{1}{\sqrt{\mu e}}\ln\tan\frac{\chi_\infty}{4} \tag{4.61}$$

(see χ_∞ in equation (4.39)).

4.2.2 Orbits of the second kind

To obtain the solution for these orbits, we now make a substitution

$$u \;= \left(\frac{1}{2M} - \frac{2}{l}\right) + \left(\frac{1}{2M} - \frac{3+e}{l}\right)\tan^2\frac{\xi}{2}\,. \tag{4.62}$$

By this substitution,

$$u \;= u_3 = \frac{1}{2M} - \frac{2}{l} \quad \text{when} \quad \xi = 0$$

and (4.63)

$$u \;\to \infty \qquad\qquad \text{as} \quad \xi \to \pi$$

we further find that equation (4.21) now reduces to

$$\left(\frac{\mathrm{d}\xi}{\mathrm{d}\varphi}\right)^2 = (1-6\mu+2\mu e)\left(1-k^2\sin^2\frac{\xi}{2}\right) \tag{4.64}$$

with the same definition of k^2 as for the orbits of the first kind. Thus we may now write

$$\varphi = \frac{2}{\sqrt{1-6\mu+2\mu e}}\,\mathrm{F}\left(\frac{\xi}{2},k\right). \tag{4.65}$$

At aphelion, $\xi = 0$ and $\varphi = 0$; and at the singularity $\xi \to \pi$ and φ takes the finite value

$$\varphi_0 = \frac{2}{\sqrt{1-6\mu+2\mu e}}\,\mathrm{K}(k)\,. \tag{4.66}$$

In fig. 4.4, an example of unbound orbits is illustrated (as given by solutions (4.60) and (4.65)).

The solution for the arc lenght τ and the coordinate time t can be obtained by integrating the equations

$$\frac{\mathrm{d}\tau}{\mathrm{d}\xi} = \frac{1}{Lu^2}\frac{\mathrm{d}\varphi}{\mathrm{d}\xi} \quad \text{and} \quad \frac{\mathrm{d}t}{\mathrm{d}\xi} = \frac{E}{Lu^2(1-2Mu)}\frac{\mathrm{d}\varphi}{\mathrm{d}\xi}\,. \tag{4.67}$$

(Numerical solution for integrals (4.50), (4.51) and (4.67) are shown in figure 4.5.) By making use of equations (4.33), (4.37), (4.62), and (4.64), we obtain

$$\begin{aligned}\tau = \frac{kl}{4\mu-1}\sqrt{\frac{\mu e^2+3\mu-1}{e}}\Bigg\{&\frac{(2\mu e+6\mu-1)\,\mathrm{E}\left(\frac{\xi}{2},k\right)}{(e+1)[2\mu(e+1)+k^2(4\mu-1)]}+\\ &+\frac{-2(2\mu e-2\mu+1)\,\mathrm{F}\left(\frac{\xi}{2},k\right)}{\mu\,(e+1)^2}+(2\mu e+6\mu-1)\Pi\left(\frac{\xi}{2},\frac{2\mu(e+1)}{1-4\mu},k\right)\cdot\\ &\cdot\frac{k^2(4\mu-1)(4\mu e+1)+4\mu(e+1)(\mu e-3\mu+1)}{2\mu(4\mu-1)\,(e+1)^2\left[4\mu-1+2\mu(e+1)\sin^2\frac{\xi}{2}\right]}+\\ &+\frac{\mu(2\mu e+6\mu-1)\left(1-k^2\sin^2\frac{\xi}{2}\right)\sin\xi\cos\frac{\xi}{2}}{[2\mu(e+1)+k^2(4\mu-1)]\left[4\mu-1+2\mu(e+1)\sin^2\frac{\xi}{2}\right]}\Bigg\}\end{aligned} \tag{4.68}$$

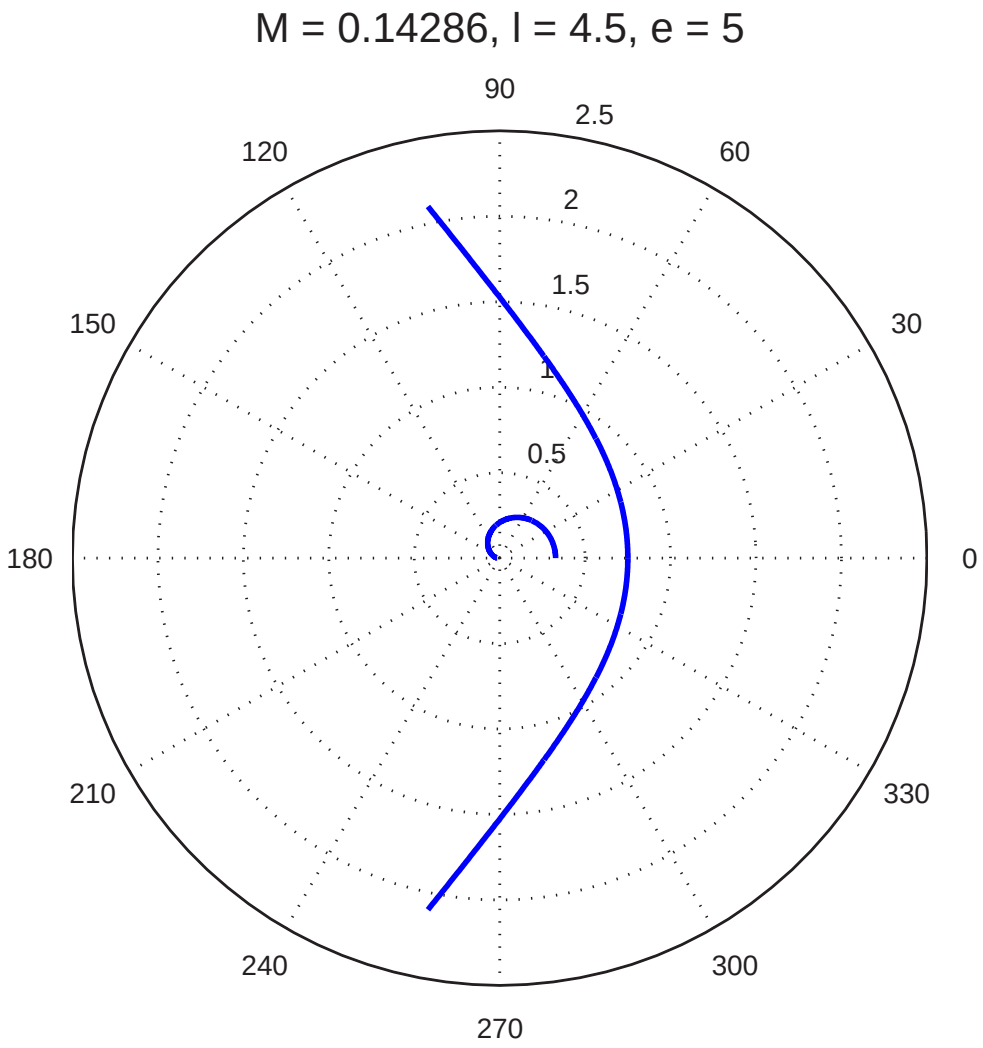

Figure 4.4: The orbit of the first kind arrives from infinity, and after reaching the perihelion, goes again to infinity. Orbit of the second, starting from a certain distance from the black hole (aphelion), falls into the singularity. Eccentricity is $e = 5$ and latus rectum is $l = 4.5$ ($M = 1/7$ in the scale along the coordinate axes.)

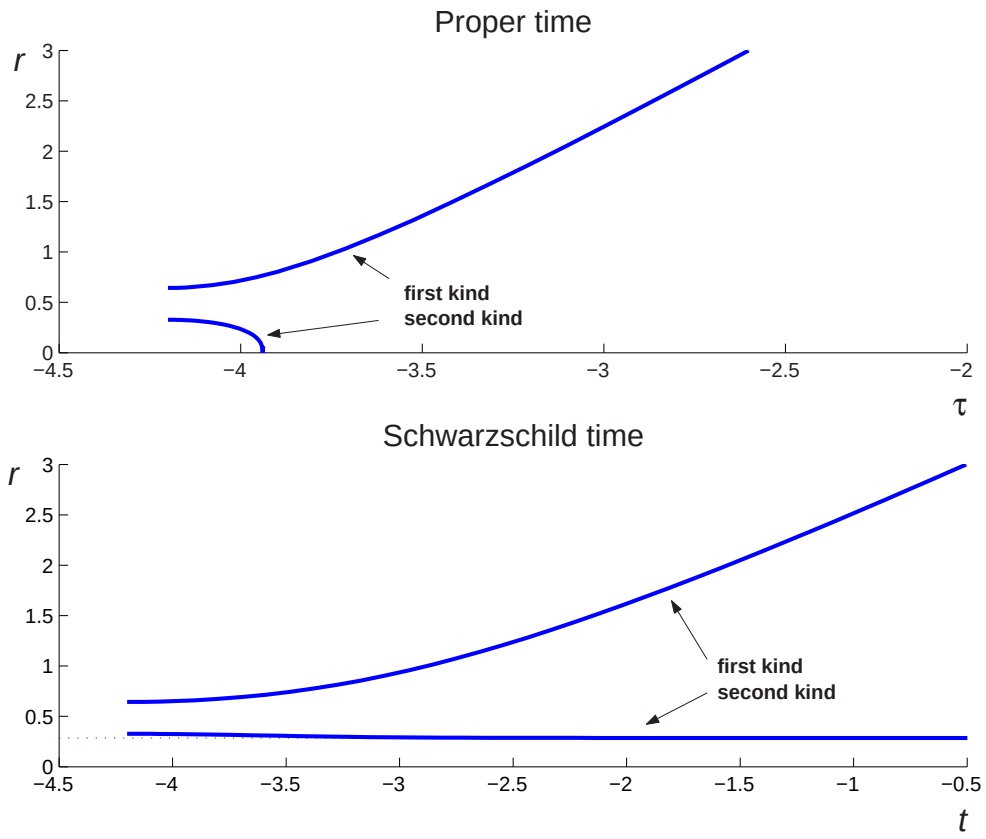

Figure 4.5: Proper time (τ) and Schwarzschild time (t) along space-like geodesics of the first and second kind; $M = 1/7$, $l = 4.5$ and $e = 6$.

and

$$t = \frac{kl}{3\mu e + 6\mu - 1 - 4\mu^2 e}\left\{\frac{(2\mu e + 6\mu - 1)^2\,\mathrm{E}\left(\frac{\xi}{2}, k\right)}{(1-4\mu)(e+1)[k^2(1-4\mu) - 2\mu(e+1)]} + \right.$$
$$+\frac{-[4\mu^3(3e^3+20e^2+31e+18) - 4\mu^2(4e^2+9e-3) + \mu(e-6)+1]\,\mathrm{F}\left(\frac{\xi}{2}, k\right)}{2\mu(1-4\mu)\,(e+1)^2\,(1-2\mu-3\mu e)} +$$
$$+\frac{(2\mu e+6\mu-1)^2\Pi\left(\frac{\xi}{2}, \frac{2\mu(e+1)}{1-4\mu}, k\right)}{2\mu\,(1-4\mu)^2\,(e+1)^2\,[k^2(1-4\mu)-2\mu(e+1)]}\cdot$$
$$\cdot\left[k^2(1-4\mu)\left(64\mu^3e^2+144\mu^3e+96\mu^3-40\mu^2-72\mu^2e-24\mu^2e^2-2\mu+\right.\right.$$
$$\left.+5\mu e-1\right) - 4\mu^3(e+1)\left(28\mu e^3 - 9e^2 - 19e + 60\mu e + 48\mu - 2\right)\Big] +$$
$$+\frac{-(3\mu e+6\mu-1)\Pi\left(\frac{\xi}{2}, \frac{1-2\mu-3\mu e}{4\mu}, k\right)}{(1-2\mu-3\mu e)(3\mu e+6\mu-1-4\mu^2 e)} +$$
$$\left.+\frac{-\mu(2\mu e+6\mu-1)\sqrt{1-k^2\sin^2\frac{\xi}{2}}\sin^2\xi}{(1-4\mu)[k^2(1-4\mu)-2\mu(e+1)]\left[1-4\mu-2\mu\sin^2\frac{\xi}{2}(e+1)\right]}\right\}\cdot$$
$$\cdot\sqrt{\frac{(1-2\mu+2\mu e)(1-2\mu-2\mu e)}{e}}\,. \quad (4.69)$$

The case $2\mu(3+e)=1$

When $2\mu(3+e)=1$, the roots of $f(u)=0$ are

$$u_1 = -\frac{1}{l}(e-1) \quad \text{and} \quad u_2 = u_3 = \frac{1}{4M} + \frac{e-1}{2l} = \frac{e+1}{l}\,; \quad (4.70)$$

and the substitution that is suggested is

$$u \;= \frac{1}{l}\left(1 + e + 2e\tan^2\frac{\xi}{2}\right)\,. \quad (4.71)$$

By this substitution,

$$u \;= u_2 = u_3 = \frac{e+1}{l} \text{ when } \xi = 0\,, \text{ and } u \;\to \infty \text{ when } \xi \to \pi\,. \quad (4.72)$$

We further find that equation (4.21) reduces to

$$\left(\frac{\mathrm{d}\xi}{\mathrm{d}\varphi}\right)^2 = 4\mu e\sin^2\frac{\xi}{2}\,. \quad (4.73)$$

We observe that this is exactly the same equation we obtained when considering the orbits of the first kind in the same context, $u_2 = u_3$ (see equation (4.59)). And, as before, we shall write

$$\varphi = -\frac{1}{\sqrt{\mu e}} \ln \tan \frac{\xi}{4} \,. \tag{4.74}$$

Along this orbit, $\varphi = 0$ when $\xi = \pi$ and $r \to 0$; and $\varphi \to \infty$ as $\xi \to \infty$ and we approach the aphelion at $r = \frac{l}{1+e}$. In fig. 4.6 there is an example of solutions (4.60) and (4.74).

4.2.3 The orbits with imaginary eccentricities

Finally, we have to consider the case when $\mathrm{f}(u) = 0$ allows only one real root and pair of complex-conjugate roots (the case (γ) of fig. 3.1). It is evident that the corresponding orbits, while arriving from infinity, will fall into the singularity though they may circle the origin one or more times before doing so. As in section 3.2.3, we shall characterize these orbits by an imaginary eccentricity ie and write roots of $\mathrm{f}(u) = 0$ as in equations (3.39). With the present definition, we can obtain the equations which replace equations (4.33) and (4.37) by simply writing $-e^2$ wherever $+e^2$ occurs and conversely. We thus obtain

$$\frac{1}{L^2} = \frac{1}{lM}\left[\mu\left(3 - e^2\right) - 1\right] \,, \quad \frac{E^2+1}{L^2} = \frac{1}{l^2}(4\mu - 1)\left(1 + e^2\right) \,,$$

and

$$\frac{E^2}{L^2} = \frac{1}{lM}\left(4\mu^2 e^2 + 4\mu^2 - 4\mu + 1\right) \,. \tag{4.75}$$

Accordingly, we must now require

$$\mu > \frac{1}{4} \quad \text{and} \quad 3\mu - \mu e^2 - 1 > 0 \,. \tag{4.76}$$

The second inequality imposes restrictions

$$e^2 < 3 - \frac{1}{\mu} \qquad \text{and} \qquad \mu > 1/3 \,. \tag{4.77}$$

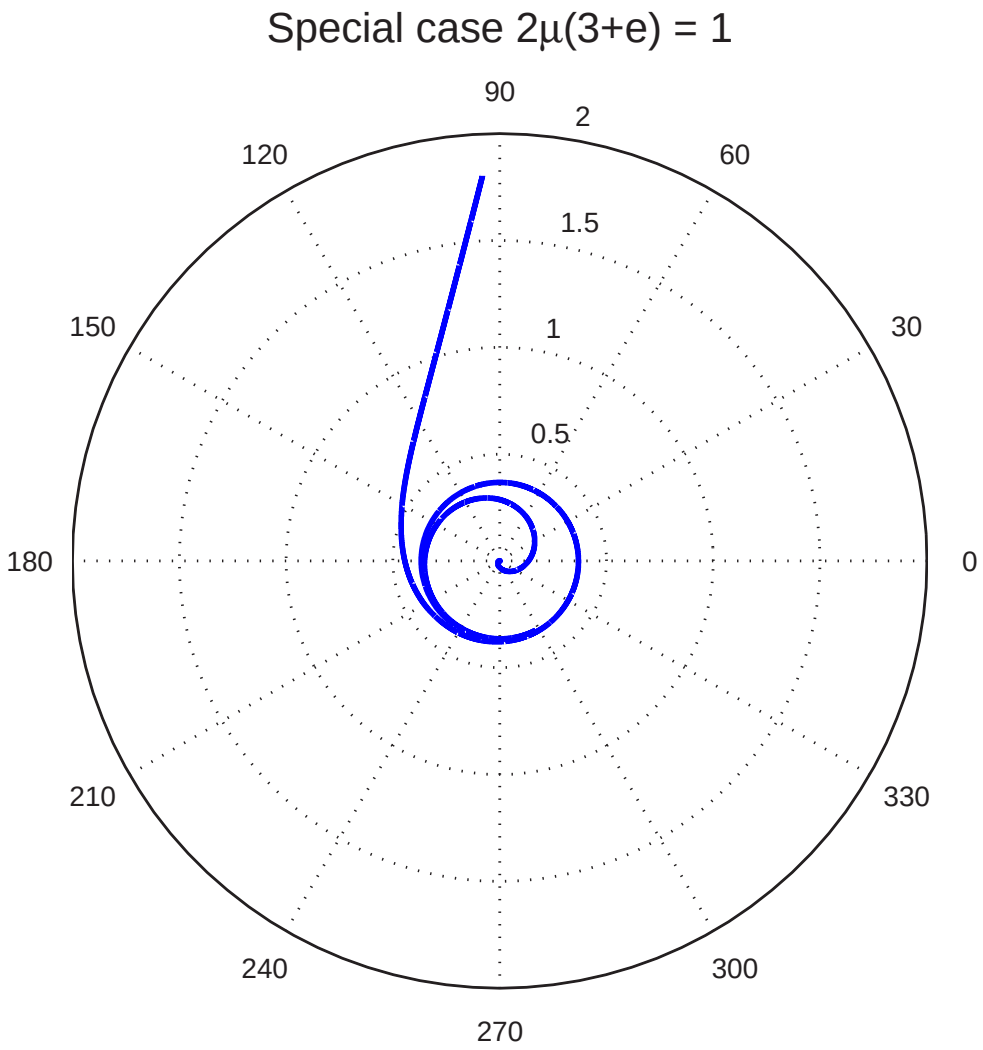

Figure 4.6: The case $2\mu(3+e) = 1$. The orbit of the first kind comes from infinity, and after spiralling infinitely around the black hole, reaches the perihelion. The orbit of the second kind starts form aphelion, and after spiralling around the black hole infinitely, reaches singularity. Eccentricity is $e = 6$ ($M = 1/7$ in the scale along the coordinate axes.)

The analysis of section 4.2.3 applies equally to the present considerations with the only proviso that (4.77) holds. Since these orbits are unbounded, the solution for φ is given by the same equation (3.48) as in section 4.2.3. The origin of φ is at the singularity (where $\xi = \pi$ and $\psi = +\pi/2$). But the lower limit on ψ, say ψ_∞, as the orbit goes off to infinity, can be obtained from equation (3.47) by inserting for $\sin\frac{\xi}{2}$ and $\cos\frac{\xi}{2}$ the values appropriate for ξ_∞ given in equation (3.42). We find

$$\sin^2\psi_\infty = \frac{1}{\triangle + 6\mu - 1}\left(\triangle + 6\mu - 1 - 2e^2\frac{4\mu - 1}{e^2 + 1}\right). \tag{4.78}$$

In fig. 4.7 an example of solution (3.48) is illustrated.

The solution for the arc lenght τ and the coordinate time t can be obtained by integrating the equations (4.67). Numerical solution for integrals (4.50) and (4.51) are shown in figure 4.8. By making use of equations (4.75), (3.41), and (3.43), we obtain

$$\begin{aligned}\tau = \frac{\mu\,(3-e^2)-1}{\sqrt{\mu}}\Bigg\{ & \frac{\tan\frac{\xi}{4}-1}{2\mu e^3\left[4\mu\,(e^2-1)-(e^2+1)\right]}\cdot \\ & \cdot \mathrm{E}\left(\sqrt{\frac{\left(\tan\frac{\xi}{4}+1\right)\left(2\mu e-\sqrt{4\mu^2e^2+36\mu^2-12\mu+1}-6\mu+1\right)}{\left(\tan\frac{\xi}{4}-1\right)\left(2\mu e-\sqrt{4\mu^2e^2+36\mu^2-12\mu+1}+6\mu-1\right)}},\right. \\ & \left.\sqrt{\frac{(6\mu-1)\sqrt{4\mu^2e^2+36\mu^2-12\mu+1}-12\mu(3\mu-1)-1}{(1-6\mu)\sqrt{4\mu^2e^2+36\mu^2-12\mu+1}-12\mu(3\mu-1)-1}}\right)\cdot \\ & \cdot\sqrt{\frac{\left(\tan\frac{\xi}{4}+1\right)\left(\sqrt{4\mu^2e^2+36\mu^2-12\mu+1}-2\mu e+6\mu-1\right)}{\left(\tan\frac{\xi}{4}-1\right)\left(\sqrt{4\mu^2e^2+36\mu^2-12\mu+1}-2\mu e-6\mu+1\right)}}\cdot \\ & \cdot\sqrt{\frac{(6\mu-1)\left(\tan^2\frac{\xi}{4}-1\right)+4\mu e\tan\frac{\xi}{4}}{(6\mu-1)\left(\tan^2\frac{\xi}{4}-1\right)-4\mu e\tan\frac{\xi}{4}}}+\end{aligned}$$

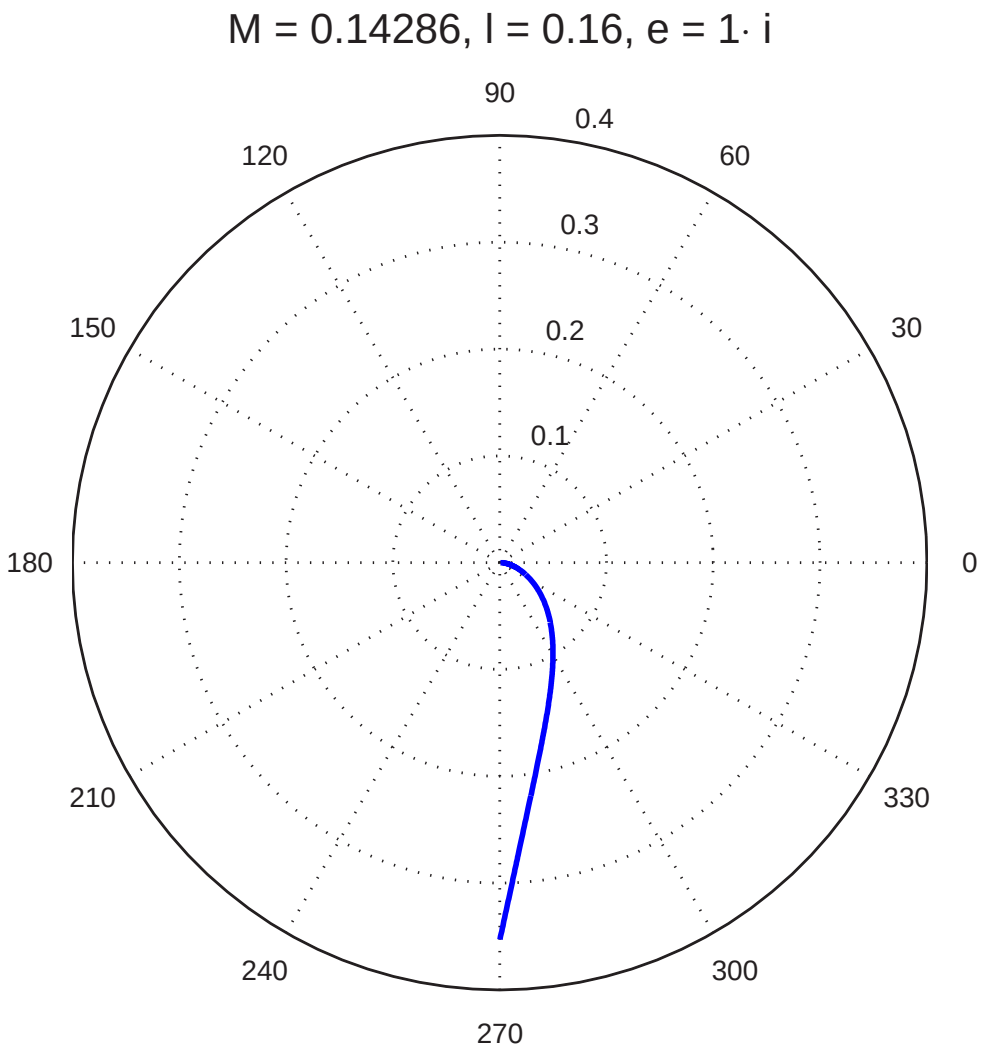

The orbit of the first kind arrives from infinity, and after reaching the perihelion, goes again to infinity. Orbit of the second, starting from a certain distance from the black hole (aphelion), falls into the singularity.

Figure 4.7: Orbits with $l = 0.16$ and with imaginary eccentricity $e = \mathrm{i}$ ($M = 1/7$ in the scale along the coordinate axes). The orbit arrives from infinity, and falls into the singularity.

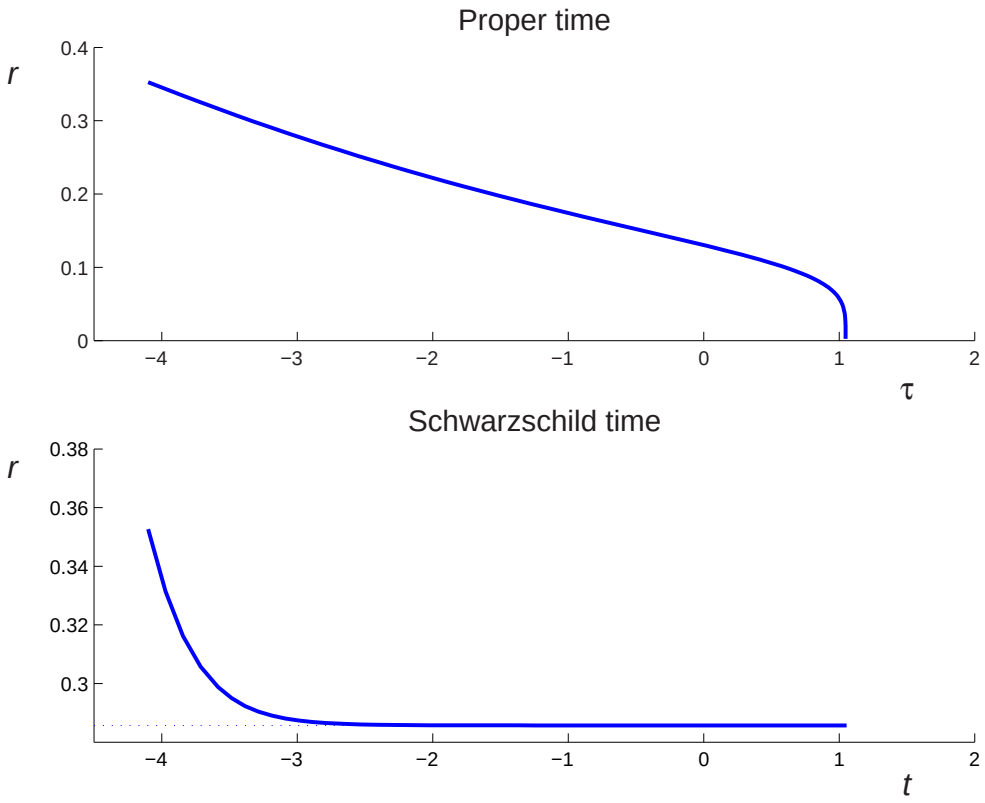

Figure 4.8: Proper time (τ) and Schwarzschild time (t) along a space-like geodesic with an imaginary eccentricity; $M = 1/7$, $l = 0.16$ and $e = \mathrm{i}$.

$$+\frac{1}{\sqrt{2(1-6\mu)(6\mu-1)+\sqrt{4\mu^2e^2+36\mu^2-12\mu+1}}}\cdot$$
$$\cdot\frac{(6\mu-1)\left(\tan^2\frac{\xi}{4}-1\right)-4\mu e\tan\frac{\xi}{4}}{\mu e\left(e^2+1\right)(4\mu-1)\left[(6\mu-1)\left(\tan^2\frac{\xi}{4}-1\right)+4\mu e\tan\frac{\xi}{4}\right]}\cdot$$
$$\cdot\mathrm{F}\left(\sqrt{\frac{\left(\tan\frac{\xi}{4}+1\right)\left(2\mu e-\sqrt{4\mu^2e^2+36\mu^2-12\mu+1}-6\mu+1\right)}{\left(\tan\frac{\xi}{4}-1\right)\left(2\mu e-\sqrt{4\mu^2e^2+36\mu^2-12\mu+1}+6\mu-1\right)}},\right.$$
$$\left.\sqrt{\frac{1-6\mu+\sqrt{4\mu^2e^2+36\mu^2-12\mu+1}}{1-6\mu-\sqrt{4\mu^2e^2+36\mu^2-12\mu+1}}}\right)\left[\left(\left(e^2+1\right)(1-4\mu)\cdot\right.\right.$$
$$\left.\cdot(2\mu e+6\mu-1)+\left(4\mu\left(e^2+1\right)+e^2-1\right)\sqrt{4\mu^2e^2+36\mu^2-12\mu+1}\right)\cdot$$
$$\cdot\sqrt{(6\mu-1)\left(1-\tan^2\frac{\xi}{4}\right)+4\mu e\tan\frac{\xi}{4}}+$$
$$+\left(\left(\mu e-4\mu e^2-3\mu+e^2+1\right)\sqrt{4\mu^2e^2+36\mu^2-12\mu+1}-3\mu e+\right.$$
$$\left.+e^2+1-2\mu e^3+12\mu+\mu^2e^3-9\mu-10e^2\mu+22\mu^2e^2\right)\cdot$$
$$\left.\cdot\sqrt{(6\mu-1)\left(1-\tan^2\frac{\xi}{4}\right)+4\mu e\tan\frac{\xi}{4}}\right]+$$
$$+\frac{1}{4e^2\left(\tan\frac{\xi}{4}-1\right)^2\left(\sqrt{4\mu^2e^2-36\mu^2-12\mu+1}-2\mu e\right)\sqrt{\mu^5\left(e^2+1\right)}}\cdot$$
$$\cdot\frac{\sqrt{\left(\tan^2\frac{\xi}{4}-1\right)(6\mu-1)+4\mu e\tan\frac{\xi}{4}}}{\left(\tan^2\frac{\xi}{4}-1\right)(6\mu-1)-4\mu e\tan\frac{\xi}{4}}\cdot$$
$$\cdot\Pi\left(\sqrt{\frac{\left(\tan\frac{\xi}{4}+1\right)\left(2\mu e-\sqrt{4\mu^2e^2-36\mu^2-12\mu+1}-6\mu+1\right)}{\left(\tan\frac{\xi}{4}-1\right)\left(2\mu e-\sqrt{4\mu^2e^2-36\mu^2-12\mu+1}+6\mu-1\right)}},\right.$$
$$\frac{\left(2\mu e-\sqrt{4\mu^2e^2-36\mu^2-12\mu+1}+6\mu-1\right)\left(e-1+\sqrt{e^2+1}\right)}{\left(2\mu e-\sqrt{4\mu^2e^2-36\mu^2-12\mu+1}-6\mu+1\right)\left(e+1+\sqrt{e^2+1}\right)},$$
$$\left.\frac{1-6\mu+\sqrt{4\mu^2e^2-36\mu^2-12\mu+1}+6\mu-1}{1-6\mu-\sqrt{4\mu^2e^2-36\mu^2-12\mu+1}+6\mu-1}\right)\cdot$$
$$\cdot\left[2(\mu e^2-3\mu+1)\left(2\mu e-\sqrt{4\mu^2e^2-36\mu^2-12\mu+1}+6\mu-1\right)\cdot\right.$$
$$\left.\cdot\left(1+2(e-1)\tan\frac{\xi}{4}-4e\tan^2\frac{\xi}{4}+2(e+1)\tan^3\frac{\xi}{4}-\tan^4\frac{\xi}{4}\right)+\right.$$

$$+ 2 + \sqrt{2}\Big] + \frac{\mu\,(3-e^2)-1}{(4\mu-1)\,(e^2+1)^{3/2}}\cdot$$

$$\cdot\,\Pi\left(\sqrt{\frac{\left(\tan^2\frac{\xi}{4}+1\right)\left(2\mu e-\sqrt{4\mu^2e^2-36\mu^2-12\mu+1}-6\mu+1\right)}{\left(\tan^2\frac{\xi}{4}-1\right)\left(2\mu e-\sqrt{4\mu^2e^2-36\mu^2-12\mu+1}+6\mu-1\right)}},\right.$$

$$\frac{\left(2\mu e-\sqrt{4\mu^2e^2-36\mu^2-12\mu+1}+6\mu-1\right)\left(e-1-\sqrt{e^2+1}\right)}{\left(2\mu e-\sqrt{4\mu^2e^2-36\mu^2-12\mu+1}-6\mu+1\right)\left(e+1-\sqrt{e^2+1}\right)},$$

$$\left.\sqrt{\frac{(6\mu-1)\sqrt{4\mu^2e^2-36\mu^2-12\mu+1}+12\mu(1-3\mu)-1}{(1-6\mu)\sqrt{4\mu^2e^2-36\mu^2-12\mu+1}+12\mu(1-3\mu)-1}}\right)\cdot$$

$$\cdot\sqrt{\frac{1-6\mu}{2e}}\sqrt{\frac{6\mu-1-2\mu e+\sqrt{4\mu^2e^2-36\mu^2-12\mu+1}}{1-6\mu-2\mu e+\sqrt{4\mu^2e^2-36\mu^2-12\mu+1}}}\cdot$$

$$\cdot\sqrt{\frac{(1-6\mu)\left(1-\tan^2\frac{\xi}{4}\right)+4\mu e\tan\frac{\xi}{4}}{(6\mu-1)\left(1-\tan^2\frac{\xi}{4}\right)+4\mu e\tan\frac{\xi}{4}}}+$$

$$+\frac{(e-1)\tan\frac{\xi}{4}+e+1}{2(e^2+1)(1-4\mu)\left(1+2e\tan\frac{\xi}{4}-\tan^2\frac{\xi}{4}\right)}\sqrt{\frac{1+\tan\frac{\xi}{4}}{1-\tan\frac{\xi}{4}}}\cdot$$

$$\cdot\sqrt{\frac{(6\mu-1)\left(1-\tan^2\frac{\xi}{4}\right)+4\mu e\tan\frac{\xi}{4}}{\mu}}\Bigg\}$$

and

$$t = l\sqrt{\frac{2\mu e-\sqrt{4\mu^2e^2+36\mu^2-12\mu+1}+6\mu-1}{2\mu e-\sqrt{4\mu^2e^2+36\mu^2-12\mu+1}-6\mu+1}}\cdot$$

$$\cdot\sqrt{\frac{(6\mu-1)\left(\tan^2\frac{\xi}{4}-1\right)+4\mu e\tan\frac{\xi}{4}}{(6\mu-1)\left(\tan^2\frac{\xi}{4}-1\right)-4\mu e\tan\frac{\xi}{4}}}\cdot$$

$$\cdot\left[\Pi\left(\sqrt{\frac{\left(\tan\frac{\xi}{4}+1\right)\left(2\mu e-\sqrt{4\mu^2e^2+36\mu^2-12\mu+1}-6\mu+1\right)}{\left(\tan\frac{\xi}{4}-1\right)\left(2\mu e-\sqrt{4\mu^2e^2+36\mu^2-12\mu+1}+6\mu-1\right)}},\right.\right.$$

$$\frac{\left(\sqrt{e^2+1}+1-e\right)\left(\sqrt{4\mu^2e^2+36\mu^2-12\mu+1}-2\mu e-6\mu+1\right)}{\left(\sqrt{e^2+1}-1-e\right)\left(\sqrt{4\mu^2e^2+36\mu^2-12\mu+1}-2\mu e+6\mu-1\right)},$$

$$\left.\sqrt{\frac{6\mu-1-\sqrt{4\mu^2e^2+36\mu^2-12\mu+1}}{6\mu-1+\sqrt{4\mu^2e^2+36\mu^2-12\mu+1}}}\right)\left(\frac{1}{\mu\sqrt{e}}+\frac{\sqrt{e^2+1}+e}{\sqrt{e^2+1}-e}\right)\cdot$$

$$\cdot\sqrt{\frac{4\mu^2e^2+4\mu^2-4\mu+1}{e^2+1}}+$$

$$+\frac{2}{\sqrt{e}}\Pi\left(\sqrt{\frac{\left(\tan\frac{\xi}{4}+1\right)\left(2\mu e-\sqrt{4\mu^2e^2+36\mu^2-12\mu+1}-6\mu+1\right)}{\left(\tan\frac{\xi}{4}-1\right)\left(2\mu e-\sqrt{4\mu^2e^2+36\mu^2-12\mu+1}+6\mu-1\right)}},\right.$$
$$\frac{\left(1-2\mu+2\mu e+\sqrt{4\mu^2e^2+4\mu^2-4\mu+1}\right)}{\left(2\mu-1+2\mu e+\sqrt{4\mu^2e^2+4\mu^2-4\mu+1}\right)}\cdot$$
$$\cdot\frac{\left(\sqrt{4\mu^2e^2+36\mu^2-12\mu+1}-2\mu e-6\mu+1\right)}{\left(\sqrt{4\mu^2e^2+36\mu^2-12\mu+1}-2\mu e+6\mu-1\right)},$$
$$\left.\sqrt{\frac{6\mu-1-\sqrt{4\mu^2e^2+36\mu^2-12\mu+1}}{6\mu-1+\sqrt{4\mu^2e^2+36\mu^2-12\mu+1}}}\right)+$$
$$+\frac{2}{\sqrt{e}}\Pi\left(\sqrt{\frac{\left(\tan\frac{\xi}{4}+1\right)\left(2\mu e-\sqrt{4\mu^2e^2+36\mu^2-12\mu+1}-6\mu+1\right)}{\left(\tan\frac{\xi}{4}-1\right)\left(2\mu e-\sqrt{4\mu^2e^2+36\mu^2-12\mu+1}+6\mu-1\right)}},\right.$$
$$\frac{\left(2\mu-1-2\mu e+\sqrt{4\mu^2e^2+4\mu^2-4\mu+1}\right)}{\left(1-2\mu-2\mu e+\sqrt{4\mu^2e^2+4\mu^2-4\mu+1}\right)}\cdot$$
$$\cdot\frac{\left(\sqrt{4\mu^2e^2+36\mu^2-12\mu+1}-2\mu e-6\mu+1\right)}{\left(\sqrt{4\mu^2e^2+36\mu^2-12\mu+1}-2\mu e+6\mu-1\right)},$$
$$\left.\sqrt{\frac{6\mu-1-\sqrt{4\mu^2e^2+36\mu^2-12\mu+1}}{6\mu-1+\sqrt{4\mu^2e^2+36\mu^2-12\mu+1}}}\right)\sqrt{\frac{\tan\frac{\xi}{4}-1}{\tan\frac{\xi}{4}+1}}\Bigg]\ . \quad (4.79)$$

Chapter 5

The time-like geodesics in the Schwarzschild space-time

Remember that freely falling particles with positive rest-mass describe time-like geodesics. This chapter is taken from [7, Chapter 3] and shortened.

For time-like geodesics $2\mathcal{L}$ has the value 1, and we can write

$$\left(\frac{\mathrm{d}r}{\mathrm{d}\tau}\right)^2 + \left(1 - \frac{2M}{r}\right)\left(1 + \frac{L^2}{r^2}\right) = E^2\,. \tag{5.1}$$

As in chapters 3 and 4 we obtain the basic equation of the problem (cf. equations (3.8) and (4.5))

$$\left(\frac{\mathrm{d}u}{\mathrm{d}\varphi}\right)^2 = 2Mu^3 - u^2 + \frac{2M}{L^2}u - \frac{1-E^2}{L^2}\,. \tag{5.2}$$

5.1 The radial geodesics

Again we shall consider trajectories of particles with $L = 0$ which start from rest at some finite distance r_i and drop towards the center.

This time the change of variables will be

$$r = \frac{M}{1-E^2}(1 + \cos\eta) = r_\mathrm{i}\cos^2\frac{\eta}{2}\,. \tag{5.3}$$

In terms of η, the equations to be integrated are (compare with equations (4.12) and (4.13))

$$\left(\frac{\mathrm{d}r}{\mathrm{d}\tau}\right)^2 = (1-E^2)\tan^2\frac{\eta}{2} \quad \text{and} \quad \frac{\mathrm{d}t}{\mathrm{d}\tau} = \frac{E\cos^2\frac{\eta}{2}}{\cos^2\frac{\eta}{2}-\cos^2\frac{\eta_{\mathrm{H}}}{2}}\,, \tag{5.4}$$

together with

$$\frac{\mathrm{d}r}{\mathrm{d}\eta} = -r_{\mathrm{i}}\sin\frac{\eta}{2}\cos\frac{\eta}{2}\,. \tag{5.5}$$

Because we are considering infalling particles,

$$\frac{\mathrm{d}r}{\mathrm{d}\tau} = -\left(1-E^2\right)^{1/2}\tan\frac{\eta}{2} = -\left(\frac{2M}{r_{\mathrm{i}}}\right)^{1/2}\tan\frac{\eta}{2}\,. \tag{5.6}$$

From equations (5.5) and (5.6) follows (compare with equation (4.15))

$$\frac{\mathrm{d}\tau}{\mathrm{d}\eta} = \left(\frac{r_{\mathrm{i}}^3}{2M}\right)^{1/2}\cos^2\frac{\eta}{2} = (1+\cos\eta)\sqrt{\frac{r_{\mathrm{i}}^3}{8M}}\,. \tag{5.7}$$

With the assumption that $\tau = 0$ at $\eta = 0$, we obtain

$$\tau = \left(\frac{r_{\mathrm{i}}^3}{8M}\right)^{1/2}(\eta+\sin\eta)\,. \tag{5.8}$$

Similarly to section 4.1 the situation differs when we consider the equation of the trajectory in coordinate time, t. To obtain t, the equation (cf. equations (5.4) and (5.7))

$$\frac{\mathrm{d}t}{\mathrm{d}\eta} = E\frac{\cos^4\frac{\eta}{2}}{\cos^2\frac{\eta}{2}-\cos^2\frac{\eta_{\mathrm{H}}}{2}}\sqrt{\frac{r_{\mathrm{i}}^3}{2M}} \tag{5.9}$$

must be integrated. After integration

$$t = E\left(\frac{r_{\mathrm{i}}^3}{2M}\right)^{1/2}\left[\frac{1}{2}(\eta+\sin\eta)+\left(1-E^2\right)\eta\right] + 2M\ln\left(\frac{\tan\frac{1}{2}\eta_{\mathrm{H}}+\tan\frac{1}{2}\eta}{\tan\frac{1}{2}\eta_{\mathrm{H}}-\tan\frac{1}{2}\eta}\right)\,. \tag{5.10}$$

Solutions (5.8) and (5.10) are illustrated in fig. 5.1. Coordinate time for time-like geodesics displays the same behavior as for space-like geodesics as can be seen in figure 5.1.

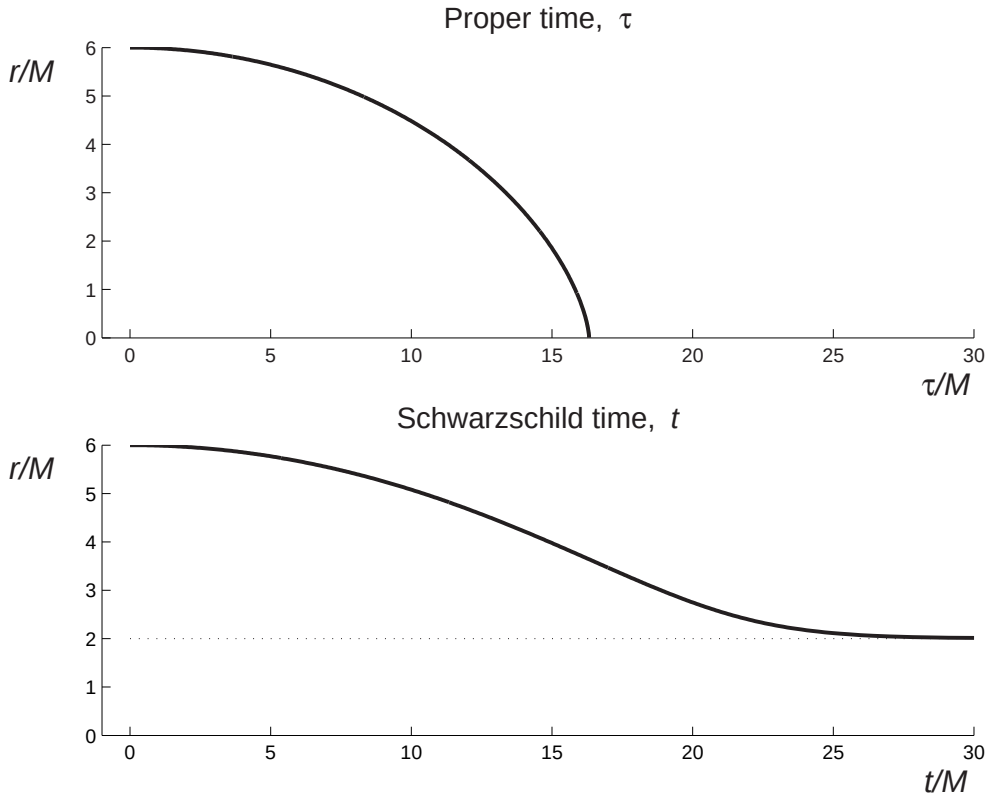

Figure 5.1: Proper time (τ) and coordinate time (t) along a time-like radial geodesic with initial condition $r_{\rm i} = 6M$.

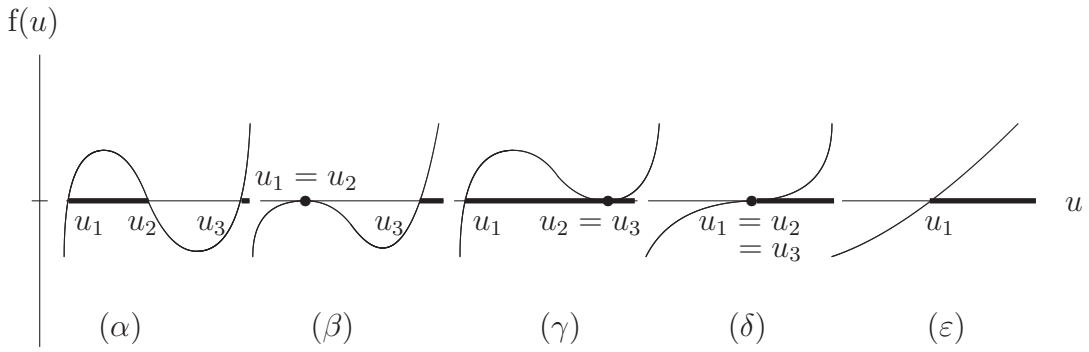

Figure 5.2: The location of the roots of a cubic $\mathrm{f}(u) = 0$ for $E^2 < 1$.

5.2 The bound orbits ($E^2 < 1$)

The consideration of equation (5.2), which governs the geometry of the paths described in the invariant plane, is divided into two sections. These two categories of orbits are characterized by $E^2 < 1$ and $E^2 \geq 1$. This difference will decide whether orbits are bound or unbound. In this section, bound orbits ($E^2 < 1$) shall be considered. These geodesics are governed by the equation (4.21), where

$$\mathrm{f}(u) = 2Mu^3 - u^2 + \frac{2M}{L^2}u - \frac{1-E^2}{L^2}\,. \tag{5.11}$$

As in sections 3.2 and 4.2, the geometry of the orbits will be decided by the location of the roots of the equation $\mathrm{f}(u) = 0$. All the allowed possibilities, [7, Chapter 3, §19(b)], are distinguished in fig. 5.2.

The different cases can also be deduced by interpreting[1]

$$\mathcal{V} = \left(1 - \frac{2M}{r}\right)\left(1 + \frac{L^2}{r^2}\right) \tag{5.12}$$

as 'potential energy' (see equation (5.1)). (In fig. 5.2 there are displayed some examples of potential energy.) The unstable circular orbits correspond to maximum potential while the stable circular orbits correspond to minimum potential.

5.2.1 Orbits of the first kind

The requirement, that

$$\mathrm{f}(u) = 2M\left(u - \frac{1-e}{l}\right)\left(u - \frac{1+e}{l}\right)\left(u - \frac{1}{2M} + \frac{2}{l}\right) \tag{5.13}$$

agrees with its definition (5.11), gives equations (cf. equations (4.33)),

$$\frac{1}{L^2} = \frac{1}{lM}\left[1 - \mu\left(3 + e^2\right)\right] \quad \text{and} \quad \frac{1-E^2}{L^2} = \frac{1}{l^2}(1-4\mu)\left(1-e^2\right)\,. \tag{5.14}$$

[1] There is $\mathcal{V}^2$ in [7, page 102].

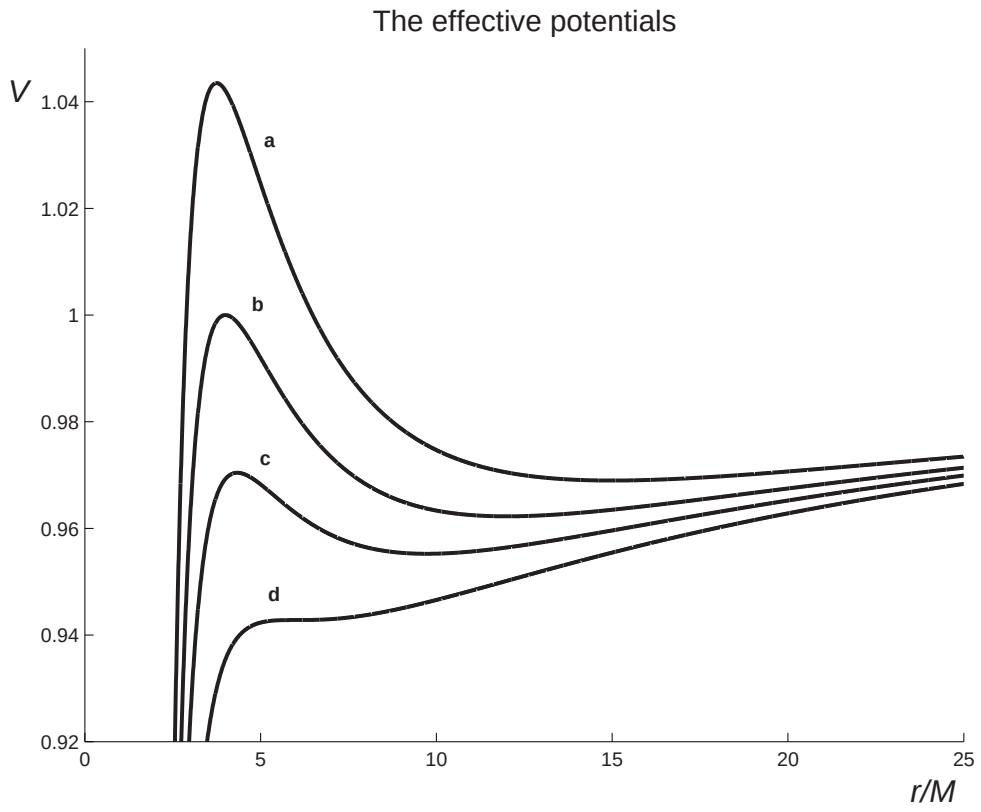

Figure 5.3: The effective potential for time-like trajectory (comp. equation (5.12)). L/M is a) 4.33, b) 4, c) 3.75, d) 3.464. The last stable circular orbit occurs at the point of inflection–case d).

A useful alternative expression for E^2 is

$$\frac{E^2}{L^2} = \frac{1}{lM}\left[(2\mu - 1)^2 - 4\mu^2 e^2\right] . \tag{5.15}$$

According to the substitution (4.38)

$$\begin{aligned} &\text{at aphelion, where} \quad u = \frac{1-e}{l}\,, \qquad \chi = \pi \\ &\text{and} \\ &\text{at perihelion, where} \quad u = \frac{1+e}{l}\,, \qquad \chi = 0\,. \end{aligned} \tag{5.16}$$

Further analysis is the same as in section 4.2.1; and the solution for φ can be expressed in terms of the elliptic integral (4.45). With the restriction (5.16) in the range of χ, we may now write the solution for φ in the form (cf. equation (4.47)).

$$\varphi = \frac{2}{\sqrt{1 - 6\mu + 2\mu e}}\ \mathrm{F}\left(\frac{\pi}{2} - \frac{\chi}{2}, k\right) , \tag{5.17}$$

where φ starts at aphelion passage where $\chi = \pi$.

The case $e = 0$

In this scenario geodesic is a circle with the radius

$$r_{\mathrm{c}} = l\,. \tag{5.18}$$

It is evident from fig. 5.2 that an orbit of zero eccentricity is compatible with one of the two roots

$$r_{\mathrm{c}} = \frac{L^2}{2M}\left(1 \pm \sqrt{1 - \frac{12M^2}{L^2}}\right) . \tag{5.19}$$

The permitted ranges for the radii of the stable and unstable orbits are

$$6M < r_{\mathrm{c}}(\text{stable}) < \infty \qquad \text{and} \qquad 3M \leq r_{\mathrm{c}}(\text{unstable}) \leq 6M\,. \tag{5.20}$$

The case $2\mu(3 + e) = 1$

The perihelion, r_{p}, and the aphelion r_{ap}, distances are given by (4.56) and

$$r_{\mathrm{ap}} = 2M\frac{3+e}{1-e}\,. \tag{5.21}$$

Perihelion distances of these geodesics are confined to the range

$$4M \leq r_{\rm p} < 6M\,. \tag{5.22}$$

For these orbits (cf. equations 4.57)

$$\frac{L^2}{M^2} = \frac{4\,(3+e)^2}{(3-e)(1+e)} \qquad \text{and} \qquad 1 - E^2 = \frac{1-e^2}{9-e^2}\,. \tag{5.23}$$

The discussion in section 4.2.1 applies in this case except that $\varphi = 0$ when $\chi = \pi$. Equation (4.60) shows that $\varphi \to \infty$ when $\chi \to 0$.

5.2.2 Orbits of the second kind

Except for different conditions for e and μ, discussion is the same as in section 4.2.2. An example of bound orbits is illustrated in fig. 5.4.

The case $e = 0$ and $\mu \neq 1/6$

In this situation the solution for u is

$$u = \frac{1}{l} + \left(\frac{1}{2M} - \frac{3}{l}\right) \sec^2\left[\frac{1}{2}(\varphi - \varphi_0)\sqrt{1-6\mu}\right]\,, \tag{5.24}$$

where φ_0 is a constant of integration. See fig. 5.5 for an example of this orbit and an associated stable circular orbit.

The case $e = 0$ and $\mu = 1/6$

In this case, all three roots coincide (case (δ) of fig 5.2) and $u_1 = u_2 = u_3 = \frac{1}{6M}$. As was shown in section 5.2.1, a circular orbit of radius $6M$ is permitted by the equations of motion as a special solution; it is the lower bound for the radii of the stable circular orbit (see equations (5.20) and (5.21)). The general solution is

$$u = \frac{1}{6M} + \frac{2}{M\,(\varphi - \varphi_0)^2}\,. \tag{5.25}$$

For example of this orbit and associated unstable circular orbit see fig. 5.6.

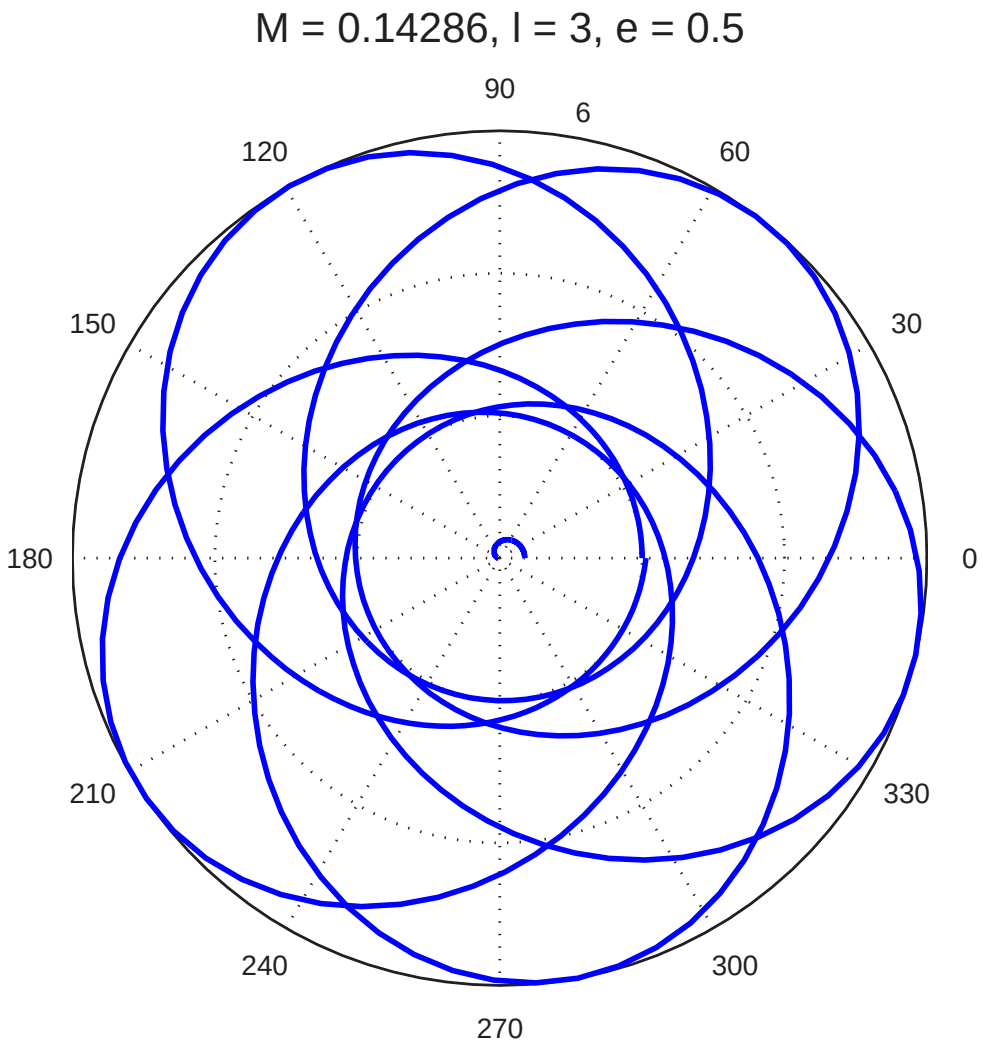

Figure 5.4: Orbits of the first and the second kind. Orbit of the first time precesses around the black hole. Orbit of the second, starting from a certain distance from the black hole (aphelion), falls into the singularity. Eccentricity is $e = 1/2$ and latus rectum $l = 3$. ($M = 1/7$ in the scale along the coordinate axes.)

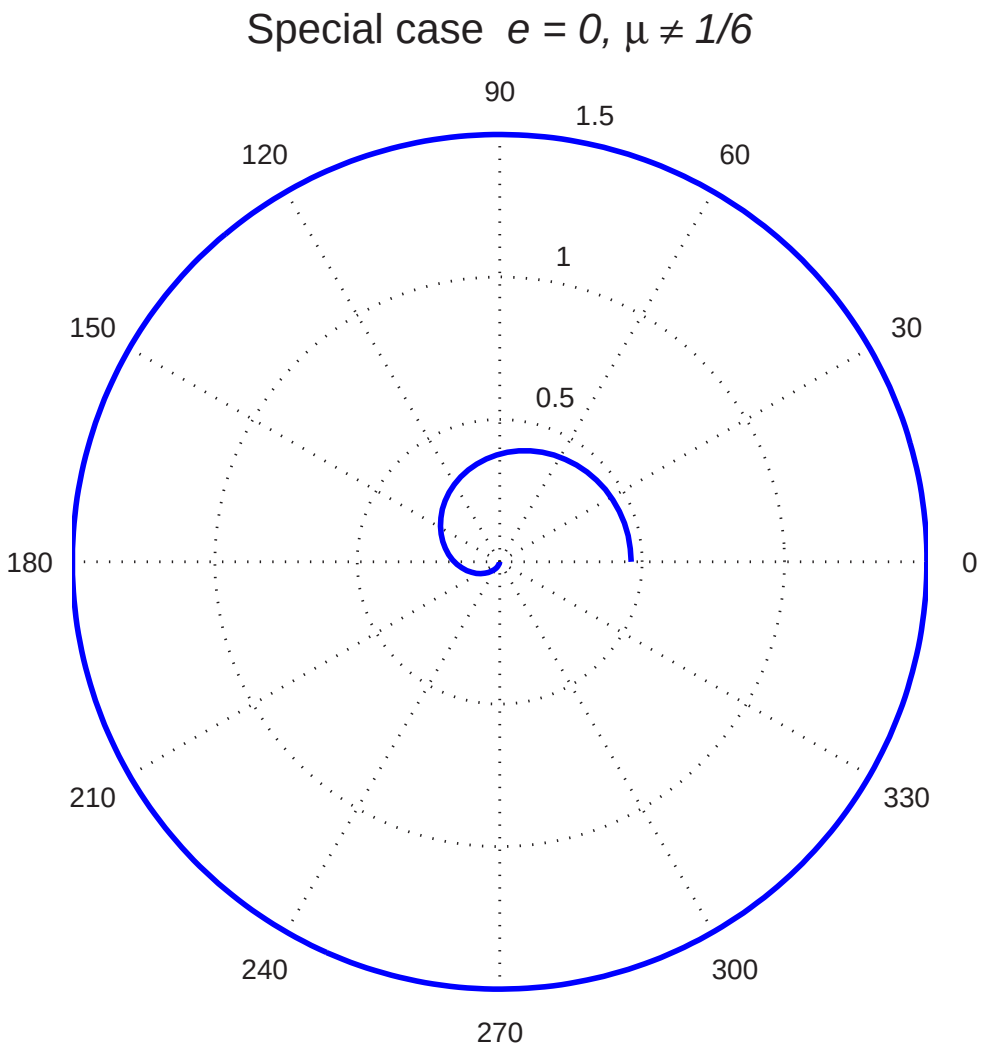

Figure 5.5: A circular orbit $e = 0$, $l = 3/2$ and the associated orbit of the second kind. Orbit of the first kind is a stable circular orbit. Orbit of the second, starting from a certain distance from the black hole (aphelion), falls into the singularity. ($M = 1/7$ in the scale along the coordinate axes.)

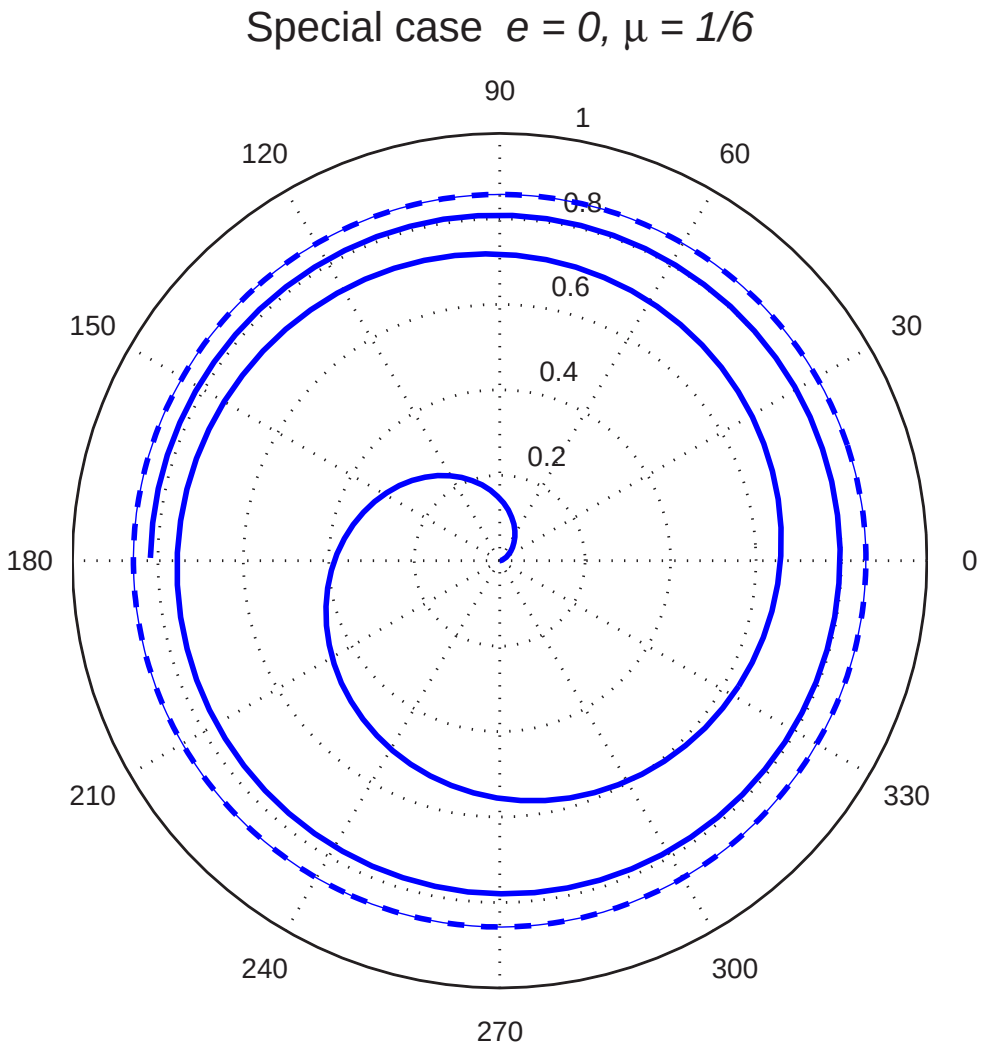

Figure 5.6: The last unstable circular orbit. The orbit of the second kind spirals out of the orbit of the first kind and falls into the singularity.($e = 0,\ \mu = 1/6$). ($M = 1/7$ in the scale along the coordinate axes.)

The case $2\mu(3+e)=1$

Formally the discussion and solution in this case has the same form as in section 4.2.2. For this orbit, $\varphi=0$ when $\xi=\pi$ and $r\to 0$; and $\varphi\to\infty$ when $\xi\to 0$ and r approaches the aphelion at $r=\frac{l}{1+e}$. The circle at $\frac{l}{1+e}$ is the perihelion for the orbits of the first kind, and it is the aphelion for the orbits of the second kind. See fig. 5.7.

5.2.3 The orbits with imaginary eccentricities

In this case f(u) = 0 allows only one real root and pair of complex-conjugate roots (see the case (ε) of fig. 5.2). The corresponding orbits start at some finite aphelion distances, and fall into the singularity. As in sections 3.2.3 and 4.2.3, these orbits will be characterized by imaginary eccentricities and roots of f(u) = 0 will be written as in equation (3.39). Again we can obtain the equations which replace equations (5.14) and (5.15) by writing $-e^2$ wherever $+e^2$ occurs and conversely. Thus (cf. equation(4.75))

$$\frac{1}{L^2}=\frac{1}{lM}\left[1-\mu\left(3-e^2\right)\right]\,,\quad \frac{1-E^2}{L^2}=\frac{1}{l^2}(1-4\mu)\left(1+e^2\right)\,,$$

and (5.26)

$$\frac{E^2}{L^2}=\frac{1}{lM}\left[(2\mu-1)^2-4\mu^2e^2\right]\,.$$

Because bound orbits with $1-E^2>0$ are considered, $\mu<1/4$; and this inequality guarantees

$$1-3\mu+\mu e^2>0\,. \tag{5.27}$$

There is no upper limit for e^2.

Further discussion is the same as in section 4.2.3, except now the range of u is

$$\frac{1}{2M}-\frac{2}{l}\le u<\infty\,, \tag{5.28}$$

and so the corresponding range of ξ is

$$\xi_0\le\xi<\pi\,, \tag{5.29}$$

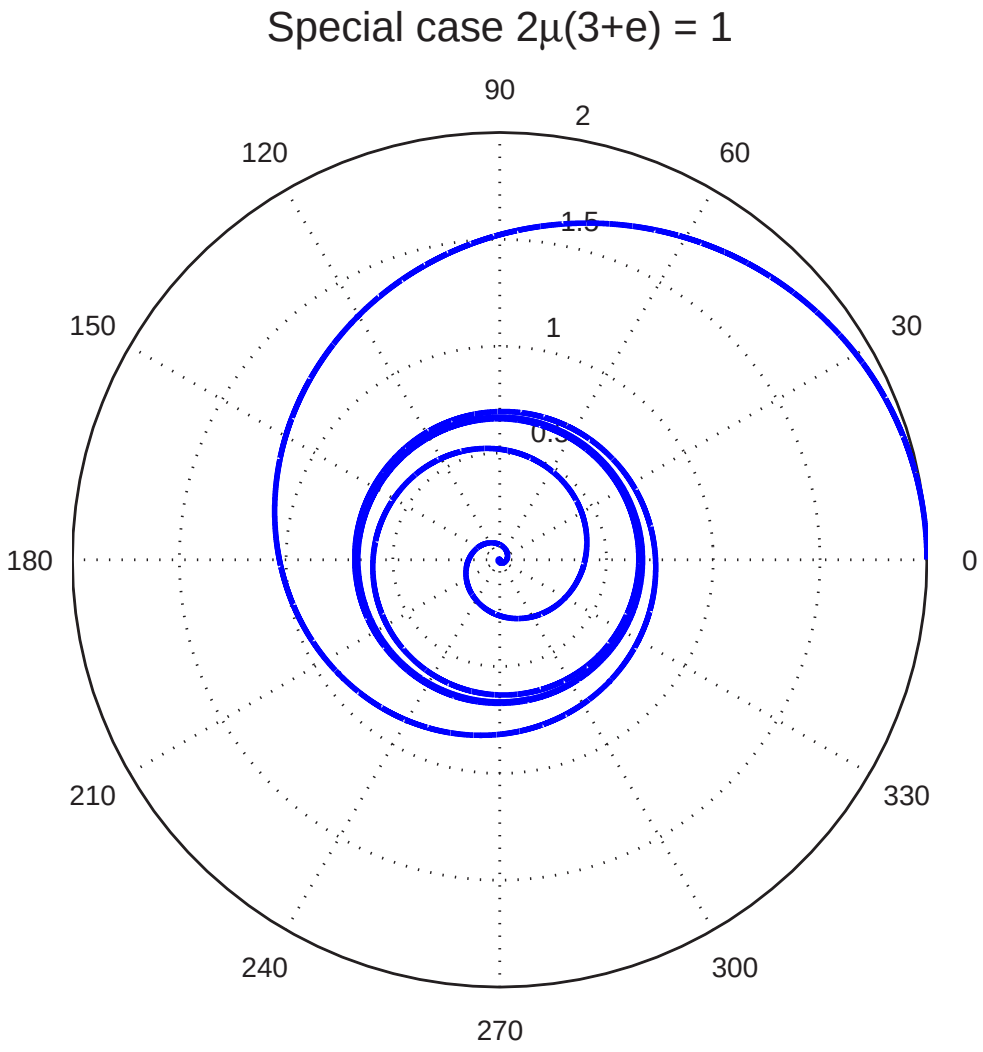

Figure 5.7: An example of a trajectory in which the orbits of the first and the second kind coalesce ($e = 1/2$). Orbit of the second, starting from a certain distance from the black hole, falls into the singularity. ($M = 1/7$ in the scale along the coordinate axes.)

where

$$\sin\frac{\xi_0}{2} = -\frac{6\mu - 1}{\triangle} \qquad \text{and} \qquad \cos\frac{\xi_0}{2} = \frac{2\mu e}{\triangle}\,, \tag{5.30}$$

where $\triangle$ is defined in equation (3.45). From equations (5.30) and (3.47), it follows that

$$\begin{aligned} \sin^2\psi = 1 \quad \text{both} \quad \text{when} \quad \xi = \xi_0 \quad & \text{(at aphelion)} \\ \text{and} \quad \xi = \pi \quad & \text{(at singularity)}\,. \end{aligned} \tag{5.31}$$

And

$$\sin^2\psi = 0 \qquad \text{when} \qquad \xi = \arctan\frac{2\mu e}{6\mu - 1}\,. \tag{5.32}$$

The range of ψ associated with the range of ξ is

$$-\frac{\pi}{2} \le \psi \le +\frac{\pi}{2} \qquad (\xi_0 \le \xi \le \pi)\,. \tag{5.33}$$

Accordingly, the solution for φ may be written as (3.48), where we have assumed $\varphi = 0$ at the singularity where $\xi = \pi$ and $\psi = \pi/2$. φ at aphelion, where $\xi = \xi_0$ and $\psi = -\pi/2$, is

$$\varphi_{\text{ap}} = 2\frac{\mathrm{K}(k)}{\sqrt{\triangle}}\,. \tag{5.34}$$

Example of an orbit with imaginary eccentricity is in fig. 5.8.

5.3 The unbound orbits ($E^2 > 1$)

In this case the constant term in f(u) is positive. Therefore, the equation f(u) = 0 allows a negative root; and the different cases to be distinguished are those shown in fig. 3.1. They look essentially as null and space-like orbits.

5.3.1 Orbits of the first and second kind

Because all three roots are real, they shall be expressed the same way as in section 4.2.1, only now $e \ge 1$. Again the inequality (4.29) continues to hold.

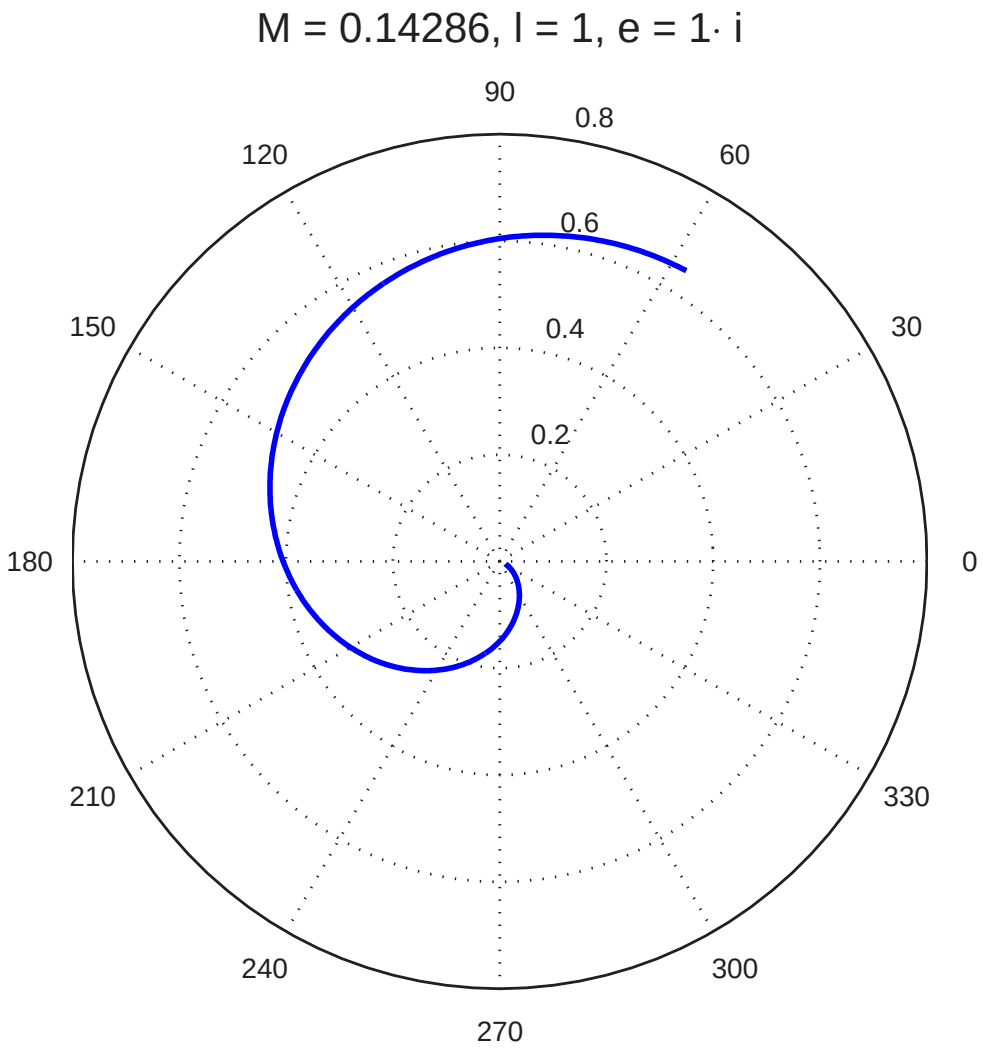

Figure 5.8: Orbit with $l = 1$ and with imaginary eccentricity $e = \mathrm{i}$ ($M = 1/7$) falls into the singularity.

The relations (5.14) also continue to hold, again with the difference that $e \geq 1$. Therefore

$$\frac{1}{L^2} = \frac{1}{lM}\left[1 - \mu\left(3 + e^2\right)\right] \quad \text{and} \quad \frac{E^2 - 1}{L^2} = \frac{1}{l^2}(1 - 4\mu)\left(e^2 - 1\right) . \tag{5.35}$$

Since we assume that$L^2 > 0$ and $E^2 - 1 \geq 0$, in addition to (4.35) we have the requirement, $\mu \leq \frac{1}{4}$, guaranteed by both inequalities (4.29) and (4.35). (4.35) ensures (4.29) for $e < 3$ while (4.29) ensures(4.35) for $e \geq 3$.

Apart from the restriction on the range of e and μ, the analysis in section 4.2.1 is applicable as it stands. An example of unbound orbits is in fig 5.9.

The case $2\mu(3 + e) = 1$

For these special orbits, the allowed range of e is

$$1 \leq e < 3\,; \tag{5.36}$$

and the corresponding perihelion-distances must lie in the range (cf. the range (5.22) for the bound orbits and (4.58) for space-like orbits)

$$3M < r_p \leq 4M\,. \tag{5.37}$$

This case is described by the same equation (4.60) (except, again, for the restriction in the range of χ). As was stated in the context of the null and space-like orbits, these unbound time-like orbits approach the circle at r_p, asymptotically, by spiralling around it an infinite number of times.

The discussion of the space-like orbits in section 4.2.2 applies to these unbound orbits without any change; only now we are concerned with values of $e \geq 1$.

5.3.2 The orbits with imaginary eccentricities

We must now require

$$\mu \geq \frac{1}{4} \tag{5.38}$$

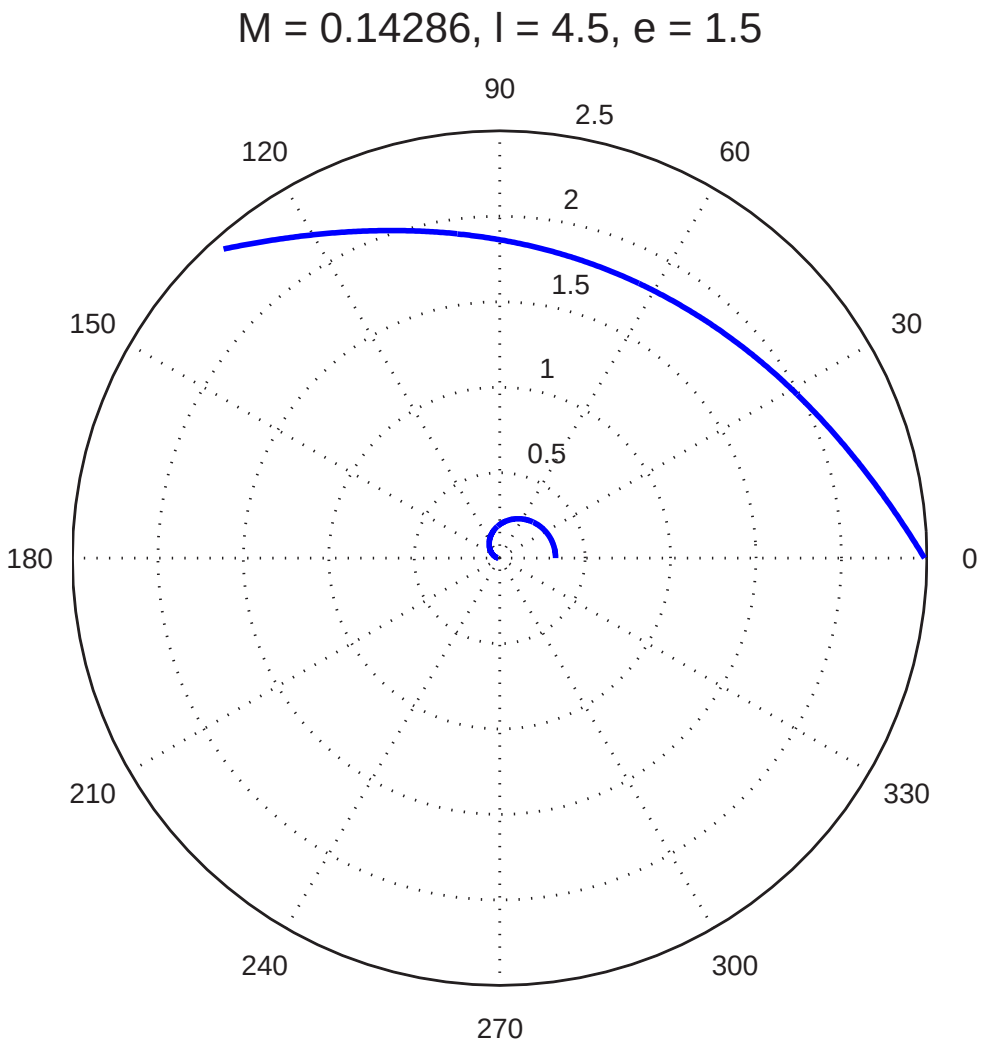

Figure 5.9: Orbits of the first and the second kind. Orbit of the first kind arrives from infinity, and after reaching the perihelion, goes again to infinity. Orbit of the second, starting from a certain distance from the black hole (aphelion), falls into the singularity. Eccentricity is $e = 3/2$, and latus rectum 4.5 ($M = 1/7$).

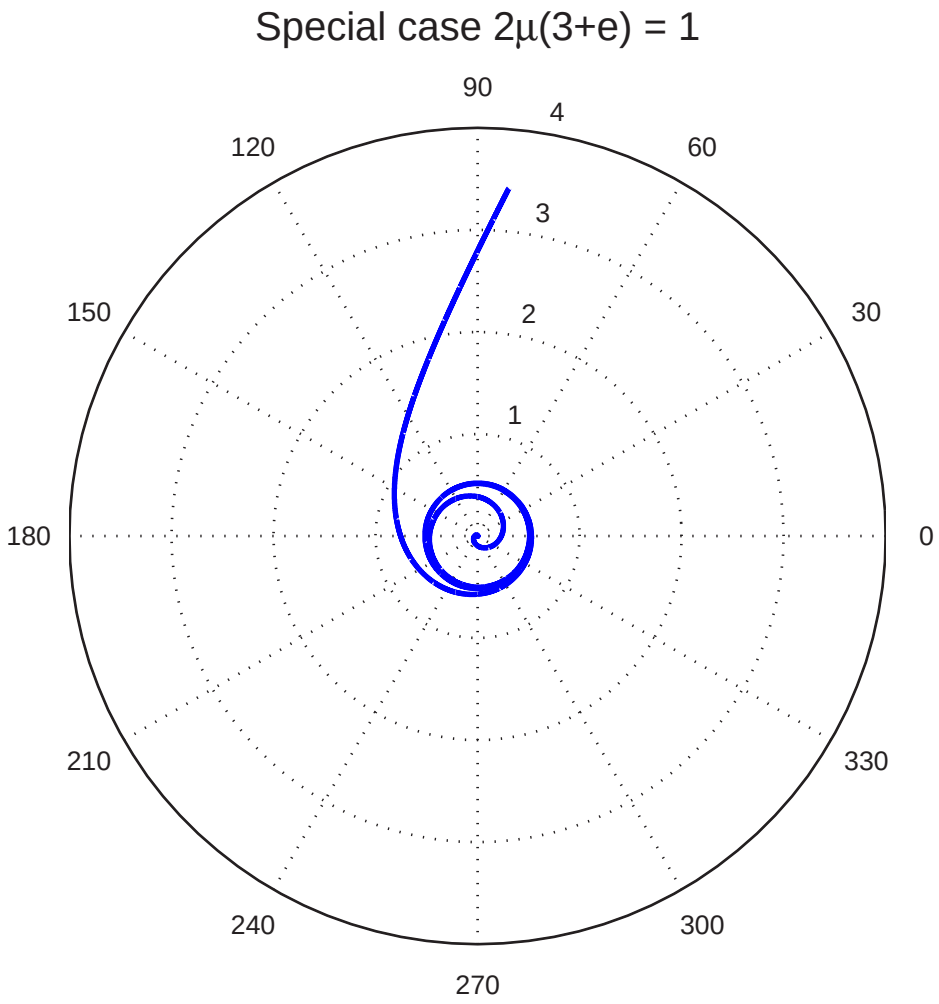

Figure 5.10: An example of a trajectory in which the orbits of the first and the second kind coalesce ($e = 3/2$) for which $2\mu(3 + e) = 1$ ($M = 1/7$). Orbit of the first kind arrives from infinity and reaches perihelion by spinning infinitely around it. Orbit of the second, starting from a certain distance from the black hole (aphelion), falls into the singularity.

and (5.27). For $\mu > \frac{1}{3}$, it is necessary to impose the restriction

$$e^2 > 3 - 1/\mu \qquad \left(\mu > \frac{1}{3}\right) . \tag{5.39}$$

Discussion of section 4.2.3 can be now applied without any change.

Chapter 6

Summary of Part I

When we look at the number of r-turning points we can see that orbits can be divided in three categories: orbits which, coming from infinity, go again to infinity, these are call *flyby orbits* and they can be of either type (null, time-like or space-like), they have one turning point; *bound orbits* which have their radial coordinate bound by two finite values (only time-like geodesics), they have two turning points; and *crash-escape orbits*, which come from infinity into the singularity (null, time-like or space-like geodesics), they have no turning point.

Flyby and bound orbits are familiar in Newtonian gravitation as Keplerian hyperbolas and Keplerian ellipses. With them are associated orbits of the second kind, which have no Newtonian analogues and which, starting from a certain distance (above horizon), plunge into the singularity (these are *not* radial geodesics in Newtonian gravitation). Crash-escape orbits are either orbits characterized by imaginary eccentricities, or, in the case of time-like and null orbits, radial geodesics. Geodesics of above types are said to be *ordinary*.

Exceptional orbits happen when the two kinds of orbits coalesce as they asymptotically approach a common circle from opposite sides by infinitely

spiralling round it.

In Chapter 3 (null geodesics) we gave explicit solutions for proper and Schwarzschild times, in addition to already known solutions for the radial coordinate.

In Chapter 4 (space-like geodesics) the explicit solutions for radial and time coordinates are evaluated. As a consequence of conditions which must be imposed on parameters we showed that there can be no repulsive orbits thus disproving result of [27].

In Chapter 5 (time-like geodesics) a minor error in [7, equation 113, page 102] was corrected.

Part II

Geodesics in the Reissner-Nordström solution

Chapter 7

Introduction to geodesics in the Reissner-Nordström space-time

In this part of the thesis we will give solutions for geodesic orbits in the Reissner-Nordström space-time (black hole characterized by mass M and charge Q_*.) We have extended the discussion in [7, chapter 5], which is concerned only with circular time-like and null orbits, to general orbits (with solutions in terms of the elliptic integrals) , and we have also included space-like geodesics and black holes with $M \leq |Q_*|$. Since these kinds of black holes (with charge larger than mass) are considered non-physical, interpretation of their orbits are unclear. Some orbits were completed manually (cyan lines), because, in some regions, the program they were generated with (Maple) failed to work adequately. In [7] charged particle are mentioned and their lagrangian given. We extend this discussion by finding explicit solutions of their orbits.

We start with the introduction of horizons. Let

$$r_+ = M + \sqrt{M^2 - Q_*^2} \qquad \text{and} \qquad r_- = M - \sqrt{M^2 - Q_*^2}\,, \tag{7.1}$$

be the roots of $\Delta = 0$, where

$$\Delta = r^2 - 2Mr + Q_*^2 \tag{7.2}$$

(cf. equation (B.14)). These roots will be real and distinct if $M^2 > Q_*^2$.

Lets assume that this inequality is satisfied. Since

$$\begin{aligned} \Delta > 0 \quad &\text{for} \qquad r > r_+ \qquad \text{and} \qquad 0 < r < r_- \\ \text{and} \quad \Delta < 0 \quad &\text{for} \qquad r_- < r < r_+ \,, \end{aligned} \tag{7.3}$$

it is clear that we must distinguish three regions:

$$\text{A:} \quad 0 < r < r_- \,; \qquad \text{B:} \quad r_- < r < r_+ \,; \qquad \text{and} \qquad \text{C:} \quad r > r_+ \,. \tag{7.4}$$

While the surface $r = r_+$ is an event horizon in the same sense that $r = 2M$ is an event horizon in the Schwarzschild space-time, the surface $r = r_-$ is called a *'Cauchy' horizon* and it is a 'horizon' in a different sense, see [7]. At the instant of crossing this horizon, the person will witness, in a flash, the entire infinite history of the external space-time, in infinite blueshift. Once under this horizon, the person's future is no longer determined by his or her past.

For $|Q_*| > M$, there is no horizon. The singularity at $r = 0$ is naked. Because of the cosmic censorship hypothesis this case could not occur in gravitational collapse ([42]). According to [28, footnote 9] this does not exclude the possibility of such singularities being created primordially. In [31, chapter 31] it is suggested that for the case of a large ratio of charge to mass, the region near $r = 0$ is unphysical.

Since the Reissner–Nordström metric differs from the Schwarzschild metric only in the definition of the 'horizon function' Δ, it follows that the basic equations governing geodesic motion are, with the redefinition of Δ, the same as those considered in part I.

Another difference between the equations governing geodesics in Schwarzschild space-time and Reissner—Nordström space-time is (as we shall see later) that f(u) will be now a biquadratic instead of a cubic. That makes an essential difference only for the orbits which cross the horizon at $r = r_+$, i.e., for the orbits, which in Schwarzschild geometry are terminated at the singularity at $r = 0$.

Chapter 8

The null geodesics in the Reissner-Nordström space-time

The equations governing the null geodesics are

$$\left(\frac{\mathrm{d}r}{\mathrm{d}\tau}\right)^2 + L^2\frac{\Delta}{r^4} = E^2\,;\ \frac{\mathrm{d}t}{\mathrm{d}\tau} = E\frac{r^2}{\Delta}\,;\quad \text{and}\quad \frac{\mathrm{d}\varphi}{\mathrm{d}\tau} = \frac{L}{r^2}\,. \tag{8.1}$$

By considering r as a function of φ and replacing r by $u = 1/r$ as the independent variable, we obtain the equation (cf. equation (4.5))

$$\left(\frac{\mathrm{d}u}{\mathrm{d}\varphi}\right)^2 = -Q_* u^4 + 2Mu^3 - u^2 + \frac{1}{D^2} = \mathrm{f}(u) \quad \text{(say)}, \tag{8.2}$$

where $D(= L/E)$ is the impact parameter.

8.1 The radial geodesics

The equations governing the radial null-geodesics can be obtained by setting $L = 0$ in equations (8.1). Accordingly,

$$\frac{\mathrm{d}r}{\mathrm{d}t} = \pm\frac{\Delta}{r^2}\,. \tag{8.3}$$

The solution of this equation is

$$t = \pm r_* + \text{constant}\,, \tag{8.4}$$

where

$$r_* = \int \frac{r^2}{\Delta}\,\mathrm{d}r = r + \frac{r_+^2}{r_+ + r_-}\ln|r - r_+| - \frac{r_-^2}{r_+ + r_-}\ln|r - r_-|\,. \tag{8.5}$$

Therefore, for an in-going null-ray, the coordinate time t *increases* from $-\infty$ to $+\infty$ as r decreases from $+\infty$ to r_+, *decreases* from $+\infty$ to $-\infty$ as r further decreases from r_+ to r_-, and *increases* again from $-\infty$ to a finite limit as r decreases from r_- to zero. All the while, the proper time decreases at a constant rate E (cf. equation (3.13)). From a finite distance $r > r_+$, a co-moving observer will arrive at the singularity in a finite proper time.

8.2 Black hole with $M^2 \geq Q_*^2$

The quartic equation (8.2), $\mathrm{f}(u) = 0$, always allows two real roots: one negative (which has no physical significance) and one positive (which occurs for $r < r_-$). We shall be concerned only with cases when the two remaining roots are *either* both real (distinct or coincident) *or* a complex-conjugate pair. Let the value of the impact parameter, D, for which $\mathrm{f}(u) = 0$ has a double root, be denoted by D_c. Then for all values of $D > D_\mathrm{c}$, we shall have orbits of two kinds (as in the Schwarzschild space-time): orbits of the *first kind* which lie entirely outside the event horizon, coming from $+\infty$ and receding again to $+\infty$ after a perihelion passage; and orbits of the *second kind* which have two turning points, one outside the event horizon and one inside the Cauchy horizon. For values of the impact parameter $D < D_\mathrm{c}$ (when $\mathrm{f}(u) = 0$ allows only one real root, $> 1/r_-$, along the positive real u-axis) the orbit coming from $+\infty$ will cross both horizons and have a turning point for a finite value of $r < r_-$. Thus, all these orbits skirt the singularity at $r = 0$.

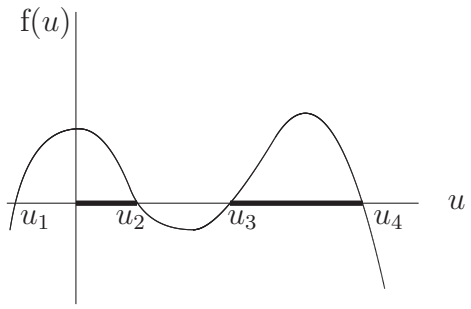

$0 < y \leq u_2$ $\qquad$ $u_3 < y \leq u_4$

Figure 8.1: The case when $\mathrm{f}(u) = 0$ has all real roots.

8.2.1 The orbits of the first kind

We now consider the case when all the roots of the biquadratic equation $\mathrm{f}(u) = 0$ are real and distinct. We rewrite equation (8.2) in the form

$$\left(\frac{\mathrm{d}u}{\mathrm{d}\varphi}\right)^2 = Q_*^2(u_1 - u)(u - u_2)(u - u_3)(u - u_4) = \mathrm{f}(u) \tag{8.6}$$

(see fig. 8.1). The solution is

$$\varphi = \int_0^y \frac{\mathrm{d}u}{\sqrt{\mathrm{f}(u)}} = \int_{u_1}^y \frac{\mathrm{d}u}{\sqrt{\mathrm{f}(u)}} - \int_{u_1}^0 \frac{\mathrm{d}u}{\sqrt{\mathrm{f}(u)}} = \frac{g}{Q_*}\mathrm{F}(\psi, k) + \int_0^{u_1} \frac{\mathrm{d}(u)}{\sqrt{\mathrm{f}(u)}} =$$

$$= \frac{g}{Q_*}[\mathrm{F}(\psi, k) + \mathrm{K}(k)]\,, \tag{8.7}$$

where

$$g = \frac{2}{\sqrt{(u_4 - u_2)(u_3 - u_1)}}\,, \tag{8.8}$$

$$\psi = \arcsin\sqrt{\frac{(u_4 - u_2)(y - u_1)}{(u_2 - u_1)(u_4 - y)}}\,, \tag{8.9}$$

$$k^2 = \frac{(u_4 - u_3)(u_2 - u_1)}{(u_4 - u_2)(u_3 - u_1)}\,. \tag{8.10}$$

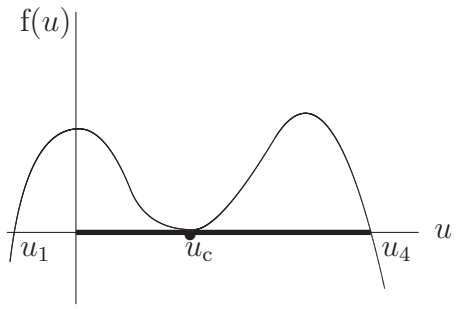

Figure 8.2: The case when $\mathrm{f}(u) = 0$ has a double root.

Geodesics with critical impact parameter

The value of the impact parameter for which $\mathrm{f}(u) = 0$ allows a double root is determined by the equations

$$\mathrm{f}(u) = \frac{1}{D^2} - u^2\left(Q_*^2 u^2 - 2Mu + 1\right) = 0 \tag{8.11}$$

and

$$\mathrm{f}'(u) = -2u\left(1 - 3Mu + 2Q_*^2 u^2\right) = 0\,. \tag{8.12}$$

Besides $u = 0$, equation (8.12) allows the roots

$$u = \frac{3M}{4Q_*^2}\left(1 \pm \sqrt{1 - \frac{8Q_*^2}{9M^2}}\right)\,. \tag{8.13}$$

At the larger of these two roots, $\mathrm{f}(u)$ has a maximum. The double root must occur at the minimum of $\mathrm{f}(u)$ where

$$u = \frac{3M}{4Q_*^2}\left(1 - \sqrt{1 - \frac{8Q_*^2}{9M^2}}\right) = u_c \qquad \text{(say)}. \tag{8.14}$$

The corresponding value of r is

$$r_c = \frac{3}{2}M\left(1 + \sqrt{1 - \frac{8Q_*^2}{9M^2}}\right)\,. \tag{8.15}$$

At this radius r_c the geodesic equation allows an unstable circular orbit.

The value of impact parameter, D_c, associated with the double root r_c follows from equation (8.11). We find

$$D_c = r_c^2/\sqrt{\Delta_c}\,, \qquad \Delta_c = r_c^2 - 2Mr_c + Q_*^2\,. \tag{8.16}$$

When $D = D_{\rm c}$,

$$\mathrm{f}(u) = (u-u_{\rm c})^2\left[-Q_*^2u^2 + 2\left(M - Q_*^2u_{\rm c}\right)u + u_{\rm c}\left(M - Q_*^2u_{\rm c}\right)\right]\,, \tag{8.17}$$

and the solution for φ is given by

$$\varphi = \pm\int \frac{\mathrm{d}u}{(u-u_{\rm c})\sqrt{-Q_*^2u^2 + 2(M-Q_*^2u_{\rm c})u + u_{\rm c}(M-Q_*^2u_{\rm c})}}\,. \tag{8.18}$$

The substitution,

$$\xi = \frac{1}{u-u_{\rm c}}\,, \tag{8.19}$$

reduces φ to the elementary integral,

$$\varphi = \mp\int \frac{\mathrm{d}\xi}{\sqrt{-Q_*^2 + b\xi + c\xi^2}}\,, \tag{8.20}$$

where

$$b = 2\left(M - 2Q_*^2u_{\rm c}\right) \qquad \text{and} \qquad c = u_{\rm c}\left(3M - 4Q_*^2u_{\rm c}\right)\,. \tag{8.21}$$

We thus obtain the solution

$$\varphi = \mp\frac{\ln\left[2c\xi + b + 2c\sqrt{c(-Q_*^2 + b\xi + c\xi^2)}\right]}{\sqrt{c}}\,, \tag{8.22}$$

for values of the argument in the following ranges:

$$-\infty < \xi < -\frac{1}{u_{\rm c}}\,, \qquad 0 \le u \le u_{\rm c}\,, \qquad \text{and} \qquad r_{\rm c} < r < \infty\,. \tag{8.23}$$

8.2.2 The geodesics of the second kind

To obtain the null geodesics, whose ranges are $u_3 < u \le u_4$, we rewrite equation (8.2) in the form

$$\left(\frac{\mathrm{d}u}{\mathrm{d}\varphi}\right)^2 = Q_*^2(u-u_1)(u-u_2)(u-u_3)(u_4-u) \tag{8.24}$$

(see fig. 8.1). The solution is

$$\varphi = \int_{u_3}^{y}\frac{\mathrm{d}u}{\sqrt{\mathrm{f}(u)}} = \frac{g}{Q_*}\mathrm{F}(\psi,k)\,, \tag{8.25}$$

where this time, unlike in the case of geodesics of the first kind,

$$\psi = \arcsin \sqrt{\frac{(u_4 - u_2)(y - u_3)}{(u_4 - u_3)(y - u_2)}}\,. \tag{8.26}$$

An example of orbits of the first and second kind can be seen in picture 8.3.

Geodesics with critical impact parameter

The orbits of the second kind are described by the same solution (8.22) for values of the argument in the ranges

$$\xi_{\min}\left(=\frac{1}{u_{\min}-u_{\rm c}}\right) < \xi < +\infty\,,\ u_{\rm c} < u \le u_{\max}\left(=\frac{1}{r_{\min}}\right) \text{ and } r_{\min} < r < r_{\rm c}\,, \tag{8.27}$$

where $r_{\min}$ is the positive root of the equation (cf. equation(8.17)),

$$u_{\rm c}\left(M - Q_*^2 u_{\rm c}\right) r^2 + 2\left(M - Q_*^2 u_{\rm c}\right) r - Q_*^2 = 0\,. \tag{8.28}$$

Both orbits of the first and second kind approach the unstable circular orbit at $r = r_{\rm c}$, asymptotically from opposite sides, by spiralling around it an infinite number of times.

8.2.3 The orbits with imaginary eccentricities

Finally, we consider the orbits when the equation f(u) = 0 has a pair of complex-conjugate roots, besides two real roots. That is true when the impact parameter, D, has values less than critical, $D_{\rm c}$, with

$$D_{\rm c} = \frac{r_{\rm c}^2}{\sqrt{\Delta_{\rm c}}}\,, \tag{8.29}$$

where the critical radius has value (8.15) and

$$\Delta_{\rm c} = r_{\rm c}^2 - 2Mr_{\rm c} + Q_*^2 = Mr_{\rm c} - Q_*^2\,. \tag{8.30}$$

We rewrite equation (8.2) in the form

$$\left(\frac{{\rm d}u}{{\rm d}\varphi}\right)^2 = Q_*^2(u - u_1)(u - u_2)(u - \bar{u}_2)(u_4 - u) \tag{8.31}$$

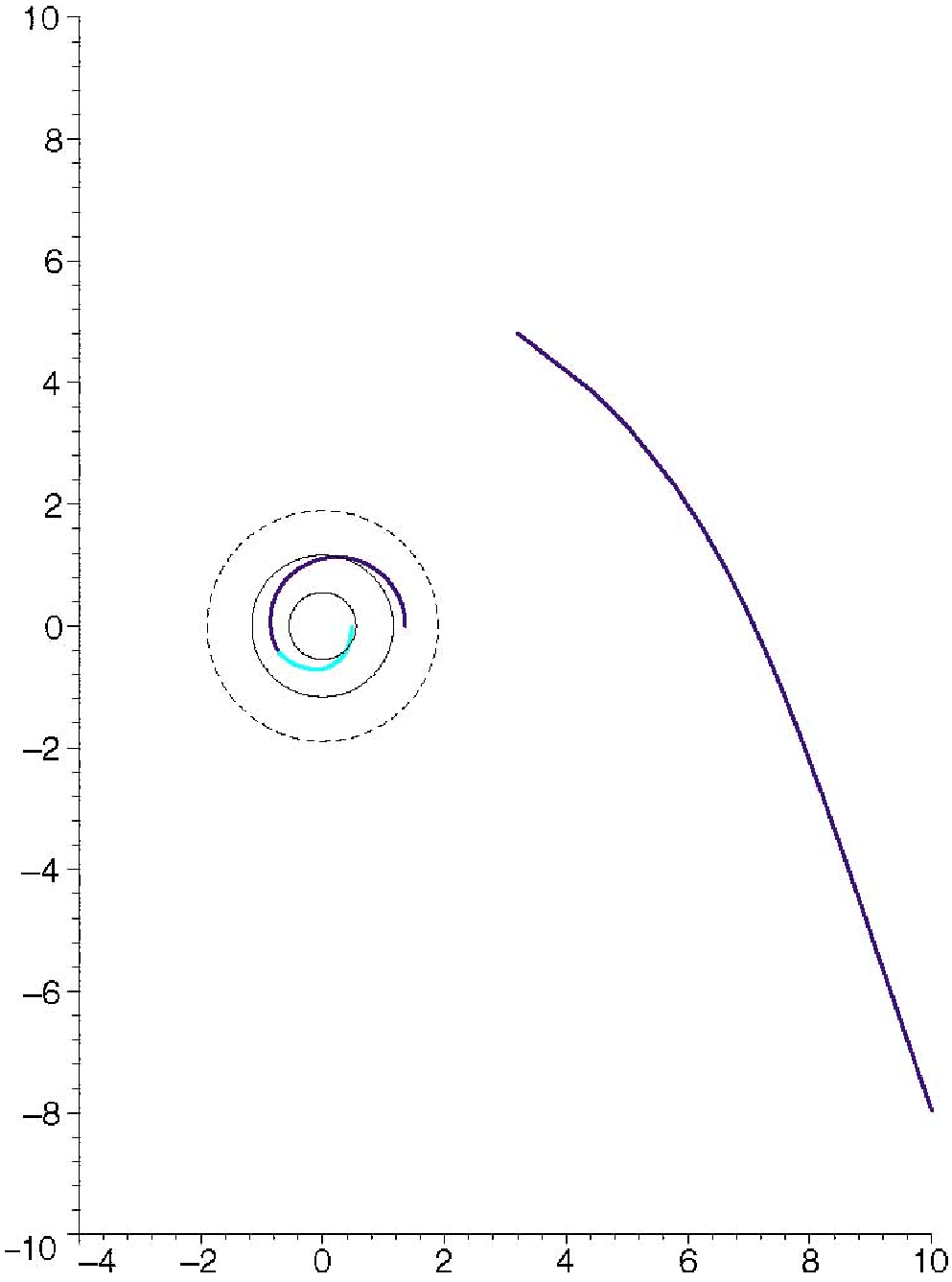

Figure 8.3: General null geodesics of the first and the second kind with $Q_* = 0.8$, $M = 6/7$ and $D = 4.658489054$. The inner and outer horizons are shown by the thin circles; the dotted circle represents the unstable circular-orbit. The orbit of the first kind starts from infinity, orbit of the second kind starts above the vent horizon and ends below the Cauchy horizon.

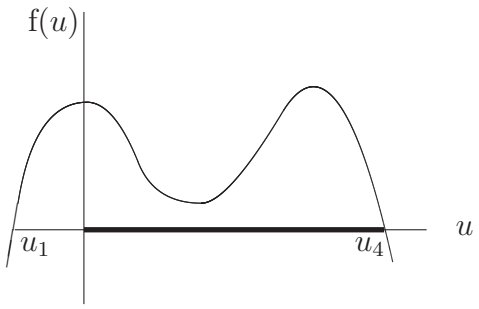

$$0 < y < u_4$$

Figure 8.4: The case when $\mathrm{f}(u) = 0$ has two complex-conjugate roots.

(see fig. 8.4). The solution is

$$\varphi = \int_0^y \frac{\mathrm{d}u}{\sqrt{\mathrm{f}(u)}} = \int_{u_1}^y \frac{\mathrm{d}u}{\sqrt{\mathrm{f}(u)}} - \int_{u_1}^0 \frac{\mathrm{d}u}{\sqrt{\mathrm{f}(u)}} = \frac{g}{Q_*}\mathrm{F}(\psi, k) + \int_0^{u_1} \frac{\mathrm{d}u}{\sqrt{\mathrm{f}(u)}} =$$

$$= \frac{g}{Q_*}[\mathrm{F}(\psi, k) + \mathrm{K}(k)]\,, \quad (8.32)$$

where

$$g = \frac{1}{\sqrt{AB}}\,, \quad (8.33)$$

$$\psi = \arccos \frac{(u_4 - y)B - (y - u_1)A}{(u_4 - y)B + (y - u_1)A}\,, \quad (8.34)$$

$$A^2 = (u_4 - b_1)^2 + a_1^2\,, \quad (8.35)$$

$$B^2 = (u_1 - b_1)^2 + a_1^2\,, \quad (8.36)$$

$$b_1 = \frac{(u_2 + \bar{u}_2)}{2}\,, \quad (8.37)$$

$$a_1^2 = -\frac{(u_2 - \bar{u}_2)^2}{4}\,, \quad (8.38)$$

$$k^2 = \frac{(u_4 - u_1)^2 - (A - B)^2}{4AB}\,. \quad (8.39)$$

An example of an orbit with imaginary eccentricity is in figure 8.5.

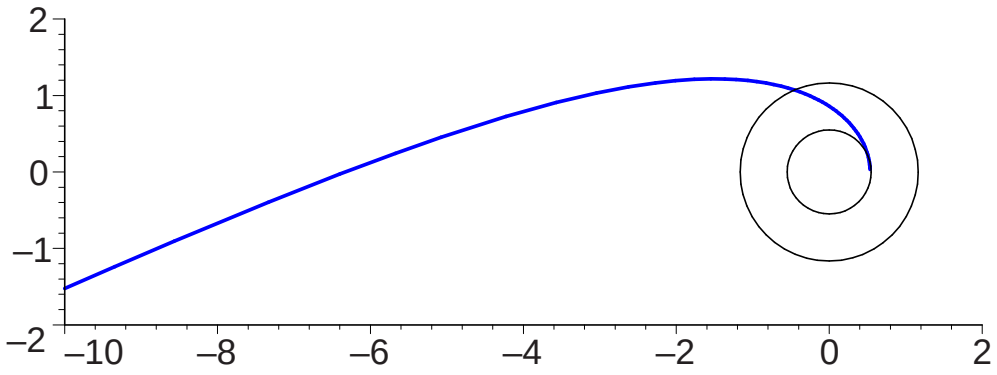

Figure 8.5: Null geodesic with imaginary eccentricity with $M = 6/7$, $Q_* = 0.8$ and $D = 3$ starts in infinity and ends below the Cauchy horizon. The inner and outer horizons are shown by the thin circles.

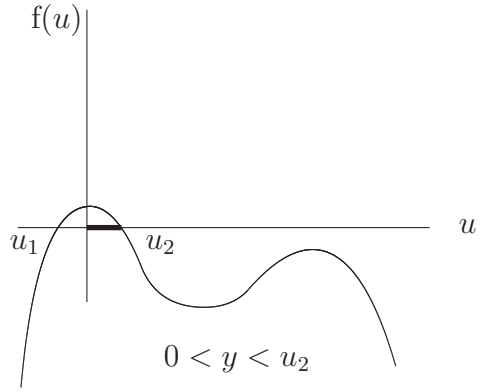

Figure 8.6: The case when $\mathrm{f}(u) = 0$ has two complex-conjugate roots.

8.3 Black hole with $M^2 < Q_*^2$

Once we allow $Q_* > M$, $r_\pm$ disappear. We must now distinguish more cases than in section 8.2 based on the relations between the coefficients M and Q_*.

8.3.1 Case $M^2 < Q_*^2 < \frac{9}{8}M^2$

For $M^2 < Q_*^2 < \frac{9}{8}M^2$ there are two circular photon orbits, one stable and one unstable, with impact parameter D_{cs} and D_{cu} respectively. For $D < D_{\mathrm{cs}}$ discussion is formally as in section 8.2.

Case $D > D_{\mathrm{cs}}$ is pictured in fig. 8.6. We can see in figure 8.7 that orbits are coming from infinity and have a turning point at $1/u_2$. The solution is

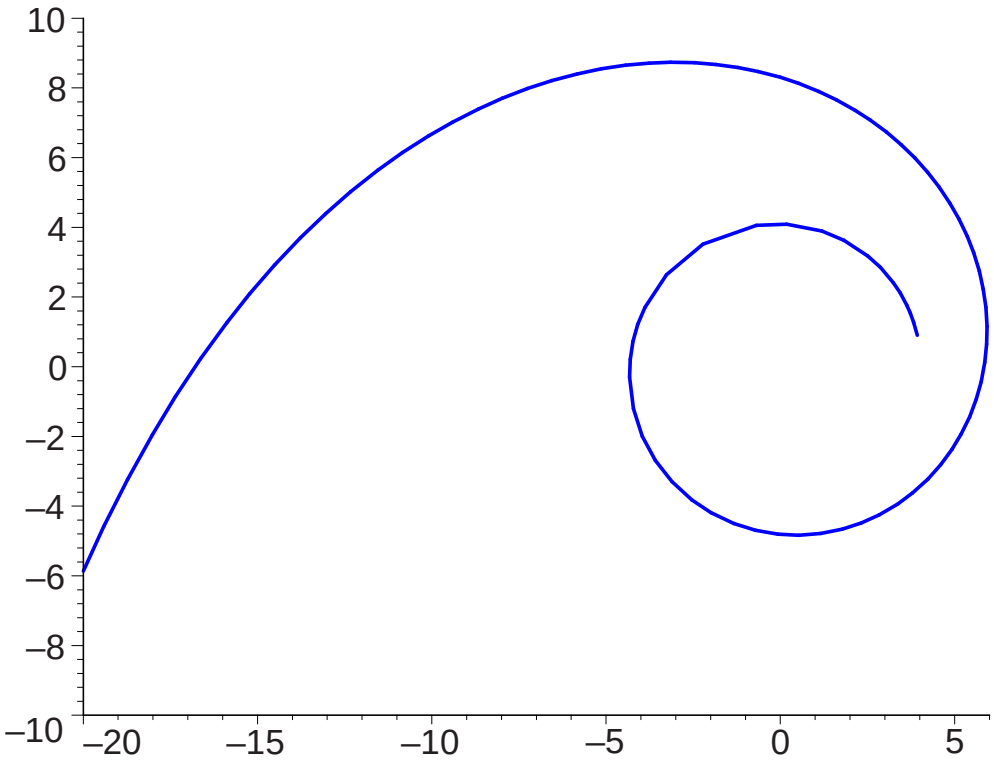

Figure 8.7: Null geodesic with imaginary eccentricity with $M = 11/14$, $Q_* = 0.8$ and $D = 5$.

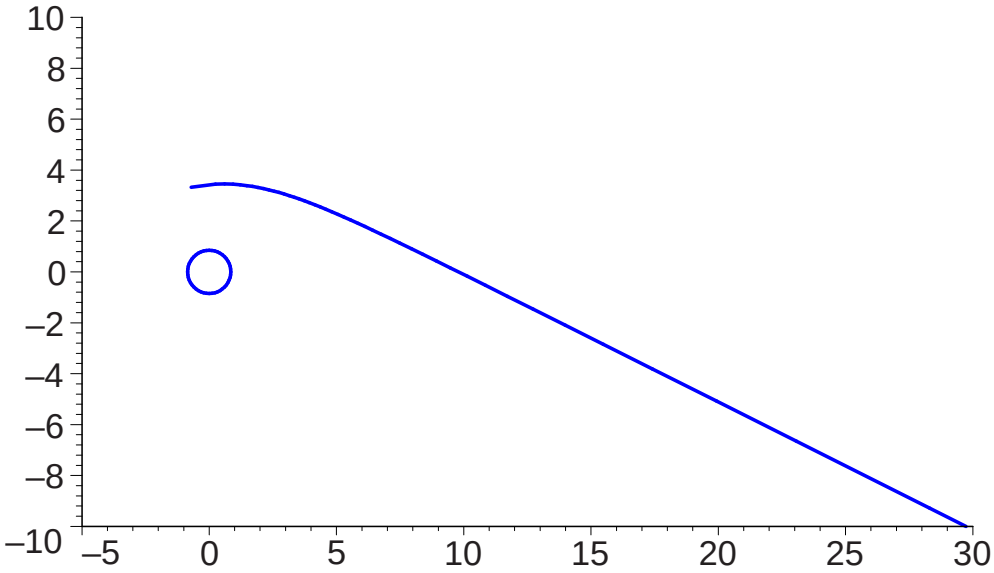

Figure 8.8: Stable circular orbit with associated orbit of the first kind. Orbit of the first kind starts from infinity. $M = 11/14$ and $Q_* = 0.8$.

formally the same as in section 8.2.3.

Special case $D = D_{\rm cs}$ (see picture 8.9) allows a stable circular photon orbit with radius

$$r_{\rm cs} = \frac{3}{2} M \left(1 - \sqrt{1 - \frac{8Q_*^2}{9M^2}} \right) . \tag{8.40}$$

For orbits of the first kind the discussion is formally as in section 8.2 with the solution in the form

$$\varphi = \pm \frac{\arcsin \dfrac{2c\xi + b}{\sqrt{4Q_*^2 c + b^2}}}{\sqrt{-c}} , \tag{8.41}$$

for values of the argument in the ranges

$$\frac{1}{u_2 - u_{\rm c}} < \xi < -\frac{1}{u_{\rm c}} , \qquad 0 \le u \le u_2 , \qquad \text{and} \qquad r_2 < r < \infty . \tag{8.42}$$

For b and c see equation (8.21). An example of such orbits is in figure 8.8.

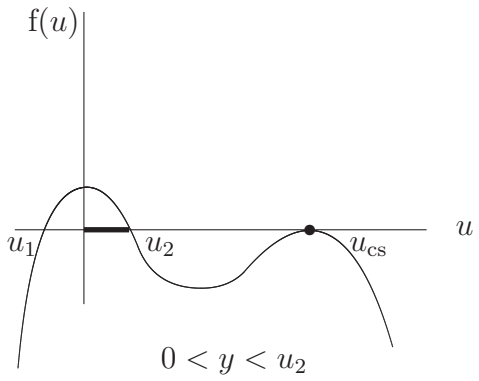

Figure 8.9: The case when $\mathrm{f}(u) = 0$ has a double root.

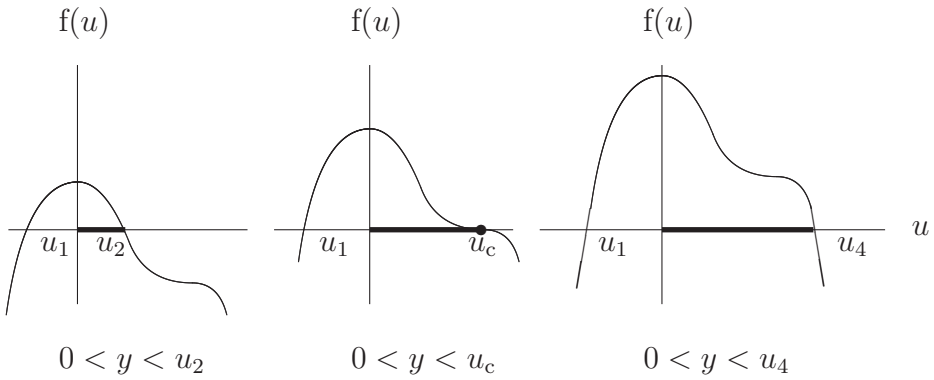

Figure 8.10: The case when $Q_*^2 = \frac{9}{8}M^2$ for $D > D_c$, $D = D_c$ and $D < D_c$ respectively.

8.3.2 Case $Q_*^2 = \frac{9}{8}M^2$

When $Q_*^2 = \frac{9}{8}M^2$, $\mathrm{f}(u) = 0$ allows only one real positive root. In case of $D = D_c$ there is a (unstable) circular orbit at $r_c = \frac{3}{2}M$ and the solution is

$$\varphi = \pm 2\sqrt{b\xi - Q_*^2}/b\,, \tag{8.43}$$

where b is defined in equation (8.21).

You can see the different possible cases in fig. 8.10. Solutions for general cases are formally as in section 8.2.3, but with different ranges of arguments. For examples see figures 8.11, 8.12 and 8.13.

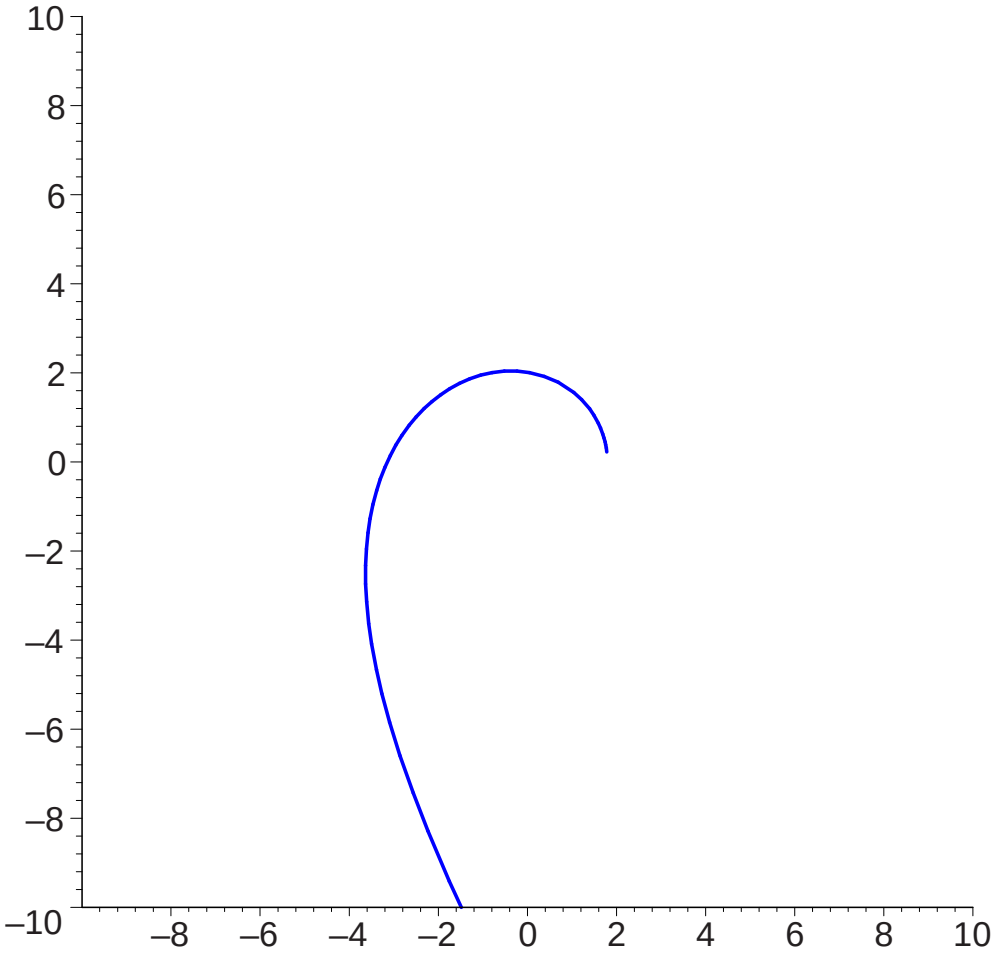

Figure 8.11: Null geodesic with $Q_*^2 = \frac{9}{8}M^2$ and $D > D_c$. It starts from infinity. ($Q_* = 0.8$ and $D = 3$.)

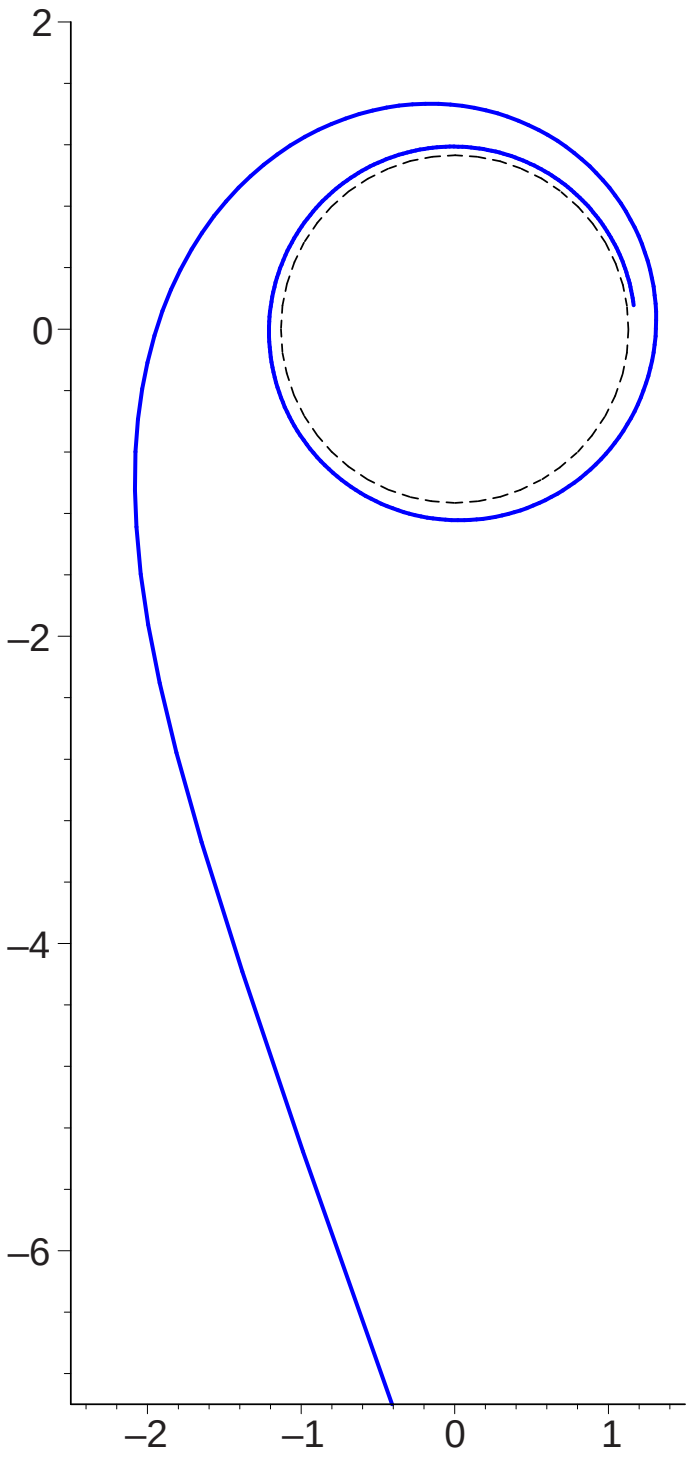

Figure 8.12: Null geodesics with $Q_*^2 = \frac{9}{8}M^2$ and $D = D_c$ associated with unstable circular orbit. It starts from infinity. ($Q_* = 0.8$.)

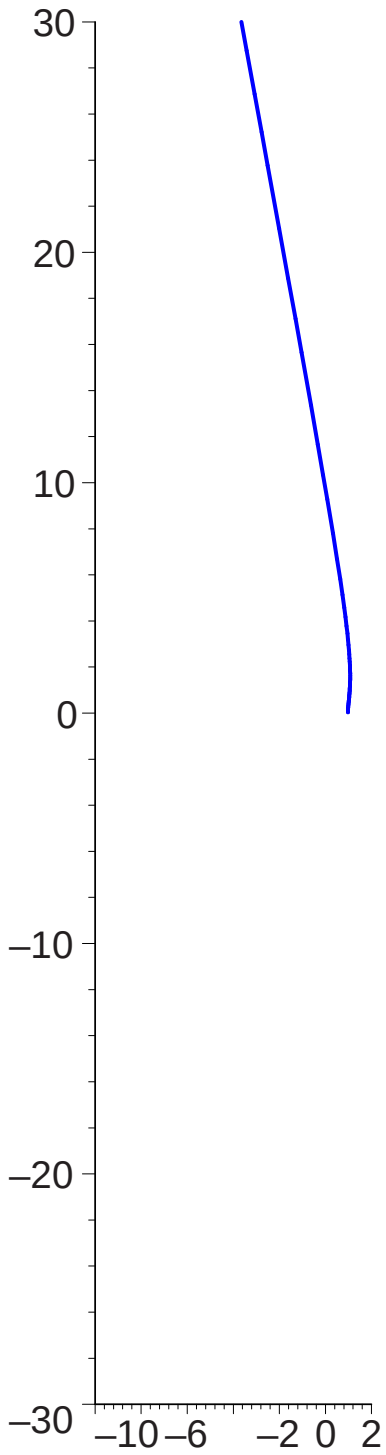

Figure 8.13: Null geodesic with $Q_*^2 = \frac{9}{8}M^2$ and $D < D_c$. It starts from infinity. ($Q_* = 0.8$ and $D = 2$.)

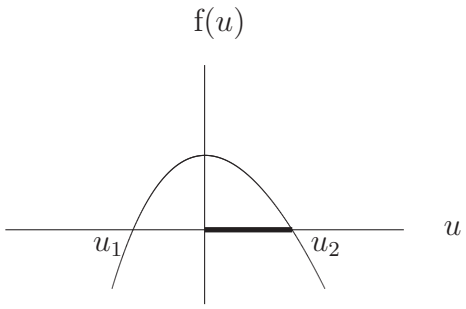

Figure 8.14: The case when $Q_*^2 > \frac{9}{8}M^2$.

8.3.3 Case $Q_*^2 > \frac{9}{8}M^2$

In this case there is no circular orbit and f(u) has only one positive root (see fig. 8.14). Again the solution is formally as in section 8.2.3 with a different range of argument. For example of this orbit see figure 8.15.

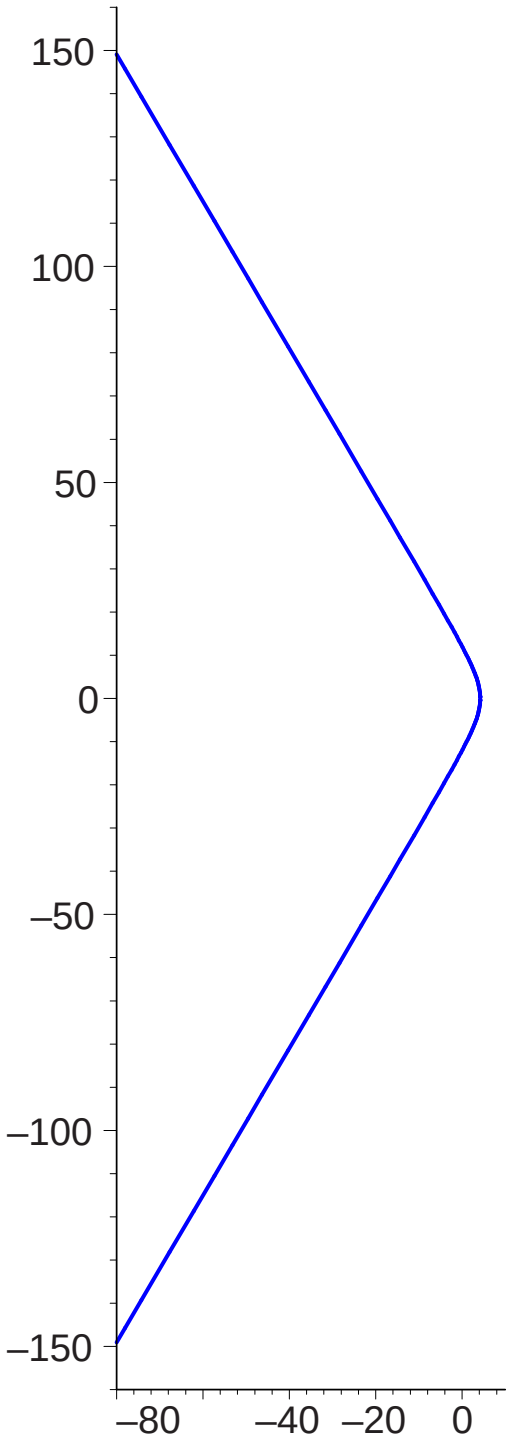

Figure 8.15: Null geodesic with $Q_*^2 > \frac{9}{8}M^2$. It starts from infinity and after reaching perihelion goes to infinity again. ($Q_* = 0.8$ and $M = 0.7$.)

Chapter 9

The space-like geodesics in the Reissner-Nordström space-time

The equations governing space-like geodesics are

$$\left(\frac{\mathrm{d}r}{\mathrm{d}\tau}\right)^2 + \frac{\Delta}{r^2}\left(\frac{L^2}{r^2} - 1\right) = E^2\,; \quad \frac{\mathrm{d}t}{\mathrm{d}\tau} = E\frac{r^2}{\Delta}\,; \quad \text{and} \quad \frac{\mathrm{d}\varphi}{\mathrm{d}\tau} = \frac{L}{r^2}\,. \tag{9.1}$$

As in part I, we interpret

$$\mathcal{V} = \frac{\Delta}{r^2}\left(\frac{L^2}{r^2} - 1\right) \tag{9.2}$$

as 'potential energy'. In the third graph of fig. 9.1, the unstable orbits correspond to maximum potential and the stable orbits correspond to minimum potential. Points of inflexion in the second graph indicate unstable orbits.

By considering r in equation (9.1) as a function of φ and replacing r by $u = 1/r$ as the independent variable we obtain the equation (cf. equation (4.5))

$$\left(\frac{\mathrm{d}u}{\mathrm{d}\varphi}\right)^2 = -Q_*^2u^4 + 2Mu^3 - \left(1 - \frac{Q_*^2}{L^2}\right)u^2 - \frac{2M}{L^2}u + \frac{E^2+1}{L^2}\,. \tag{9.3}$$

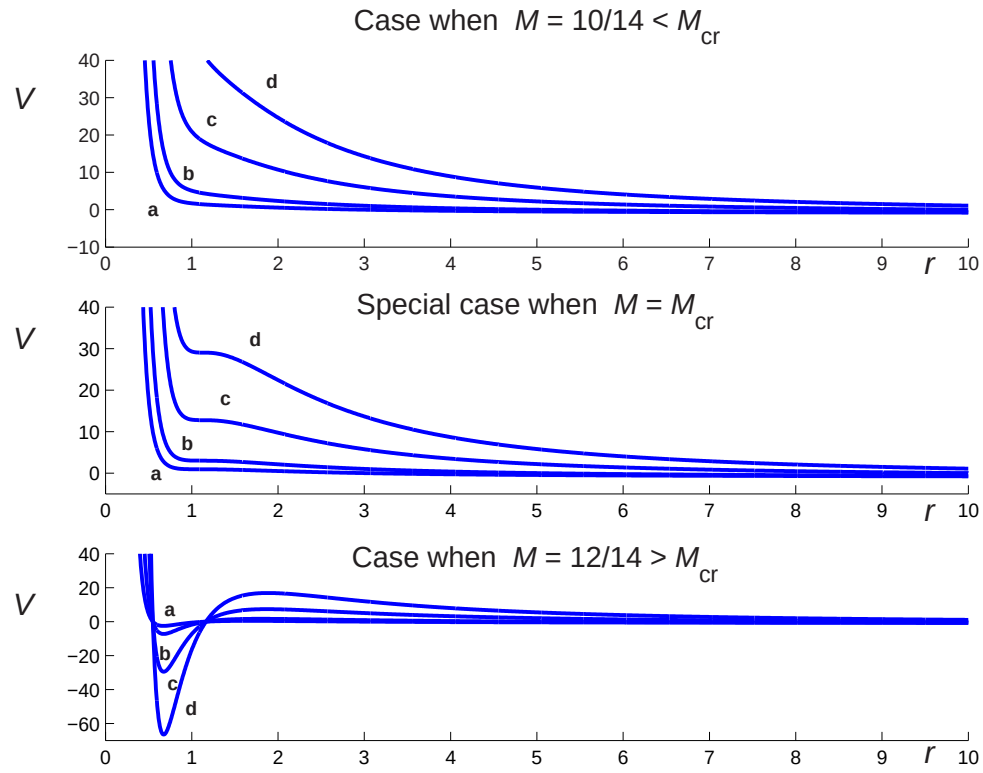

Figure 9.1: The effective potential appropriate for space-like trajectory (comp. equation 9.2). $Q = 0.8$ and L is a) 3, b) 5, c) 10 and d) 15.

9.1 The radial geodesics

The equations governing the radial space-like geodesics can be obtained by setting $L = 0$ in equations (9.1); thus,

$$\left(\frac{\mathrm{d}r}{\mathrm{d}\tau}\right)^2 = E^2 + \frac{\Delta}{r^2}\,, \quad \frac{\mathrm{d}t}{\mathrm{d}\tau} = E\frac{r^2}{\Delta}\,, \quad \text{and} \quad \frac{\mathrm{d}\theta}{\mathrm{d}\tau} = \frac{\mathrm{d}\varphi}{\mathrm{d}\tau} = 0\,. \tag{9.4}$$

Accordingly,

$$\frac{\mathrm{d}r}{\mathrm{d}t} = \pm\left(\frac{\Delta}{Er^2}\right)\sqrt{E^2 + \frac{\Delta}{r^2}}\,. \tag{9.5}$$

The solution for the arc lenght, τ, is

$$\tau = \frac{r_\mathrm{i}\sqrt{E^2 + \frac{\Delta_\mathrm{i}}{r_\mathrm{i}^2}} - r\sqrt{E^2 + \frac{\Delta}{r^2}}}{E^2+1} + \frac{M}{\left(E^2+1\right)^{3/2}}\cdot$$
$$\cdot\left(\operatorname{arctanh}\frac{E^2 + 1 - \frac{M}{r_\mathrm{i}}}{\sqrt{E^2+1}\sqrt{E^2 + \frac{\Delta_\mathrm{i}}{r_\mathrm{i}^2}}} - \operatorname{arctanh}\frac{E^2 + 1 - \frac{M}{r}}{\sqrt{E^2+1}\sqrt{E^2 + \frac{\Delta}{r^2}}}\right) \tag{9.6}$$

and for coordinate t,

$$t = \frac{M(4M+1)}{\left(E^2+1\right)^{3/2}}\cdot$$
$$\cdot\left(\operatorname{arctanh}\frac{E^2 + 1 - \frac{M}{r_\mathrm{i}}}{\sqrt{E^2+1}\sqrt{E^2 + \frac{\Delta_\mathrm{i}}{r_\mathrm{i}^2}}} - \operatorname{arctanh}\frac{E^2 + 1 - \frac{M}{r}}{\sqrt{E^2+1}\sqrt{E^2 + \frac{\Delta}{r}}}\right) +$$
$$+\left(Q_*^2 - \frac{4M^2}{E^2+1}\right)\ln\frac{r\sqrt{E^2 + \frac{\Delta}{r^2}}}{r_\mathrm{i}\sqrt{E^2 + \frac{\Delta_i}{r_\mathrm{i}^2}}} +$$
$$+ 2M\sqrt{E^2+1}\ln\frac{r(E^2+1) - M + r\sqrt{E^2+1}\sqrt{E^2 + \frac{\Delta}{r^2}}}{r_\mathrm{i}(E^2+1) - M + r_\mathrm{i}\sqrt{E^2+1}\sqrt{E^2 + \frac{\Delta_\mathrm{i}}{r_\mathrm{i}^2}}} +$$
$$+\frac{Q_*^2}{2}\left(\frac{\sqrt{E^2 + \frac{\Delta_\mathrm{i}}{r_\mathrm{i}^2}}}{r_\mathrm{i}} - \frac{\sqrt{E^2 + \frac{\Delta}{r^2}}}{r}\right) - 2M\left(\sqrt{E^2 + \frac{\Delta_\mathrm{i}}{r_\mathrm{i}^2}} - \sqrt{E^2 + \frac{\Delta}{r^2}}\right) +$$
$$+\frac{r_\mathrm{i}\sqrt{E^2 + \frac{\Delta_\mathrm{i}}{r_\mathrm{i}^2}} - r\sqrt{E^2 + \frac{\Delta}{r^2}}}{E^2+1}\,, \tag{9.7}$$

where the initial condition for r is given by

$$E^2 + 1 = \frac{Q_*^2 + 2Mr_\mathrm{i}}{r_\mathrm{i}^2} \tag{9.8}$$

for $r(0) = r_\mathrm{i}$ and $\dot{r}(0) = 0$.

9.2 Unbound orbits

These orbits are governed by equation (4.21), where

$$\mathrm{f}(u) = -Q_*^2 u^4 + 2Mu^3 - \left(1 - \frac{Q_*^2}{L^2}\right) u^2 - \frac{2M}{L^2} u + \frac{E^2+1}{L^2}\,. \tag{9.9}$$

Letting u_1, u_2, u_3, and u_4 denote the roots of the quartic equation $\mathrm{f}(u) = 0$, we have again several possibilities of their location (cf. figures 8.1, 8.2, 8.4, 8.6, 8.10 and 8.14 in Chapter 8).

First we find the condition for parameters M, L and Q_* for the limiting case in fig. 8.10, which happens when

$$\mathrm{f}'(u) = -4Q_*^2 u^3 + 6Mu^2 - 2\left(1 - \frac{Q_*^2}{L^2}\right) u - \frac{2M}{L^2} = 0 \tag{9.10}$$

and

$$\mathrm{f}''(u) = -12Q_*^2 u^2 + 12Mu - 2\left(1 - \frac{Q_*^2}{L^2}\right) = 0\,. \tag{9.11}$$

Since we require M to be positive we have

$$M = \frac{\sqrt{6\left[16Q_*^2L^2 - (L^2+Q_*^2)^2\right] \pm 2\sqrt{3(3L^2 - Q_*^2)\,(5Q_*^2 + L^2)^3}}}{12L} \tag{9.12}$$

or

$$\begin{aligned} L^2 = \Bigg| \Bigg\{ & 3M^{2/3} \Bigg[2Q_*^4 \left(8Q_*^2 - 9M^2\right) \sqrt{(Q_*^2 - M^2)\,(4Q_*^2 - 5M^2)^3} + \\ & + 8154Q_*^4M^6 - 5177Q_*^6M^4 + 1472Q_*^8M^2 - 128Q_*^{10} + \\ & + 1728M^{10} - 6040Q_*^2M^8 \Bigg]^{1/3} \\ & - 3M^{4/3}\left(64Q_*^6 - 257Q_*^4M^2 - 144M^6 + 336Q_*^2M^4\right) \\ & \Bigg/ \Bigg[2Q_*^4\left(8Q_*^2 - 9M^2\right) \sqrt{(Q_*^2 - M^2)\,(4Q_*^2 - 5M^2)^3} \\ & + 8154Q_*^4M^6 - 5177Q_*^6M^4 + 1472Q_*^8M^2 - 128Q_*^{10} + 1728M^{10} \\ & - 6040Q_*^2M^8 \Bigg]^{1/3} + 36M^4 + 8Q_*^4 - 42M^2Q_*^2 \Bigg\} \Big/ \left(8Q_*^2 - 9M^2\right) \Bigg|\,. \end{aligned} \tag{9.13}$$

The conditions for the occurrence of circular orbits are equations

$$\mathrm{f}(u) = 0 \tag{9.14}$$

and (9.10). From these equations it follows that energy E and the angular momentum L of a circular orbit of radius $r_{\mathrm{c}} = 1/u_{\mathrm{c}}$ is given by

$$E^2 = -\frac{(1 - 2Mu_{\mathrm{c}} + Q_*^2 u_{\mathrm{c}}^2)^2}{1 - 3Mu_{\mathrm{c}} + 2Q_*^2 u_{\mathrm{c}}^2} \tag{9.15}$$

and

$$L^2 = -\frac{M - u_{\mathrm{c}} Q_*^2}{u_{\mathrm{c}}(1 - 3Mu_{\mathrm{c}} + 2Q_*^2 u_{\mathrm{c}}^2)}\,. \tag{9.16}$$

These equations require, in particular, that

$$1 - 3Mu_{\mathrm{c}} + 2Q_*^2 u_{\mathrm{c}}^2 < 0\,. \tag{9.17}$$

and

$$\frac{M}{Q_*^2} \geq u_{\mathrm{c}} \tag{9.18}$$

Inequality (9.17) shows that the maximum radius for space-like circular orbits, in the case $M^2 \geq Q_*^2$, is the radius of the circular photon-orbit. Since for $M^2 < Q_*^2 < 9M^2/8$ we have two distinct circular photon-orbits (one stable and one unstable), space-like circular orbits exist in the region $r_{\mathrm{cs}} < r < r_{\mathrm{cu}}$. When $Q_*^2 \geq 9M^2/8$, there is no space-like circular orbit at all. Inequality (9.18) shows minimum radius for space-like circular orbit. So in figure 9.1 the stable orbits in the last picture are not allowed. Analytical solutions for general and circular orbits are formally the same as in Chapter 8.

Chapter 10

The time-like geodesics in the Reissner-Nordström space-time

The equations governing the time-like geodesics are

$$\left(\frac{\mathrm{d}r}{\mathrm{d}\tau}\right)^2 + \frac{\Delta}{r^2}\left(1+\frac{L^2}{r^2}\right) = E^2\,; \quad \frac{\mathrm{d}t}{\mathrm{d}\tau} = E\frac{r^2}{\Delta}\,; \quad \text{and} \quad \frac{\mathrm{d}\varphi}{\mathrm{d}\tau} = \frac{L}{r^2}\,. \tag{10.1}$$

As before, we can interpret

$$\mathcal{V} = \frac{\Delta}{r^2}\left(1+\frac{L^2}{r^2}\right)\,, \tag{10.2}$$

as 'potential energy'. (Cf. equations (5.12), (4.25) and (9.2).)

By considering r as a function of φ and replacing r by $u = 1/r$ as the independent variable, we obtain the equation (cf. equation (4.5))

$$\left(\frac{\mathrm{d}u}{\mathrm{d}\varphi}\right)^2 = -Q_*^2u^4 + 2Mu^3 - u^2\left(1+\frac{Q_*^2}{L^2}\right) + \frac{2M}{L^2}u - \frac{1-E^2}{L^2} = \mathrm{f}(u) \quad \text{(say)}. \tag{10.3}$$

10.1 The radial geodesics

Considering first the radial geodesics, we can obtain governing equations by setting $L = 0$ in equations (10.1). Accordingly,

$$\frac{\mathrm{d}r}{\mathrm{d}t} = \pm\left(\frac{\Delta}{Er^2}\right)\sqrt{E^2 - \frac{\Delta}{r^2}}\,. \tag{10.4}$$

The solution for the proper time, τ, is

$$\tau = \frac{r_{\rm i}\sqrt{E^2-\frac{\Delta_{\rm i}}{r_{\rm i}^2}} - r\sqrt{E^2-\frac{\Delta}{r^2}}}{E^2-1} + \\ + \frac{M}{(E^2+1)^{3/2}} \ln\left(\frac{r}{r_{\rm i}} \cdot \frac{E^2-1+\frac{M}{r}+\sqrt{E^2-\frac{\Delta}{r^2}}\sqrt{E^2-1}}{E^2-1+\frac{M}{r_{\rm i}}+\sqrt{E^2-\frac{\Delta_{\rm i}}{r_{\rm i}^2}}\sqrt{E^2-1}}\right) \quad (10.5)$$

and for coordinate t,

$$t = \frac{ME(2E^2-3)}{(E^2-1)^{3/2}} \ln \frac{r(E^2-1)+M+r\sqrt{E^2-1}\sqrt{E^2-\frac{\Delta}{r^2}}}{r_{\rm i}(E^2-1)+M+r_{\rm i}\sqrt{E^2-1}\sqrt{E^2-\frac{\Delta_{\rm i}}{r_{\rm i}^2}}} + \\ + \frac{4M^3-3Q_*^2M-(Q_*^2-4*M^2)\sqrt{M^2-Q_*^2}}{2Q_*^2\sqrt{M^2-Q_*^2}} \cdot \\ \cdot \sqrt{2M^2-Q_*^2+2M\sqrt{M^2-Q_*^2}} \ln\left\{\frac{r_{\rm i}-M+\sqrt{M^2-Q_*^2}}{r-M+\sqrt{M^2-Q_*^2}} \cdot \right. \\ \cdot \left[M^2-Q_*^2-\left(M+r(E^2-1)\right)\sqrt{M^2-Q_*^2}+\right. \\ \left. + rE\left(ME+\sqrt{2M^2-Q_*^2-2M\sqrt{M^2-Q_*^2}}\sqrt{E^2-\frac{\Delta}{r^2}}\right)\right] / \\ / \left[M^2-Q_*^2-\left(M+r_{\rm i}(E^2-1)\right)\sqrt{M^2-Q_*^2}+\right. \\ \left. \left. + r_{\rm i}E\left(ME+\sqrt{2M^2-Q_*^2-2M\sqrt{M^2-Q_*^2}}\sqrt{E^2-\frac{\Delta_{\rm i}}{r_{\rm i}^2}}\right)\right]\right\} + \\ + \frac{3Q_*^2M-4M^3-(Q_*^2-4M^2)\sqrt{M^2-Q_*^2}}{2Q_*^2\sqrt{M^2-Q_*^2}} \cdot \\ \cdot \sqrt{2M^2-Q_*^2-2M\sqrt{M^2-Q_*^2}} \ln\left\{\frac{r_{\rm i}-M-\sqrt{M^2-Q_*^2}}{r-M-\sqrt{M^2-Q_*^2}} \cdot \right. \\ \cdot \left[M^2-Q_*^2+\left(M+r(E^2-1)\right)\sqrt{M^2-Q_*^2}+\right. \\ \left. + rE\left(ME+\sqrt{2M^2-Q_*^2+2M\sqrt{M^2-Q_*^2}}\sqrt{E^2-\frac{\Delta}{r^2}}\right)\right] / \\ / \left[M^2-Q_*^2+\left(M+r_{\rm i}(E^2-1)\right)\sqrt{M^2-Q_*^2}+\right. \\ \left. \left. + r_{\rm i}E\left(ME+\sqrt{2M^2-Q_*^2+2M\sqrt{M^2-Q_*^2}}\sqrt{E^2-\frac{\Delta_{\rm i}}{r_{\rm i}^2}}\right)\right]\right\} +$$

$$+\frac{E}{E^2-1}\left(r_{\rm i}\sqrt{E^2-\frac{\Delta_{\rm i}}{r_{\rm i}^2}}-r\sqrt{E^2-\frac{\Delta}{r^2}}\right)\,, \quad (10.6)$$

where the initial condition for r is given by

$$E^2-1=-\frac{Q_*^2+2Mr_{\rm i}}{r_{\rm i}^2} \quad (10.7)$$

for $r(0)=r_{\rm i}$ and $\dot{r}(0)=0$.

10.2 Circular orbits

[7] gives the solution for these orbits in case of $M^2>Q_*^2$ and [28] discusses these orbits in general. We combine these two together to get a full description and, whenever necessary, complete it.

The conditions for the occurrence of circular orbits are $\mathrm{f}(u)=0$ and

$$\mathrm{f}'(u)=-4Q_*^2u^3+6Mu^2-2u\left(1+Q_*^2/L^2\right)+2M/L^2=0\,. \quad (10.8)$$

From these equations, it follows that the energy E and the angular momentum L of a circular orbit of radius $r_{\rm c}=1/u_{\rm c}$ is given by

$$E^2=\frac{(1-2Mu_{\rm c}+Q_*^2u_{\rm c}^2)^2}{1-3Mu_{\rm c}+2Q_*^2u_{\rm c}^2} \quad (10.9)$$

and

$$L^2=\frac{M-Q_*^2u_{\rm c}}{u_{\rm c}(1-3Mu_{\rm c}+2Q_*^2u_{\rm c}^2)}\,. \quad (10.10)$$

These equations require (9.18) and

$$1-3Mu_{\rm c}+2Q_*^2u_{\rm c}^2>0 \quad (10.11)$$

(cf. inequality (9.17)). This inequality shows that the minimum radius for a time-like circular orbit, in case $M^2\geq Q_*^2$, is the radius of the unstable circular photon-orbit. Since for $M^2<Q_*^2<9M^2/8$ we have two distinct circular photon-orbits (one stable and one unstable), particle circular orbits exist in

the regions $Q_*^2/M < r < r_{\rm cs}$ (all stable) and $r > r_{\rm cu}$ (some unstable). When $Q_*^2 = 9M^2/8$, particle orbits exist for all $r \geq Q_*^2/M$ except $r = r_{\rm c} = 3M/2$, which is an unstable photon-orbit. When $Q_*^2 > 9M^2/8$, particle orbits are allowed everywhere in the region $r \geq Q_*^2/M$.

When E and L have the values (10.9) and (10.10), appropriate for a circular orbit of radius $r_{\rm c} = 1/u_{\rm c}$, equation (10.3) becomes (cf. equation (8.17))

$$\left(\frac{{\rm d}u}{{\rm d}\varphi}\right)^2 = (u-u_{\rm c})^2\left[-Q_*^2u^2 + 2\left(M - Q_*^2u_{\rm c}\right)u + \left(M - Q_*u_{\rm c} - M/L^2u_{\rm c}^2\right)u_{\rm c}\right] . \tag{10.12}$$

Therefore, besides the circular orbit of radius $r_{\rm c} = 1/u_{\rm c}$, equation (10.12) provides an orbit of the second kind determined by (cf. equation (8.18))

$$\varphi = \pm\int \frac{{\rm d}u}{(u-u_{\rm c})\sqrt{-Q_*^2u^2 + 2(M-Q_*^2u_{\rm c})u + u_{\rm c}(M - Q_*^2u_{\rm c} - M/L^2u_{\rm c}^2)}} . \tag{10.13}$$

With the substitution (8.19) we obtain the same solution (8.22) with, however,

$$b = 2\left(M - 2Q_*^2u_{\rm c}\right) \qquad \text{and} \qquad c = u_{\rm c}\left(3M - 4Q_*^2u_{\rm c} - M^2/L^2u_{\rm c}^2\right) . \tag{10.14}$$

When the circular orbit is unstable, the solution has the form (8.41) for values of the argument in the following ranges:

$$\xi_{\rm min}\left(= \frac{1}{u_{\rm min} - u_{\rm c}}\right) < \xi < +\infty\,,\ u_{\rm c} < u \leq u_{\rm max}\left(= \frac{1}{r_{\rm min}}\right) \text{ and } r_{\rm min} < r < r_{\rm c}\,. \tag{10.15}$$

The limiting case in fig. 10.1 (where the second picture illustrates the last unstable circular orbit) happens for (10.8) and

$$\mathrm{f}''(u) = -6Q_*^2u^2 + 6Mu - 1 - \frac{Q_*^2}{L^2} = 0\,. \tag{10.16}$$

Since we require M to be positive, the condition for parameters M, L and Q_* is

$$M = \frac{\sqrt{6\left[12Q_*^2L^2 + \left(L^2+Q_*^2\right)^2\right] \pm 2\sqrt{\left(Q_*^2+3L^2\right)\left(L^2-5Q_*^2\right)^3}}}{12L} \tag{10.17}$$

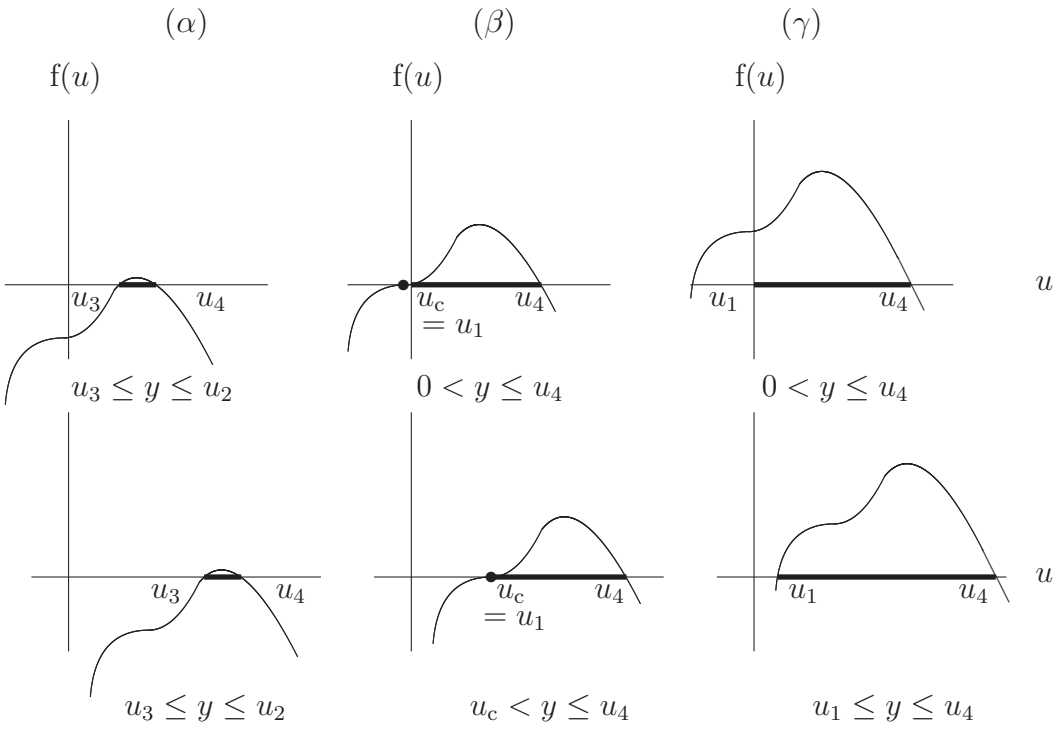

Figure 10.1: Limiting case for (α) $E < E_c$, (β) $E = E_c$ and (γ) $E > E_c$. (See equation (10.9).) The top row are orbits with $E^2 > 1$ and the bottom row are orbits with $E^2 < 1$.

or

$$L = \text{sqrt}\left\{3M^{2/3}\left[2Q_*^4\left(8Q_*^2-9M^2\right)\sqrt{\left(Q_*^2-M^2\right)\left(4Q_*^2-5M^2\right)^3}+\right.\right.$$
$$+8154Q_*^4M^6-5177Q_*^6M^4+1472Q_*^8M^2-128Q_*^{10}+$$
$$\left.+1728M^{10}-6040Q_*^2M^8\right]^{1/3}$$
$$-3M^{4/3}\left(64Q_*^6-257Q_*^4M^2-144M^6+336Q_*^2M^4\right)$$
$$/\left[2Q_*^4\left(8Q_*^2-9M^2\right)\sqrt{\left(Q_*^2-M^2\right)\left(4Q_*^2-5M^2\right)^3}\right.$$
$$+8154Q_*^4M^6-5177Q_*^6M^4+1472Q_*^8M^2-128Q_*^{10}+1728M^{10}$$
$$\left.\left.-6040Q_*^2M^8\right]^{1/3}+36M^4+8Q_*^4-42M^2Q_*^2\right\}/\sqrt{9M^2-8Q_*^2}. \quad (10.18)$$

Eliminating L^2 in equation (10.16) with the aid of equation (10.10), we

obtain the equation

$$4Q_*^4 u_c^3 - 9MQ_*^2 u_c^2 + 6M^2 u_c - M = 0\,, \tag{10.19}$$

When all three equations $\mathrm{f}(u) = 0$, (10.8), and (10.16), are satisfied, equation (10.3) takes form

$$\left(\frac{\mathrm{d}u}{\mathrm{d}\varphi}\right)^2 = (u - u_c)^3 \,(2M - 3Q_*^2 u_c - Q_*^2 u)\,; \tag{10.20}$$

and the solution of this equation is (cf. equation (5.25))

$$u = u_c + \frac{2(M - 2Q_*^2 u_c)}{(M - 2Q_*^2 u_c)^2(\varphi - \varphi_0)^2 + Q_*^2}\,. \tag{10.21}$$

10.3 The bound orbits ($E^2 < 1$)

The consideration of equation (10.3), governing the geometry of the orbits described in the invariant plane, is separated to two parts (similarly as it was in chapter 5). These two classes of orbits are characterized by $E^2 < 1$ and $E^2 \geq 1$. This distinction is one which will determine whether orbits are bound or unbound. In this section, we shall restrict ourselves to bound orbits ($E^2 < 1$). The geometry of the geodesics will be determined by the disposition of the roots of the equation $\mathrm{f}(u) = 0$ (see figure 10.2).

10.3.1 Orbits of the first kind

We now consider the case when all the roots of the biquadratic equation $\mathrm{f}(u) = 0$ are real and distinct. Letting u_1, u_2, u_3 and u_4 denote the roots, we rewrite equation (10.3) in the form (8.6) (see fig. 10.2 (α)). The solution is

$$\varphi = \int_{u_1}^{y} \frac{\mathrm{d}u}{\sqrt{\mathrm{f}(u)}} = \frac{g}{Q_*}\mathrm{F}(\psi, k)\,, \tag{10.22}$$

where g, ψ and k^2 are defined in equations (8.8) – (8.10).

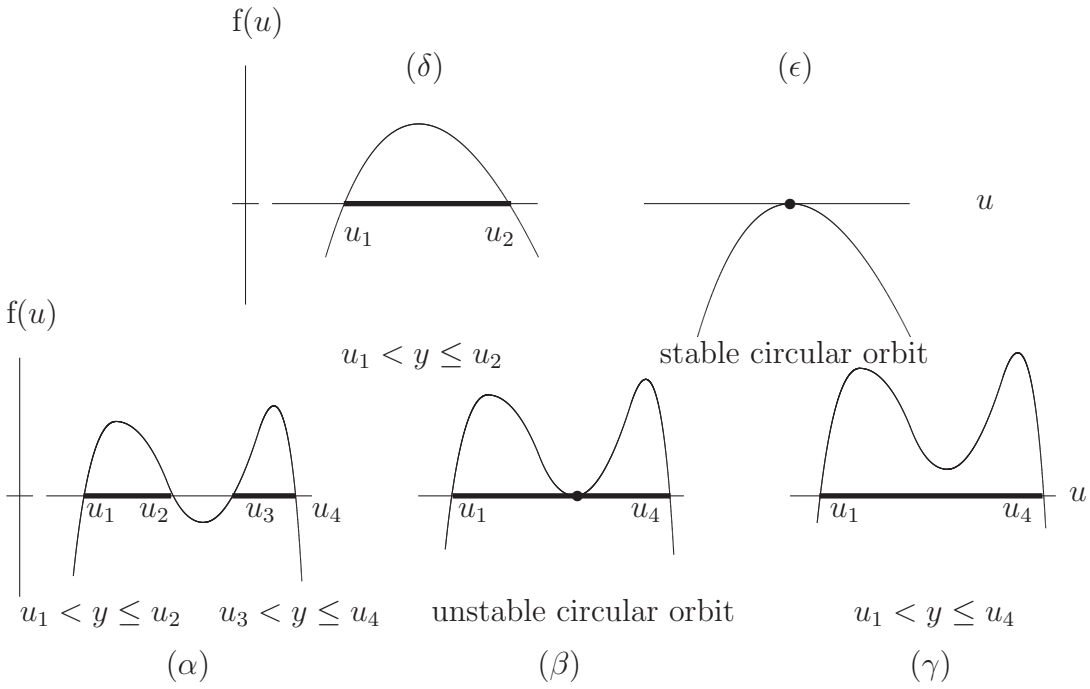

Figure 10.2: The case when f(u) has (α) four real roots, (β) double root, (γ) two complex conjugate roots, (δ) two real roots, and (ϵ) one real root.

10.3.2 Orbits of the second kind

To obtain the time-like geodesics, whose ranges are $u_3 < u \leq u_4$, we rewrite equation (10.3) in the form (8.24). Solution is then formally as in section 8.2.2. An example of the orbit of the first kind and associated orbit of the second kind is in figure 10.3.

10.3.3 The orbits with imaginary eccentricities

Finally, we consider the orbits when the equation f(u) = 0 has a pair of complex-conjugate roots, besides two real roots. We rewrite equation (10.3) in the form (8.31). Unlike in section 8.2.3 this time solution is (10.22) where constants g, ψ, A, B, b_1, a_1 and k are defined by (8.33) – (8.39). The case (δ) in figure 10.2 has the same formal solution.

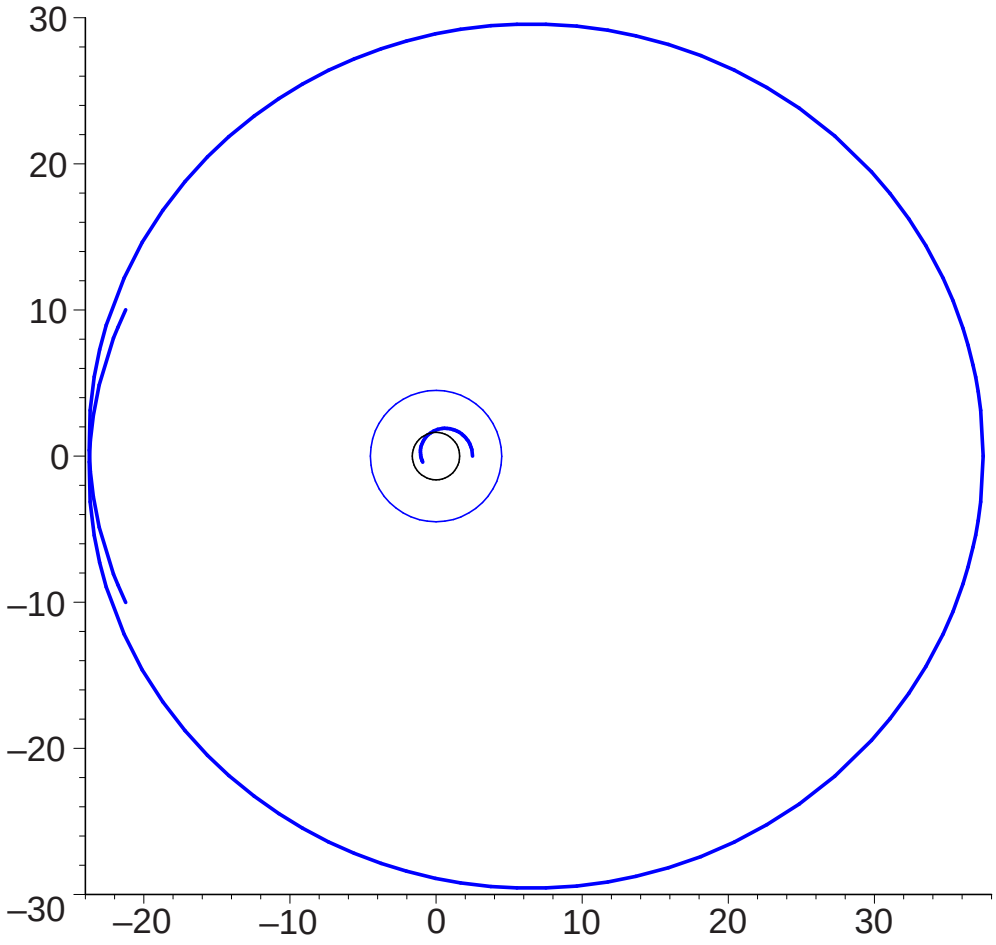

Figure 10.3: Time-like geodesics of the first and the second kind with $Q_* = 0.8$, $M = 1.2$, $L = 6$ and $E = 0.98$. The thin blue circle represents the circular-orbit r_c ($u_c = 1/r_c = 0.2225$); the thin black circle represents radius below which no circular orbits are allowed. Orbit of the first kind precesses around the black hole. Orbit of the second kind starts above the event horizon and ends below the Cauchy horizon.

10.4 The unbound orbits ($E^2 > 1$)

When $E^2 > 1$, the constant term in f(u) is positive. The equation f(u) = 0 must, therefore, allow a negative root. The cases we must distinguish look essentially as space-like and null orbits. Analytical solution are formally the same as in Chapter 8.

Chapter 11

The motion of a charged particle

A charged test particle does not follow a geodesic path, but we will look briefly at them to compare their motion with particles without charge. Their motion is determined by Lagrangian (from [7, chapter 5])

$$2\mathcal{L} = \left[\frac{\Delta}{r^2}\left(\frac{\mathrm{d}t}{\mathrm{d}\tau}\right)^2 - \frac{r^2}{\Delta}\left(\frac{\mathrm{d}r}{\mathrm{d}\tau}\right)^2 - r^2\left(\frac{\mathrm{d}\theta}{\mathrm{d}\tau}\right)^2 - r^2\sin^2\theta\left(\frac{\mathrm{d}\varphi}{\mathrm{d}\tau}\right)^2\right] + 2\frac{qQ_*}{r}\frac{\mathrm{d}t}{\mathrm{d}\tau}\,, \tag{11.1}$$

where q denotes the charge per unit mass of the test particle. It is the last term in which the Lagrangian of the charged particle differs from Lagrangian of particle without charge. The equations of motion which follow from Lagrangian (11.1) are (cf. equations (10.1))

$$p_t = \frac{\Delta}{r^2}\frac{\mathrm{d}t}{\mathrm{d}\tau} + \frac{qQ_*}{r} = E = \text{constant}\,, \qquad r^2\frac{\mathrm{d}\varphi}{\mathrm{d}\tau} = L = \text{constant}\,, \tag{11.2}$$

and

$$\left(\frac{\mathrm{d}r}{\mathrm{d}\tau}\right)^2 + \frac{\Delta}{r^2}\left(1 + \frac{L^2}{r^2}\right) = \left(\frac{\Delta}{r^2}\frac{\mathrm{d}t}{\mathrm{d}\tau}\right)^2 = \left(E - \frac{qQ_*}{r}\right)^2\,; \tag{11.3}$$

and in place of equation (10.3) we now have

$$\left(\frac{\mathrm{d}u}{\mathrm{d}\varphi}\right)^2 = -Q_*^2u^4 + 2Mu^3 - \left[1 + Q_*^2\frac{(1-q^2)}{L^2}\right]u^2 + \frac{2}{L^2}(M - qQ_*E)u - \frac{1-E^2}{L^2}\,. \tag{11.4}$$

If a particle should have a turning point as it arrives at the event horizon,

then its energy, according to equation (11.3), will be

$$E = qQ_*/r_+\,; \tag{11.5}$$

and this will be negative if $qQ_* < 0$. This fact gives rise to the possibility of extracting energy from the black hole, energy that is associated with its charge. (Processes of this kind are considered in [7, chapter 7].)

11.1 Radial motion

Let us briefly examine radial motion of a charged particle. The governing equations can be obtained by setting $L = 0$ in equation (11.3); thus

$$\left(\frac{\mathrm{d}r}{\mathrm{d}\tau}\right)^2 = \left(E - \frac{qQ_*}{r}\right)^2 - \frac{\Delta}{r^2}\,, \qquad \text{and} \qquad \frac{\mathrm{d}t}{\mathrm{d}\tau} = \left(E - \frac{qQ_*}{r}\right)\frac{r^2}{\Delta}\,. \tag{11.6}$$

Accordingly,

$$\frac{\mathrm{d}r}{\mathrm{d}t} = \pm\frac{\Delta}{r^2\left(E - \dfrac{qQ_*}{r}\right)^2}\sqrt{\left(E - \frac{qQ_*}{r}\right)^2 - \frac{\Delta}{r^2}}\,. \tag{11.7}$$

Since $\Delta > 0$ in the interval $0 \le r < r_-$, then for $q^2 < 1$, $(Er - qQ_*)^2 - \Delta$ will vanish for some finite value of $0 < r < r_-$ and the trajectory will have a turning point inside the Cauchy horizon (like in the case of a particle without charge). If $qQ_* > 0$ the particle can have a turning point anywhere depending on relations between parameters E , q , M and Q_*. And finally if $qQ_* < 0$ there is turning point only if $E^2 < 1$ (if $q^2 > 1$ holds).

The formal solutions of equations (11.6) and (11.7) can be readily written down in terms of elementary integrals. We shall not write them since they are too complicated to exhibit any more features that what can be deduced from a simple inspection of the equations.

11.2 Circular orbits

The conditions for the occurrence of circular orbits are

$$\begin{aligned} \mathrm{f}(u) = &-Q_*^2 u^4 + 2Mu^3 - \left[1 + Q_*^2 \frac{(1-q^2)}{L^2}\right] u^2 + \\ &+ \frac{2}{L^2}(M - qQ_*E)u - \frac{1-E^2}{L^2} = \\ &= 0\,, \end{aligned} \tag{11.8}$$

and

$$\mathrm{f}'(u) = -4Q_*^2 u^3 + 6Mu^2 - 2\left(1 + Q_*^2 \frac{1-q^2}{L^2}\right) u + 2\frac{M - qQ_*E}{L^2} = 0\,. \tag{11.9}$$

From these equations, it follows that the energy E and the angular momentum L of a circular orbit of radius $r_{\mathrm{c}} = 1/u_{\mathrm{c}}$ is given by (cf. equations (10.9) and (10.10))

$$\begin{aligned} E^2 = \{&1 - (4M - qQ_*E)u_c + \\ &+ 2\left[Q_*^2 + 2M(M - qQ_*E)\right] u_c^2 - Q_*^2\left[3(M - qQ_*E) + \right. \\ &\left. + M\left(1 - q^2\right)\right] u_c^3 + Q_*^4(1-q^2)u_c^4\} \,/\, \left(1 - 3Mu_c + 2Q_*^2 u_c^2\right) \end{aligned} \tag{11.10}$$

and

$$L^2 = \frac{M - qQ_*E - Q_*^2(1-q^2)u_c}{u_c(1 - 3Mu_c + 2Q_*^2 u_c^2)}\,. \tag{11.11}$$

It is possible to give explicit solutions of these equations, but for easier comparison with time-like geodesic and a clearer understanding of the roles of signs of qQ_* and $(1-q^2)$, we have left them in this implicit form.

The minimum radius for a stable circular orbit will occur at a point of inflexion of the function $\mathrm{f}(u)$ (see figure 10.1), i.e., we must supplement equation (11.8) and (11.9) with the further equation

$$\mathrm{f}''(u) = -12Q_*^2 u^2 + 12Mu - 2\left(1 + Q_*^2 \frac{1-q^2}{L^2}\right) = 0\,. \tag{11.12}$$

Eliminating L^2 in this equation with the aid of equation (11.11), we obtain the equation (cf. equation (10.19))

$$4Q_*^4\left(q^2-1\right)u^3+ \tag{11.13}$$
$$+3Q_*^2\left[2(M-qQ_*E)+M\left(1-q^2\right)\right]u^2-6M(M-qQ_*E)u+M-qQ_*E=0\,,$$

or, alternatively

$$r_c^3-6Mr_c^2+3Q_*^2\frac{\left[2(M-qQ_*E)-M\left(1-q^2\right)\right]r_c}{M-qQ_*E}-4Q_*^4\frac{1-q^2}{M-qQ_*E}=0\,. \tag{11.14}$$

(It may be noted here that equation (11.14) gives $r_c=6M$ when $Q_*^2=0$, in agreement with the value for the Schwarzschild geometry; and when $q=0$ is identical to the equation for time-like geodesic (cf. [7, §40(b)]).)

11.3 The bound orbits $\left(E^2<1\right)$

As in chapter 10, the geometry of the orbits described in the invariant plane is separated to two parts distinguished by $E^2<1$ and $E^2\geq 1$ (see equation (11.4)). This will determine which orbits are bound and which ones are unbound. The geometry of the orbits will be determined by the disposition of the roots of the equation $\mathrm{f}(u)=0$ (see figure 10.2). Orbits look essentially as time-like geodesics. Analytical solutions are formally the same as in Chapter 10.

11.4 The unbound orbits $\left(E^2>1\right)$

When $E^2>1$, the constant term in $\mathrm{f}(u)$ is positive. The equation $\mathrm{f}(u)=0$ must, therefore, allow a negative root. The cases we must distinguish look essentially as space-like, unbound time-like and null geodesics. Analytical solutions are formally the same as in Chapter 8. An example of unbound orbits of a charged particle is in figure 11.1.

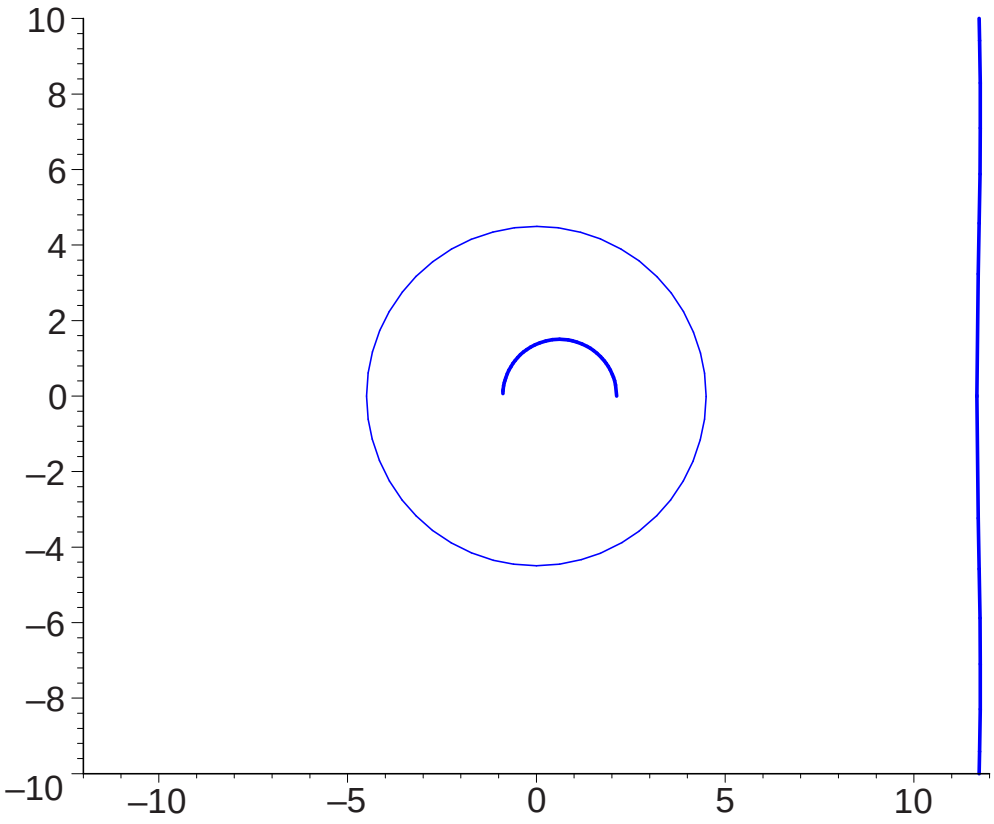

Figure 11.1: Orbits of the first and the second kind of a charged particle with $Q_* = 0.8,\ M = 1.2,\ L = 6,\ E = 1.1$ and $q = 2$. The thin circle represents the unstable circular-orbit $r_{\rm c}$ ($u_{\rm c} = 1/r_{\rm c} = 0.2225$). The orbit of the first kind starts from infinity and ends in infinity, the orbit of the second kind starts and ends certain distance from the black hole.

Chapter 12

Summary of Part II

The main difference between geodesics in Schwarzschild and Reissner-Nordström solutions comes from the function f(u), which is, in the Schwarzschild black hole, cubical, and in the Reissner-Nordström black hole, quartic. That means that, while orbits of the first kind (bound or unbound) look essentially the same, orbits of the second kind fall into the singularity of the Schwarzschild black hole, unlike in the case of the Reissner-Nordsröm black hole, where they end at some finite distance from the singularity.

Again there are similarities between null, space-like and time-like unbound geodesics in the Reissner-Nordström space-time (all of them are unbounded), and, as before, only time-like geodesics can be bound.

Radius of a circular orbit depends on relation of black hole parameters M and Q_*. To see how charge of a black hole affects the circular orbit one may look at time-like geodesic in Schwarzschild space-time, where circular orbits have radius $r \geq 3M$, and compare it with circular geodesic in Reissner-Nordström space-time, which have radius $r \geq \frac{3}{2}M(1 + \sqrt{1 - \frac{8Q_*^2}{9M^2}})$ when $M^2 \geq Q_*^2$, and $r \geq Q_*^2/M$ otherwise.

The solution for charged particles are formally the same as the solution for time-like geodesics, however the conditions for existence of circular orbits

differ. Since there is one more parameter to consider (q – charge of the particle), discussion of the occurrence of different cases is not trivial. We expect the orbits of charged particles to look the same as those that are not charged, with the addition of repulsive orbits when $qQ_* > 0$.

The main contribution of the thesis is in providing general solutions of the time-like and the null geodesics as opposed to special circular orbits which can be found in [7], and discussion of the space-like geodesics. All three types of geodesics are considered for black holes with $M > |Q_*|$ as well as $M \leq |Q_*|$.

In Chapter 11 the solutions for orbits of the charged particles are given, extending the prior work of [7].

Part III

Geodesics in the Kerr space-time

Chapter 13

Introduction to geodesics in the Kerr space-time

In this part we will deal with geodesics in Kerr space-time (black hole characterized by mass M and angular momentum per unit mass a, see Appendix B.3). We shall use the following terminology:

slowly rotating Kerr space-time occurs when $0 < a^2 < M^2$

extreme Kerr space-time occurs when $a^2 = M^2$

rapidly rotating Kerr space-time occurs when $M^2 < a^2$

with Schwarzschild space time occurring when $a = 0$. In this chapter there is a brief derivation of equations of motion, and discussion of different types of orbits in relation to relationship among parameters (energy, angular momentum, Carter constant). This will make later chapters easier to follow. Lemmas from [34] are in this thesis without proofs (only with relevant references). Lemmas modified or additional ones are followed by their proofs. The pictures are in "spherical" coordinates; the accurate definitions can be found in Appendix A in the files that generate the figures.

A first indication of the differences between these *rotation types* is given by the horizon function (B.31).

- For Schwarzschild space-time, Δ has roots $0,\ 2M$ (see Part I).
- For slow Kerr, Δ has two roots: $0 < r_\pm = M \pm \sqrt{M^2 - a^2} < 2M$.
- For extreme Kerr, $\Delta = (r - M)^2$, so $r = M$ is a double root.
- For fast Kerr (rapidly rotating), Δ has no real roots.

There are four independent first-integrals on the Kerr space-time: $\delta_1 = \langle \dot\gamma, \dot\gamma \rangle$, energy E, angular momentum about the axis L and the fourth, called the *Carter constant*.

13.1 The nature of the Kerr space-time

Unlike the Schwarzschild and the Reissner-Nordström space-times, in the Kerr metric there are three subsets on which the metric fails (see [34, Section 2.2]).

1. On the *horizon* $H :\ \Delta = 0$. For the fast Kerr space-time there is no horizon; for the extreme Kerr space-time there is a single horizon $H :\ r = M$; and for the slow Kerr space-time there are *two* horizons $H_+ :\ r = r_+$ and $H_- :\ r = r_-$. As in the Reissner-Nordsrtöm geometry the surface $r = r_+$ represents an event horizon, and surface $r = r_-$ represents a Cauchy horizon.

2. On the *ring singularity* $\Sigma :\ \rho^2 = 0$, because $\rho^2 = 0$ iff both $r = 0$ and $\cos\theta = 0$. Thus Σ is the equatorial circle $\theta = \pi/2$ in S^2 at radius $r = 0$. Sometimes the circle itself is called the ring singularity, with $\Sigma = S^1 \times \mathbf{R}^1$ its history through time. *Singularity along this ring is the only singularity of the Kerr space-time.*

3. On the *axis* $A:\ \sin\theta = 0$. For spherical coordinates, $\sin\theta = 0$ gives the z-axis, but now there are *two* such axes (enduring through time). t

As in the case of the Reissner-Nordström space-time, we must distinguish three regions $A,\ B,\ C$:

- For slow Kerr, where there are two horizons $r = r_{\pm}$,

  $A\ :\ r < r_-$,

  $B\ :\ r_- < r < r_+$,

  $C\ :\ r > r_+$.

- For extreme Kerr, where there is a single horizon $r = M$,

  $A\ :\ r < M$,

  $C\ :\ r > M$.

- For fast Kerr , since there is no horizon, $\mathbf{R}^2 \times S^2 - \Sigma$ itself can be regarded as a single block $A = C$.

13.2 The general equations of motion

In this section, we shall consider the reduction of the equations of geodesic motion, which follows from discoveries of Carter, and Walker and Penrose ([7]). Alternative derivation of the basic equations follows from separability of the Hamilton-Jacobi equation and can be found in [7, §62(a)].

From the general Lagrangian we derive the energy and the angular momentum integrals:

$$+p_t = \left(1 - \frac{2Mr}{\rho^2}\right)\dot{t} + \frac{2aMr\sin^2\theta}{\rho^2}\dot{\varphi} = E = \text{constant} \tag{13.1}$$

and

$$-p_\varphi = -\frac{2aMr\sin^2\theta}{\rho^2}\dot{t} + \left(r^2 + a^2 + \frac{2a^2Mr}{\rho^2}\sin^2\theta\right)\left(\sin^2\theta\right)\dot{\varphi} = L = \text{constant}. \tag{13.2}$$

Further, there are the integrals ([7, chapter 7])

$$2\rho^2(\boldsymbol{k}\cdot\boldsymbol{l})(\boldsymbol{k}\cdot\boldsymbol{n}) - r^2|\boldsymbol{k}|^2 = K \tag{13.3}$$

and

$$2\rho^2(\boldsymbol{k}\cdot\boldsymbol{m})(\boldsymbol{k}\cdot\bar{\boldsymbol{m}}) + \left(a^2\cos^2\theta\right)|\boldsymbol{k}| = K\,, \tag{13.4}$$

where $\boldsymbol{l}$, $\boldsymbol{n}$, $\boldsymbol{m}$, and $\bar{\boldsymbol{m}}$ are the basis null vectors, and $\boldsymbol{k}$ is an affinely parametrized geodesic. We set

$$|\boldsymbol{k}|^2 = \delta_1 = \begin{cases} 1 & \text{for time-like geodesics,} \\ 0 & \text{for null geodesics,} \\ -1 & \text{for space-like geodesics.} \end{cases} \tag{13.5}$$

In the Kerr geometry the integrals (13.3) and (13.4) have the explicit forms

$$\frac{\left[\Delta\dot{t} - \left(a\Delta\sin^2\theta\right)\dot{\varphi}\right]^2}{\Delta} - \frac{\rho^4}{\Delta}\dot{r}^2 - \delta_1 r^2 = K \tag{13.6}$$

and

$$\left[(a\sin\theta)\dot{t} - \left(r^2+a^2\right)(\sin\theta)\dot{\varphi}\right]^2 + \rho^4\dot{\theta}^2 + \delta_1 a^2\cos^2\theta = K\,. \tag{13.7}$$

Also, by equations (13.1) and (13.2), we can write

$$(a\sin\theta)\dot{t} - \left[\left(r^2+a^2\right)\sin\theta\right]\dot{\varphi} = aE\sin\theta - L\csc\theta \tag{13.8}$$

and

$$\Delta\dot{t} - \left(a\Delta\sin^2\theta\right)\dot{\varphi} = \left(r^2+a^2\right)E - aL\,. \tag{13.9}$$

After inserting these expressions in equations (13.6) and (13.7), equations

$$\rho^4\dot{r}^2 = \mathrm{R}(r) = \left[\left(r^2+a^2\right)E - aL\right]^2 - \Delta\left(\delta_1 r^2 + K\right) \tag{13.10}$$

and

$$\rho^4\dot{\theta}^2 = \Theta(\theta) = -\left(aE\sin\theta - L\csc\theta\right)^2 + \left(-\delta_1 a^2\cos^2\theta + K\right) \tag{13.11}$$

are obtained. Equations (13.8) and (13.9) also provide the complementary pair of equations

$$\rho^2\dot{t} = \frac{\Sigma^2 E - 2aMrL}{\Delta} \tag{13.12}$$

and

$$\rho^2\dot{\varphi} = \frac{2aMrE + (\rho^2 - 2Mr)L\csc^2\theta}{\Delta}\,. \tag{13.13}$$

Any function of first-integrals is again a first-integral. A particularly useful case is the first-integral Q defined by the relation

$$K = Q + (L - aE)^2\,. \tag{13.14}$$

Following [34], we call Q or K, *the Carter constant*. Each form has its advantages. Often K gives simpler formulas, and $K \geq 0$ *holds for nonspace-like geodesics* (by the θ-equation (13.11)), but the geometric meaning of Q is usually clearer. For example, Q is crucial for the behavior of geodesics near $r = 0$, and Q decisively influences the θ-motion of geodesics.

With the above identification, the equations of motions (13.10)–(13.13) are equivalent to

$$\int^r \frac{\mathrm{d}r}{\sqrt{\mathrm{R}}} = \int^\theta \frac{\mathrm{d}\theta}{\sqrt{\Theta}}\,, \tag{13.15}$$

$$\tau = \int^r \frac{r^2}{\sqrt{\mathrm{R}}}\mathrm{d}r + a^2\int^\theta \frac{\cos^2\theta}{\sqrt{\Theta}}\mathrm{d}\theta\,, \tag{13.16}$$

$$t = \tau E + 2M\int^r r\left[r^2E - a(L - aE)\right]\frac{\mathrm{d}r}{\Delta\sqrt{\mathrm{R}}}\,, \tag{13.17}$$

and

$$\varphi = a\int^r \left[\left(r^2 + a^2\right)E - aL\right]\frac{\mathrm{d}r}{\Delta\sqrt{\mathrm{R}}} + \int^\theta \left(L\csc^2\theta - aE\right)\frac{\mathrm{d}\theta}{\sqrt{\Theta}}\,. \tag{13.18}$$

13.3 Control of the r coordinate

In this section, effect of the inequality $R \geq 0$ on the r coordinate of a Kerr geodesic γ will be studied. The radial coordinate r determines such critical issues as escape to infinity and passage through a horizon. Substituting[1] $\Delta = r^2 - 2Mr + a^2$ and $\mathbb{P} = (r^2 + a^2)E - aL$ into the definition $\mathrm{R}(r) = \mathbb{P}^2 - \Delta(\delta_1 r^2 + K)$ gives fundamental result:

Proposition 13.1 *For a geodesic γ with $\delta_1 = \langle \dot{\gamma}, \dot{\gamma} \rangle$, energy E, angular momentum L, and Carter constant Q,*

$$\mathrm{R}(r) = \left(E^2 - \delta_1\right) r^4 + 2M\delta_1 r^3 + \mathfrak{X} r^2 + 2MKr - a^2 Q \,,$$

where $\mathfrak{X} = a^2(E^2 - \delta_1) - L^2 - Q$ and $K = Q + (L - aE)^2$.

$\mathrm{R}(r)$ is unchanged if the pair $E,\ L$ is replaced by $-E,\ -L$. On the other hand, $\mathrm{R}(r)$ *is* changed (provided $E \neq L \neq 0$) if only *one* of the two parameters $E,\ L$ changes sign, because $K = Q + L^2 - 2aLE + a^2E^2$. Therefore, in Kerr space-time the direct and retrograde orbits with the same $\delta_1,\ E,\ K$ and $|L|$ generally vary in their radial motion (except in the special cases $E = 0$ or $L = aE$).

The polynomial $\mathrm{R}(r)$ of a Kerr geodesic γ is determined by the first-integrals $\delta_1,\ E,\ L,\ Q$.

13.4 r-L plots

In this section we follow [34], who concentrates on time-like geodesics. We expand his discussion to null geodesics (which are analogous and are usually easier to deal with), and space-like geodesics (which have more varied trajectories).

[1] comp. with [34, page 208]

If the Kerr parameters $M,\ a$ and the causal parameter δ_1 are fixed then the function $\mathrm{R}(r)$ of Proposition 13.1 depends on $E,\ L,\ Q$. Since the resulting r-line cannot enter the region $\mathrm{R} < 0$, the set Z: $\mathrm{R} = 0$ in $\mathbf{R}^4$ is the key as it provides the boundary points of $\mathrm{R} < 0$. However, it is possible to show the qualitative character of orbits by considering R only as a function of the variables r and L–for a few selected constant values of E and Q. The region of Z in the r-L plane is said to be *allowed* if $\mathrm{R} > 0$, and *forbidden* if $\mathrm{R} < 0$. A diagram of this situation is called the r-L plot.

The set Z: $\mathrm{R} = 0$ is usually a smooth curve.

The abbreviation $e = E^2 - \delta_1$ is often convenient. This first-integral is called *effective energy*. It could also be called the *escape parameter* ([34]). (In the literature the notation Γ has also been used.)

Initially some properties of r-L plots that are independent of causal character will be examined.

In some contexts it is useful to regard the function in Proposition13.1 as a polynomial $\mathrm{R}(L)$ in L, with coefficients determined by the remaining first-integrals and r. Specifically,

$$\mathrm{R}(L) = r(2M - r)L^2 - 4MaErL + \mathrm{R}(r, 0)\,, \tag{13.19}$$

where $\mathrm{R}(r, 0)$ is the function R with $L = 0$ (r-axis).

Using (13.19) explicit formulas for the implicitly defined set $\mathrm{R} = 0$ can be derived.

Lemma 13.2 *In any r-L plot the set $\mathrm{R} = 0$ is the union of the graphs of (the real values of) the two functions*

$$L_\pm(r) = \frac{2MaEr \pm \sqrt{\mathrm{D}(r)}}{r(2M - r)}\,,$$

for $r \neq 0,\ \neq 2M$, where $\mathrm{D}(r) = r\Delta(r)\phi(r)$ is one fourth of the discriminant of $\mathrm{R}(L)$, and the discriminant polynomial $\phi(r)$ is

$$\phi(r) = \left(E^2 - \delta_1\right) r^3 + 2M\delta_1 r^2 - Qr + 2MQ\,.$$

For a proof of this lemma see [34, page 215].

The polynomial $\mathrm{R}(L)$ is quadratic in L (except when $r = 0$ and $r = 2M$), so its graph is parabolic with *vertex* at $L_{\mathrm{v}}(r) = 2MaE/(2M-r)$. The number $\mu(r)$ of points on any vertical line is 0, 1, or 2 as the modified discriminant $\mathrm{D}(r)$ is negative, zero or positive, respectively. When $\mu(r) = 2$ the two points are placed symmetrically on both sides of $L_{\mathrm{v}}(r)$. The curve $r \to (r, L_{\mathrm{v}}(r))$ in an r-L plot is called the *midline*.

When $\mu(r) = 1$, there is just one point of $\mathrm{R} = 0$ on the line $L \to (r, L)$, the vertex $(r, L_{\mathrm{v}}(r))$.

The formula (13.19) shows that when $r = 0$, R has the constant value $-a^2Q$, and that the behavior of R on and near the line $r = 2M$ is following:

Lemma 13.3 *In an r-L plot the function $L \to \mathrm{R}(2M, L)$ is linear with negative slope (if $E > 0$). Thus there is a critical momentum L_0 such that $\mathrm{R}(2M, L) < 0$ if $L > L_0$ and*[2] *$\mathrm{R}(2M, L) > 0$ if $L < L_0$. Furthermore, if $0 < \delta \ll M$, then $\mathrm{R}(2M + \delta) < 0$ and $\mathrm{R}(2M - \delta) > 0$ for all sufficiently large $|L|$.*

Proof of this lemma is in [34, page 216].

Investigation of r-L plots frequently comes in vertical strips: The B strip $r_- < r < r_+$ is particularly simple for nonspacelike geodesics; because they cannot turn in B, R is never zero there.

Lemma 13.4 *In the r-L plot of a time-like (or null) geodesic γ in slow Kerr space-time, we have $\mathrm{R} > 0$ on the closed vertical strip $r_- \le r \le r_+$* except *that $\mathrm{R} = 0$ at the two points (r_-, L_-) and (r_+, L_+), where*

$$L_\pm = L_v(r_\pm) = 2MaE/(2M - r_\pm) = 2MaE/r_\mp = 2Mr_\pm E/a\,. \qquad (13.20)$$

At these points the curve $\mathrm{R} = 0$ is smooth and tangent (from outside the strip) to the lines $r = r_-$ and $r = r_+$.

[2] comp. [34, lemma 4.7.2]

Proof. For any geodesic, the formula $\mathrm{R} = \mathbb{P}^2 - \Delta(\delta_1 r^2 + K)$ yields[3] $\mathrm{R}(r_\pm) = \mathbb{P}(r_\pm)^2$, where $\mathbb{P}(r_\pm) = (r_\pm^2 + a^2)E - La$. So $\mathrm{R}(r_\pm) > 0$ except when $\mathbb{P}(r_\pm) = 0$, and that is at $L_\pm$. The other formulas follow because $r_- + r_+ = 2M$ and $r_- r_+ = a^2$.

Since R is never zero on the B strip, therefore $\mathrm{R} > 0$ there.

Because $L_\pm$ is a minimum point on $r = r_\pm$, then $\frac{\partial \mathrm{R}}{\partial L} = 0$ at the points $(r_\pm, L_\pm)$.

To show that $\frac{\partial \mathrm{R}}{\partial r} \neq 0$ at these point we write

$$\frac{\partial \mathrm{R}}{\partial r} = 2\mathbb{P}\frac{\partial \mathbb{P}}{\partial r} - 2(r - M)\left(\delta_1^2 + K\right) - 2\delta_1 r\Delta\,, \tag{13.21}$$

which at $(r_\pm, L_\pm)$ becomes $-2(r_\pm - M)(\delta_1 r^2 + K) \neq 0$. This inequality holds for both $\delta_1 = 0$ and $\delta_1 = 1$ (null and time-like geodesics respectively). □

Remark 1 *A crucial effect of the Carter constant Q on (time-like) orbits derives from the fact that the function* R*, which depends quadratically on L, depends* linearly *on Q. In fact, the formulas $\mathrm{R} = \mathbb{P}^2 - \Delta(r^2 + K)$ and $K = Q + (L - aE)^2$ give $\mathrm{R}(r) = -\Delta(r)Q + \mathrm{R}_0(r)$, where $\mathrm{R}_0(r)$ is obtained by setting $Q = 0$. (Thus $\mathrm{R}_0(r)$ governs the r-equation for geodesics in the equator.) It follows that when the other first-integrals are held constant,* as Q increases, forbidden regions expand. *In fact, the strip $r_- \leq r \leq r_+$, where $\Delta \leq 0$, is always in a allowed*[4] *region; so elsewhere, as Q increases, $\mathrm{R}(r)$ decreases.*

Lemma 13.5 *For time-like geodesics, $\phi(r) = er^3 + 2Mr^2 - Qr + 2MQ$, where $e = E^2 - 1$.*

1. *If $Q > 0$, then ϕ has no roots in $0 \leq r \leq 2M$. If also $e > 0$, then ϕ has exactly one negative root, hence either zero or two positive roots. If $e < 0$, ϕ has no negative roots, hence either one or three positive roots*[5].

[3] cf. [34, page 217]

[4] cf. [34, Remark 4.7.7]

[5] [34, lemma 4.7.5] has the following statement in addition to the above: For $e = 0$,

2. *If $Q < 0$, so $e > 0$ then ϕ has a unique root in $0 < r < 2M$, and either zero or two roots in $r < 0$.*

Proof of this lemma can be found in [34, page 218].

Lemma 13.6 *For null geodesics, $\phi(r) = er^3 - Qr + 2MQ$, where $e = E^2$.*

1. *If $Q > 0$, then ϕ has no roots in $0 \leq r \leq 2M$. If also $e > 0$, then ϕ has exactly one negative root, hence either zero or two positive roots. For $e = 0$, ϕ has one real positive root $r = 2M$.*

2. *As for time-like geodesics.*

Proof. 1. For $e > 0$, proof is the same as for time-like geodesics. For $e = 0$ direct solution of the equation $-Qr + 2MQ = 0$ gives $2M$.

2. As for time-like geodesics.

□

Lemma 13.7 *For space-like geodesics $\phi(r) = er^3 - 2Mr^2 - Qr + 2MQ$, where $e = E^2 + 1$, ϕ has exactly one negative root, hence either zero or two positive roots.*

Proof. For $r < 0$ the signs for Descartes' rule are - - + +, so there is a unique negative root. □

The ambiguities 0/2 and 1/3 in the preceding lemmas can be settled precisely. The discriminant d of a real cubic polynomial determines the number of its real roots: one if $d < 0$, three if $d > 0$, and repeated roots if $d = 0$.

ϕ has no real roots. That is not true, because if $e = 0$ then we have the polynomial $2Mr^2 - Qr + 2MQ$, which has discriminant $Q(Q - 16M^2)$. That is negative only when $Q < 16M^2$.

For the time-like geodesics we find the discriminant of the polynomial ϕ to be $d = d(e, Q) = \operatorname{discrim} \phi(r) = -4Q\mathrm{f}(e, Q)$, where

$$\mathrm{f}(e, Q) = -eQ^2 + M^2(27e^2 + 18e - 1)Q + 16M^4 \,. \tag{13.22}$$

The regions in the e-Q plane where $d > 0,\ d = 0$, or $\ d < 0$, have to be found. Let $\beta = \beta(e) = 27e^2 + 18e - 1$. Then $\mathrm{f} = 0$ for

$$Q_{\pm}(e) = \frac{M^2\left(\beta \pm \sqrt{\beta^2 + 64e}\right)}{2e} \,. \tag{13.23}$$

The functions (13.23) are real only when $\beta^2 + 64e \geq 0$, which always holds if $e > 0$. The factorization

$$\beta^2 + 64e = \left(27e^2 + 18e - 1\right)^2 + 64e = (e + 1)\,(9e + 1)^3 \tag{13.24}$$

demonstrates that $\beta^2 + 64e > 0$ iff $e > -1/9$. The zero at $e = -1$ can be neglected since $Q < 0$ there ([34, chapter 4]). Thus the explicit formula emerges:

$$Q_{\pm}(e) = \frac{M^2[27e^2 + 18e - 1 \pm (e + 1)^{1/2}(9e + 1)^{3/2}]}{2e} \,. \tag{13.25}$$

Finally, the functions $Q_-(e),\ Q_+(e)$ on $e \geq -1/9$ will be examined. They have the same value at $e = -1/9$ $(12M^2)$, but thereafter they differ considerably. For Q_+, solving the equation $\mathrm{f} = 0$, where f is introduced by the equation (13.22), we define $Q_+(0) = 16M^2$. For $e \gg 1$, $Q_+(e) \sim \beta(e)/e \sim M^2(27e{+}18)$, so Q_+ becomes almost linear (see figure 13.1).

However, Q_- approaches $+\infty$ as $e \to 0$ from the left. This is clear from[6]

$$(Q_+ + Q_-)/2 = \frac{1}{2}\frac{M^2(27e^2 + 18e - 1)}{e} \,. \tag{13.26}$$

since Q_+ is bounded near $e = 0$. For $e < 0$, $Q_-(e) > Q_+(e)$.

$Q_-(e)$ is always negative for $e > 0$, approaching $-\infty$ when $e \to 0$, and approaching 0 when $e \to +\infty$.

[6] cf. [34, p. 219]

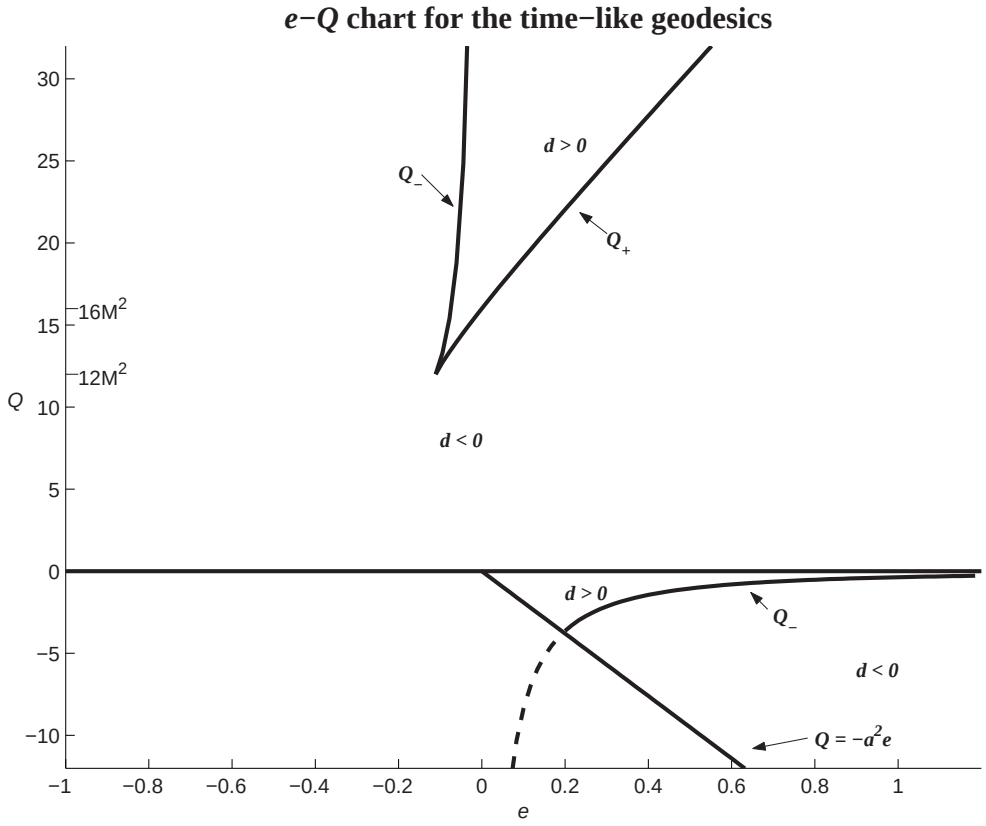

Figure 13.1: The sign of $d(e, Q) = \text{discrim}(\phi, r)$ on the relevant portion of the e-Q plane for the time-like geodesics is showed on this e-Q *chart*. If $d(e, Q) < 0$, then in the r-L plot determined by (e, Q), the curve $\mathrm{R} = 0$ has only one vertical tangent in addition to those at $(r_\pm, L_\pm)$. When $d > 0$ there are three such points. Repeated roots occur when $d = 0$. (In this plot $a = \sqrt{19}$.)

There are three restrictions for a point of the e-Q plane to correspond to an r-L plot:

1. $e \geq -1$, because $e = E^2 - 1$,
2. $Q > 0$ if $e < 0$, because vortical geodesics have escape energy,
3. $Q \geq -a^2 e$ if $e > 0$, by Carter's inequality (see [34, chapter 4]).

Therefore in figure 13.1 the third quadrant is irrelevant, and so is the area in the fourth quadrant below the line $Q = -a^2 e$.

For the null geodesics the discriminant of the polynomial ϕ is $d = d(e, Q) = \text{discrim}\,\phi(r) = -4eQ^2\mathrm{f}(e, Q)$, where

$$\mathrm{f}(e, Q) = -Q + 27M^2 e\,. \tag{13.27}$$

Again, we will find the region in the e-Q plane where $d > 0$, $d = 0$ and $d < 0$. The solution of equation $\mathrm{f} = 0$ is

$$Q = 27M^2 e\,, \tag{13.28}$$

which is a real-valued linear function (see figure 13.2).

There are two restrictions or the point of the e-Q plane to correspond to an r-L plot:

1. $e \geq 0$, since $e = E^2$; and
2. $Q \geq -a^2 e$, by Carter's inequality.

Thus in figure 13.2 the region in fourth quadrant below the line $Q = -a^2 e$ is irrelevant.

For the space-like geodesics the discriminant of the polynomial ϕ is, as for time-like geodesics, $d = d(e, Q) = \text{discrim}(\phi r) = -4Q\mathrm{f}(e, Q)$, but this time

$$\mathrm{f}(e, Q) = -eQ^2 + M^2(27e^2 - 18e - 1)Q - 16M^4\,. \tag{13.29}$$

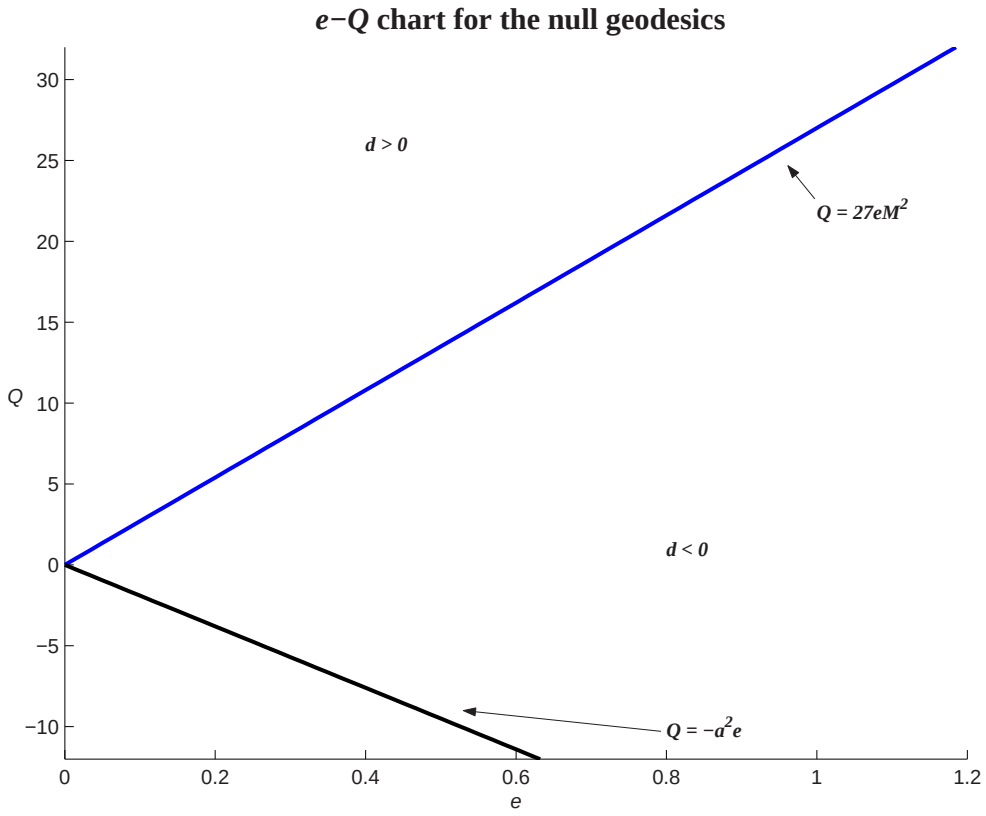

Figure 13.2: This *e-Q chart* shows the sign of $d(e, Q) = \text{discrim}(\phi, r)$ on the relevant portion of the *e-Q* plane for the null geodesics. When $d(e, Q) < 0$, then in the r-L plot determined by (e, Q) the curve $\mathrm{R} = 0$ has only one vertical tangent except those at $(r_\pm, L_\pm)$. When $d > 0$ there are three such points. Repeated roots occur when $d = 0$. (In this plot $a = \sqrt{19}$.)

As before, our goal is to find the regions in the e-Q plane where $d > 0$, $d = 0$, $d < 0$, respectively. This time, let $\beta = 27e^2 - 18e - 1$. Again we solve the equation f $= 0$. In this case, the solution is (cf. equation (13.23))

$$Q_{\pm}(e) = \frac{M^2\left(\beta \pm \sqrt{\beta^2 - 64e}\right)}{2e}\,. \tag{13.30}$$

These functions are real only when $\beta^2 - 64e \geq 0$. The factorization

$$\beta^2 - 64e = \left(27e^2 - 18e - 1\right)^2 - 64e = (e-1)\,(9e-1)^3 \tag{13.31}$$

shows that $\beta^2 - 64e > 0 \Leftrightarrow e > 1$. Thus we get the explicit formula:

$$Q_{\pm}(e) = \frac{M^2[27e^2 - 18e - 1 \pm (e-1)^{1/2}(9e-1)^{3/2}]}{2e}\,. \tag{13.32}$$

At $e = 1$ the functions $Q_-(e)$, $Q_+(e)$ have the same value, $4M^2$, but thereafter are quite different. For $e \gg 1$, $Q_+(e) \sim \beta(e)/e \sim M^2(27e - 18)$, so as figure 13.3 shows, Q_+ becomes almost linear.

For $e \geq 1$, $Q_-(e)$ is always positive, approaching 0 as $e \to \infty$. (Note that $Q_-(e) > Q_+(e)$ for $e > 1$.)

For the point of the e-Q plane to correspond to an r-L plot the following inequalities must hold:

1. $e \geq 1$, since $e = E^2 + 1$, and

2. $Q \geq -a^2 e$, by Carter's inequality.

Thus, as before, the area in the fourth quadrant below the line $Q = -a^2 e$ is irrelevant, as is the region $e < 1$.

Remark 2 *Summary: The number of zero the discriminant polynomial* $\phi(r) = er^3 + 2M\delta_1 r^2 - Qr + 2MQ$ *has determines the qualitative character of* r-L. *For given* e *and* Q, *the sign of a second discriminant,* $d(e, Q) =$ discrim(ϕ, r) *determines this number. Therefore* d *becomes a function on the*

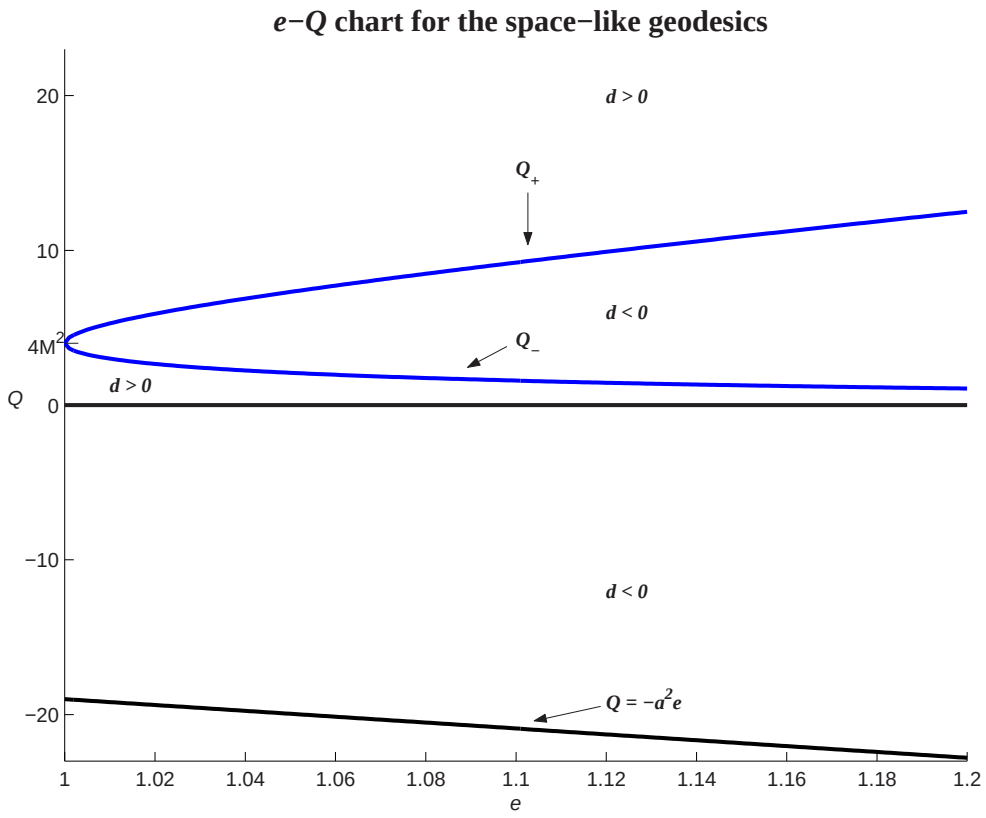

Figure 13.3: This *e-Q chart* shows the sign of $d(e, Q) = \text{discrim}(\phi, r)$ on the relevant portion of the e-Q plane for the space-like geodesics. When $d(e, Q) < 0$, then in the r-L plot determined by (e, Q) the curve R $= 0$ has only one vertical tangent apart from those at $(r_\pm, L_\pm)$. There are three such points for $d > 0$. Repeated roots occur when $d = 0$. (In this plot $a = \sqrt{19}$.)

e-Q chart in figures 13.1, 13.2 and 13.3 (for time-like, null and space-like geodesics respectively). The regions $d > 0$ and $d < 0$ in the chart are separated by graphs of the functions

$$Q_\pm = \frac{M^2}{2e}\left[27e^2 + 18e - 1 \pm (e+1)^{1/2}(9e+1)^{3/2}\right] \quad \textit{for time-like geodesics,} \tag{13.33}$$

$$Q = 27M^2 e \quad \textit{for null geodesics,} \tag{13.34}$$

$$Q_\pm = \frac{M^2}{2e}\left[27e^2 - 18e - 1 \pm (e-1)^{1/2}(9e-1)^{3/2}\right] \quad \textit{for space-like geodesics.} \tag{13.35}$$

Hence, for the time-like geodesics, if $e > 0$, the negative root of ϕ is its only root when $0 < Q < Q_\pm$, but when $Q > Q_\pm$, then ϕ has three roots. These roots are all simple, so they represent the vertical tangents in the r-L plot determined by e and Q. Similarly, if $e < 0$, the negative root of ϕ is its only root unless both $-1/9 < e \leq 0$ and $Q_+ < Q < Q_-$ hold[7]*, giving three roots. If $Q < 0$ the conditions giving three roots of ϕ are $Q > -a^2 e$ and $Q > Q_-$.*

For the null geodesics, we can see from the chart that when $-a^2 e < Q < 27M^2 e$ the negative root of ϕ is its only root, but if $Q > 27M^2 e$, then ϕ has three roots.

For the space-like geodesics, ϕ has three roots when $0 < Q < Q_-$ or $Q > Q_+$ otherwise, that is for $-a^2 e < Q < 0$ and for $Q_- < Q < Q_+$, the negative root is its only root.

Lemma 13.8 *For $e \neq 0$ and $Q > 0$, let $L_0 = L_{\rm v}(r_0)$, where r_0 is a root of $\phi(r)$. Then:*

1. R *= 0 has a vertical tangent at $(r_0, L_0) \Leftrightarrow r_0$ is a simple root of $\phi(r)$; and*

[7] cf. [34, Remark 4.7.6]

2. *(r_0, L_0) is a critical point of the function $\mathrm{R}(r, L) \Leftrightarrow r_0$ is a repeated root of $\phi(r)$. If $\phi''(r_0) > 0$, then (r_0, L_0) is a saddle point, with adjacent allowed regions along the midline, and if $\phi''(r_0) < 0$, then (r_0, L_0) is an isolated maximum point, surrounded by a forbidden region.*

For the proof of this lemma see [34, section 4.7].

Proposition 13.9 *For $Q > 0$, consider the r-L plot of (e, Q) where $d(e, Q) = 0$ (so $e \geq -1/9$ and $Q = Q_{\pm}(e) > 0$). Excluding $e = -1/9$ and[8] $e = 0$, $\mathrm{R} = 0$ has a unique vertical tangent point (r_1, L_1) with $r_1 \neq \mathrm{R}_{\pm}$ and a unique critical point (r_2, L_2), both necessary on the midline, so $L_i = L_{\mathrm{v}}(r_i)$. There are three cases:*

1. *If $e > 0$ and $Q = Q_+(e)$, then $r_1 < 0 < 2M < r_2$. Further, (r_2, L_2) is a saddle point of the function $\mathrm{R}(r, L)$, with adjacent allowed regions along the midline.*

2. *If $-1/9 < e < 0$ and $Q = Q_+(e)$, then $2M < r_2 < r_1$, in fact,*

$$2M < r_2 < \frac{2M}{3|e|} < r_1 < \frac{2M}{|e|}\,, \tag{13.36}$$

   and (r_2, L_2) is a saddle point, as above.

3. *If $-1/9 < e < 0$ and $Q = Q_-(e)$, then $2M < r_1 < r_2$, in fact,*

$$2M < r_1 < \frac{2M}{3|e|} < r_2 < \frac{2M}{|e|}\,, \tag{13.37}$$

   and (r_2, L_2) is an isolated $\mathrm{R} = 0$ point in a forbidden region.

Proof. See [34, page 222]. □

To find the critical points (r_2, L_2) in proposition 13.9 we know that r_2 is a solution of both quadratic equations

$$Mr^2 - Qr + 3MQ = 0\,, \qquad \text{and} \qquad er^2 - M(3e-1)r - 4M^2 = 0\,, \tag{13.38}$$

[8] [34, proposition 4.7.8] does not exclude $e = 0$.

which come from eliminating e and Q, respectively, from the equations $\phi(r) = 0$, $\phi'(r) = 0$. Then, by the general midline formula (13.20), $L_2 = L_{\mathrm{v}}(r_2) = 2MaE/(2M - r_2)$.

For $e = 1$ and $d = 0$ we have a double root at $r = 4M$, which is a saddle point, since $\phi''(4M) > 0$.

13.5 First-integrals and orbits

The most important question about a time-like geodesic is whether or not it has escape energy (determined by the sign of $e = E^2 - 1$). Next (also for a null and space-like geodesic) is the sign of the Carter constant Q. This section deals with the "standard" case $Q > 0$. Such geodesics do not reach $r = 0$ and have θ motion oscillating about $\pi/2$.

Depending on shape of allowed and forbidden regions for slow black holes we distinguish four cases. "Continents" configuration has two large forbidden areas – one for direct and one for retrograde orbits. In "barrier" configuration these two "continents" are joined and form a barrier preventing geodesics to fall in a black hole. "Bay" configuration has an allowed region in a shape of bay, and in "lake" configuration this bay is reduced to a "lake" – an allowed region surrounded by a forbidden area.

13.5.1 Continents configuration

Perhaps the most common is case of escape energy $e > 0$ and moderate Carter constant $0 < Q < Q_+(e)$ ([34, section 4.8]), where $Q_+(e)$ are given precisely by the formulas in Remark 2. See figures 13.4 and 13.5 for r-L plots for the time-like geodesics, figures 13.6 and 13.7 for the null geodesics, and 13.8, 13.9, 13.10 and 13.11 for the space-like geodesics ($Q < Q_+(e)$, $Q < Q_-(e)$). These plots are distinguished by two "continents" on the $r > 0$ side. There the situation

is similar to Newtonian gravitation. Particles falling from $r = +\infty$ have flyby orbit if their angular momentum $|L|$ is large, those with smaller $|L|$ continue through the horizons.

In the strip $0 < r < 2M$ there are many bound orbits, both direct and retrograde. No particle, no matter how high is its energy, can reach $r = 0$ in $r > 0$ region.

13.5.2 Barrier configuration

As Q increases from small values, the continents N and S become larger. At the critical point of the function $\mathrm{R}(r, L)$ they meet ([34, section 4.8]) and then they merge into a single *barrier* as shown in figures 13.12, 13.13, 13.14, 13.15, 13.16 and 13.17. Hence the large values of the Carter constant Q provide the complete protection against a crush into a black hole, no matter how small angular momentum L may be.

13.5.3 Bay configuration

If a particle has less than escape energy, all orbits are bound and none meet $r < 0$ ([34, section 4.8]). Figures 13.18 and 13.19 show r-L plots for this case.

Comparison with figures 13.4 and 13.5 shows that for the same value of Q, the decrease of energy from $e > 0$ to $e < 0$ (that is, from $E > 1$ to $E < 1$) has enclosed the large allowed region on the $r > 0$ side.

For fixed Q, there are both retrograde and direct orbits in the exterior when $e < 0$ is near zero, but for e nearer -1 all bound orbits disappear. (See [34, section 4.8].)

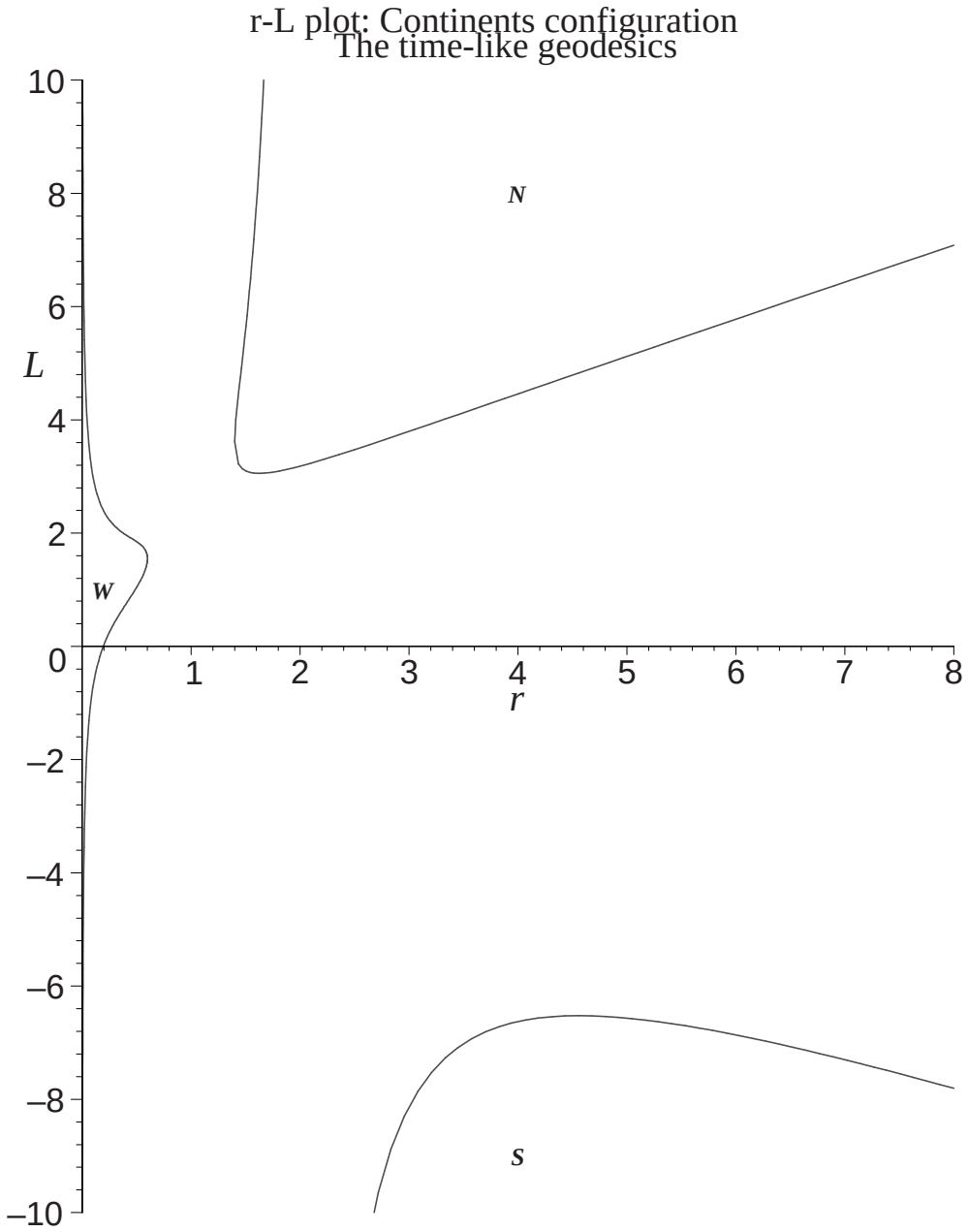

Figure 13.4: Plot for a time-like geodesic with escape energy $e = 0.4$ and Carter constant $Q = 1$. Forbidden regions are the continents W, N and S. On each horizontal line $L = \text{const}$, the maximal segments on which $R \geq 0$ give ranges of $r(\tau)$ for a geodesics with that angular momentum. Most particles infalling from $r = +\infty$ have flyby orbit. (Additional parameters: $M = 1,\ a^2 = 0.84$.)

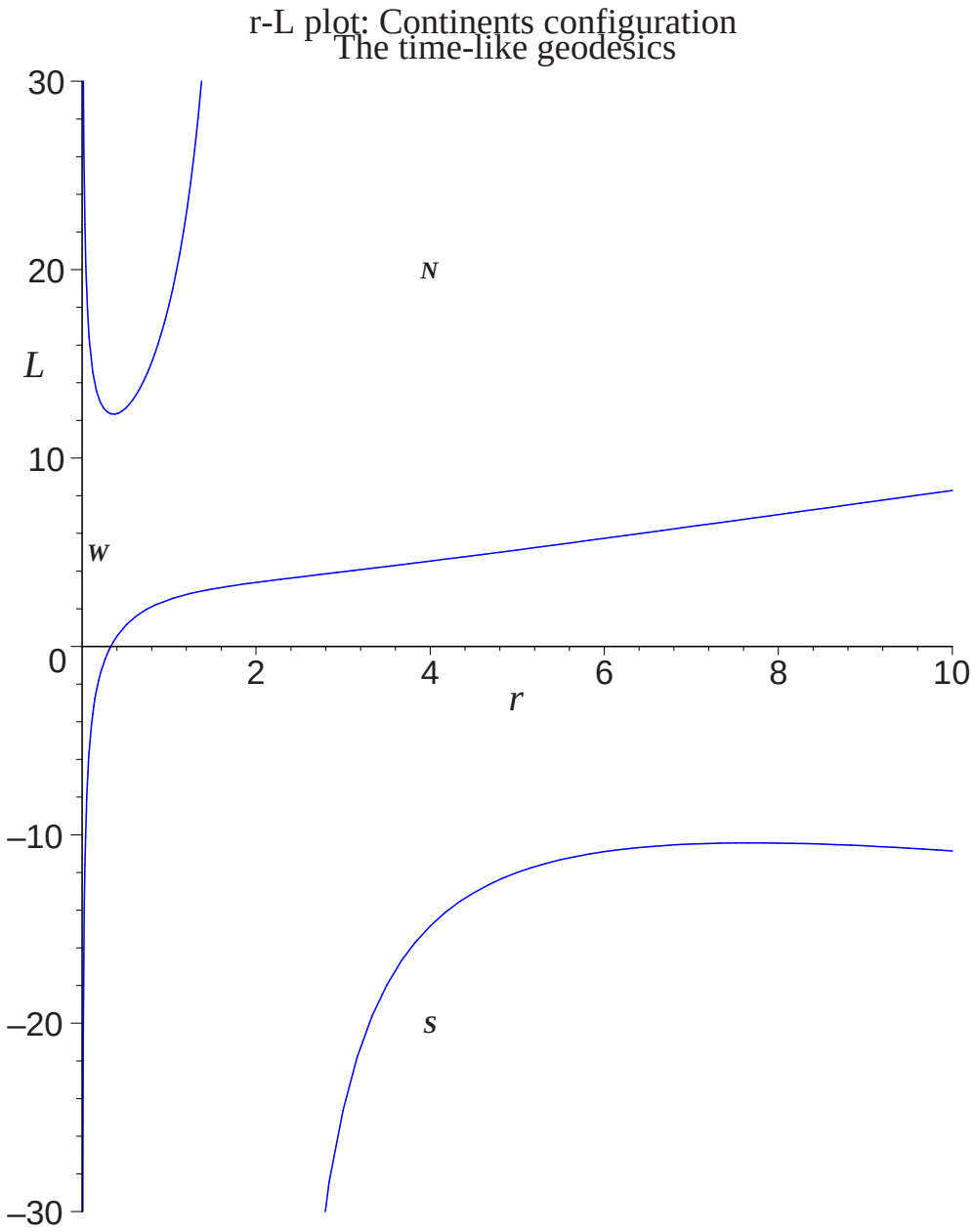

Figure 13.5: Plot for a time-like geodesic with escape energy $e = 0.4$ and Carter constant $Q = 1$. In a fast black hole forbidden regions W and N are joined (there is only one vertical tangent–in $r < 0$ region, see lemma 13.8). On each horizontal line $L = \text{const}$, the maximal segments on which $R \geq 0$ give ranges of $r(\tau)$ for a geodesics with that angular momentum. Most particles infalling from $r = +\infty$ have flyby orbit. (Additional parameters: $M = 1,\ a^2 = 19$.)

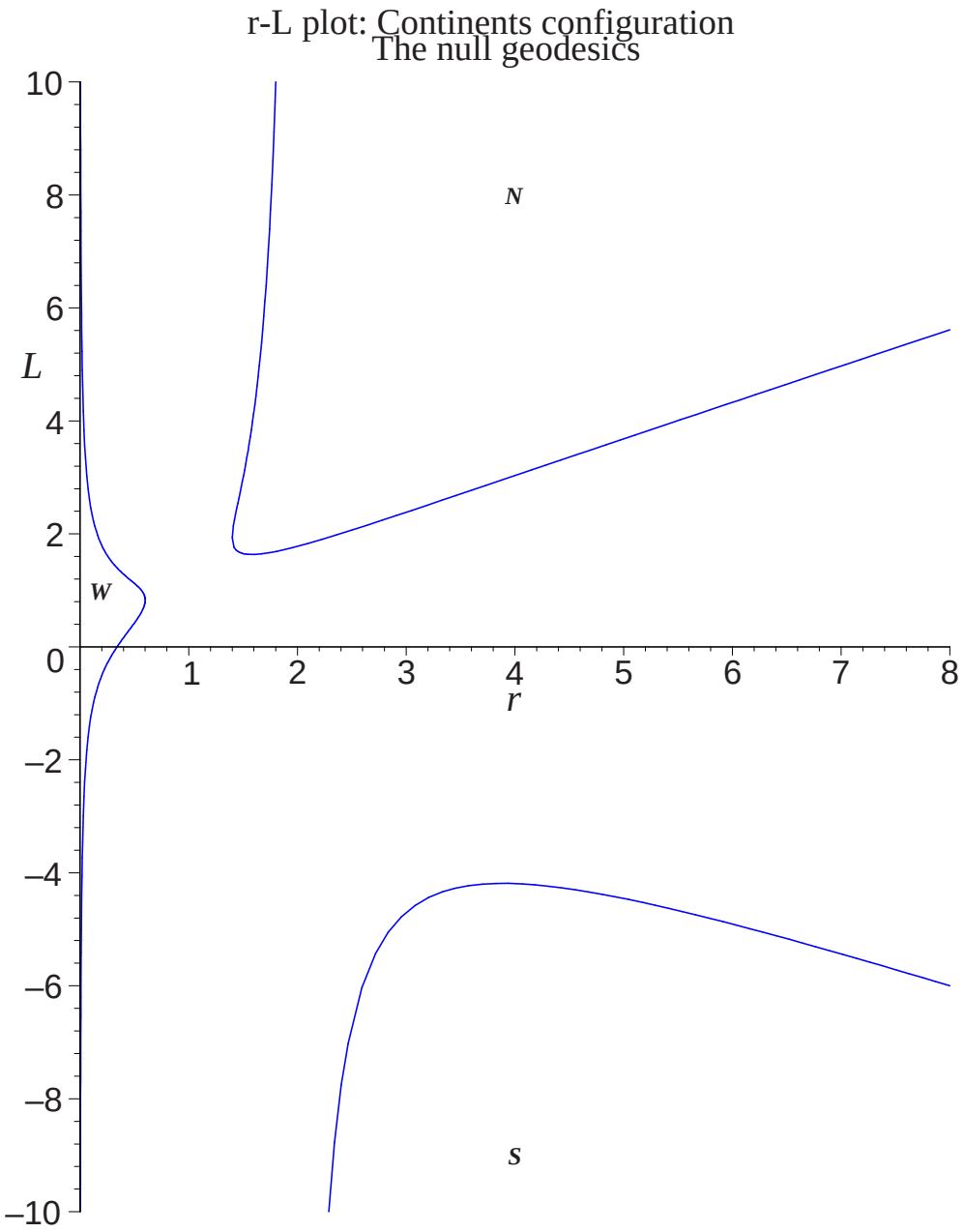

Figure 13.6: Continents configuration: an r-L plot for a null geodesic with escape energy $e = 0.4$ and Carter constant $Q = 1$. Forbidden regions are the continents W, N and S. On each horizontal line $L = \text{const}$, the maximal segments on which $R \geq 0$ give ranges of $r(\tau)$ for a geodesics with that given angular momentum. Most particles infalling from $r = +\infty$ have flyby orbit. (Additional parameters: $M = 1,\ a^2 = 0.84$.)

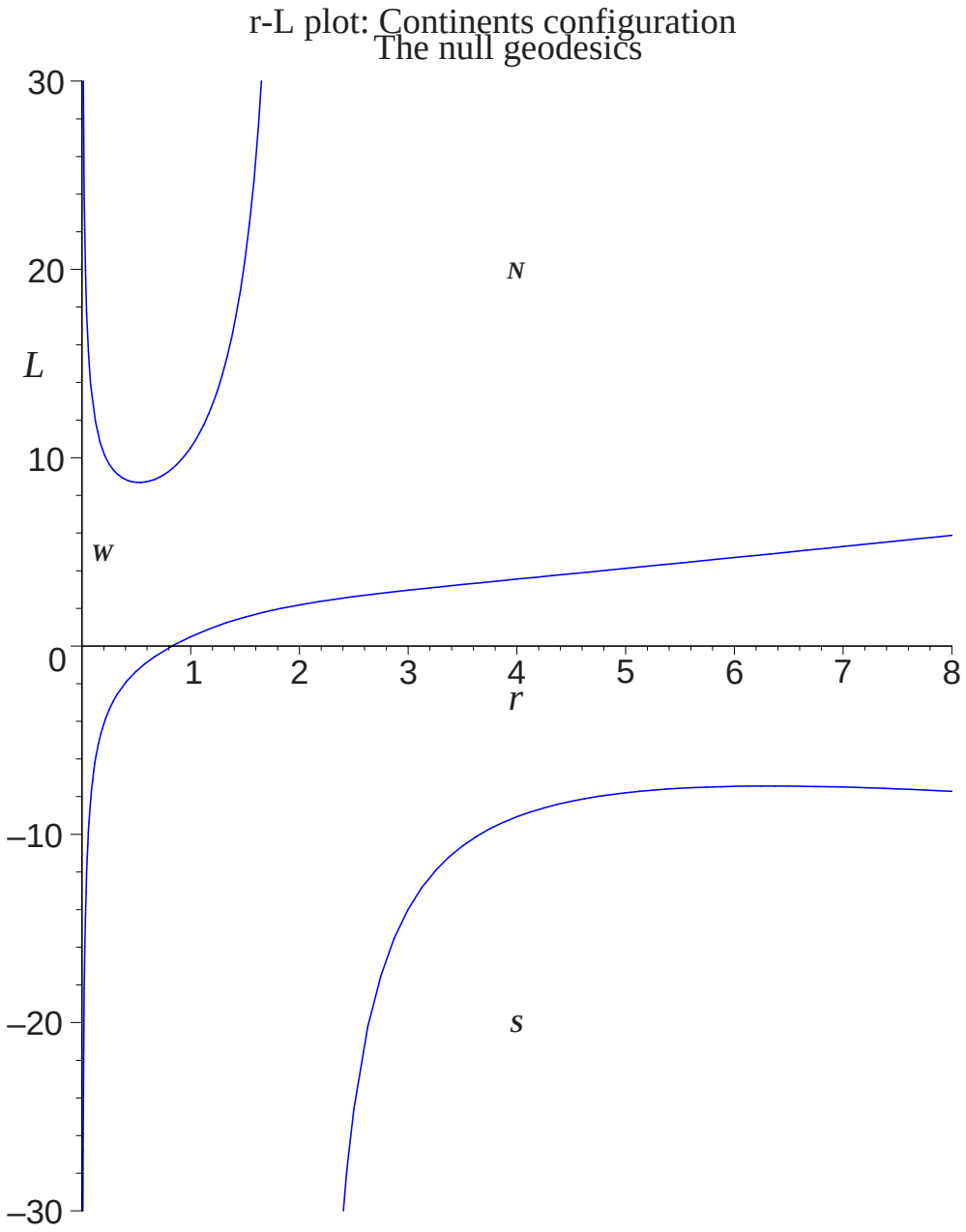

Figure 13.7: Continents configuration: an r-L plot for a null geodesic with escape energy $e = 0.4$ and Carter constant $Q = 1$. The continents W, N are joined and together with continent S are forbidden for a photon to enter. On each horizontal line $L = \text{const}$, the maximal segments on which $R \geq 0$ give ranges of $r(\tau)$ for a geodesics with that given angular momentum. Most particles infalling from $r = +\infty$ have flyby orbit. (Additional parameters: $M = 1,\ a^2 = 19$.)

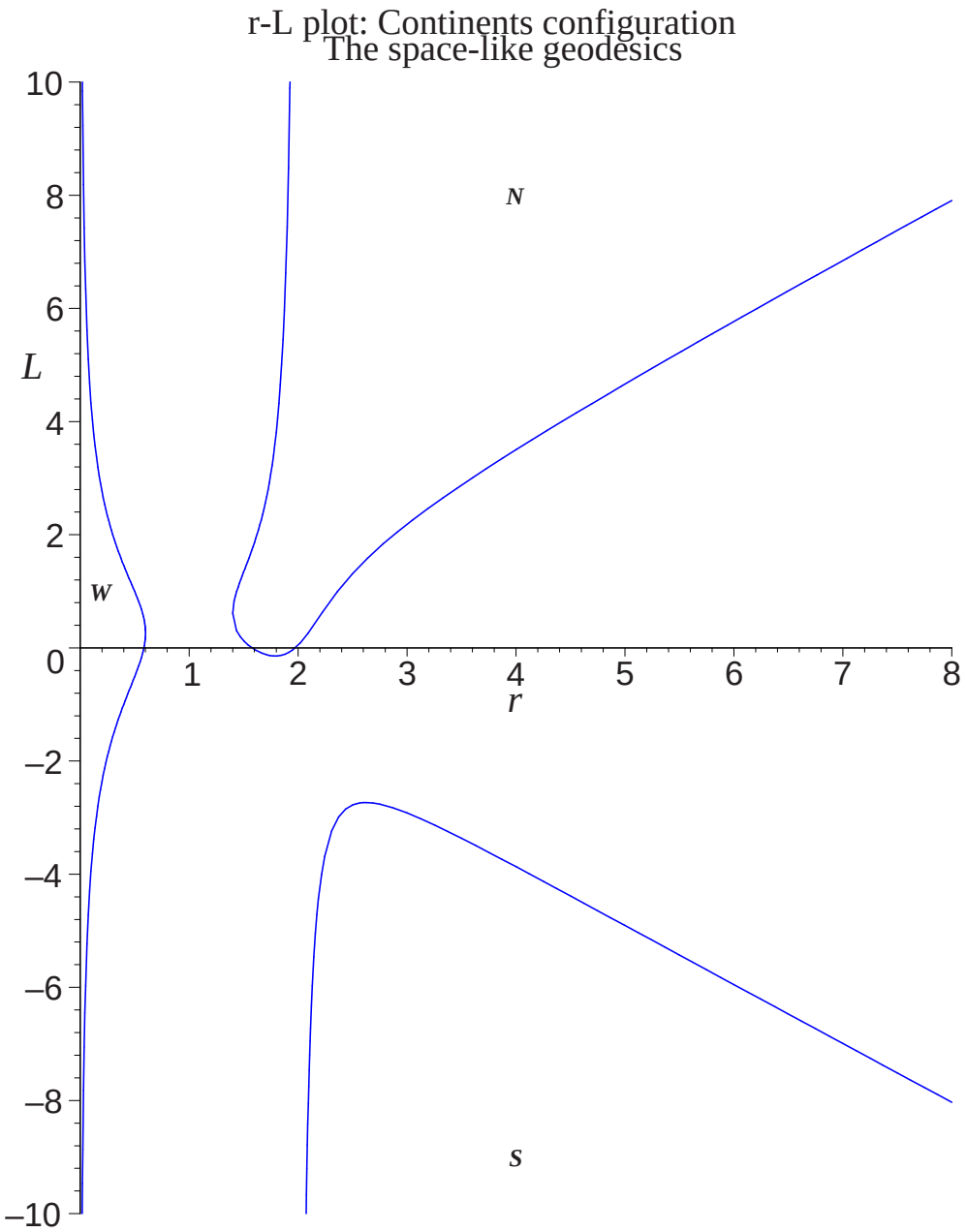

Figure 13.8: Continents configuration: an r-L plot for a space-like geodesic with escape energy $e = 1.04$ and Carter constant $Q = 5$. Forbidden regions are the continents W, N and S. On each horizontal line $L = \text{const}$, the maximal segments on which $R \geq 0$ give ranges of $r(\tau)$ for a geodesics with that angular momentum. Most particles infalling from $r = +\infty$ have flyby orbit. (Additional parameters: $M = 1,\ a^2 = 0.84$.)

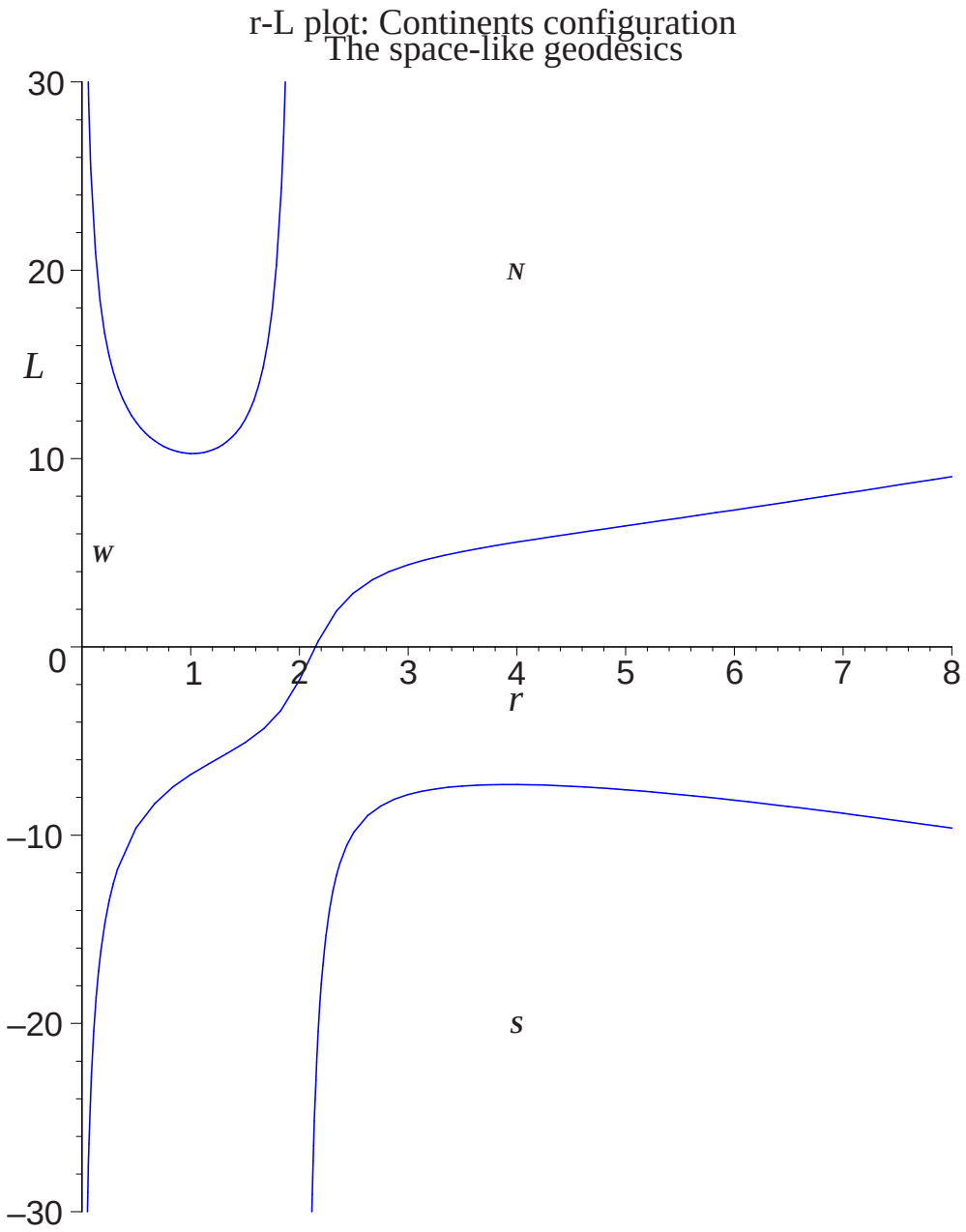

Figure 13.9: Continents configuration: an r-L plot for a space-like geodesic with escape energy $e = 1.04$ and Carter constant $Q = 5$. In a fast black hole forbidden regions W and N are joined. On each horizontal line $L = \text{const}$, the maximal segments on which $R \geq 0$ give ranges of $r(\tau)$ for a geodesics with that given angular momentum. Most particles infalling from $r = +\infty$ have flyby orbit. (Additional parameters: $M = 1,\ a^2 = 19$.)

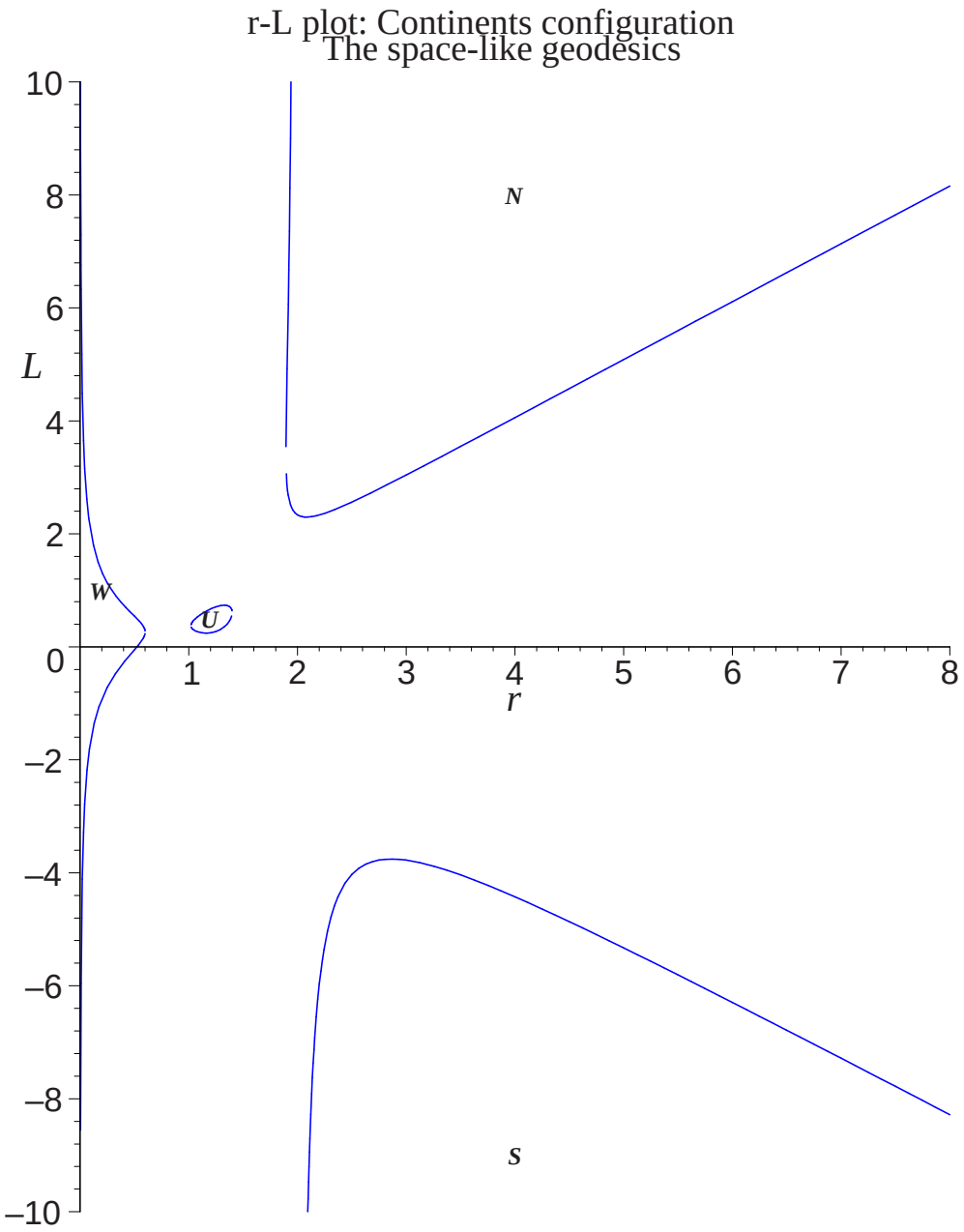

Figure 13.10: Continents configuration: an r-L plot for a space-like geodesic with escape energy $e = 1.04$ and Carter constant $Q = 1$. Forbidden regions are the continents W, N, S and the oval U. On each horizontal line $L = \text{const}$, the maximal segments on which $R \geq 0$ give ranges of $r(\tau)$ for a geodesics with that angular momentum. Most particles infalling from $r = +\infty$ have flyby orbit. (Additional parameters: $M = 1,\ a^2 = 0.84$.)

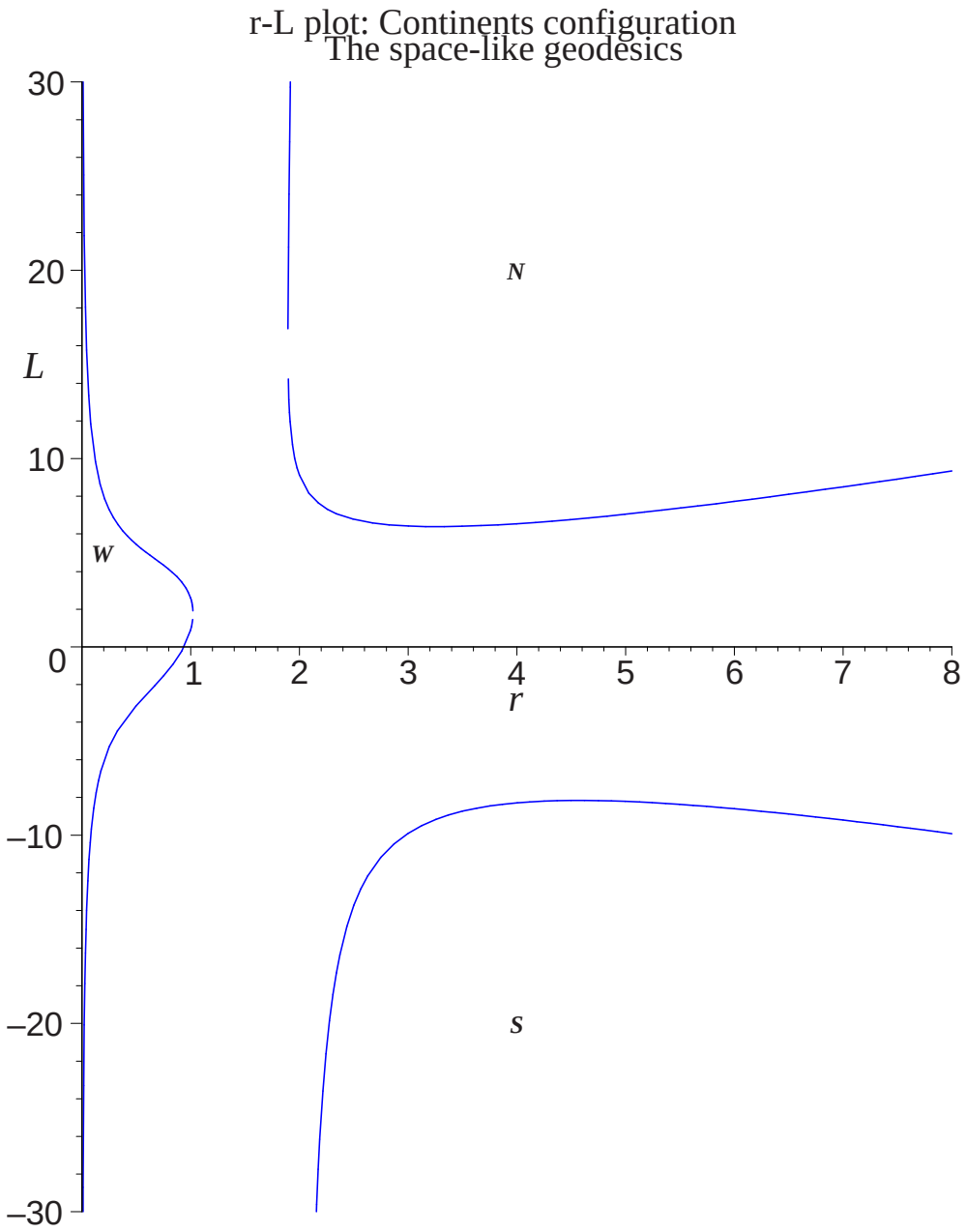

Figure 13.11: Continents configuration: an r-L plot for a space-like geodesic with escape energy $e = 1.04$ and Carter constant $Q = 1$. In a fast black hole oval U disappears. On each horizontal line $L = \text{const}$, the maximal segments on which $R \geq 0$ give ranges of $r(\tau)$ for a geodesics with that given angular momentum. Most particles infalling from $r = +\infty$ have flyby orbit. (Additional parameters: $M = 1,\ a^2 = 19$.)

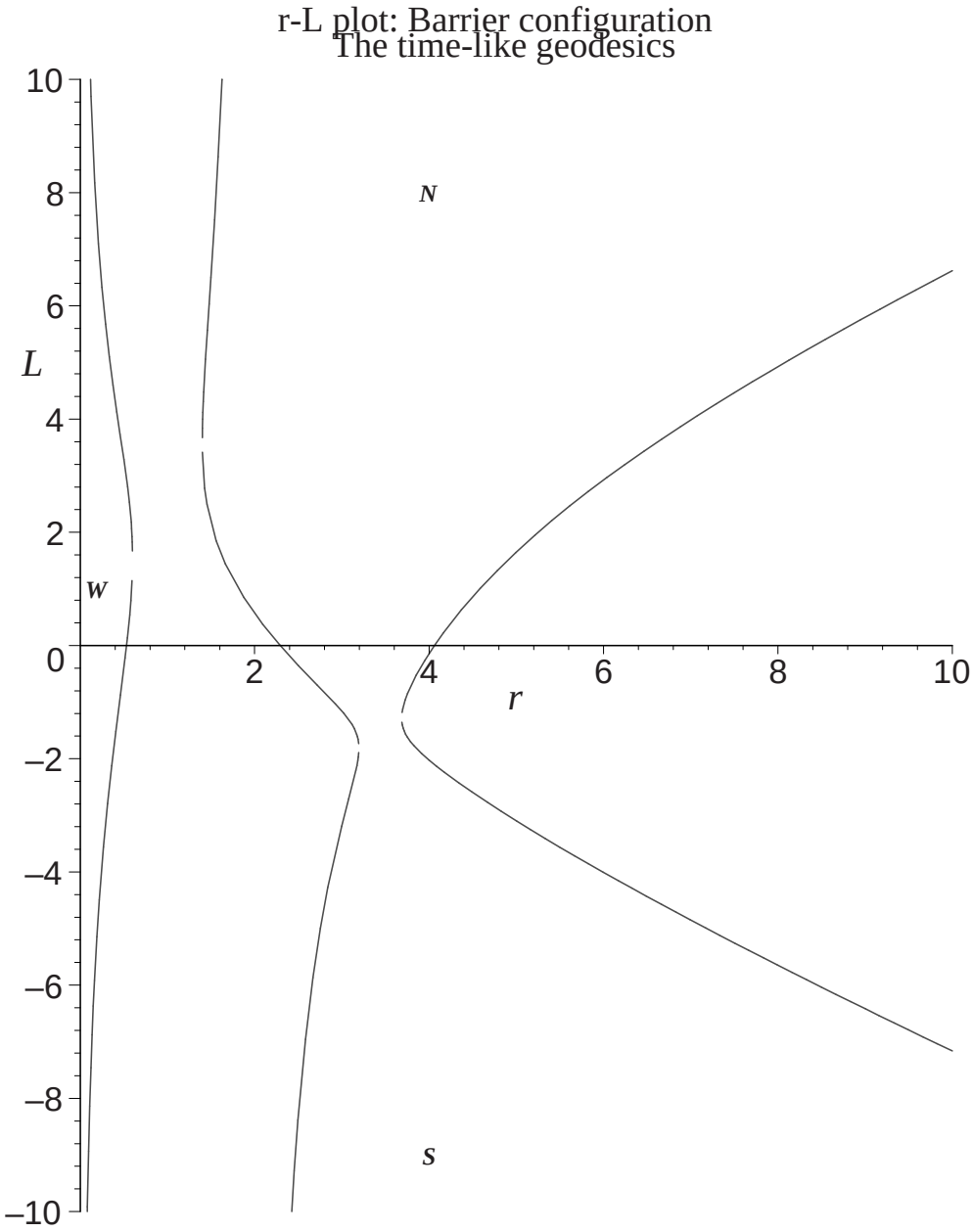

Figure 13.12: Barrier configuration: an r-L plot for a time-like geodesic with escape energy $e = 0.4$ and Carter constant $Q = 28$. Regions N and S merge, forming a barrier between $r = +\infty$ and the horizons. On each horizontal line $L = \text{const}$, the maximal segments on which $R \geq 0$ give ranges of $r(\tau)$ for a geodesics with that angular momentum. All particles infalling from $r = +\infty$ have flyby orbit. (Additional parameters: $M = 1,\ a^2 = 0.84$.)

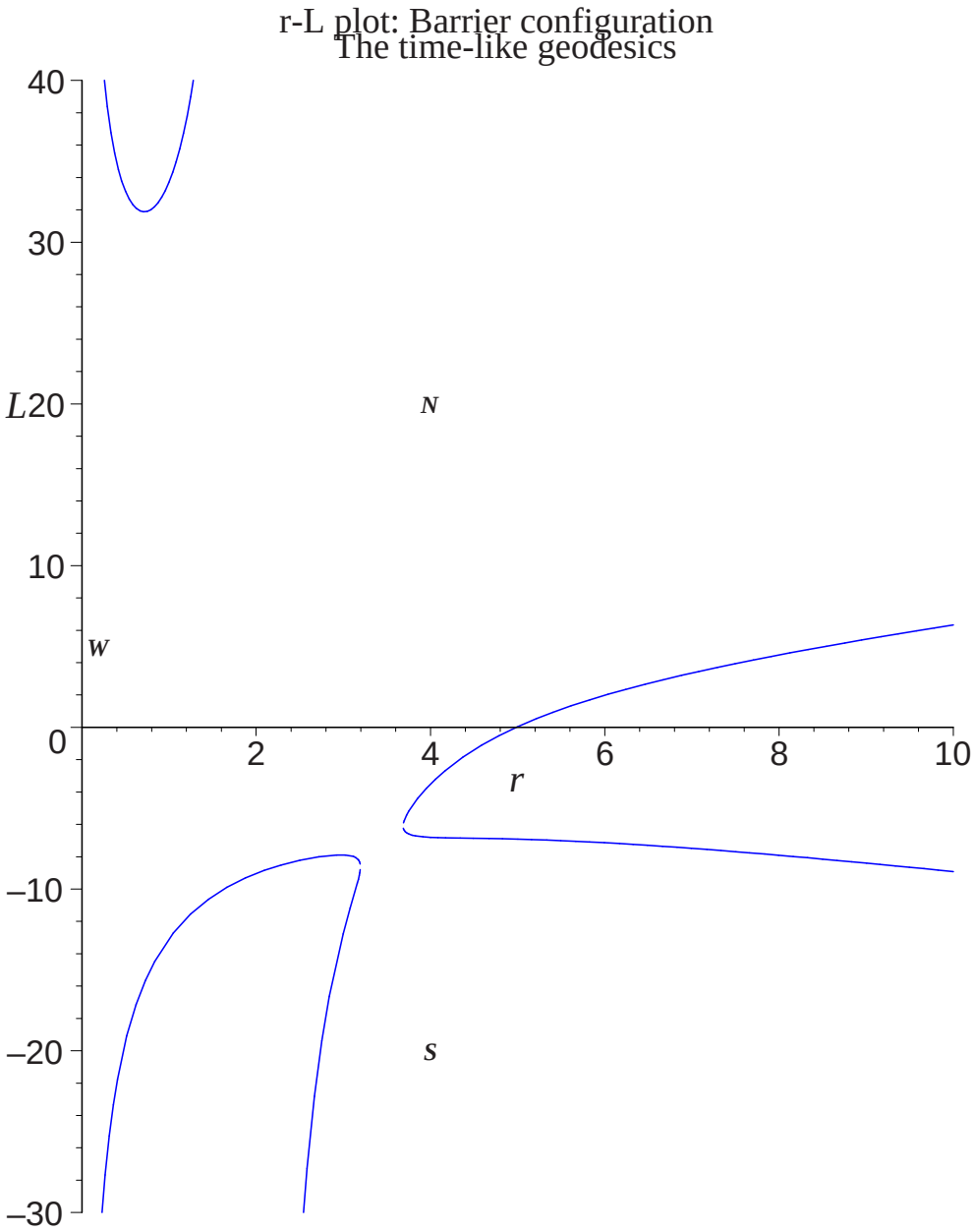

Figure 13.13: Barrier configuration: an r-L plot for a time-like geodesic with escape energy $e = 0.4$ and Carter constant $Q = 28$. Regions W, N and S merge. On each horizontal line $L = \text{const}$, the maximal segments on which $R \geq 0$ give ranges of $r(\tau)$ for a geodesics with that particular angular momentum. All particles infalling from $r = +\infty$ have flyby orbits. (Additional parameters: $M = 1,\ a^2 = 19$.)

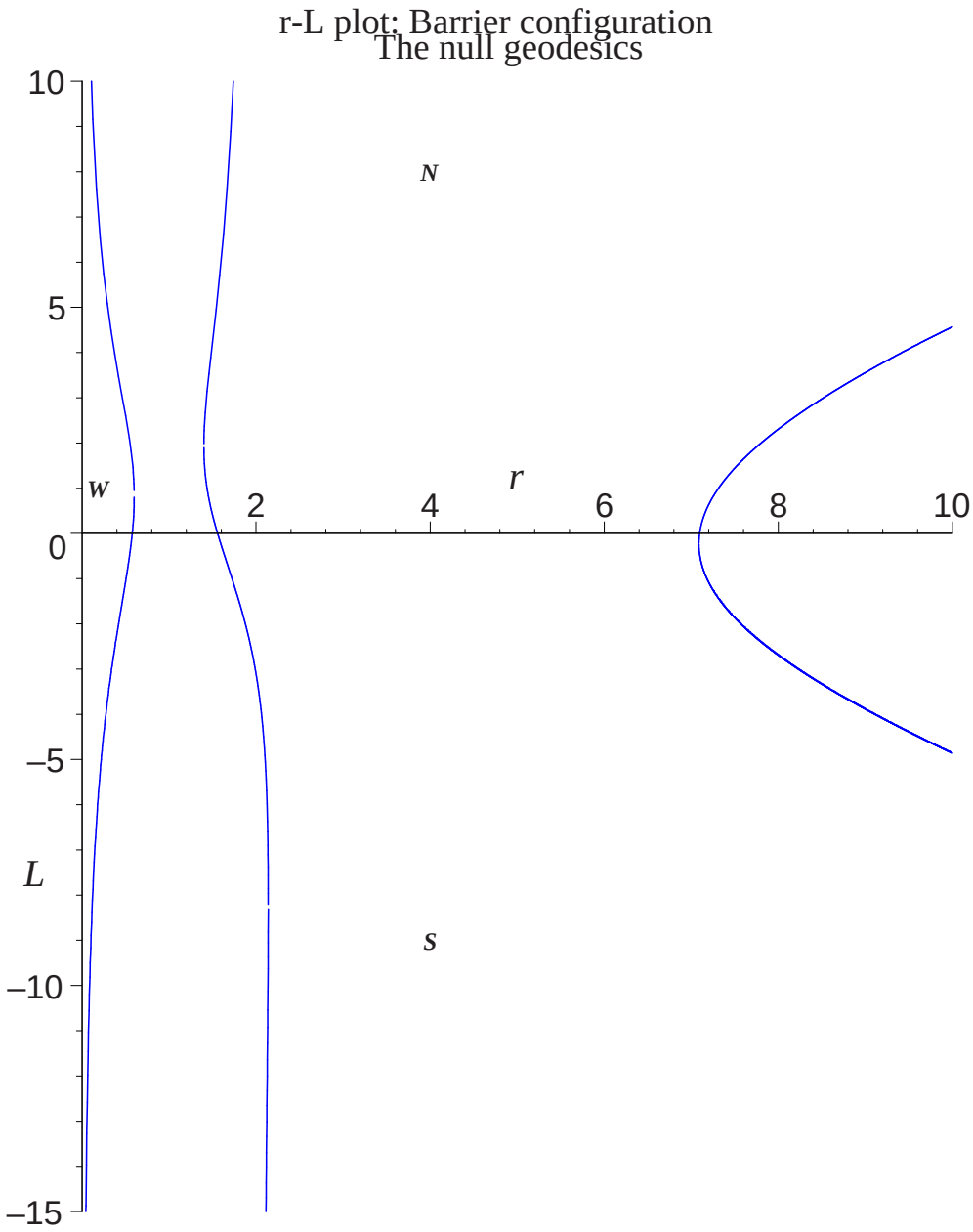

Figure 13.14: Barrier configuration: an r-L plot for a null geodesic with escape energy $e = 0.4$ and Carter constant $Q = 28$. Regions N and S merge, forming a barrier between $r = +\infty$ and the horizons. On each horizontal line $L = \text{const}$, the maximal segments on which $R \geq 0$ give ranges of $r(\tau)$ for a geodesics with that particular angular momentum. All particles falling from $r = +\infty$ have flyby orbits. (Additional parameters: $M = 1,\ a^2 = 0.84$.)

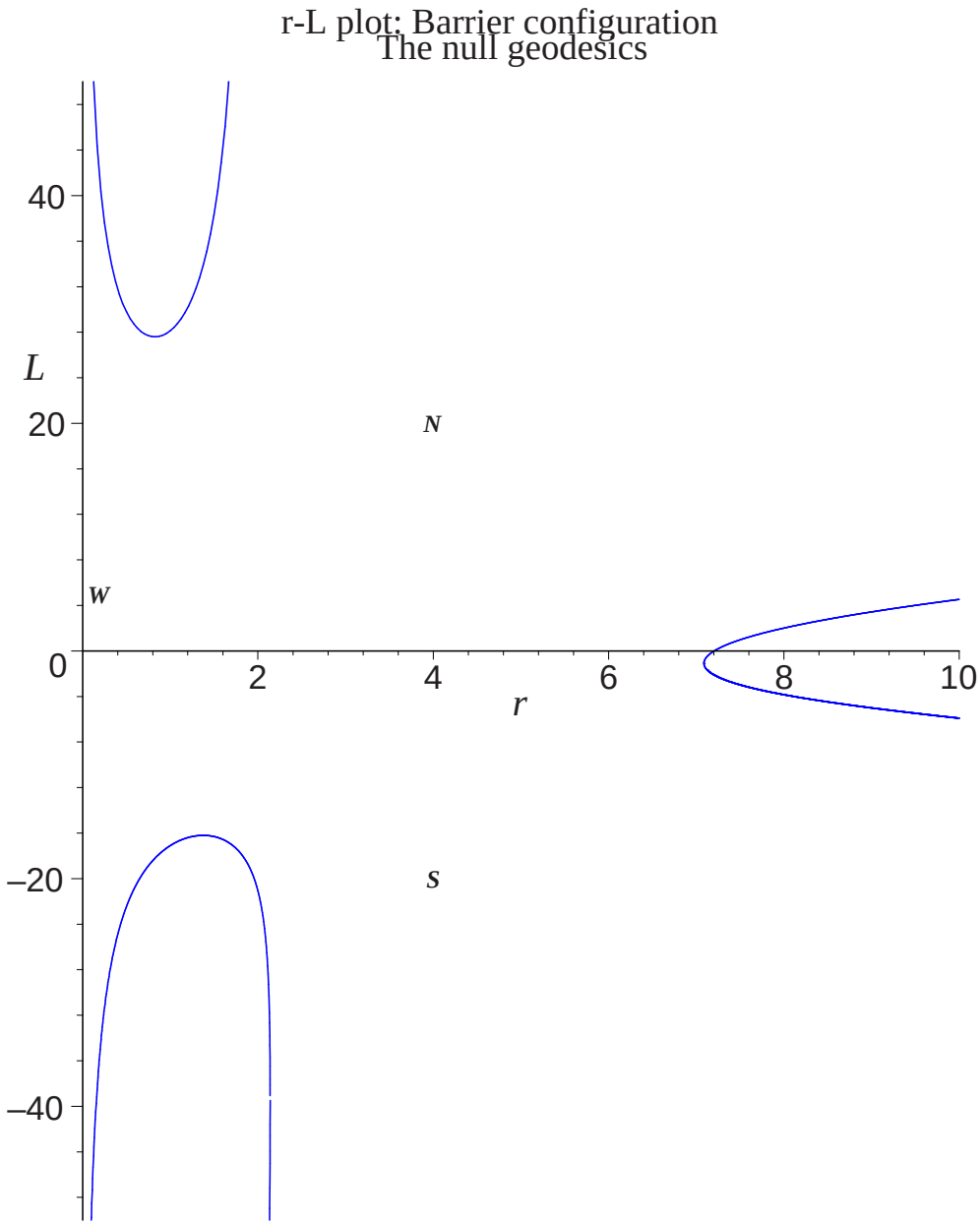

Figure 13.15: Barrier configuration: an r-L plot for a null geodesic with escape energy $e = 0.4$ and Carter constant $Q = 28$. In a fast black hole regions N, W and S merge. On each horizontal line $L = \text{const}$, the maximal segments on which $R \geq 0$ give ranges of $r(\tau)$ for a geodesics with that particular angular momentum. All particles falling from $r = +\infty$ have flyby orbit. (Additional parameters: $M = 1,\ a^2 = 0.84$.)

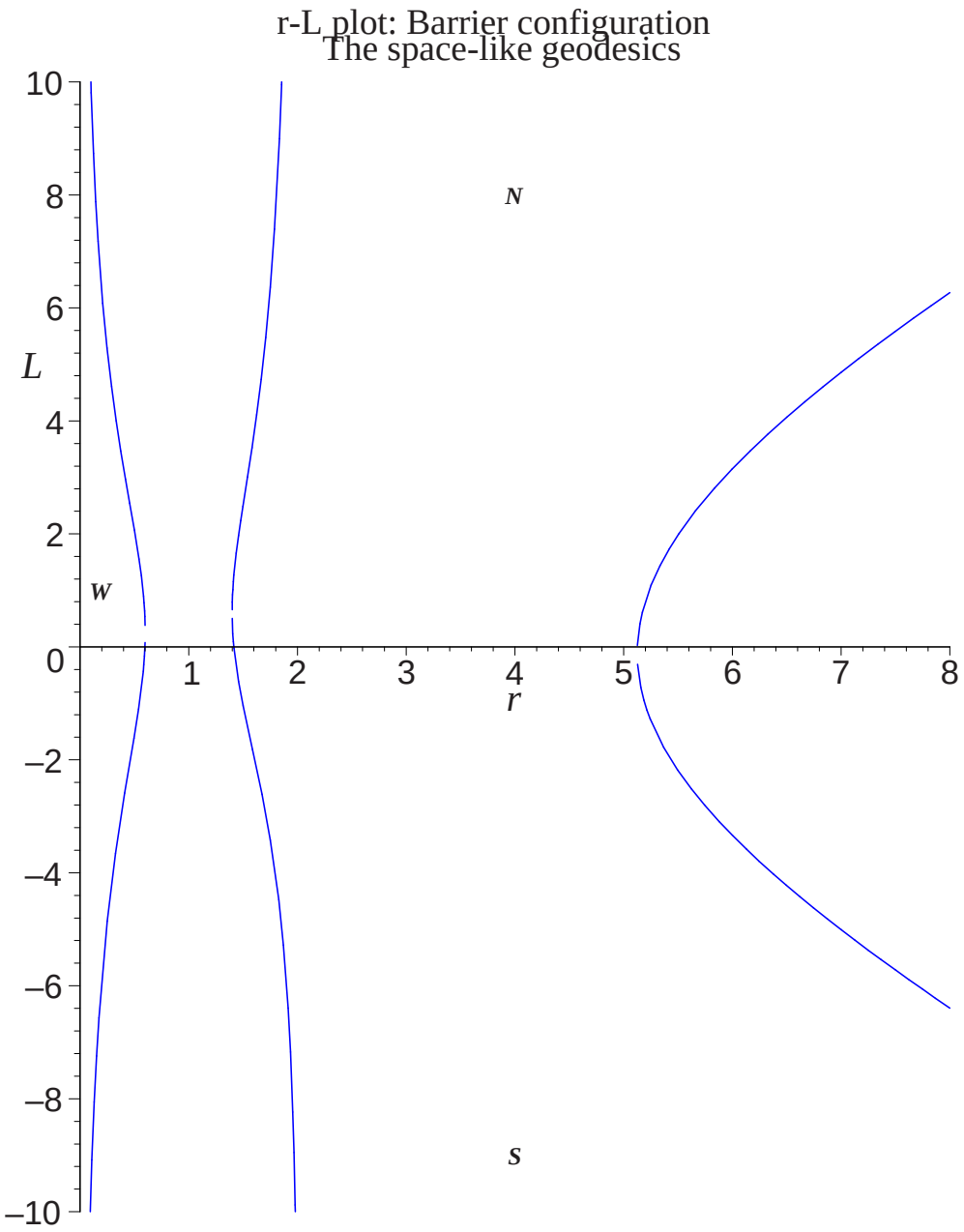

Figure 13.16: Barrier configuration: an r-L plot for a space-like geodesic with escape energy $e = 1.04$ and Carter constant $Q = 28$. Regions N and S merge, forming a barrier between $r = +\infty$ and the horizons. On each horizontal line $L = \text{const}$, the maximal segments on which $R \geq 0$ give ranges of $r(\tau)$ for a geodesics with that particular angular momentum. All particles falling from $r = +\infty$ have flyby orbits. (Additional parameters: $M = 1,\ a^2 = 0.84$.)

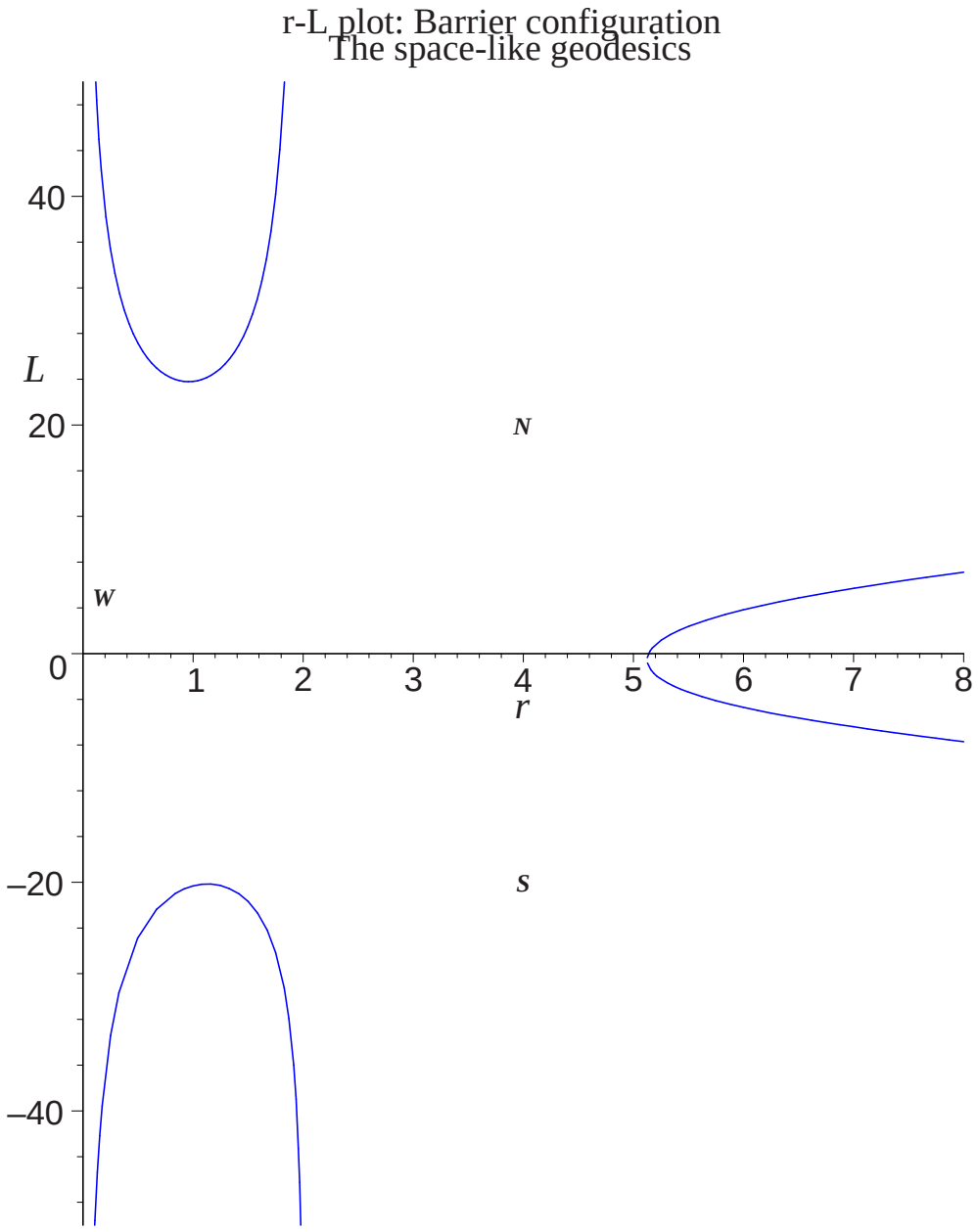

Figure 13.17: Barrier configuration: an r-L plot for a space-like geodesic with escape energy $e = 1.04$ and Carter constant $Q = 28$. Regions N, W and S merge. On each horizontal line $L = \text{const}$, the maximal segments on which $R \geq 0$ give ranges of $r(\tau)$ for a geodesics with that particular angular momentum. All particles falling from $r = +\infty$ have flyby orbits. (Additional parameters: $M = 1,\ a^2 = 19$.)

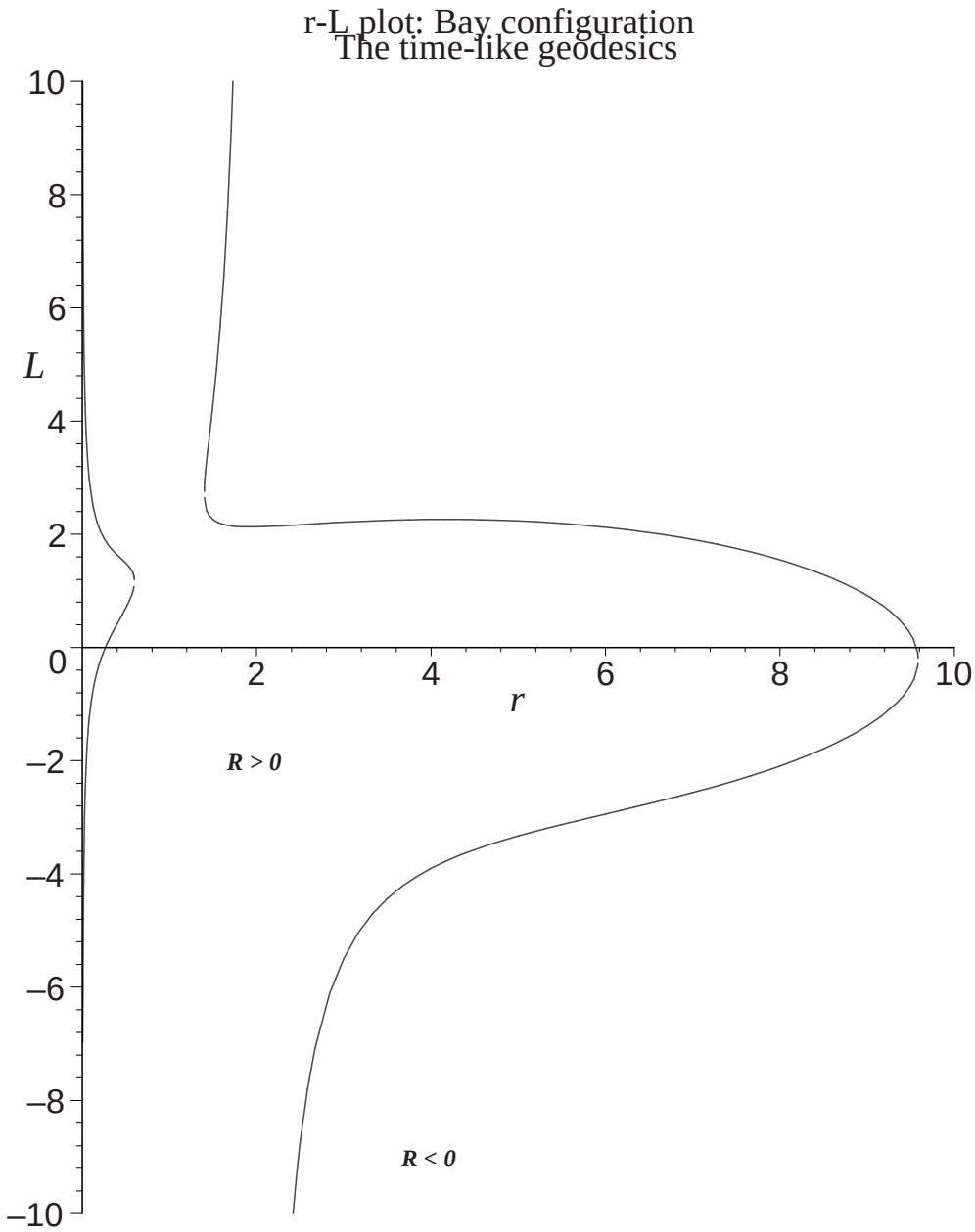

Figure 13.18: Bay configuration: an r-L plot for a time-like geodesic with escape energy $e = -0.2$ and Carter constant $Q = 1$. Forbidden regions are those with $R < 0$. For $r < r_-$ the plot still resembles the $e > 0$ case in figure 13.4. On each horizontal line $L = \text{const}$, the maximal segments on which $R \geq 0$ give ranges of $r(\tau)$ for a geodesics with that angular momentum. All orbits are bound. (Additional parameters: $M = 1,\ a^2 = 0.84$.)

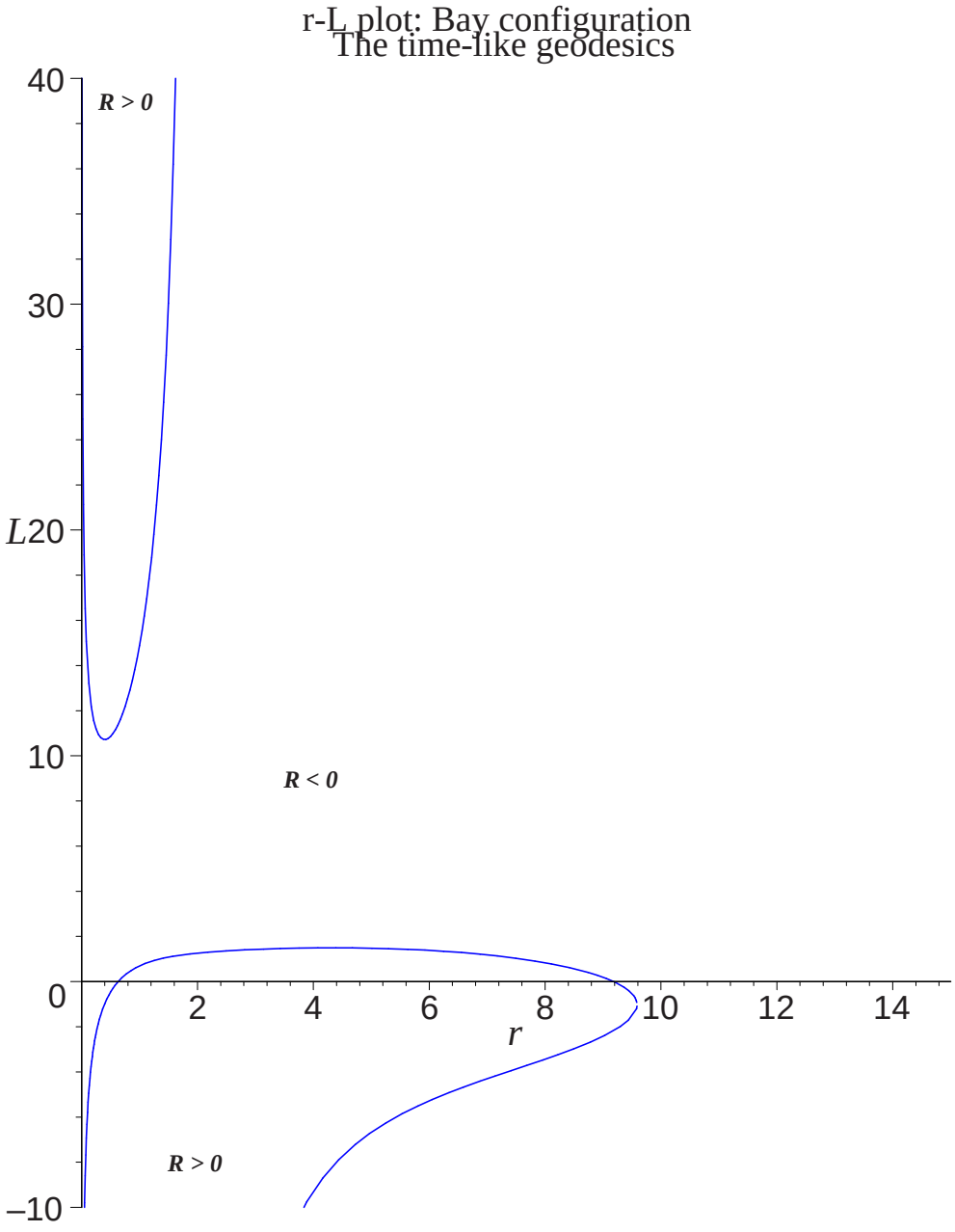

Figure 13.19: Bay configuration: an r-L plot for a time-like geodesic with escape energy $e = -0.2$ and Carter constant $Q = 1$. Forbidden regions are those with $R < 0$. On each horizontal line $L = \text{const}$, the maximal segments on which $R \geq 0$ give ranges of $r(\tau)$ for a geodesics with that particular angular momentum. All orbits are bound. (Additional parameters: $M = 1,\ a^2 = 19$.)

13.5.4 Lake configuration

For $-1/9 < e < 0$ and $Q_+(e) \leq Q \leq Q_-(e)$, forbidden regions enlarge with increasing Q ([34, section 4.8]). When $Q = Q_+(e)$ they meet (at a saddle point of $\mathrm{R}(r, L)$, see the second assertion of Proposition 13.9) and thereafter they merge, forming a "lake" as shown in figures 13.20 and 13.21 .

Every r-L plot with $-1/9 < e < 0$ and $Q_+(e) < Q < Q_-(e)$ has this lake. Because $d > 0$, ϕ has two simple roots $2M < r_1 < r_2$. The boundary of the lake is the closed curve formed by the two curves $L_-(r)$ and $L_+(r)$, which meet with vertical tangents at r_1 and r_2. The midline runs along the middle of the lake.

Hence there are many bound orbits in the Kerr exterior, given by horizontal lines within the lake, and they all are stably bound.

If Q continues to increase, the forbidden regions grow and therefore the lake shrinks until at $Q = Q_-(e)$ it vanishes. But, as specified by the third assertion of Proposition 13.9, there remains an isolated maximum point of $\mathrm{R}(r, L)$ at which $\mathrm{R} = 0$. This point represents a stable spherical orbit.

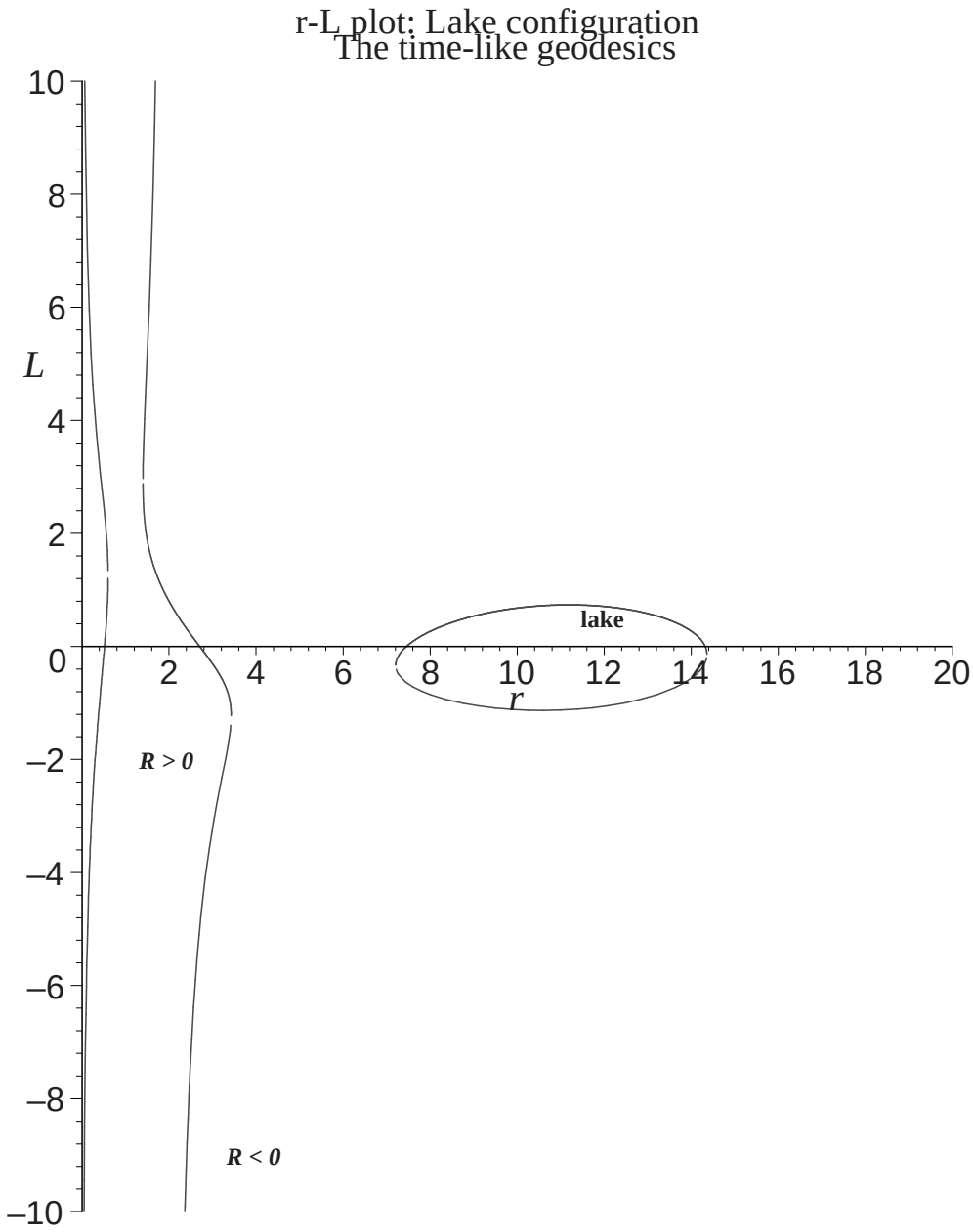

Figure 13.20: Lake configuration: an r-L plot for a time-like geodesic with escape energy $e = -0.08$ and Carter constant $Q = 14.2$. Forbidden regions are those with $R < 0$. For $r < r_-$ the plot still resembles the $e > 0$ case in figure 13.4. On each horizontal line $L = \text{const}$, the maximal segments on which $R \geq 0$ give ranges of $r(\tau)$ for a geodesics with that particular angular momentum. All orbits are bound. (Additional parameters: $M = 1,\ a^2 = 0.84$.)

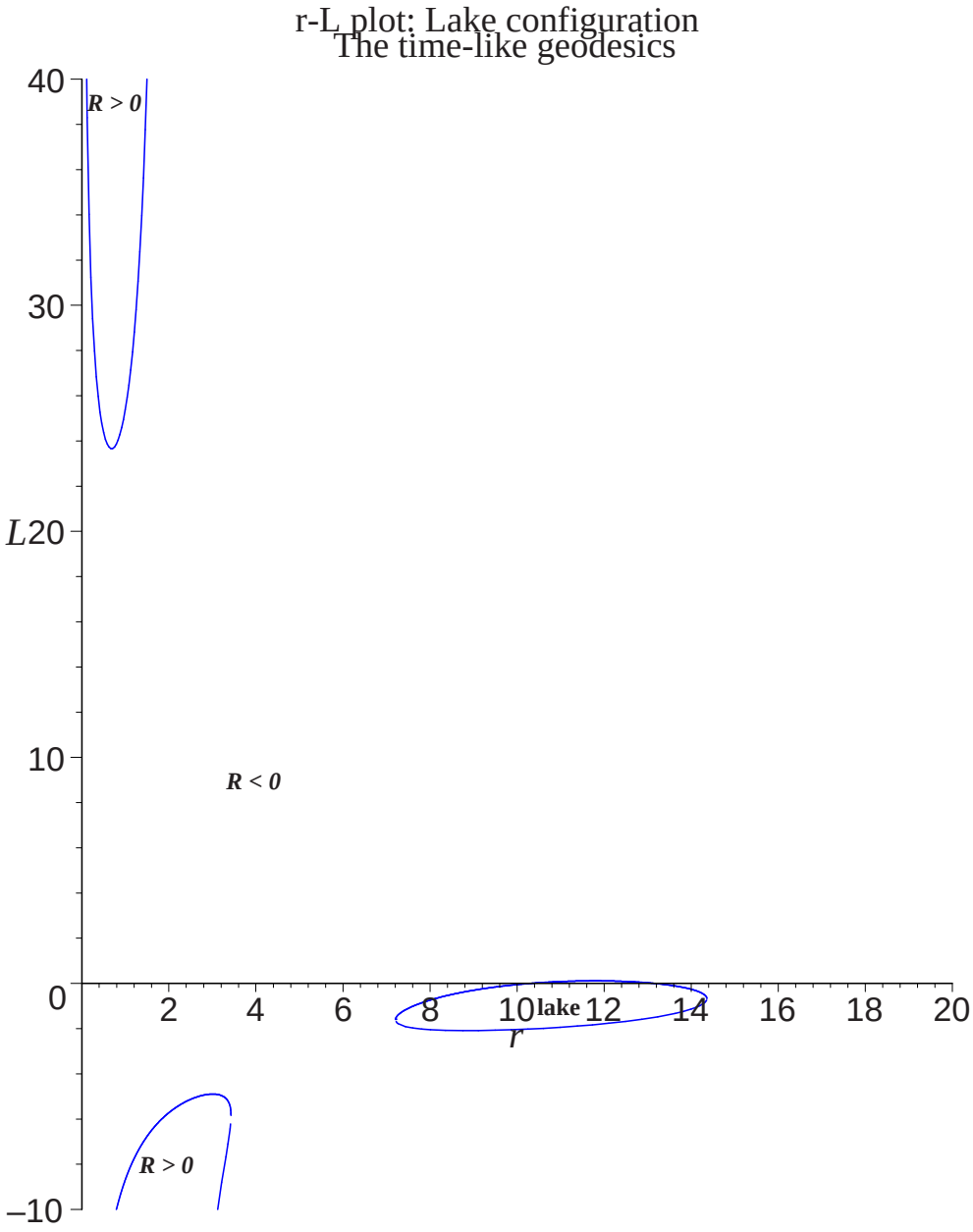

Figure 13.21: Lake configuration: an r-L plot for a time-like geodesic with escape energy $e = -0.08$ and Carter constant $Q = 14.2$. Forbidden regions are those with $R < 0$. On each horizontal line $L = \text{const}$, the maximal segments on which $R \geq 0$ give ranges of $r(\tau)$ for a geodesics with that particular angular momentum. All orbits are bound. (Additional parameters: $M = 1,\ a^2 = 19$.)

Chapter 14

The geodesics in the equatorial plane

In the early study of Kerr space-time equatorial geodesics were emphasized, because when compared with Schwarzschild geodesics the consequences of rotation stand out.

While geodesics in the equator are included in the broader class of geodesics with Carter constant $Q = 0$, orbital consequences are radically different for the equatorial and non-equatorial cases.

Motion in the equatorial plane is described by Lagrangian

$$2\mathcal{L} = \left(1 - \frac{2M}{r}\right)\dot{t}^2 + \frac{4aM}{r}\dot{t}\dot{\varphi} - \frac{r^2}{\Delta}\dot{r}^2 - \left[(r^2 + a^2) + \frac{2a^2M}{r}\right]\dot{\varphi}^2\,; \qquad (14.1)$$

and we deduce from it that the generalized momenta are given by

$$p_t = \left(1 - \frac{2M}{r}\right)\dot{t} + \frac{2aM}{r}\dot{\varphi} = E = \text{constant}\,, \qquad (14.2)$$

$$-p_\varphi = -\frac{2aM}{r}\dot{t} + \left(r^2 + a^2 + \frac{2a^2M}{r}\right)\dot{\varphi} = L = \text{constant} \qquad (14.3)$$

and

$$-p_r = \frac{r^2}{\Delta}\dot{r}\,. \qquad (14.4)$$

Stationary and axisymmetric character of the Kerr Geometry is evident from the fact that the Lagrangian does not depend on t or φ. Therefore p_t and p_φ are constant.

The Hamiltonian is

$$\begin{aligned}\mathcal{H} &= p_t\dot{t} - p_\varphi\dot{\varphi} + p_r\dot{r} - \mathcal{L} = \\ &= \frac{1}{2}\left(1-\frac{2M}{r}\right)\dot{t}^2 + \frac{2aM}{r}\dot{t}\dot{\varphi} - \frac{r^2}{2\Delta}\dot{r}^2 - \frac{1}{2}\left(r^2+a^2+\frac{2a^2M}{r}\right)\dot{\varphi}^2\,; \quad (14.5)\end{aligned}$$

and from the independence of the Hamiltonian on t

$$\begin{aligned}2\mathcal{H} &= \\ &= \left[\left(1-\frac{2M}{r}\right)\dot{t} + \frac{2aM}{r}\dot{\varphi}\right]\dot{t} - \left[\left(r^2+a^2+\frac{2a^2M}{r}\right)\dot{\varphi} - \frac{2aM}{r}\dot{t}\right]\dot{\varphi} - \frac{r^2}{\Delta}\dot{r}^2 \\ &= E\dot{t} - L\dot{\varphi} - \frac{r^2}{\Delta}\dot{r}^2 = \delta_1 = \text{constant}\,. \quad (14.6)\end{aligned}$$

Solving equations (14.2) and (14.3) for $\dot{\varphi}$ and $\dot{t}$

$$\dot{\varphi} = \frac{1}{\Delta}\left[\left(1-\frac{2M}{r}\right)L + \frac{2aM}{r}E\right]\,, \quad (14.7)$$

$$\dot{t} = \frac{1}{\Delta}\left[\left(\dot{r}^2+a^2+\frac{2a^2M}{r}\right)E - \frac{2aM}{r}L\right]\,; \quad (14.8)$$

and inserting these solutions in the third line of equation (14.6), the radial equation can be deduced

$$r^2\dot{r}^2 = r^2E^2 + \frac{2M}{r}\left(aE-L\right)^2 + \left(a^2E^2-L^2\right) - \delta_1\Delta\,. \quad (14.9)$$

We write this as the following corollary

Corollary 14.1 *For a geodesic γ with $Q = 0$, we have $\mathrm{R}(r) = r\psi(r)$ where the function ψ is given by*

$$\psi(r) = E^2r^3 + \left(a^2E^2-L^2\right)r + 2M\left(L-aE\right)^2 - \delta_1 r\Delta\,.$$

When $Q = 0$, r-L plots are determined solely by E, thus the e-Q chart (figure 13.1) shows that time-like r-L plots have either bay or continents configurations and that null and space-like r-L plots have continents configurations (figures 13.2 and 13.3 respectively).

The previous results from section 13.4 can be written down as follows.

Corollary 14.2 *Let γ be a $Q = 0$ geodesic, with ψ as in Corollary 14.1.*

1. *As a polynomial in L,*

$$\psi(r, L) = (2M - r)L^2 - 4MaEL + \psi_0(r)\,, \tag{14.10}$$

   where $\psi_0(r) = \psi(r, L = 0) = E^2(r^3 + a^2r + 2Ma^2) - \delta_1 r\Delta(r)$.

2. *If $r \neq 2M$, the discriminant of ψ as a polynomial in L is $4D(r) = r\Delta(r)(E^2r - \delta_1 r + 2M\delta_1)$.*

3. *The set Z of zeros of $\psi(r, L)$ (or of $\mathrm{R}(r, L)$) is the union of the graphs of the two functions*

$$L_\pm = \frac{2MaE \pm \sqrt{r\Delta(E^2r - \delta_1 r + 2M\delta_1)}}{2M - r} \tag{14.11}$$

   defined on maximal r intervals on which $\mathrm{D}(r) \geq 0$.

Therefore, after the reduction of R to ψ, the discriminant polynomial ϕ of section 13.4 is replaced by the linear expression $(E^2 - \delta_1)r + 2M\delta_1$. As in section 13.4 the discriminant is essential in determining the configuration of the set Z, because (for $r \neq 2M$) the sign $(-, 0, +)$ of $\mathrm{D}(r)$ establishes whether there are zero, one, or two points, respectively, of $\mathrm{R} = 0$ on the vertical line $L \to (r, L)$.

For the exceptional line $r = 2M$, the function $L \to \psi(2M, L)$ is linear with negative slope for $E > 0$. Therefore as L increases, the line $r = 2M$ enters a forbidden region at $L_{2M} = \frac{\psi(r,0)}{4MaE}$ and remains there. (When $E = 0$, ψ is constant on $r = 2M$.)

Proposition 14.3 *In a $Q = 0$ r-L plot with $E^2 - \delta_1 \neq 0$ and $E \neq 0$, the only vertical lines that contain a unique point (r, L_r) of Z are $r = 0$, r_-, r_+, $2M$,*

or $w = \frac{2M\delta_1}{\delta_1 - E^2}$. *The corresponding angular momenta are* L_{2M} *(as above) for* $r = 2M$, *and* $L_r = \frac{2MaE}{2M-r}$ *for the others. Explicitly,*

$$L_0 = aE\,, \qquad L_\pm = 2MaE/r_\mp\,, \qquad L_w = a\left(E^2 - \delta_1\right)\,.$$

For proof see [34, page 275].

14.1 The null geodesics

For null geodesics $\delta_1 = 0$ and the radial equation (14.9) becomes

$$\dot{r}^2 = E^2 + \frac{2M}{r^3}\left(L - aE\right)^2 - \frac{1}{r^2}\left(L^2 - a^2E^2\right) = \mathrm{f}(r)\,. \tag{14.12}$$

As in Chapters 3 and 8, it will be more convenient to distinguish the geodesics by the impact parameter (3.9) rather than by L. So a single r-D plot is sufficient to characterize the radial motion of all equatorial null geodesics.

Corollaries 14.1 and 14.2 lead to the following corollary.

Corollary 14.4 *For* $Q = 0$ *null geodesics with* $E \neq 0$,

$$\psi = \mathrm{R}/r = r^3 + \left(a^2 - D^2\right)r + 2M\left(D - a\right)^2\,. \tag{14.13}$$

The zero set $Z:\ \psi = 0$ *is the union of the graphs of the two functions*

$$D_\pm(r) = \frac{2Ma \pm r\sqrt{\Delta}}{2M - r} \qquad \textit{where} \qquad \Delta > 0. \tag{14.14}$$

Therefore there are two points of Z on each vertical line in the strip $0 < r < r_-$ and in $r > 2M$, one on the lines $r = r_\pm$ and $r = 2M$, and none between the horizons. Like in the non-equatorial case (section 13.5.1), the r-D plot has two continental forbidden regions N and S in the exterior $r > r_+$, but in the strip $0 < r < r_-$ the forbidden region is a "tongue" W, first observed by [3] (although their "tongue" pointed "southward" not "northward"). W starts from $r = 0$ at the $(0, a)$ and ends in $r = r_-$. The principal line $D = a$

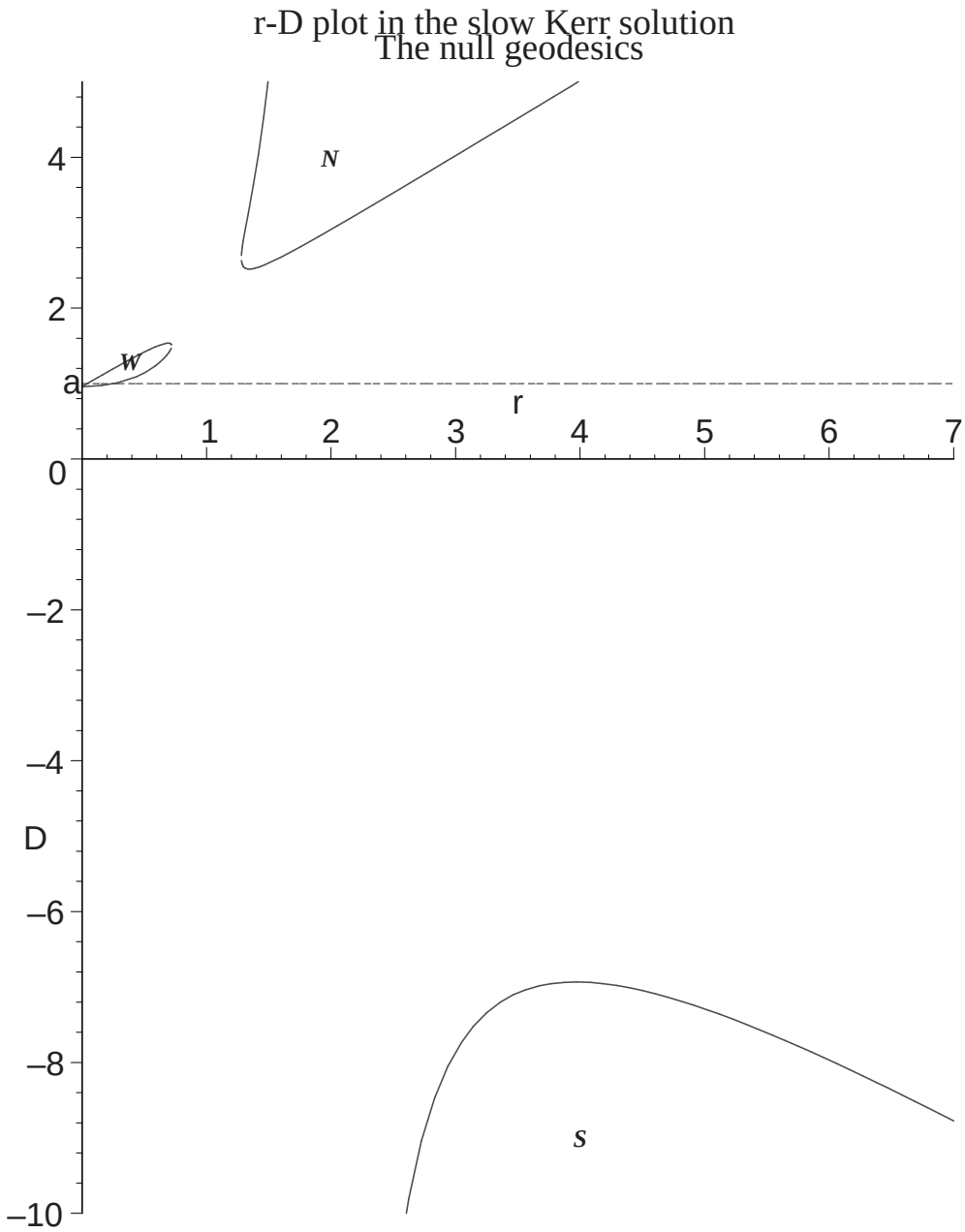

Figure 14.1: The r-D plot for equatorial null geodesics in the slow Kerr black hole. Forbidden regions are N, S and W; their boundaries define the turning points for null rays. ($M = 1,\ a = 0.96$)

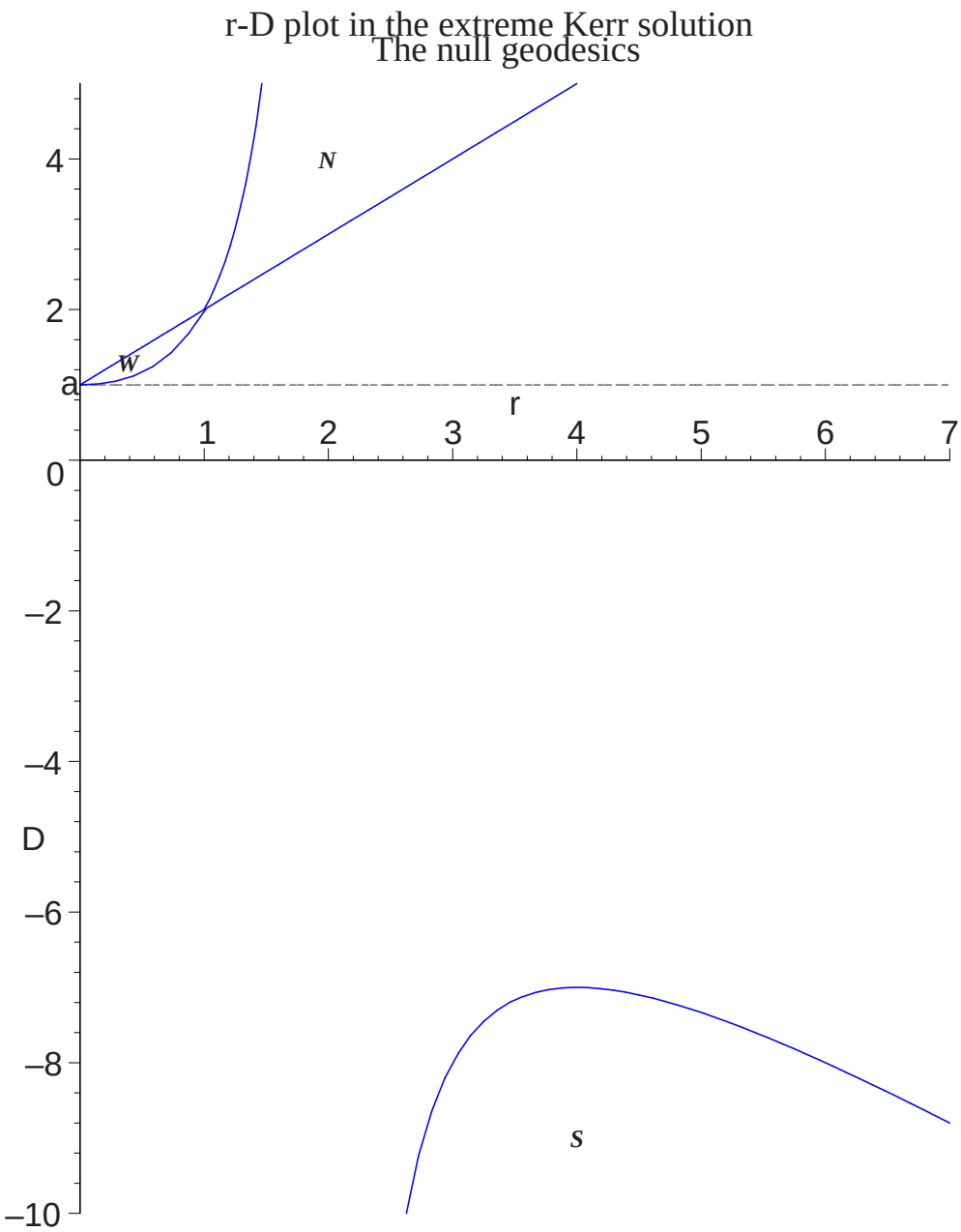

Figure 14.2: The r-D plot for equatorial null geodesics in the extreme Kerr black hole. Forbidden regions are N, S and W; their boundaries define the turning points for null rays. ($a = M = 1$)

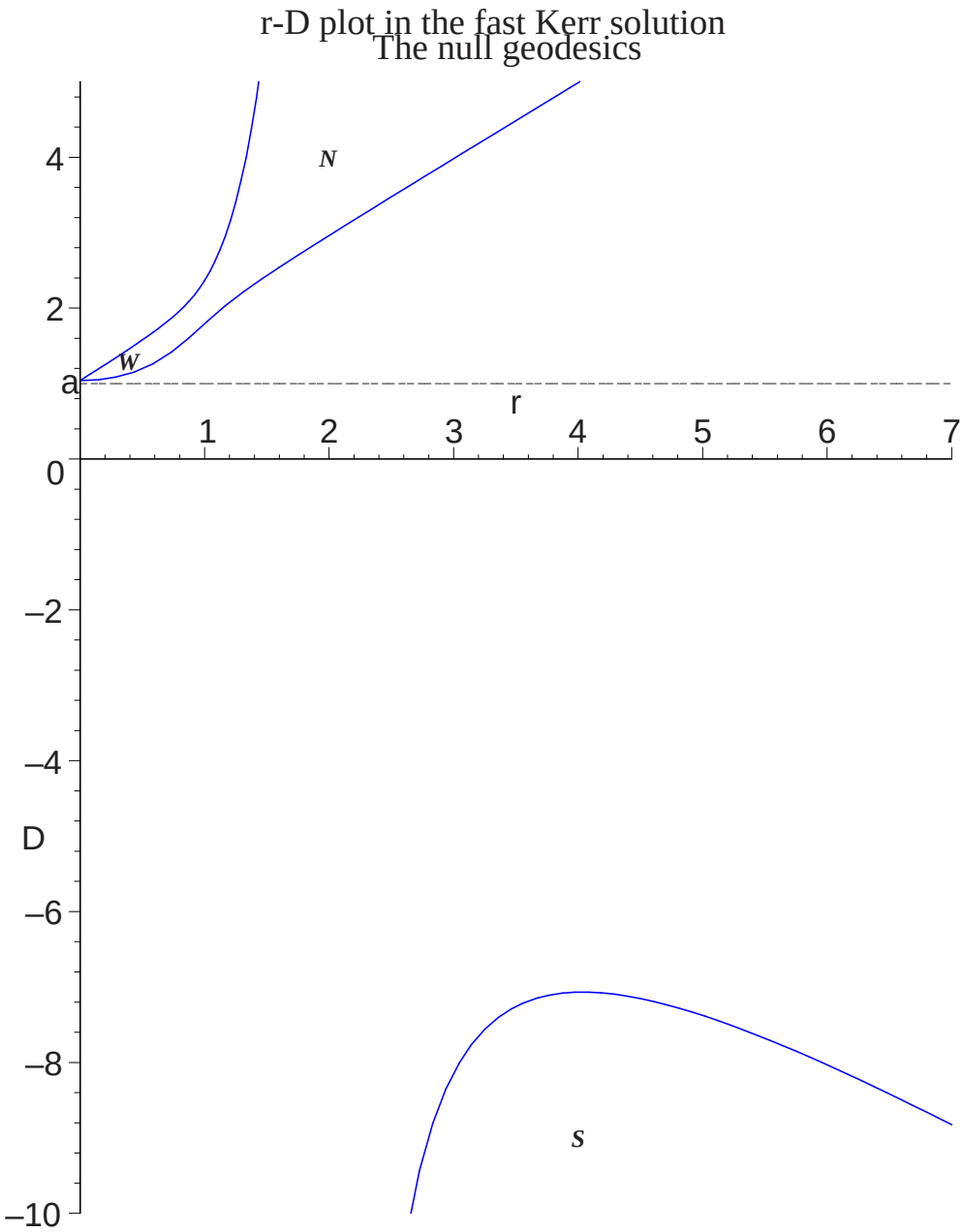

Figure 14.3: The r-D plot for equatorial null geodesics in the fast Kerr black hole. Forbidden regions are N, S and W (regions W and N merge); their boundaries define the turning points for null rays. ($M = 1,\ a = 1.04$)

(corresponding to $L = aE$) is tangent to W from below (see figures 14.1, 14.2 and 14.3 and cf. with [3, figure 8]).

As figures 14.1, 14.2 and 14.3 show, a null geodesics γ coming in from $r = +\infty$ has flyby orbit if $|D|$ is large ($|L| \gg E$) and may hit the ring singularity if $|D|$ is small. But because of the tongue, in the slow Kerr black hole, if D is just larger than the principal level $D = a$, it meets the tongue in an r-turning point, and so the geodesic has a long flyby orbit ([34]); in the fast Kerr black hole the tongue meets the continent N, thus a null geodesics with $D > a$ does not reach the singularity.

14.1.1 The special case $D = a$

Geodesics with impact parameter

$$D = a\,, \quad \text{when} \quad L = aE\,, \tag{14.15}$$

have, in the rotating black hole, the same role as the radial geodesics in the Schwarzschild and in the Reissner-Nordström geometry. They meet the ring singularity and have crash-escape orbit type. And so equations (14.7), (14.8), and (14.12) are reduced to

$$\dot{r} = \pm E\,, \qquad \dot{t} = \frac{(r^2 + a^2)E}{\Delta}\,, \qquad \text{and} \qquad \dot{\varphi} = \frac{aE}{\Delta}\,. \tag{14.16}$$

The radial coordinate is described uniformly with respect to the affine parameter, and the equations governing t and φ are

$$\frac{\mathrm{d}t}{\mathrm{d}r} = \pm\frac{r^2 + a^2}{\Delta} \qquad \text{and} \qquad \frac{\mathrm{d}\varphi}{\mathrm{d}r} = \pm\frac{a}{\Delta}\,. \tag{14.17}$$

Slow black hole

The solutions of equations (14.17) are

$$\pm t = r + \frac{r_+^2 + a^2}{r_+ - r_-}\ln\left(\frac{r}{r_+} - 1\right) - \frac{r_-^2 + a^2}{r_+ - r_-}\ln\left(\frac{r}{r_-} - 1\right)\,, \tag{14.18}$$

$$\pm\varphi = \frac{a}{r_+ - r_-}\ln\left(\frac{r}{r_+} - 1\right) - \frac{a}{r_+ - r_-}\ln\left(\frac{r}{r_+} - 1\right)\,. \tag{14.19}$$

They display the typical behaviors of t and φ of approaching $\pm\infty$ near the horizons r_+ and r_-.

Extreme black hole

The solutions of equations (14.17) are

$$\pm t = r - r_{\rm in} + 2M^2\left(\frac{1}{r_{\rm in}-M} - \frac{1}{r-M}\right) + 2M\ln\left|\frac{r-M}{r_{\rm in}-M}\right|, \qquad (14.20)$$

$$\pm\varphi = M\left(\frac{1}{r_{\rm in}-M} - \frac{1}{r-M}\right) \qquad (14.21)$$

with initial condition $r = r_{\rm in}$ for $t = \varphi = 0$.

Fast black hole

The solutions of equations (14.17) are

$$\pm\, t = r - r_{\rm in} + M\ln\left|\frac{\Delta}{\Delta_{\rm in}}\right| + \\ + \frac{2M}{\sqrt{a^2-M^2}}\left(\arctan\frac{r-M}{\sqrt{a^2-M^2}} - \arctan\frac{r_{\rm in}-M}{\sqrt{a^2-M^2}}\right) \qquad (14.22)$$

and

$$\pm\varphi = a\left(\arctan\frac{r-M}{\sqrt{a^2-M^2}} - \arctan\frac{r_{\rm in}-M}{\sqrt{a^2-M^2}}\right) \qquad (14.23)$$

with initial condition $r = r_{\rm in}$ for $t = \varphi = 0$.

14.1.2 General orbits

Unlike in the general $Q > 0$ case, it is now simple to find the horizontal tangents to Z, which represent the circular photons–and therefore to specify all null orbits types.

Proposition 14.5 *In the slow Kerr equator there are, aside from restphotons, exactly three circular null orbits. For $E > 0$, these have radii and impact parameters (r_τ, D_τ), (r_ρ, D_ρ), (r_δ, D_δ) with*

$$0 < r_\tau < r_- < r_+ < r_\delta < 3M < r_\rho < 4M\,,$$

and

$$D_\rho < -7a < 0 < a < D_\tau < 2a < D_\delta \,.$$

The radii are the roots of the polynomial $\mathrm{p}(r) = r(r-3M)^2 - 4Ma^2$, *and the impact parameters are the roots of* $\mathrm{q}(D) = (D+a)^3 - 27M^2(D-a)$.

For proof see [34, page 278][1].

Proposition 14.6 *In the extreme Kerr equator there are, aside from restphotons, exactly three circular null orbits. For* $E > 0$, *these have radii and impact parameters* (r_τ, D_τ), (r_ρ, D_ρ), (r_δ, D_δ) *with*

$$0 < r_\tau = r_\pm = r_\delta < 3M < r_\rho = 4M \,, \tag{14.24}$$

and

$$D_\rho = -7a < 0 < a < D_\tau = 2a = D_\delta \,. \tag{14.25}$$

The radii are the roots of the polynomial $\mathrm{p}(r) = r(r-3M)^2 - 4Ma^2$, *and the impact parameters are the roots of* $\mathrm{q}(D) = (D+a)^3 - 27M^2(D-a)$.

Proof. The circular orbits occur at simultaneous solutions (r, D) of the equations $\psi = 0$, $\frac{\partial \psi}{\partial r} = 0$. The second equations yields to

$$D^2 = 3r^2 + a^2 \,. \tag{14.26}$$

Substituting $r^2 = \frac{D^2 - a^2}{3}$ into $\psi(r, D) = r^3 + (a^2 - D^2)R + 2M(D-a)^2 = 0$ gives $r(a^2 - D^2) + 3M(D-a)^2 = 0$. Therefore

$$r = \frac{3M(D-a)}{D+a} \,. \tag{14.27}$$

Equations (14.26) and (14.27) are the basic relations between the radius and the impact parameter of a circular null geodesic. Substituting equation

[1] with correction that $\mathrm{p}(4M) = 4M^3 - 4Ma^2$

(14.27) into $\frac{\partial\psi}{\partial r} = 3r^2 + a^2 - D^2 = 0$ leads to $27M^2\frac{(D-a)^2}{(D+a)^2} + a^2 - D^2 = 0$. By omitting the principal null geodesics $D = a$, $D - a$ is cancelled from the preceding equation. That leaves

$$\mathrm{q}(D) = (D+a)^3 - 27M^2(D-a) = 0\,. \tag{14.28}$$

Solving equation (14.27) for $D = -a\frac{r+3M}{r-3M}$, and substituting this into equation (14.28) yields

$$\mathrm{p}(r) = r\,(r-3M)^2 - 4Ma^2\,. \tag{14.29}$$

This polynomial has no negative roots, and $\mathrm{p}(0) < 0$, $\mathrm{p}(3M) < 0$, $\mathrm{p}(4M) = 0$. The placing of $r_\pm$ derives from

$$\mathrm{p}(r_\pm) = \mathrm{p}(M) = 0\,. \tag{14.30}$$

It follows that $\mathrm{p}(r)$ has three roots obeying equation (14.24). $D(r_\rho) = D(4M)$, which gives $D_\rho = -7a$. The function $D(r) = a\frac{3M+r}{3M-r}$ is strictly increasing on $\{r < 3M\}$ and $\{r > 3M\}$, hence $D(0) < D(r_\tau) = D(M) = D(r_\delta)$, which gives $a < D_\tau = 2a = D_\delta$. □

Proposition 14.7 *In the fast Kerr equator there is, aside from restphotons, exactly one circular null orbit. For $E > 0$, this has radius and impact parameter (r_ρ, D_ρ) with*

$$r_\rho > 4M\,, \tag{14.31}$$

and

$$D_\rho > -7a\,. \tag{14.32}$$

The radius is the real root of the polynomial $\mathrm{p}(r) = r(r-3M)^2 - 4Ma^2$, and the impact parameter is the real root of $\mathrm{q}(D) = (D+a)^3 - 27M^2(D-a)$.

Proof. Evidently the polynomial (14.29) is approaching $+\infty$ with $r \to +\infty$, and $\mathrm{p}(4M) = 4M^3 - 4Ma^2 < 0$. The discriminant of $\mathrm{p}(r)$ is $432M^2a^2(M^2 - a^2) < 0$, so there is only one real solution, and it obeys the stated inequality. With the same reasoning as in previous proof, $D(r_\rho) > D(4M)$ gives $D_\rho > -7a$. □

Once the circular photons are found in the null r-D plot, the equatorial null orbit types can be described. Principal null geodesics hit the ring singularity ([34, chapter 4]). There are no bound null orbits except for (unstable) circular orbits. For $E \neq 0$ the remaining flyby and crash orbits can be characterized in terms of impact parameter, as follows:

1. Flyby orbits (for r large) or crash orbits (for r small) iff the impact parameter $D = L/E$ is in one of the intervals: $(-\infty, D_\rho)$, (a, D_τ), (D_δ, ∞) (for the fast black holes that means $D > a$ or $D < D_\rho$).

2. Crash-escape orbit iff D lies in the interval $(D_\rho, a]$ or (D_τ, D_δ) (for the fast black holes only the first interval applies).

3. Circular orbit (or associated asymptotic orbit) iff $D = D_\rho$, D_τ, or D_δ.

In the remaining case $E = 0$, γ is a restphoton if $L = 0$, other than that it has crash-crash orbit in $0 < r \leq 2M$. When $L = 0$, all the first integrals of γ are zero, which is possible only for restphotons ([34, chaper 4]). If $L \neq 0$, then (from 14.10) $\psi(r, L) = (2M - r)L^2$, and so γ is in the strip $0 < r \leq 2M$. The r-equation is (from 14.9) $r^3\dot{r}^2 = L^2(2M - r)$, therefore γ hits Σ at both ends, with a turn at $r = 2M$.

The null geodesics are *central* in the sense that, for large E, both space-like and the time-like sets Z resemble that of the null case ([34, chapter 4]).

Now we will find the general solution for all three types of orbits. From (14.12) it is clear that turning points occur at the zeros of the cube polynomial

$$f(u) = 2Mu^3 \left(L - aE\right)^2 - u^2 \left(L^2 - a^2E^2\right) + E^2 \,. \tag{14.33}$$

Then for orbits of the first kind (flyby orbits)

$$\tau = \frac{g}{k^4 u_3^4 \sqrt{2M}} \Bigg\{ u_2 \big[\mathrm{F}(\phi,k) + \mathrm{K}(k) \big] + \\ + 2\left(k^2 u_3^2 - u_2^2\right) \left[\Pi\left(\phi, \frac{k^2 u_3^4}{u_2^2}, k\right) + \Pi\left(\frac{k^2 u_3^4}{u_2^2}, k\right) \right] + \\ + \frac{u_2^2 - k^2 u_3^2}{2(k^4 u_3^2 - u_2^2)} \Bigg[k^2 u_3^2 \, \mathrm{E}(\phi,k) + \left(u_2^2 - k^2 u_3^2\right) v + \\ + \left(2k^4 u_3^2 2k^2 u_3^2 + \frac{k^6 u_3^2}{u_2^2} - 3u_2^2 \right) \Pi\left(\phi, \frac{k^2 u_3^4}{u_2^2}, k\right) - \frac{k^6 u_3^4 \operatorname{sn} v \operatorname{cn} v \operatorname{dn} v}{u_2^2 - k^4 u_3^2 \operatorname{sn}^2 v} + \\ + k^2 u_3^2 \, \mathrm{E}(k) + \left(u_2^2 - k^2 u_3^2\right) \mathrm{K}(k) + \\ + \left(2k^4 u_3^2 2k^2 u_3^2 + \frac{k^6 u_3^2}{u_2^2} - 3u_2^2 \right) \Pi\left(\frac{k^2 u_3^4}{u_2^2}, k\right) \Bigg] \Bigg\} \,, \quad (14.34)$$

where

$$g = \frac{2}{\sqrt{u_3 - u_1}} \,, \quad (14.35)$$

$$\phi = \operatorname{am} v = \arcsin \sqrt{\frac{(u_3 - u_1)(u_2 - u)}{(u_2 - u_1)(u_3 - u)}} \,, \quad (14.36)$$

$$k^2 = \frac{u_2 - u_1}{u_3 - u_1} \,, \quad (14.37)$$

for orbits of the second kind (crash orbits)

$$\tau = \frac{\sqrt{2}}{\alpha^4 \left(u_3 - u_1\right)^{3/2} \sqrt{M}} \Bigg\{ \mathrm{F}(\phi,k) - 2\Pi\left(\phi, \alpha^2, k^2\right) + \\ + \frac{1}{2(\alpha^2 - 1)(k^2 - \alpha^2)} \Bigg[\alpha^2 \, \mathrm{E}(\phi,k) + \left(k^2 - \alpha^2\right) \mathrm{F}(\phi,k) + \\ + \left(2\alpha^2 k^2 + 2\alpha^2 - \alpha^4 - 3k^2\right) \Pi\left(\phi, \alpha^2, k^2\right) - \frac{\alpha^4 \operatorname{sn} v \operatorname{cn} v \operatorname{dn} v}{1 - \alpha^2 \operatorname{sn}^2 v} \Bigg] \Bigg\} \,, \quad (14.38)$$

where u_1, u_2 and u_3 are the roots of $\mathrm{f}(u) = 2M(u - u_1)(u - u_2)(u - u_3)$, k is defined in (14.37), g in (14.35), and

$$\alpha^2 = \frac{u_1}{u_1 - u_3} \,, \quad (14.39)$$

$$\phi = \operatorname{am} v = \arcsin \sqrt{\frac{u_3 - u_1}{u - u_1}} \,. \quad (14.40)$$

The solution for the crash-escape orbits can be also expressed in terms of elliptic integrals, but we do not write it here because it is long and not essentially different from the previous two solutions.

We can write the solution of

$$\varphi = \int \frac{D - 2Mu(a-D)}{\Delta(u)\sqrt{2M(a-D)^2u^3 + (a^2-D^2)u^2 + 1}}\mathrm{d}u\,, \tag{14.41}$$

in the form

$$\varphi = \frac{gp}{(M^2-a^2)\sqrt{8M}}\left[\frac{\Pi\left(\phi,\alpha_+^2,k\right)+\Pi\left(\alpha_+^2,k\right)}{u_+-u_1} - \frac{\Pi\left(\phi,\alpha_-^2,k\right)+\Pi\left(\alpha_-^2,k\right)}{u_--u_1}\right] \tag{14.42}$$

for the orbits of the first kind (flyby orbits), where

$$p = 2M(a-D)\left(M^2-a^2\right) + \left[a^2D - 2M^2(a-D)\right]\sqrt{M^2-a^2}\,, \tag{14.43}$$

$$g = \frac{2}{u_3-u_1}\,, \tag{14.44}$$

$$\phi = \arcsin\sqrt{\frac{u-u_1}{u_2-u_1}}\,, \tag{14.45}$$

$$\alpha_+^2 = \frac{u_2-u_1}{u_+-u_1}\,, \tag{14.46}$$

$$\alpha_-^2 = \frac{u_2-u_1}{u_--u_1}\,, \tag{14.47}$$

k^2 is defined in (14.37), u_+ and u_- are the roots of

$$\Delta(u) = a^2u^2 - 2M + 1\,; \tag{14.48}$$

and

$$\varphi = \frac{gp}{(M^2-a^2)\sqrt{8M}}\left[\frac{\Pi\left(\phi,\alpha_-^2,k\right)-\mathrm{F}(\phi,k)}{u_--u_1} - \frac{\Pi\left(\phi,\alpha_+^2,k\right)-\mathrm{F}(\phi,k)}{u_+-u_1}\right] \tag{14.49}$$

for the orbits of the second kind (crash orbits), where g, p and k^2 are same as before and

$$\alpha_+^2 = \frac{u_+-u_1}{u_3-u_1}\,, \tag{14.50}$$

$$\alpha_-^2 = \frac{u_--u_1}{u_3-u_1}\,, \tag{14.51}$$

$$\phi = \arcsin\sqrt{\frac{u_3-u_1}{u-u_1}}\,, \tag{14.52}$$

and

$$\varphi = \frac{gp}{(M^2-a^2)\sqrt{8M}}\left[\frac{-v+\frac{\Pi\left(\phi,\frac{\alpha_-^2}{\alpha_-^2-1},k\right)-\alpha_- f_-}{1+\alpha_-}}{\alpha_-(A+a-u_-)} - \frac{-v+\frac{\Pi\left(\phi,\frac{\alpha_+^2}{\alpha_+^2-1},k\right)-\alpha_+ f_+}{1+\alpha_+}}{\alpha_+(A+a-u_+)}\right] \tag{14.53}$$

for crash-escape orbits, where p is the same as before, and

$$g = 1/\sqrt{A}\,, \tag{14.54}$$

$$\operatorname{cn} v = \cos\phi\,, \tag{14.55}$$

$$\phi = \arccos\frac{u-u_1-A}{u-u_1+A}\,, \tag{14.56}$$

$$k^2 = \frac{A+b_1-u_1}{2A}\,, \tag{14.57}$$

$$A^2 = (b_1-u_1)^2 + a_1^2\,, \tag{14.58}$$

$$b_1 = \frac{u_2+\bar{u}_2}{2}\,, \tag{14.59}$$

$$a_1^2 = -\frac{(u_2-\bar{u}_2)^2}{4}\,, \tag{14.60}$$

$$\alpha_- = \frac{A-u_1+u_-}{A+u_1-u_-}\,, \tag{14.61}$$

$$\alpha_+ = \frac{A-u_1+u_+}{A+u_1-u_+}\,, \tag{14.62}$$

$$f_\pm = \begin{cases} \arctan\left(\sqrt{\dfrac{k^2+k'^2\alpha_\pm^2}{1-\alpha_\pm^2}}\operatorname{sn} u\right)\sqrt{\dfrac{1-\alpha_\pm^2}{k^2+k'^2\alpha_\pm^2}}\,, & \text{if } \dfrac{\alpha_\pm^2}{\alpha_\pm^2-1} < k^2\,; \\ \operatorname{sd} u\,, & \text{if } \dfrac{\alpha_\pm^2}{\alpha_\pm^2-1} = k^2\,; \\ \sqrt{\dfrac{\alpha_\pm^2-1}{k^2+k'^2\alpha_\pm^2}}\ln\dfrac{\sqrt{k^2+k'^2\alpha_\pm^2}\operatorname{dn} u+\sqrt{\alpha_\pm^2-1}\operatorname{sn} u}{\sqrt{k^2+k'^2\alpha_\pm^2}\operatorname{dn} u-\sqrt{\alpha_\pm^2-1}\operatorname{sn} u}\Big/2\,, & \text{if } \dfrac{\alpha_\pm^2}{\alpha_\pm^2-1} > k^2\,, \end{cases} \tag{14.63}$$

where k' is

$$k' = \sqrt{1-k^2} \tag{14.64}$$

and u_1, u_2, $\bar{u}_2$ are the roots of $\mathrm{f}(u) = 2M(u-u_1)(u-u_2)(u-\bar{u}_2)$. An example of orbits of the first and second kind is in figure 14.4.

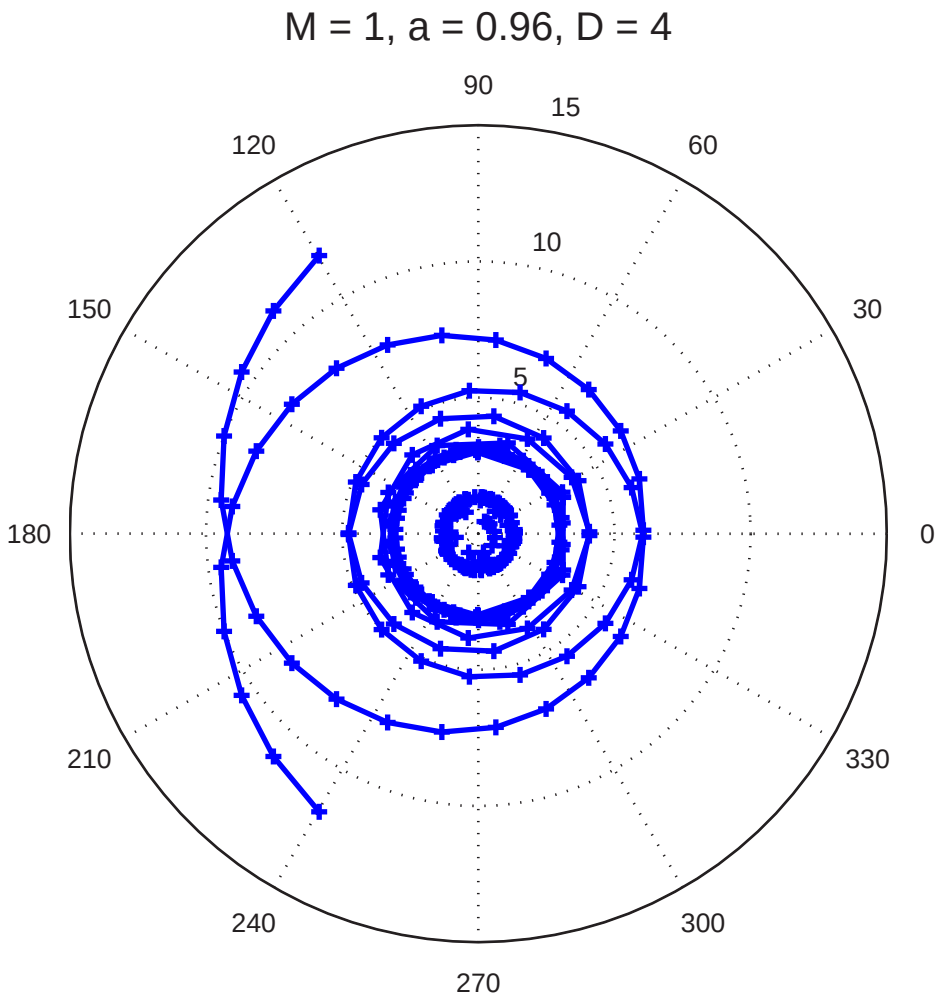

Figure 14.4: The flyby and the associated crash null orbits in the equatorial plane. Numerical values of points '+' are listed in section A.1.19. The flyby orbit is coming from infinity and after circling around singularity several times it goes off to infinity again. Crash orbit starts from a certain distance from singularity and after twice reversing direction of its rotation it plunges into singularity.

Unstable circular orbits

The radius r_c of the unstable circular orbit is determined by the equations (cf. equation (14.12))

$$E^2 + \frac{2M}{r_c^3}(L - aE)^2 - \frac{1}{r_c^2}\left(L^2 - a^2E^2\right) = 0 \tag{14.65}$$

and

$$-\frac{6M}{r_c^4}(L - aE)^2 + \frac{2}{r_c^3}\left(L^2 - a^2E^2\right) = 0\,. \tag{14.66}$$

From equation (14.66)

$$r_c = 3M\frac{L - aE}{L + aE} = 3M\frac{D_c - a}{D_c + a}\,. \tag{14.67}$$

Inserting this relation in equation (14.65), we get

$$E^2 = \frac{1}{27M^2}\frac{(L + aE)^3}{L - aE} \tag{14.68}$$

or

$$(D_c + a)^3 = 27M^2(D_c - a)\,. \tag{14.69}$$

Substitution

$$y = D_c + a\,, \tag{14.70}$$

leads to the cubic equation

$$y^3 - 27M^2y + 54aM^2 = 0\,. \tag{14.71}$$

- Slow and extreme black hole: Cases with $a > 0$ and $a < 0$ corresponding to the direct and retrograde orbits are distinguished. For $a > 0$,

$$\begin{gathered} y = 6M\cos\left(\frac{\pi}{3} \pm \frac{\vartheta}{3}\right) \qquad \text{where} \qquad \cos\vartheta = a/M\,, \\ D_c = y - a \qquad \text{and} \qquad r_c = 3M(1 - 2a/y)\,; \end{gathered} \tag{14.72}$$

and for $-a = |a| > 0$,

$$\begin{gathered} y = 6M\cos\frac{\vartheta}{3} \qquad \text{where} \qquad \cos\vartheta = |a|/M \\ D_c = y + |a| \qquad \text{and} \qquad r_c = 3M(1 + 2|a|/y)\,. \end{gathered} \tag{14.73}$$

It can be directly verified that the solution for $r_{\rm c}$, expressed directly in terms of ϑ, is given by

$$r_{\rm c} = 4M\cos^2\frac{\pi \pm \vartheta}{3} = 4M\cos^2\frac{\pi \pm \arccos\frac{a}{M}}{3} \tag{14.74}$$

for direct orbits, and

$$r_{\rm c} = 4M\cos^2\frac{\vartheta}{3} = 2M\left[1+\cos\left(\frac{2}{3}\arccos\frac{|a|}{M}\right)\right] \tag{14.75}$$

for retrograde orbits.

- Fast black hole: Circular orbits appear only for retrograde orbits. We have

$$\begin{aligned} &y = 6M\cosh(\vartheta/3) \qquad \text{where} \qquad \cosh\vartheta = |a|/M \\ &D_{\rm c} = y + |a| \qquad\qquad \text{and} \qquad r_{\rm c} = 3M(1+2|a|/y)\,, \end{aligned} \tag{14.76}$$

with condition

$$|a|/M < \pi/2\,. \tag{14.77}$$

Then

$$r_{\rm c} = 4M\cosh^2\frac{\vartheta}{3} = 2M\left[1+\cosh\left(\frac{2}{3}\text{arccosh}\frac{|a|}{M}\right)\right]\,. \tag{14.78}$$

When the impact parameter has the critical value $D_{\rm c}$, and $\mathrm{f}(r) = 0$ allows a double root, the governing equation (14.12) can be reduced to

$$\dot{u}^2 = ME^2\left(D_{\rm c}-a\right)^2 u^4\left(u-u_{\rm c}\right)^2\left(2u+u_c\right), \tag{14.79}$$

where

$$u = \frac{1}{r} \qquad \text{and} \qquad u_{\rm c} = \frac{1}{r_{\rm c}} = \frac{D_{\rm c}+a}{3M(D_{\rm c}-a)}\,. \tag{14.80}$$

Equation (14.79) directly integrated gives

$$[E(D_{\rm c}-a)\sqrt{M}]\tau = \pm\int \frac{{\rm d}u}{u^2(u-u_{\rm c})\sqrt{2u+u_{\rm c}}} = \\ = \pm\frac{1}{u_{\rm c}^2}\left(\frac{\sqrt{2u+u_{\rm c}}}{u}+\frac{1}{\sqrt{3u_{\rm c}}}\ln\left|\frac{\sqrt{2u+u_{\rm c}}-\sqrt{3u_{\rm c}}}{\sqrt{2u+u_{\rm c}}+\sqrt{3u_{\rm c}}}\right|\right) . \quad (14.81)$$

To show the orbit in the equatorial plane, we combine it with equation

$$\dot{\varphi} = \frac{Eu^2}{3(a^2u^2-2Mu+1)u_{\rm c}}[3D_{\rm c}u_{\rm c}-2(D_{\rm c}+a)u] \quad (14.82)$$

(which follows directly from equation (14.7)). We obtain

$$\frac{{\rm d}u}{{\rm d}\varphi} = \pm\frac{D_{\rm c}+a}{\sqrt{M}}(a^2u^2-2Mu+1)\frac{(u-u_{\rm c})\sqrt{2u+u_{\rm c}}}{3D_{\rm c}u_{\rm c}-2(D_{\rm c}+a)u} , \quad (14.83)$$

or

$$\varphi = \pm\frac{\sqrt{M}}{a^2(D_{\rm c}+a)}\int\frac{3D_{\rm c}u_{\rm c}-2(D_{\rm c}+a)u}{(u-u_+)(u-u_-)(u-u_{\rm c})\sqrt{2u+u_{\rm c}}} . \quad (14.84)$$

The explicit expression of this integral is

$$\varphi = \pm\frac{\sqrt{M}}{a^2(D_{\rm c}+a)}\left\{\frac{[3D_{\rm c}u_{\rm c}-2u_+(D_{\rm c}+a)]\ln\left|\frac{\sqrt{2u+u_{\rm c}}-\sqrt{2u_++u_{\rm c}}}{\sqrt{2u+u_{\rm c}}+\sqrt{2u_++u_{\rm c}}}\right|}{(u_+-u_-)(u_+-u_{\rm c})\sqrt{2u_++u_{\rm c}}}+\right. \\ +\frac{[3D_{\rm c}u_{\rm c}-2u_-(D_{\rm c}+a)]\ln\left|\frac{\sqrt{2u+u_{\rm c}}-\sqrt{2u_-+u_{\rm c}}}{\sqrt{2u+u_{\rm c}}+\sqrt{2u_-+u_{\rm c}}}\right|}{(u_+-u_-)(u_{\rm c}-u_-)\sqrt{2u_-+u_{\rm c}}}+ \\ \left.+\sqrt{\frac{u_{\rm c}}{3}}\frac{(2a-D_{\rm c})\ln\left|\frac{\sqrt{2u+u_{\rm c}}-\sqrt{3u_{\rm c}}}{\sqrt{2u+u_{\rm c}}+\sqrt{3u_{\rm c}}}\right|}{(u_{\rm c}-u_-)(u_+-u_{\rm c})}\right\} . \quad (14.85)$$

14.2 Space-like geodesics

For space-like geodesics $\delta_1 = -1$, therefore we have the radial equation

$$r^2\dot{r}^2 = r^2E^2+\frac{2M}{r}(aE-L)^2+\left(a^2E^2-L^2\right)+\Delta \quad (14.86)$$

Corollary 14.8 *For space-like equatorial geodesics*[2]*,*

$$\psi(r,L) = (E^2+1)-2Mr^2+\left[a^2\left(E^2+1\right)-L^2\right]r+2M\left(L-aE\right)^2 , \quad (14.87)$$

[2] cf. [34, Corollary 4.14.12]

and the set $Z:\ \psi = 0$ *is the union of the graphs of*

$$L \pm (r) = \frac{2MaE \pm \sqrt{\mathrm{D}(r)}}{2M - r}\,, \tag{14.88}$$

defined on intervals where $\mathrm{D}(r) = r\Delta(r)[(E^2+1)r - 2M]$ *is non-negative.*

Outside the region B the r-L plots usually look like the null case (figures 14.1, 14.2 and 14.3). But the vertical tangent $w(E) = \frac{2M}{E^2+1}$ is positive, and its interaction with the horizon radii $r_\pm$ creates many different types of orbits.

When E is large, the only important difference from the null case is that W has moved from the L-axis at the short distance $w(E) > 0$. In the slow case it has become an island. In the fast case W is connected to N (see figure 14.15). But as E decreases, this distance increases, while (in the slow and extreme cases) the right side of W remains pinned at (r_-, L_-) (see figures 14.5 and 14.14). Thus the island diminishes, until it is reduced to the single point (r_-, L_-) at $w = r_-$. This happens when $E = \sqrt{r_+/r_-}$, with $L_- = L_w = 2M$. Therefore, in the slow case, $(r_-, 2M)$ is an isolated maximum of $\psi(r, L)$. This point represents an unstable circular orbit in the intersection of the equator and the horizon H_- (see figure 14.6).

In the slow case, when E decreases below $\sqrt{r_+/r_-}$, $w(E)$ increases past r_- and the island reemerges, now running from $r = r_-$ to $r = w(E) > r_-$. Hence, unlike null and time-like geodesics, space-like ones can turn in region B. As w approaches r_+ the island expands toward N. When $E = \sqrt{r_-/r_+}$, w reaches r_+, and the island meets N at the critical point $(r_+, 2M)$ (see figure 14.8). This is the unstable circular orbit in H_+. In the extreme case there is only one unstable orbit in H at the critical point $(r_\pm, 2ME)$ (see figures 14.11, 14.12 and 14.13).

Further decrease of E moves w past r_+ where it drives N eastward (see figures 14.9, 14.12 and 14.16). In the slow case the island is left behind, extending from r_- to r_+. Thereafter, it moves south until at $E = 0$ a symmetry

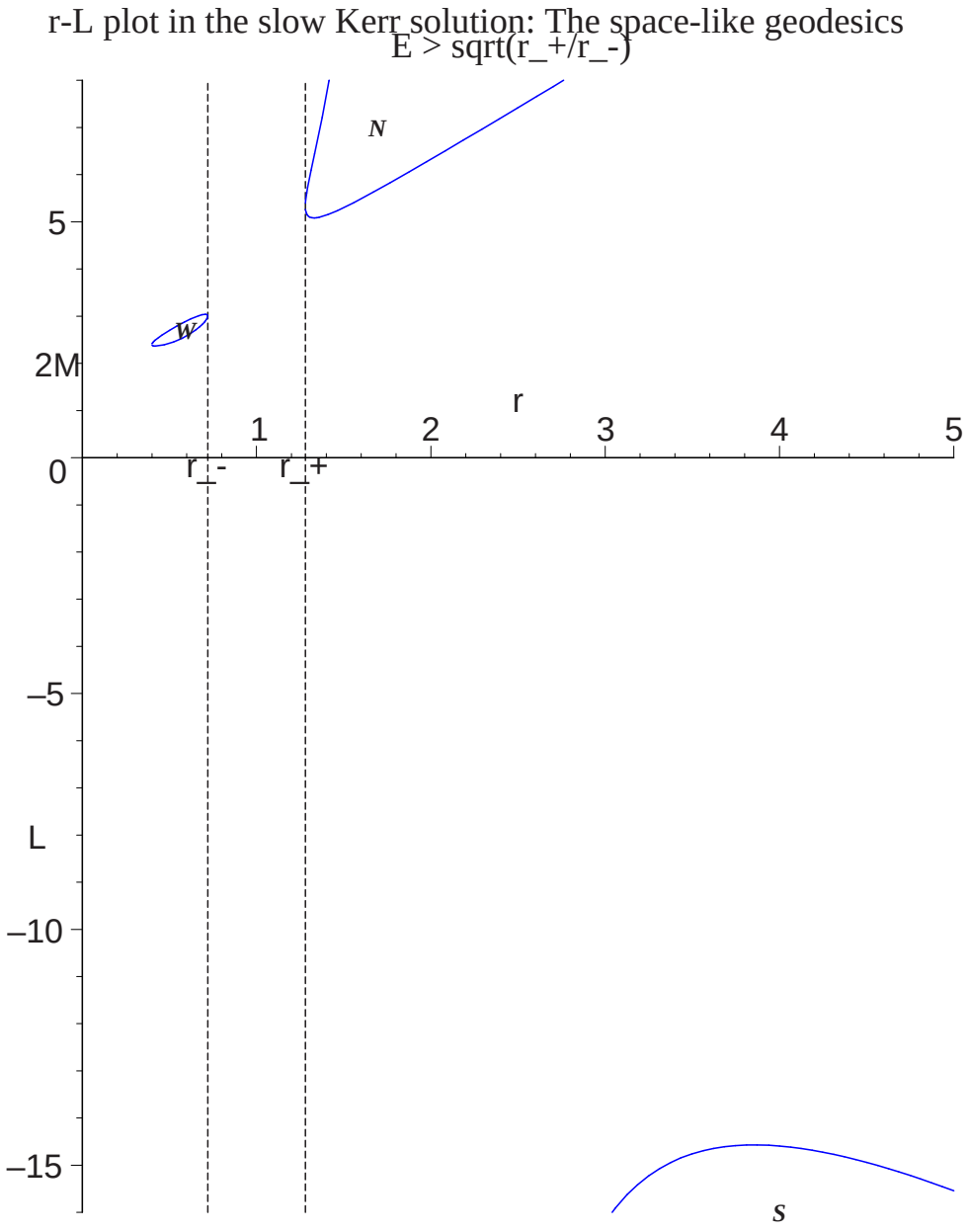

Figure 14.5: Space-like r-L plots for equatorial geodesics. As E decrease from $+\infty$, the island W shrinks. ($M = 1$, $a = 0.96$ and $E = 2$.)

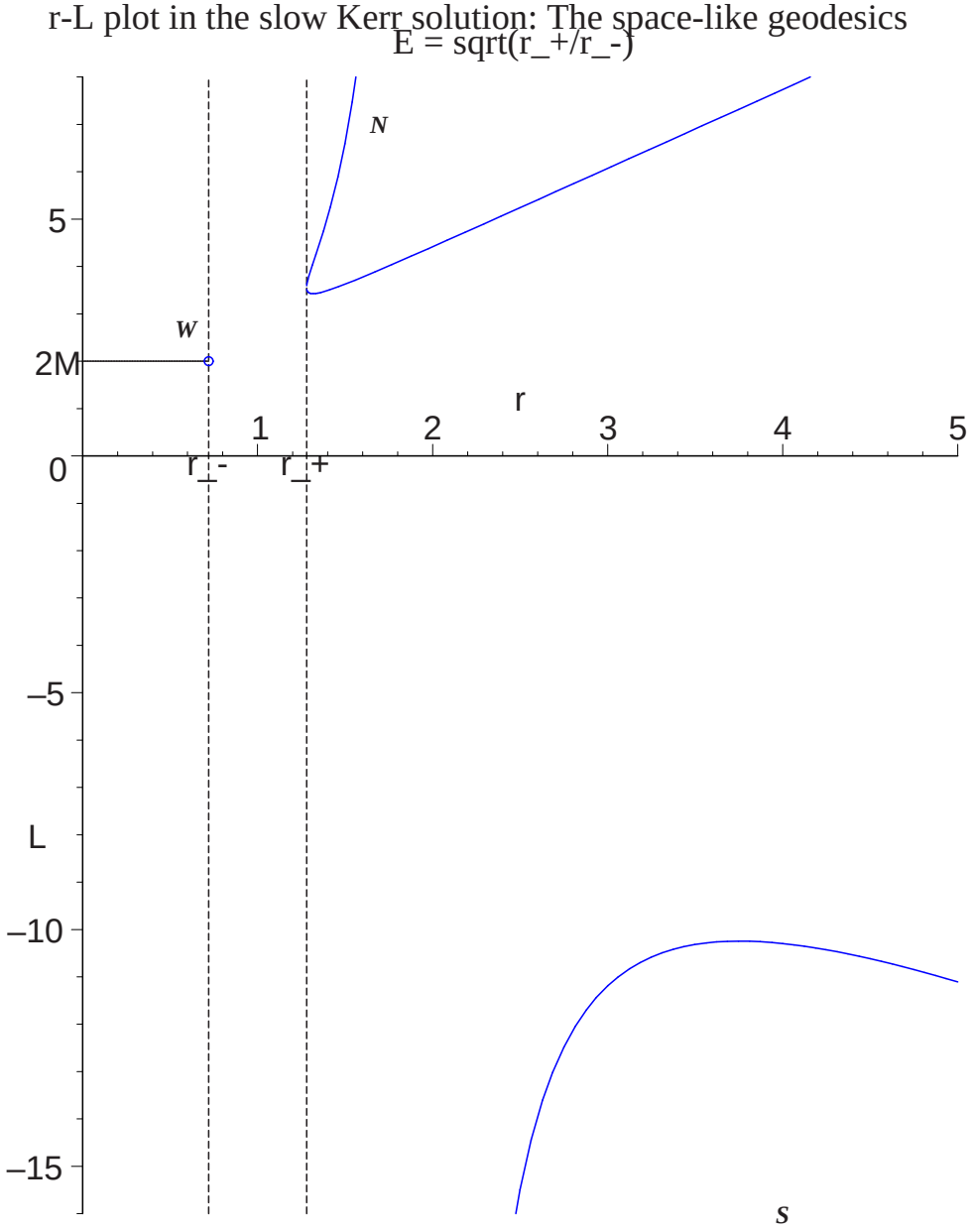

Figure 14.6: Space-like r-L plots for equatorial geodesics. The island W is reduced to a single point $(r_-, 2M)$. ($M = 1$, $a = 0.96$ and $E = \sqrt{\frac{r_+}{r_-}}$.)

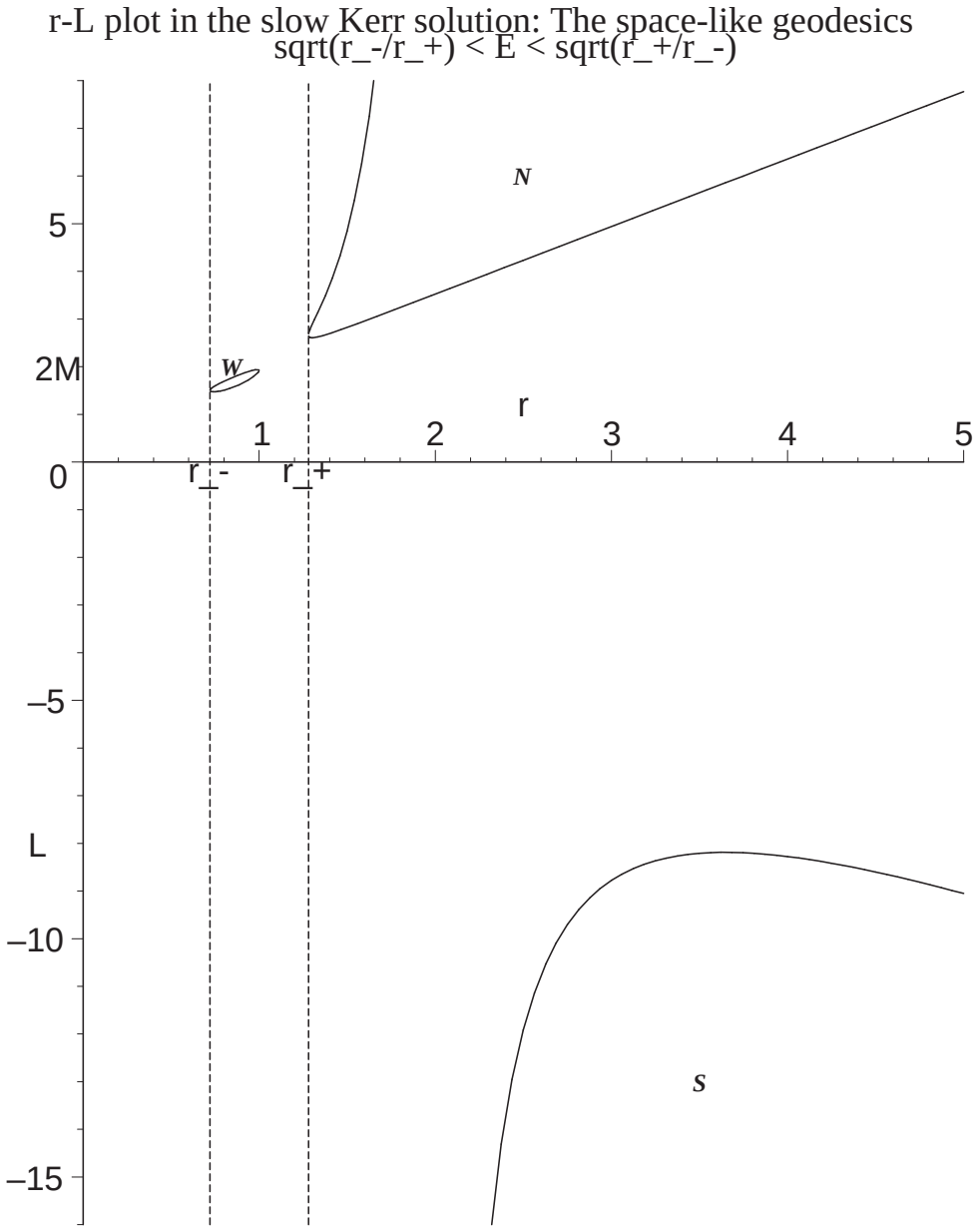

Figure 14.7: Space-like r-L plots for equatorial geodesics. As E decrease from $+\infty$, the island W moves through region B. ($M = 1$, $a = 0.96$ and $E = 1$.)

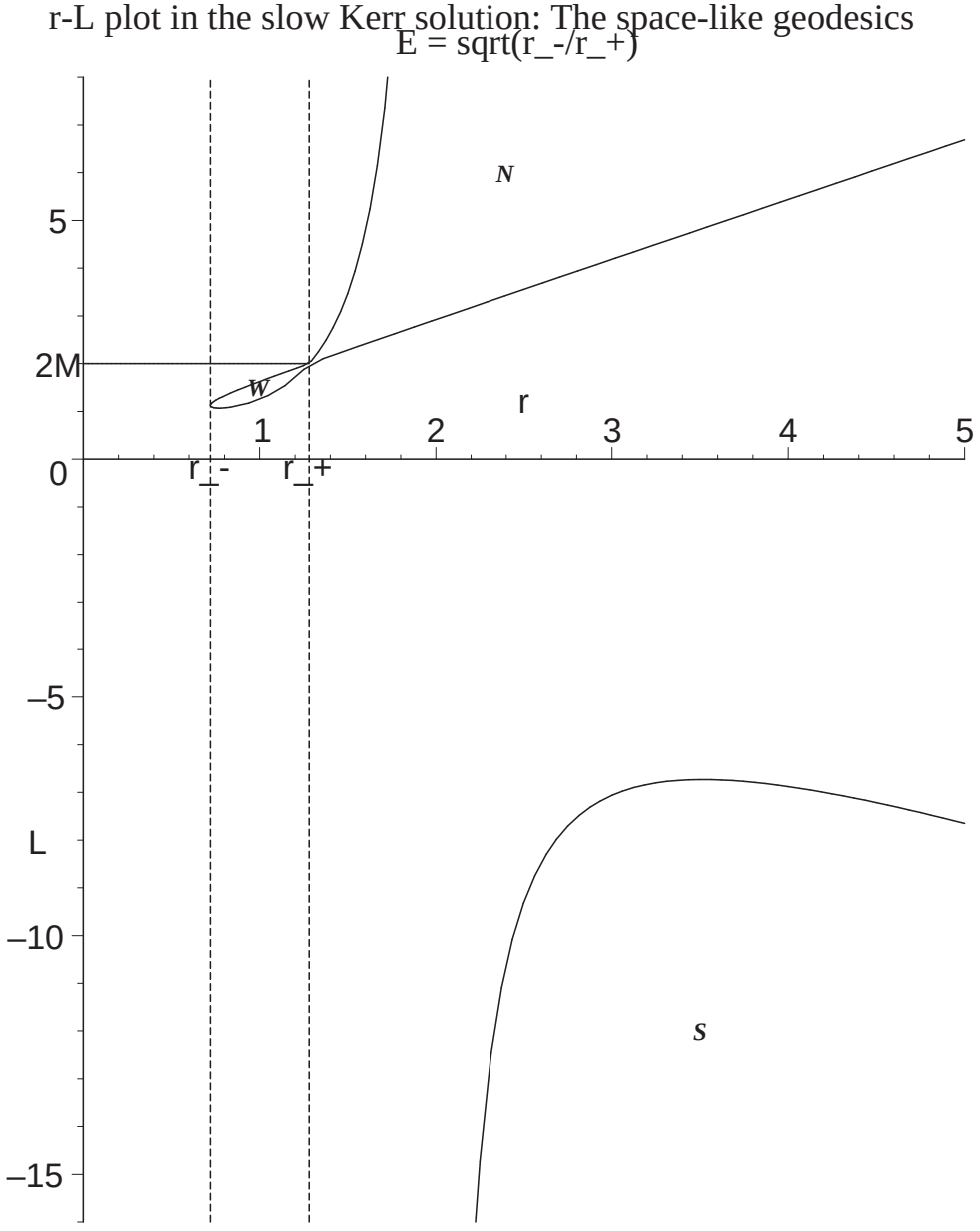

Figure 14.8: Space-like r-L plots for equatorial geodesics. The island W meets with the north continent N. ($M = 1$, $a = 0.96$ and $E = \sqrt{\frac{r_-}{r_+}}$.)

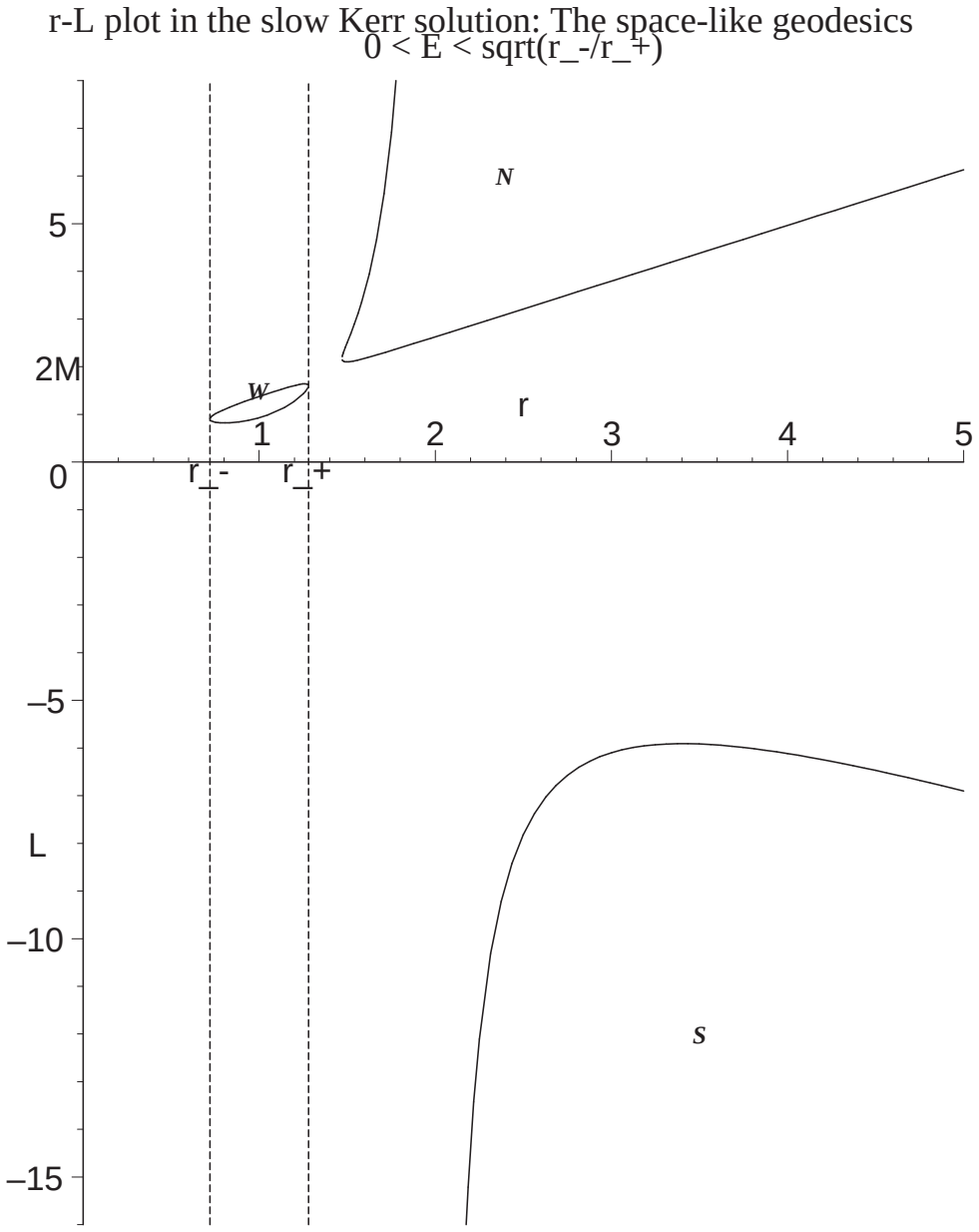

Figure 14.9: Space-like r-L plots for equatorial geodesics. The island W approaches the r-axis. ($M = 1$, $a = 0.96$ and $E = 0.6$.)

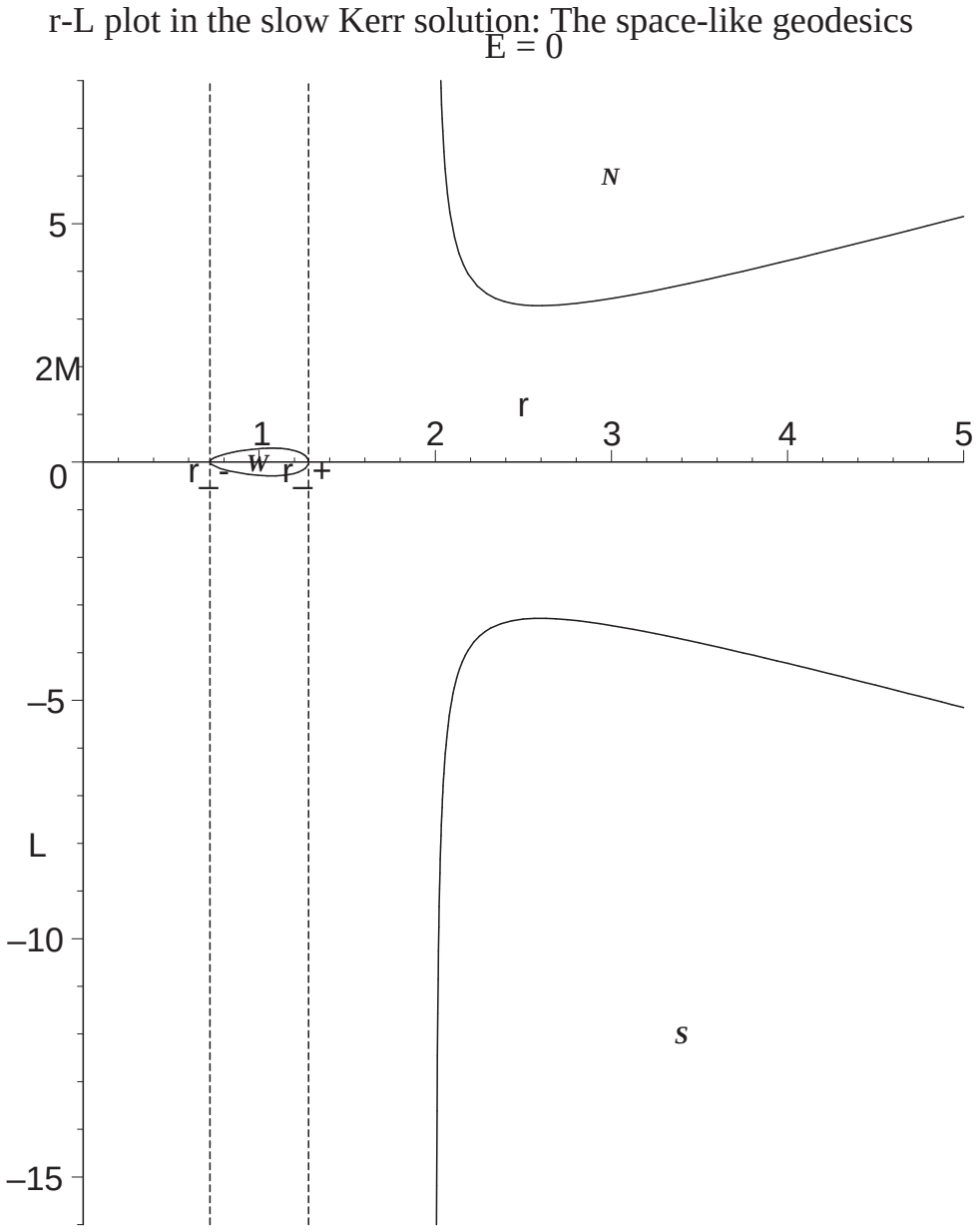

Figure 14.10: Space-like r-L plots for equatorial geodesics. The island W lays symmetrically around the r-axis. ($M = 1$, $a = 0.96$ and $E = 0$.)

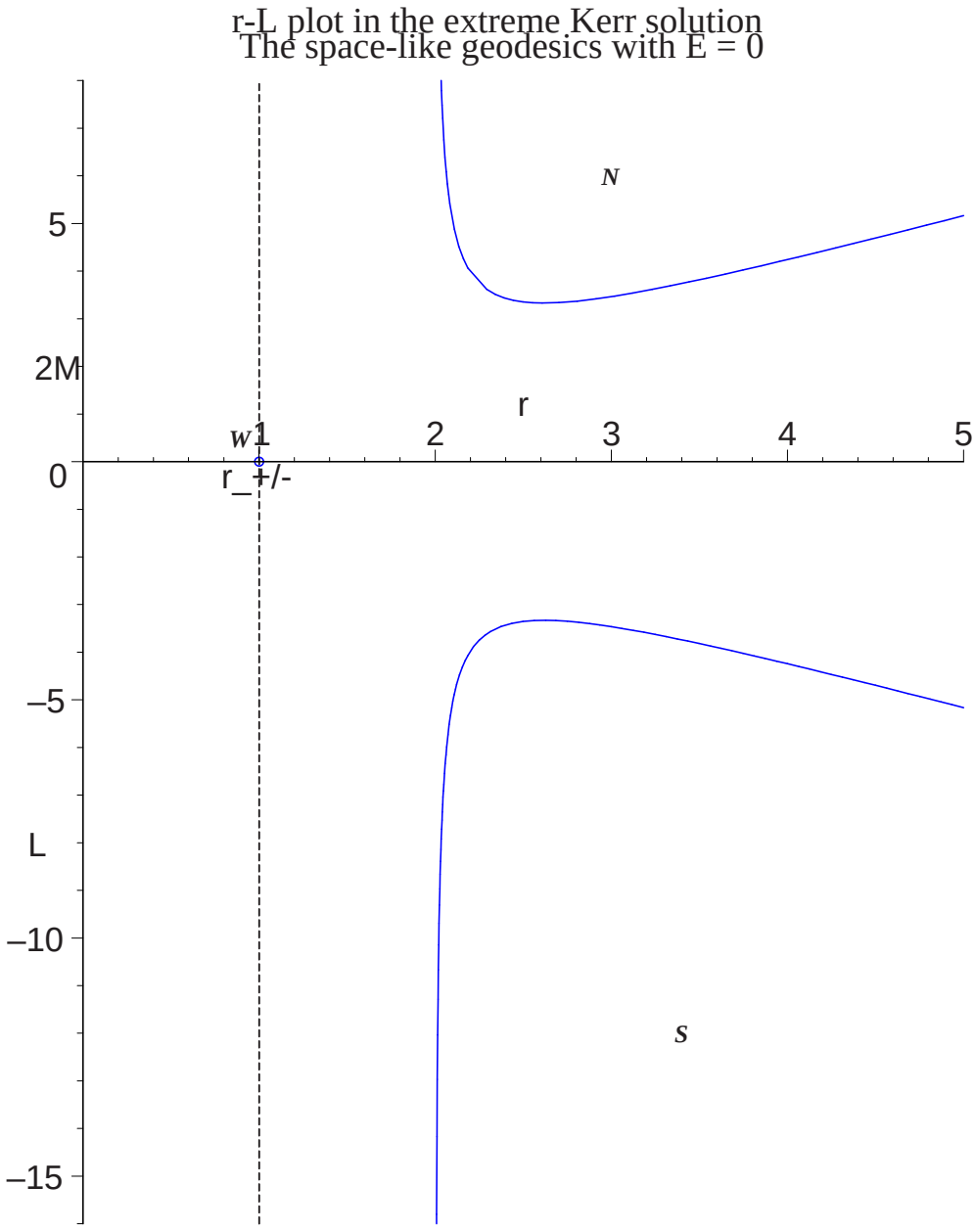

Figure 14.11: Space-like r-L plots for equatorial geodesics. The island W is reduced to a single point $(r_{\pm}, 0)$. ($M = a = 1$ and $E = 0$.)

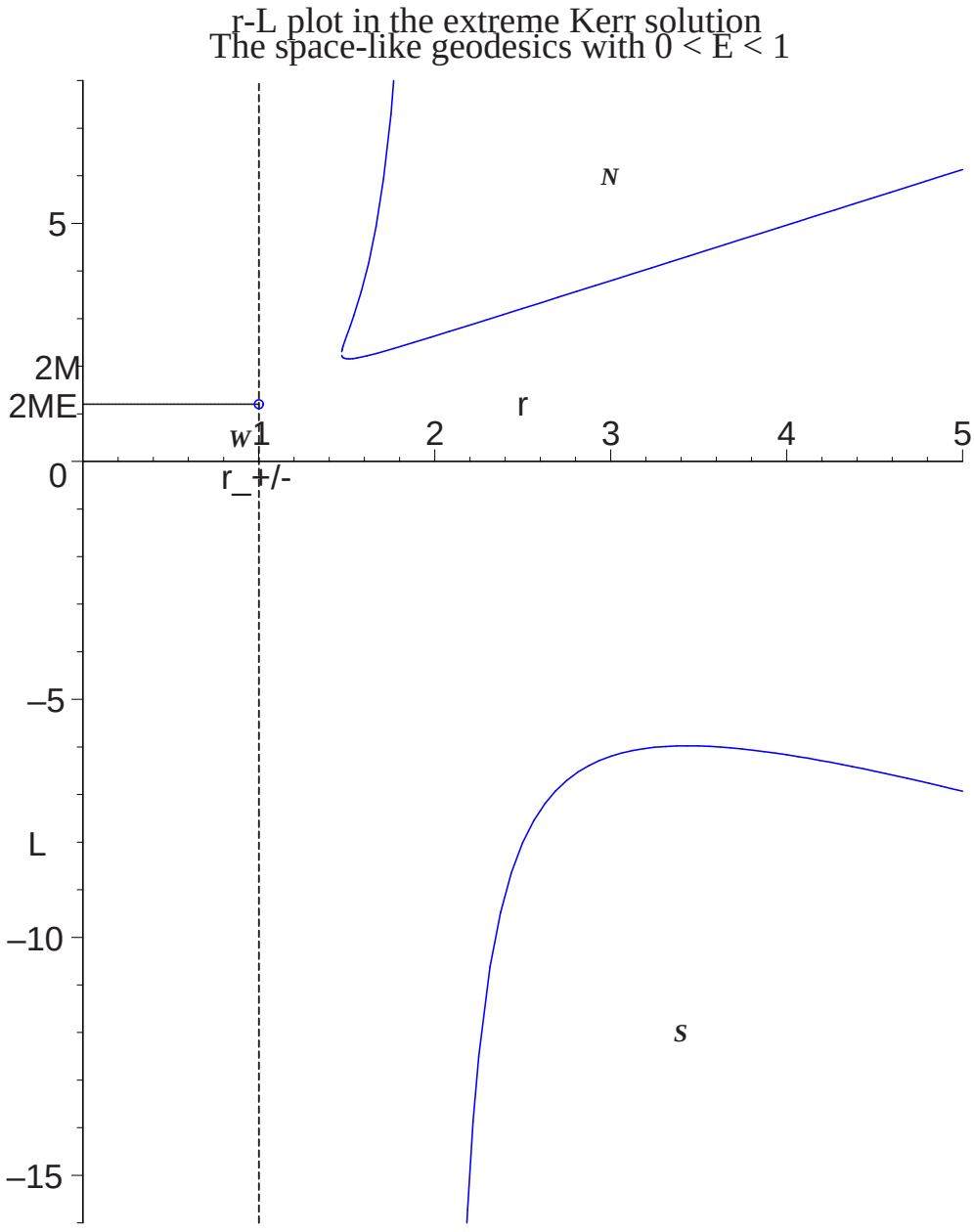

Figure 14.12: Space-like r-L plots for equatorial geodesics. The island W, reduced to a single point $(r_{\pm}, 2ME)$, is moving north from the r-axis. ($M = a = 1$ and $E = 0.6$.)

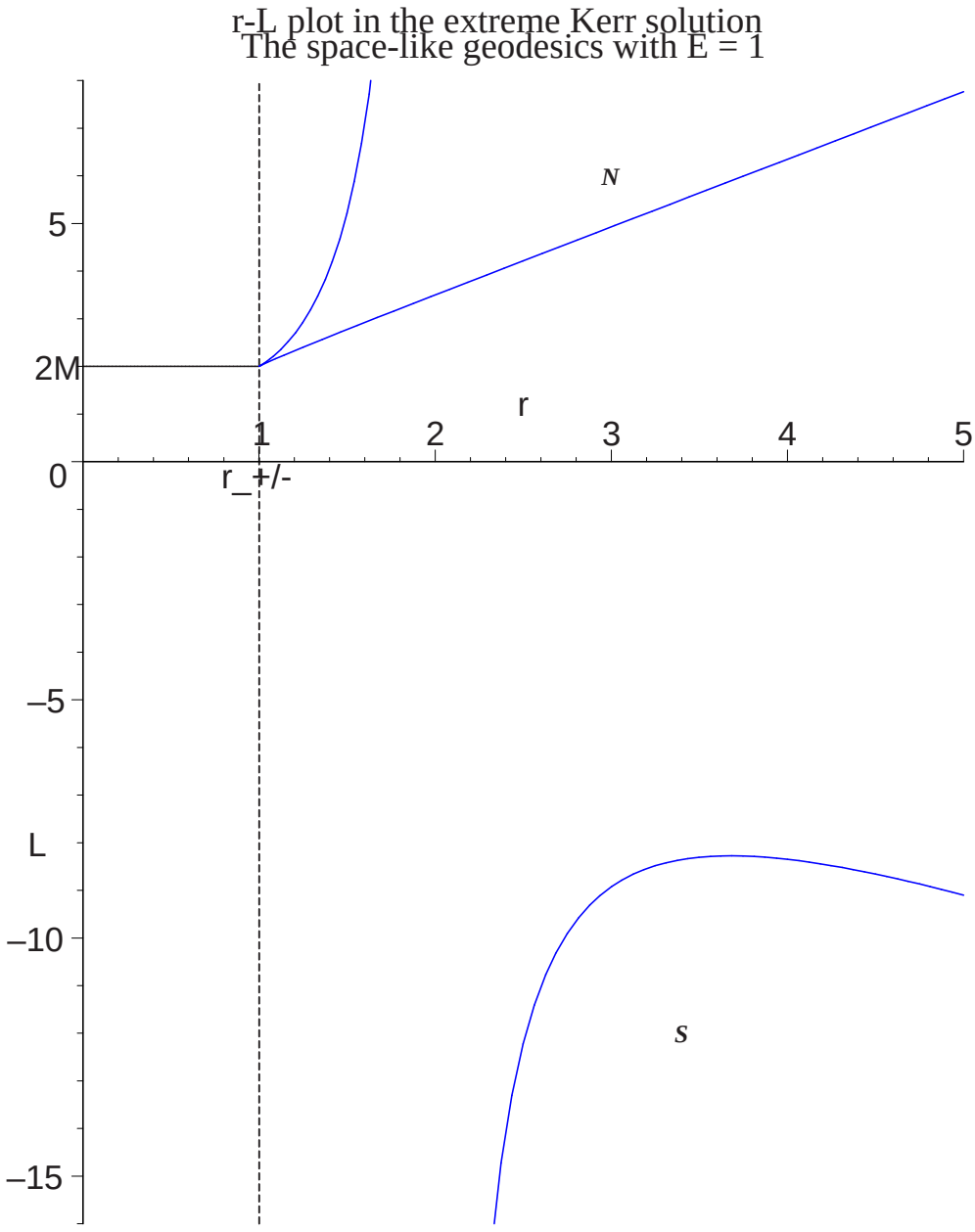

Figure 14.13: Space-like r-L plots for equatorial geodesics. The point W joins the north continent N. ($M = a = 1$ and $E = 1$.)

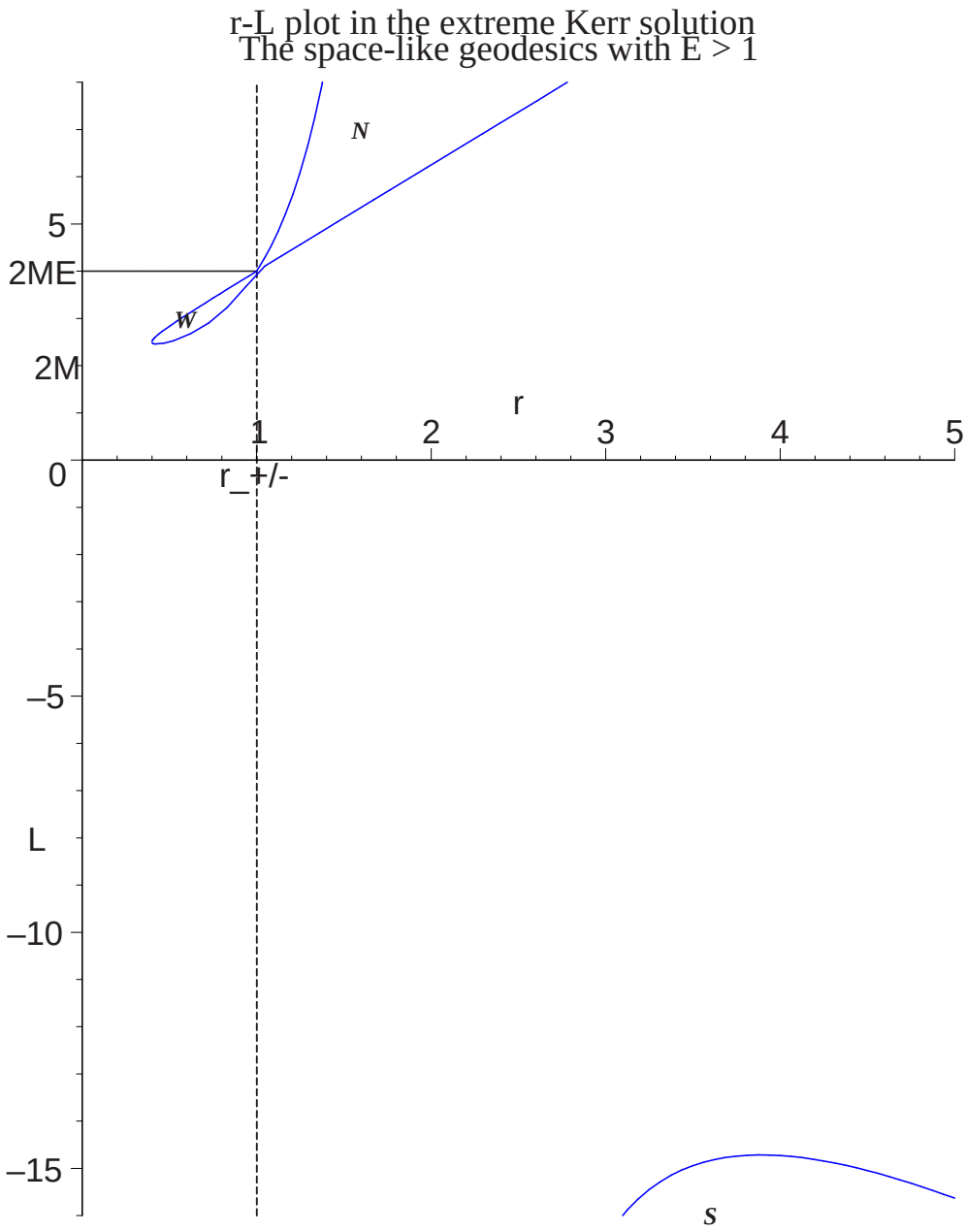

Figure 14.14: Space-like r-L plots for equatorial geodesics. The island W emerges from the north continent N staying connected with N in the point $(r_{\pm}, 2ME)$. W grows with increasing E. ($M = a = 1$ and $E = 2$.)

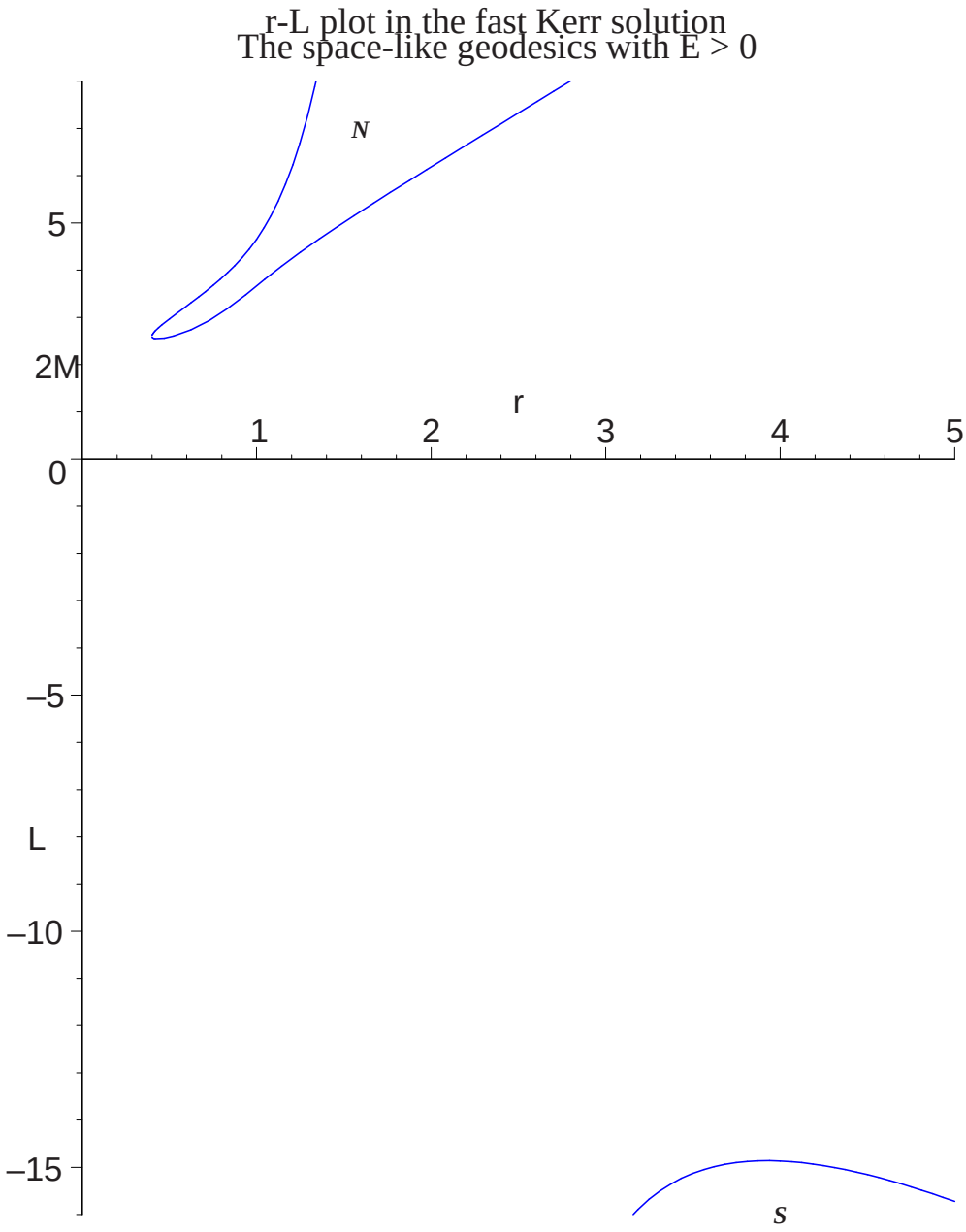

Figure 14.15: Space-like r-L plots for equatorial geodesics. The island W and the north continent N form a single continent. ($M = 1$, $a = 1.04$ and $E = 2$.)

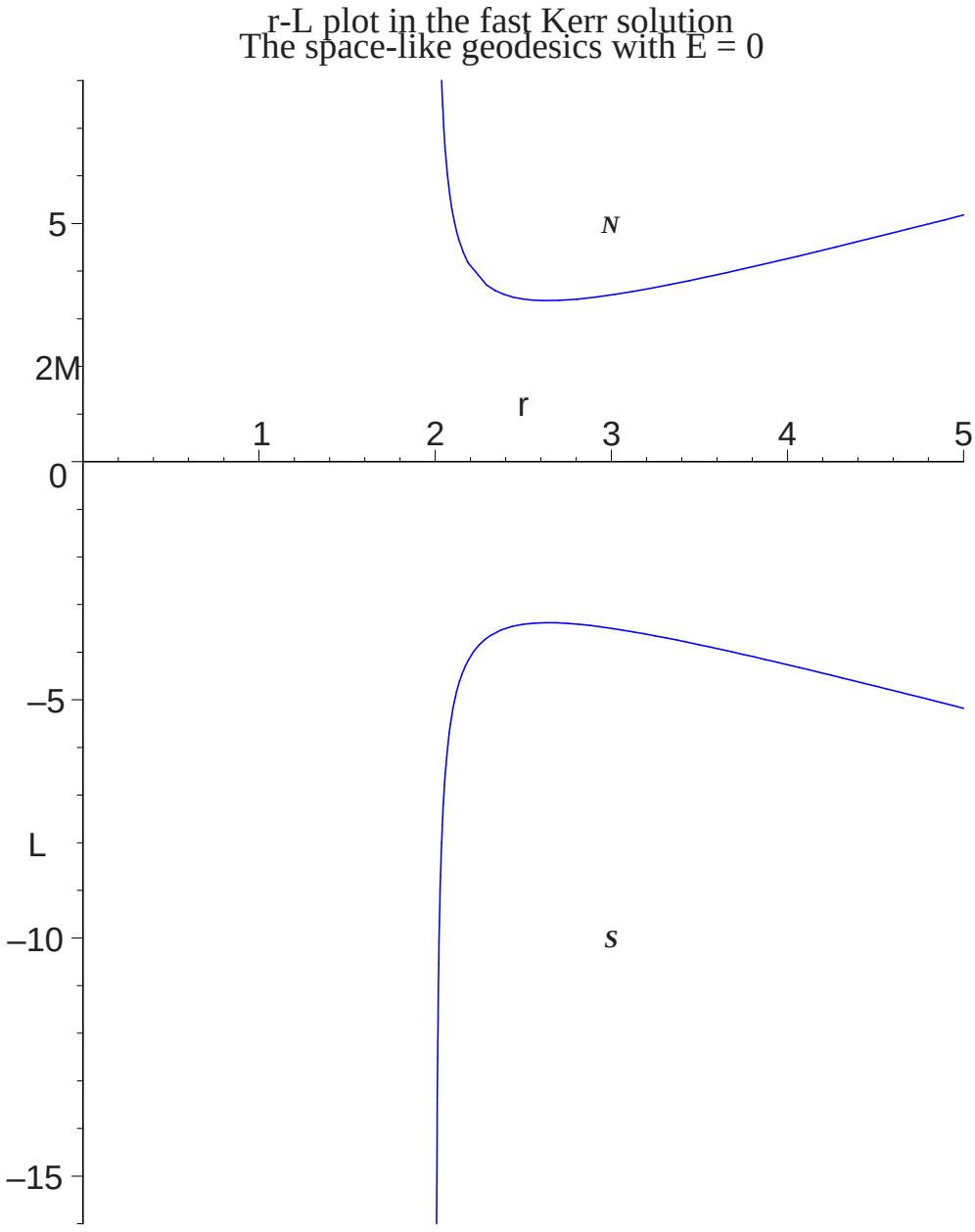

Figure 14.16: Space-like r-L plots for equatorial geodesics. With decreasing E the continent N shrinks. ($M = 1$, $a = 1.04$ and $E = 0$.)

is achieved (see figures 14.10 and 14.11).

14.2.1 The special case, $L = aE$

In this case equations (14.86) reduces to

$$r^2\dot{r} = (E^2+1)r^2 - 2Mr + a^2\,, \tag{14.89}$$

while the equations for $\dot{\varphi}$ and $\dot{t}$ are the same as for the null geodesics (cf. equations (14.16)). Equation (14.89) on integration gives

$$\tau = \frac{1}{E^2+1}\left[\sqrt{(E^2+1)r^2-2Mr+a^2}+ \right. \\ \left. +\frac{M}{\sqrt{E^2+1}}\,\mathrm{arcsinh}\,\frac{(E^2+1)\,r-M}{\sqrt{(E^2+1)a^2+M^2}}\right]\,. \tag{14.90}$$

Alternatively, we may combine equations governing $\dot{r}$ and $\dot{\varphi}$ in the manner

$$\frac{\mathrm{d}u}{\mathrm{d}\varphi} = \frac{1-2Mu+a^2u^2}{aE}\sqrt{E^2+1-2Mu+a^2u^2}\,, \tag{14.91}$$

and obtain the solution

$$\varphi = \frac{E\sqrt{M^2-a^2}}{2}\left[\mathrm{arctanh}\,\frac{a^2(E^2+1)-(a^2u-M)\sqrt{M^2-a^2}-M^2}{a^2E\sqrt{E^2+1-2Mu+a^2u^2}} \right. \\ \left. -\,\mathrm{arctanh}\,\frac{a^2(E^2+1)+(a^2u-M)\sqrt{M^2-a^2}-M^2}{a^2E\sqrt{E^2+1-2Mu+a^2u^2}}\right]\,, \tag{14.92}$$

where we assume E to be positive. An example of an orbit derived with the aid of the equation (14.92) is illustrated in figure 14.17.

14.2.2 General orbits

In this section we will find general solutions for all three types of orbits. From equation (14.86) it is clear that turning points occur at the zeros of the cubic polynomial

$$f(u) = 2Mu\,(aE-L)^2\,u^3 + \left(a^2e-L^2\right)u^2 - 2Mu + e. \tag{14.93}$$

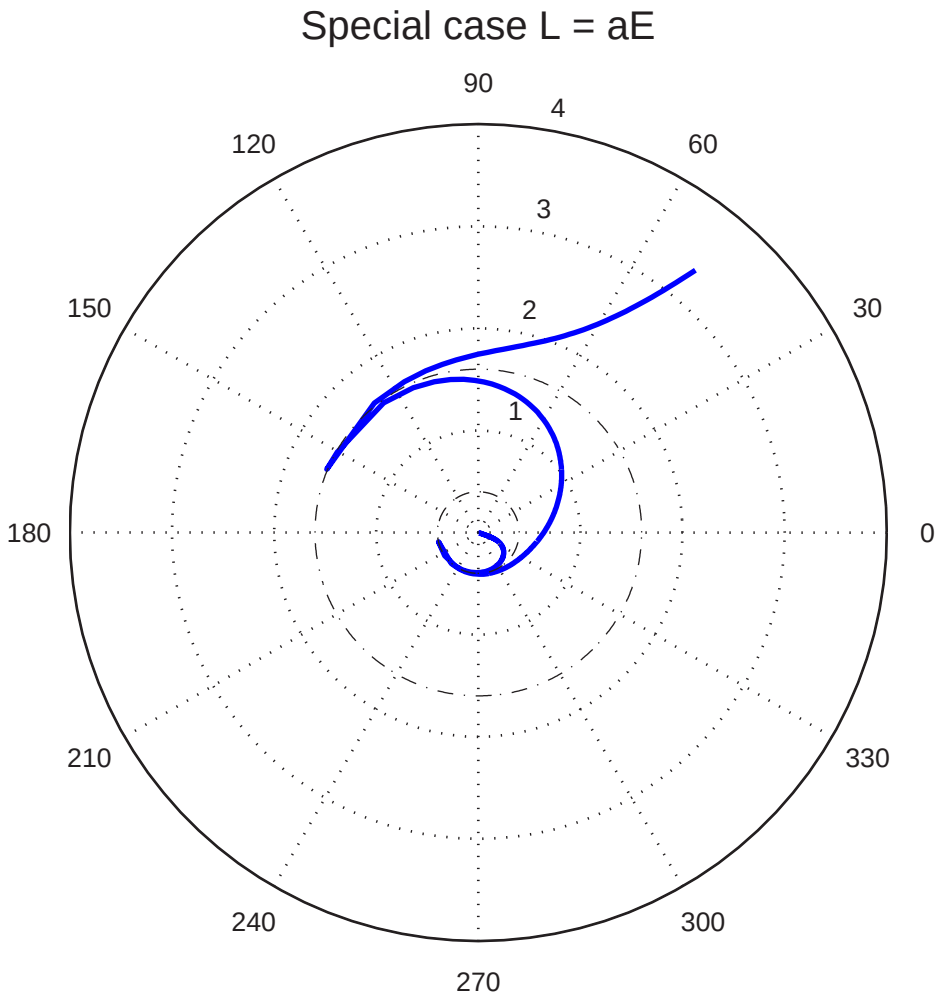

Figure 14.17: An example of a space-like geodesic with $L = aE$, described in the equatorial plane of a Kerr black hole with $M = 1$ and $a = 0.8$. For the orbit illustrated, $E = 2$. An equivalent of radial geodesic this orbit comes from infinity to singularity, reversing its direction on both horizons. The two horizons are represented by dash-dotted circles.

With this polynomial instead of (14.33) the solutions for τ and φ are formally the same as in section 14.1.2.

Unstable circular orbits

We look for the values of L and E which a circular orbit at some assigned radius, $r = 1/u$, will have. When L and E have these values, the cubic polynomial (14.93) will have a double root. The conditions for a double root are

$$a^2u^2 - 2Mu + 1 + E^2 + 2Mx^2u^3 - \left(x^2 + 2aEx\right) = 0 \tag{14.94}$$

and

$$a^2u - M + 3Mx^2u^2 - \left(x^2 + 2aEx\right)u = 0\,, \tag{14.95}$$

where we have written

$$x = L - aE\,. \tag{14.96}$$

Equations (14.94) and (14.95) can be combined to give

$$E^2 = (Mu - 1) + Mx^2u^3 \tag{14.97}$$

and

$$2axEu = x^2(3Mu - 1)u + a^2u - M\,. \tag{14.98}$$

By eliminating E between these equations, we obtain the following quadratic equation for x:

$$\begin{aligned} &x^4u^2\left[(3Mu-1)^2 - 4a^2Mu^3\right] \\ &\quad + 2x^2u\left[(3Mu - a)\left(a^2u - M\right) - 2a^2u(Mu - 1)\right] + \left(a^2u - M\right)^2 = 0\,. \end{aligned} \tag{14.99}$$

The discriminant of this equation is

$$-4a^2M\Delta^2(u)u\,, \tag{14.100}$$

where $\Delta(u)$ is defined in (14.48); and the solution of equation (14.99) takes a simple form by writing

$$(3Mu-1)^2 - 4a^2Mu^3 = Q_+Q_-\,, \tag{14.101}$$

where

$$Q_\pm = 1 - 3Mu \pm 2a\sqrt{Mu^3}\,. \tag{14.102}$$

Thus, we find

$$x^2u^2 = -\frac{Q_\pm\Delta(u) - Q_+Q_-}{Q_+Q_-} = -\frac{\Delta(u) - Q_\mp}{Q_\mp}\,. \tag{14.103}$$

But

$$\Delta(u) - Q_\mp = u\left(a\sqrt{u} \pm \sqrt{M}\right)^2\,. \tag{14.104}$$

Therefore the solution for x takes the form

$$x = -\frac{a\sqrt{u} \pm \sqrt{M}}{\sqrt{uQ_\mp}}\,. \tag{14.105}$$

Inserting the solution (14.105) for x in equation (14.97), we find

$$E = \sqrt{\frac{4Mu - 1 - 2M^2u^2 + Mu^3a^3 \pm a\sqrt{Mu^3}}{Q_\mp}}\,; \tag{14.106}$$

and the value of L to be associated with this value of E is

$$L = aE = \frac{\pm\sqrt{M} + a\sqrt{u}\left(\sqrt{4Mu - 1 - 2M^2u^2 + Mu^3a^3 \pm a\sqrt{Mu^3}} - 1\right)}{\sqrt{uQ_\mp}}\,. \tag{14.107}$$

E and L given by equations (14.106) and (14.107) are the energy and the angular momentum (per unit mass) of a particle describing a circular orbit of reciprocal radius u.

14.3 The time-like geodesics

For time-like geodesics, equations (14.7) and (14.8) for $\dot\varphi$ and $\dot t$ remain the same. On the other hand, equation (14.12) is replaced by

$$r^2\dot r^2 = -\Delta + r^2E^2 + \frac{2M}{r}(L - aE)^2 - \left(L^2 - a^2E^2\right)\,, \tag{14.108}$$

where E is now the energy per unit mass of the particle.

14.3.1 The special case, $L = aE$

The time-like geodesics with $L = aE$, are like null geodesics with $D = a$, in that that their behavior as they cross the horizons is characteristic of the orbits in general.

For $L = aE$, equation (14.108) reduces to

$$r^2\dot{r}^2 = (E^2-1)r^2 + 2Mr - a^2\,, \tag{14.109}$$

while the equations for $\dot{\varphi}$ and $\dot{t}$ remain the same as for the null geodesics (cf. equations (14.16)):

$$\dot{\varphi} = aE/\Delta \qquad \text{and} \qquad \dot{t} = E\left(r^2+a^2\right)/\Delta\,. \tag{14.110}$$

Equation (14.109) yields

$$\tau = \pm\int \frac{r\,\mathrm{d}r}{\sqrt{(E^2-1)r^2+2Mr-a^2}}\,. \tag{14.111}$$

Since we are considering infalling particles, we take equation (14.111) with the negative sign. After integration we get[3]

$$\begin{aligned}\tau =& \frac{1}{1-E^2}\left\{\sqrt{(E^2-1)r^2+2Mr-a^2}\right.\\ &\left.-\frac{M}{\sqrt{E^2-1}}\ln\left[\sqrt{(E^2-1)r^2+2Mr-a^2}+r\sqrt{E^2-1}+\frac{M}{\sqrt{E^2-1}}\right]\right\}\\ &\text{(for } E^2>1)\,,\end{aligned} \tag{14.112}$$

$$\tau = -\frac{Mr+a^2}{3M^2}\sqrt{2Mr-a^2} \qquad \text{(for } E^2=1) \tag{14.113}$$

and

$$\begin{aligned}\tau =& \frac{1}{1-E^2}\left[\sqrt{(E^2-1)r^2+2Mr-a^2}+\right.\\ &\left.+\frac{M}{\sqrt{1-E^2}}\arcsin\frac{M-(1-E^2)r}{\sqrt{M^2-a^2(1-E^2)}}\right] \qquad \text{(for } 1-M^2/a^2<E^2<1).\end{aligned} \tag{14.114}$$

[3] Compare [7, page 333, equation (100)] and (14.114).

Alternatively, for a slow black hole, equations governing $\dot{r}$ and $\dot{\varphi}$ can be combined as follows

$$\frac{\mathrm{d}u}{\mathrm{d}\varphi} = \pm\frac{a}{E}(u-u_+)(u-u_-)\sqrt{(E^2-1)+2Mu-a^2u^2}\,, \tag{14.115}$$

where $u = 1/r$ and $u_\pm = 1/r_\pm$. The solution is

$$\varphi = \frac{1}{a(u_+-u_-)}\left\{\ln\left[2E\sqrt{E^2\xi_+^2+2(M-a^2u_+)\xi_+-a^2}+2E^2\xi_+ + \right.\right. \\ \left. + 2\left(M-a^2u_+\right)\right] - \ln\left[2E\sqrt{E^2\xi_-^2+2(M-a^2u_-)\xi_--a^2}+2E\xi_- + \right. \\ \left.\left. + 2M\left(M-a^2u_-\right)\right]\right\}, \tag{14.116}$$

where

$$\xi_\pm = (u-u_\pm)^{-1}\,. \tag{14.117}$$

For an extreme or fast black hole, we may combine equations governing $\dot{r}$ and $\dot{\varphi}$ in the manner

$$\frac{\mathrm{d}u}{\mathrm{d}\varphi} = \pm\frac{aE}{1-2Mu+a^2u^2}\sqrt{E^2-1+2Mu-a^2u^2}\,, \tag{14.118}$$

and obtain the solution

$$\varphi = \frac{-aE}{2u_2(a^2u_2^2+1+2Mu_2)\sqrt{A}}\left\{2Bu_2\left(a^2Mu_2^2+2M^2u_1-a^2+2M^2u_2+ \right.\right. \\ \left. +a^2Mu_1u_2-a^2u_1\right)+2\sqrt{A}\left(a^2u_2^2+1+ \right. \\ \left. +2Mu_2\right)\ln\left(u_1z^2-u_2\right)-u_2\sqrt{A}\left(2M+a^2u_2\right)\ln\left[z^4\left(1-2Mu_1+a^2u_1^2\right)+ \right. \\ \left.\left. +2z^2\left(Mu_2-Mu_1-a^2u_1u_2+1\right)+a^2u_2^2+2Mu_2+1\right]\right\} \\ \text{(for } E^2 > 1-M^2/a^2\text{)}, \tag{14.119}$$

where u_1 and u_2 are the solutions of polynomial $a\left(\frac{E^2-1}{a^2}+\frac{2M}{a^2}u-u^2\right)$, and

$$z^2 = \frac{u_2-u}{u-u_1}\,, \tag{14.120}$$

$$A = \left(a^2-M^2\right)\left(u_2-u_1\right)^2\,, \tag{14.121}$$

$$B = \arctan\frac{a^2u_1^2z^2+z^2-2Mu_1z^2-a^2u_1u_2+Mu_2-Mu_1+1}{\sqrt{A}}\,. \tag{14.122}$$

14.3.2 General orbits

As before in the case of the null and space-like geodesics, we will find solutions for all three types of orbits. We have the same polynomial (14.93) as in the case of the space-like geodesics with redefinition of the effective energy e. (In the space-like case $e = E^2 + 1$, now $e = E^2 - 1$.) Solutions for the unbound orbits ($e \leq 1$) look formally the same as in section 14.1.2, but in the case of $e < 1$ we have bound orbits. For them

$$\tau = \frac{gk^4}{{u_2}^2\alpha^4|L-aE|\sqrt{2M}}\Bigg\{\mathrm{F}(\phi,k)+ \\ + \frac{2(\alpha^2-k^2)}{k^2}\Pi\left(\phi,\alpha^2,k\right) - \frac{\alpha^2-k^2}{2k^4(\alpha^2-1)}\Bigg[\alpha^2\,\mathrm{E}(\phi,k) - \left(\alpha^2-k^2\right)\mathrm{F}(\phi,k)+ \\ + \left(2\alpha^2k^2+2\alpha^2-\alpha^4-3k^2\right)\Pi\left(\phi,\alpha^2,k\right) - \frac{\alpha^4\,\mathrm{sn}\,v\,\mathrm{cn}\,v\,\mathrm{dn}\,v}{1-\alpha^2\,\mathrm{sn}^2\,v}\Bigg]\Bigg\}\,, \quad (14.123)$$

where g is defined in (14.35), k in (14.37), ϕ and v in (14.36), $u_1 < u_2 < u_3$ are roots of $f(u)$, and

$$\alpha^2 = \frac{u_3k^2}{u_2}\,; \quad (14.124)$$

$$\varphi = \frac{g}{u_+-u_-}\Bigg\{\frac{L-2Mu_-(L-aE)}{\alpha_-^2(u_--u_2)}\left[k^4\,\mathrm{F}(\phi,k)+ \right. \\ \left. + \left(\alpha_-^2-k^2\right)\Pi\left(\phi,\alpha_-^2,k\right)\right] - \frac{L-2Mu_+(L-aE)}{\alpha_+^2(u_+-u_2)}\left[k^4\,\mathrm{F}(\phi,k)+ \right. \\ \left. + \left(\alpha_+^2-k^2\right)\Pi\left(\phi,\alpha_+^2,k\right)\right]\Bigg\}\,, \quad (14.125)$$

where u_1, u_2, u_3, ϕ, v and k are the same as for solution for τ, g is defined in (14.44), and

$${\alpha_\pm}^2 = \frac{k^2(u_\pm-u_3)}{u_\pm-u_2}\,, \quad (14.126)$$

where $u_\pm$ are the solutions of $\Delta(u) = 1 - 2Mu + a^2u^2$.

For the orbits of the second kind, which are associated with the bound

orbits

$$\tau = \frac{g}{\alpha^4(u_3-u_1)^2|L-aE|\sqrt{2M}}\Bigg\{\mathrm{F}(\phi,k) - 2\Pi\left(\phi,\alpha^2,k\right) + \\ + \frac{1}{2(\alpha^2-1)(k^2-\alpha^2)}\Bigg[\alpha^2\,\mathrm{E}(\phi,k) + \left(k^2-\alpha^2\right)\mathrm{F}(\phi,k) + \\ + \left(2\alpha^2k^2+2\alpha^2-\alpha^4-3k^2\right)\Pi\left(\phi,\alpha^2,k\right) - \frac{\alpha^4\,\mathrm{sn}\,v\,\mathrm{cn}\,v\,\mathrm{dn}\,v}{1-\alpha^2\,\mathrm{sn}^2\,v}\Bigg]\Bigg\}\,, \quad (14.127)$$

where we have the same u_1, u_2, u_3, k and g as in the case of orbits of the first kind, α is defined in (14.39), and ϕ and v in (14.40);

$$\varphi = \frac{g}{(u_+-u_-)(u_3-u_1)}\left\{\frac{L-2Mu_+(L-aE)}{{\alpha_+}^2}\left[\Pi\left(\phi,{\alpha_+}^2,k\right)-\mathrm{F}(\phi,k)\right]\right. \\ \left. -\frac{L-2Mu_-(L-aE)}{{\alpha_-}^2}\left[\Pi\left(\phi,{\alpha_-}^2,k\right)-\mathrm{F}(\phi,k)\right]\right\}\,, \quad (14.128)$$

where ϕ, v, u_1, u_2, u_3 are the same as in the above solution for τ, g is defined in (14.35), α_+ is in (14.50), α_- in (14.51), k in (14.57), and $u_\pm$ have the same meaning as in the case of orbits of the first kind.

The last type of orbit is the crash-escape orbit. Solution for τ can be again written in terms of elliptic integrals, but we will not do it here, because it is long and does not bring any new features. Solution for φ is

$$\varphi = \frac{g[L-2Mu_+(L-aE)]}{\alpha_+(u_+-u_-)(A+u_3-u_+)}\left\{\frac{1}{1-\alpha_+}\left[\Pi\left(\phi,\frac{{\alpha_+}^2}{{\alpha_+}^2-1},k\right)-\alpha_+ f_+\right]\right\} \\ -\frac{g[L-2Mu_+(L-aE)]}{\alpha_-(u_+-u_-)(A+u_3-u_-)}\left\{\frac{1}{1-\alpha_-}\left[\Pi\left(\phi,\frac{{\alpha_-}^2}{{\alpha_-}^2-1},k\right)-\alpha_- f_-\right]\right\}\,, \quad (14.129)$$

where g is defined in (14.54), k as above in (14.57), ϕ in (14.56), α_+ in (14.62), α_- in (14.61), and A in (14.58).

The circular and associated orbit

We will follow [7, chapter 7] to find conditions for E and L for circular orbits. With the reciprocal radius $u = 1/r$ as the independent variable, the radial equation (14.108) becomes

$$u^{-4}\dot{u}^2 = -\left(a^2u^2-2Mu\right)+E^2+2M\left(L-aE\right)^2u^3-\left(L^2-a^2E^2\right)u^2\,. \quad (14.130)$$

When L and E have the values which a circular orbit at some assigned radius, $r = 1/u$, will have, the cubic polynomial on the right-hand side of equation (14.130) will have a double root. The conditions for a double root are

$$-\left(a^2u^2 - 2Mu + 1\right) + E^2 + 2Mx^2u^3 - \left(x^2 + 2aEx\right)u^2 = 0 \qquad (14.131)$$

and

$$-\left(a^2u - M\right) + 3Mx^2u^2 - \left(x^2 + 2aEx\right)u = 0\,, \qquad (14.132)$$

where x is defined in (14.96). The equations above can be combined to give

$$E^2 = (1 - Mu) + Mx^2u^3 \qquad (14.133)$$

and

$$2axEu = x^3(3Mu - 1)u - \left(a^2u - M\right)\,. \qquad (14.134)$$

Eliminating E between these equations leads to the following quadratic equation for x:

$$\begin{aligned} &x^4u^2\left[(3Mu-1)^2 - 4a^2Mu^3\right] \\ &\quad - 2x^2u\left[(3Mu-1)\left(a^2u - M\right) - 2a^2u(Mu-1)\right] + \left(a^2u - M\right)^2 = 0\,. \end{aligned} \qquad (14.135)$$

Its discriminant is

$$4a^2M\Delta^2(u)u\,, \qquad (14.136)$$

where $\Delta(u)$ is defined in (14.48); and by using (14.101) and (14.102), the solution of equation (14.135) takes a simple form. Hence

$$x^2u^2 = \frac{Q_\pm\Delta(u) - Q_+Q_-}{Q_+Q_-} = \frac{\Delta(u) - Q_\mp}{Q_\mp}\,. \qquad (14.137)$$

With the use of (14.104) the solution for x takes a simple form (14.105). Inserting it in equation (14.133), we find

$$E = \frac{1 - 2Mu \mp a\sqrt{Mu^3}}{\sqrt{Q_\mp}}\,; \qquad (14.138)$$

and the value of L associated with this value of E is

$$L = aE + x = \mp \left(a^2u^2 + 1 \pm 2a\sqrt{Mu^3} \right) \sqrt{\frac{M}{uQ_{\mp}}} \,. \tag{14.139}$$

E and L given by the above equations are the energy and the angular momentum (per unit mass) of a particle in a circular orbit of reciprocal radius u.

Chapter 15

The null geodesics

In this section we follow [7, section 63] with a few of our additions.

For the null geodesics $\delta_1 = 0$, and it is convenient to minimize the number of parameters by letting

$$\xi = L/E \qquad \text{and} \qquad \eta = Q/E^2\,, \tag{15.1}$$

and writing R and Θ in place of R/E^2 and Θ/E^2:

$$\mathrm{R} = r^4 + \left(a^2 - \xi^2 - \eta\right) r^2 + 2M\left[\eta + (\xi - a)^2\right] r - a^2\eta \tag{15.2}$$

and

$$\Theta = \eta + a^2\cos^2\theta - \xi^2\cot^2\theta\,. \tag{15.3}$$

The equation governing the projection of the orbit in the (r, θ)-plane is

$$\int_{r_i}^{r} \frac{\mathrm{d}r}{\sqrt{\mathrm{R}}} = \int_{\theta_i}^{\theta} \frac{\mathrm{d}\theta}{\sqrt{\Theta}}\,, \tag{15.4}$$

where r_i and θ_i are certain assigned initial values of r and θ. Also while the signs of $\sqrt{\mathrm{R}}$ and $\sqrt{\Theta}$ can be chosen independently, they must be adhered to once the choice has been made.

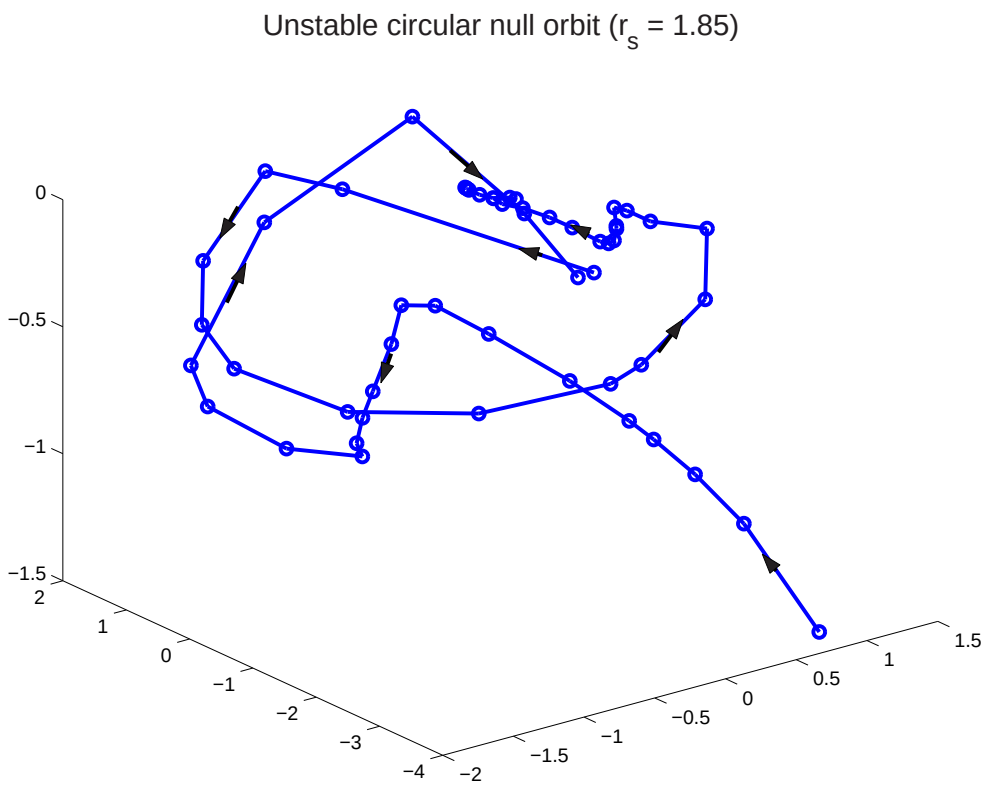

Figure 15.1: Critical null geodesic in "spherical" coordinates with $r_s = 1.85$, $M = 1$ and $a = 0.8$. The orbit does not reach the singularity.

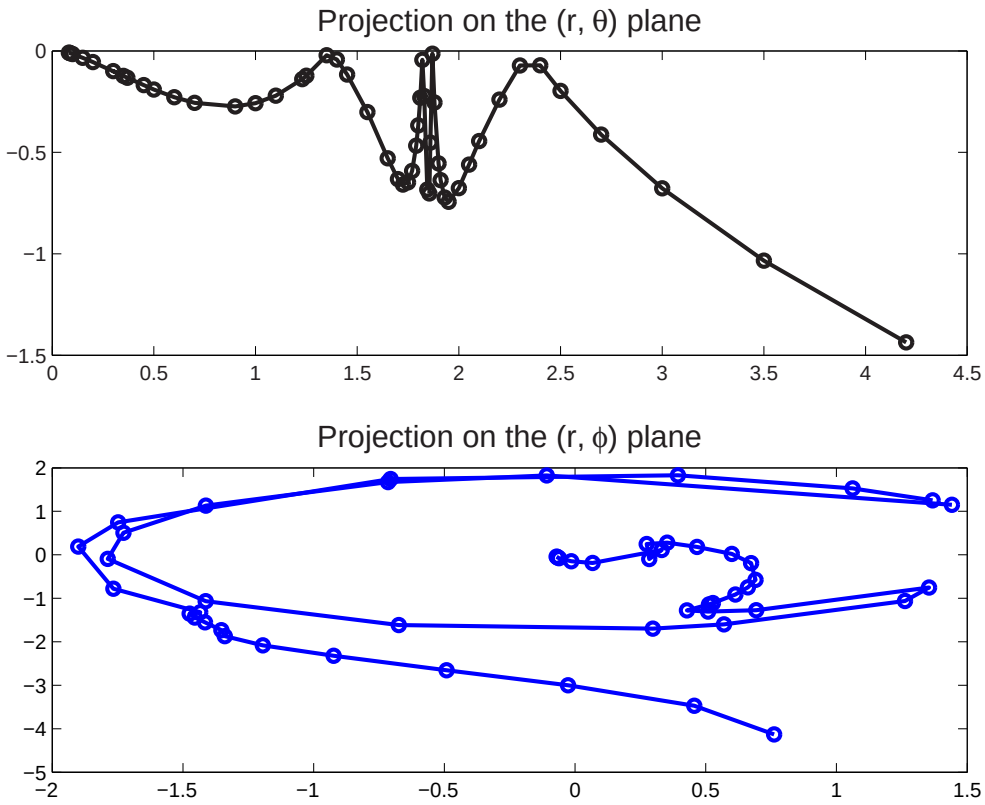

Figure 15.2: The projections of the critical null geodesic with $r_s = 1.85$, $M = 1$ and $a = 0.8$ on (r, θ) and (r, φ) respectively. The orbit does not reach the singularity. The first "reversal" is actually where the orbits of the first and second kind coalesce. Other reversal are similar to those occurring for orbits in equatorial plane.

15.1 The θ-motion

In this section the θ-motion, as specified by the integral over $\Theta^{-1/2}$ in equation (15.4), will be investigated. The condition on Θ being non negative restricts the constants ξ and η by the inequality

$$\eta + (a - \xi) \geq 0\,, \tag{15.5}$$

which follows from Θ written as follows:

$$\Theta = \eta + (a - \xi)^2 - (a \sin\theta - \xi \csc\theta)^2\,. \tag{15.6}$$

$\cos\theta = \mu$ replaces θ as the variable of integration. The integral

$$I_\mu = \int \frac{\mathrm{d}\mu}{\sqrt{\Theta_\mu}}\,, \tag{15.7}$$

where

$$\Theta_\mu = \eta - \left(\xi^2 + \eta - a^2\right)\mu^2 - a^2\mu^4 \tag{15.8}$$

is considered instead. When $\eta > 0$, and for $\Theta \geq 0$, μ^2 will lay between $\mu^2 = 0$ and a certain maximum ${\mu_{\max}}^2$: $0 \leq \mu^2 \leq {\mu_{\max}}^2$.

15.1.1 $\eta > 0$

Explicit expression for the integral I_μ can be written down as follows :

$$\Theta_\mu = a^2\left({\mu_-}^2 + \mu^2\right)\left({\mu_+}^2 + \mu^2\right) \qquad (0 \leq \mu^2 \leq {\mu_+}^2)\,, \tag{15.9}$$

where

$${\mu_+}^2 = \frac{\sqrt{(\xi^2 + \eta - a^2)^2 + 4a^2\eta} - (\xi^2 + \eta - a^2)}{2a^2}\,, \tag{15.10}$$

$${\mu_-}^2 = \frac{\sqrt{(\xi^2 + \eta - a^2)^2 + 4a^2\eta} + (\xi^2 + \eta - a^2)}{2a^2}\,; \tag{15.11}$$

and

$$\int_\mu^{\mu_+} \frac{\mathrm{d}\mu}{\sqrt{\Theta_\mu}} = \frac{\mathrm{F}(\psi, k)}{a\sqrt{\mu_+^2 + \mu_-^2}}\,, \tag{15.12}$$

where

$$k^2 = \frac{{\mu_+}^2}{{\mu_+}^2 + {\mu_-}^2} \qquad \text{and} \qquad \cos\psi = \mu/\mu_+\,. \tag{15.13}$$

15.1.2 $\eta = 0$

Integral I_μ can be written down explicitly:

$$\Theta_\mu = \left(a^2 - \xi^2\right)\mu^2 - a^2\mu^4 \qquad \left(0 \le \mu^2 \le {\mu_{\max}}^2\right), \tag{15.14}$$

where

$${\mu_{\max}}^2 = 1 - \xi^2/a^2 \qquad \left(|\xi|^2 \le |a|^2\right), \tag{15.15}$$

and

$$\int_\mu^{\mu_{\max}} \frac{\mathrm{d}\mu}{\sqrt{\Theta}} = -\frac{\operatorname{arcsech}\frac{\mu}{\mu_{\max}}}{\sqrt{a^2 - \xi^2}}. \tag{15.16}$$

15.1.3 $\eta < 0$

Integral I_μ written explicitly is, in this case

$$\Theta_\mu = a^2\left(\mu^2 - \mu_-^2\right)\left(\mu_+^2 - \mu^2\right) \qquad \left(\mu_-^2 \le \mu^2 \le \mu_+^2\right), \tag{15.17}$$

where

$$\mu_\pm^2 = \frac{|\eta| + a^2 - \xi^2 \pm \sqrt{\left(|\eta| + a^2 - \xi^2\right)^2 - 4a^2|\eta|}}{2a^2}, \tag{15.18}$$

and

$$\int_{\mu_-}^{\mu} \frac{\mathrm{d}\mu}{\sqrt{\Theta_\mu}} = \frac{\mathrm{F}(\psi, k)}{a\mu_+}, \tag{15.19}$$

where

$$k^2 = \frac{\mu_+^2 - \mu_-^2}{\mu_+^2}, \tag{15.20}$$

$$|\eta| \le a^2, \tag{15.21}$$

$$0 \le |\xi| \le |a| - \sqrt{|\eta|}, \tag{15.22}$$

and

$$\sin\psi = \sqrt{\frac{\mu_+^2(\mu^2 - \mu_-^2)}{\mu^2(\mu_+^2 - \mu_-^2)}}. \tag{15.23}$$

15.1.4 The principal null-congruences

From equations (15.5) and (15.6) it can be seen that the case

$$\eta + (a - \xi)^2 = 0 \tag{15.24}$$

is distinguished because it is compatible with the condition $\Theta_\mu \geq 0$ only if

$$\theta = \theta_0 = \text{a constant}\,, \tag{15.25}$$

and

$$\xi = a \sin^2 \theta_0\,, \tag{15.26}$$

when $\Theta_\mu = 0$ for $\theta = \theta_0$ (see equation (13.11) for equation for $\dot{\theta}$). Now the condition for equation (15.24) is that

$$\eta = -a^2 \cos^4 \theta_0\,. \tag{15.27}$$

Inserting the above values of ξ and θ in equation (15.2), it yields

$$\mathrm{R} = \left(r^2 + a^2 \cos^2 \theta_0\right)^2 E^2\,, \tag{15.28}$$

where the previously suppressed factor E^2 was restored. Now from equation (13.10) it follows that

$$\dot{r} = \pm E\,. \tag{15.29}$$

Similarly, from equation(13.13) it can be concluded that

$$\dot{\varphi} = aE/\Delta \tag{15.30}$$

and from equation (13.12)

$$\dot{t} = \left(r^2 + a^2\right) E/\Delta\,. \tag{15.31}$$

These special null geodesics are described by

$$\frac{\mathrm{d}t}{\mathrm{d}\tau} = E\frac{r^2 + a^2}{\Delta}\,, \quad \frac{\mathrm{d}r}{\mathrm{d}\tau} = \pm E\,, \quad \frac{\mathrm{d}\theta}{\mathrm{d}\tau} = 0\,, \quad \text{and} \quad \frac{\mathrm{d}\varphi}{\mathrm{d}\tau} = E\frac{a}{\Delta}\,. \tag{15.32}$$

Solutions for $t(r)$ and $\varphi(r)$ can be found in section 14.1.1.

15.2 The r-motion

In this section we turn to a consideration of the radial motion as specified by the integral over $\mathrm{R}^{-1/2}$.

In the non-planar case there must be a distinction of whether the constants of the motion, ξ and η, are on one side or the other of a critical locus, (ξ_s, η_s), in the (ξ, η)-plane, with the orbits, with the constants of the motion on the locus itself, representing unstable orbits with $r =$ constant.

15.2.1 The unstable orbits of constant radius

The equations which determine the unstable orbits of constant radius are

$$\mathrm{R} = r^4 + \left(a^2 - \xi^2 - \eta\right) r^2 + 2M\left[\eta + (\xi - a)^2\right] r - a^2\eta = 0\,, \tag{15.33}$$

and

$$\frac{\partial \mathrm{R}}{\partial r} = 4r^3 + 2\left(a^2 - \xi^2 - \eta\right) r + 2M\left[\eta + (\xi - a)^2\right] = 0\,. \tag{15.34}$$

They can be combined to give

$$3r^4 + r^2a^2 - \eta\left(r^2 - a^2\right) = r^2\xi^2 \tag{15.35}$$

and

$$r^4 - a^2Mr + \eta\left(a^2 - Mr\right) = Mr\left(\xi^2 - 2a\xi\right)\,. \tag{15.36}$$

The above equations can be solved for ξ and η. Therefore, eliminating η between them yields

$$a^2(r - M)\xi^2 - 2aM\left(r^2 - a^2\right)\xi - r\left(r^2 + a^2\right)\left[r\left(r^2 + a^2\right) - M\left(3r^2 - a^2\right)\right] = 0\,. \tag{15.37}$$

We find the discriminant of this equation to be

$$a^2r^2\Delta^2 \tag{15.38}$$

and the solution of equation (15.37) is

$$\xi = \frac{M\,(r^2 - a^2) \pm r\Delta}{a(r - M)}\,. \tag{15.39}$$

To be consistent with our present requirements, we must choose the lower sign in this equation ([7, section 63]). Then

$$\xi = \frac{M\,(r^2 - a^2) - r\Delta}{a(r - M)} \tag{15.40}$$

and

$$\eta = \frac{r^3\,[4a^2M - r(r - 3M)^2]}{a^2(r - M)^2} = \frac{r^3\,[4M\Delta - r(r - M)^2]}{a^2(r - M)^2}\,. \tag{15.41}$$

These equations parametrically determine the critical locus (ξ_s, η_s).

There are no orbits of constant radius with $\eta < 0$ and when $\eta = 0$, the orbits lie entirely in the equatorial plane ([7, section 63§(c)]).

For an orbit to have constant radius r_s, the constants of motions, ξ and η, have the values ξ_s and η_s. That means ξ_s and η_s have the values given by equations (15.40) and (15.41) with substitution $r = r_s$. Then r_s is a double root of $\mathrm{R} = 0$; and R is reduced to

$$\mathrm{R} = (r - r_s)^2\left(r^2 + 2rr_s - a^2\eta_s/{r_s}^2\right)\,. \tag{15.42}$$

Then the integral to be considered is

$$\int \frac{\mathrm{d}r}{\sqrt{\mathrm{R}}} = \int \frac{\mathrm{d}r}{(r - r_s)\sqrt{r^2 + 2rr_s - a^2\eta_s/{r_s}^2}}\,. \tag{15.43}$$

From this equation, it can be seen that the trajectory consists of two parts: a part exterior to $r = r_s$ and a part interior to $r = r_s$. Because η_s is positive the orbit will terminate before $r = 0$ ([7, section 63§(c)].

Substituting

$$x = \frac{1}{r - r_s}\,, \tag{15.44}$$

and integrating (15.43), the equation of the projection of the orbit on the $(r, \theta = \arccos \mu)$-plane is found. Thus,

$$\int \frac{\mathrm{d}\mu}{\sqrt{\Theta_\mu}} = \pm \frac{\ln\left[4r_s + 2cx + 2\sqrt{c(1 + 4r_s x + cx^2)}\right]}{\sqrt{c}}\,, \tag{15.45}$$

where ([7, page 353])

$$c = 3{r_s}^2 - a^2\eta_s/{r_s}^2 > 0\,. \tag{15.46}$$

The integral over μ on the left-hand[1] side is given by equation (15.13).

In the first picture of the figure 15.2 there is an example of a trajectory derived from equation (15.45).

15.2.2 The case $\eta = 0$

All orbits of constant radius with $\eta = 0$ lie entirely in the equatorial plane. Also, all orbits in the equatorial plane have the Carter constant being zero. But *not all orbits with* $\eta = 0$ *are in the equatorial plane*, because when $\eta = 0$, the r-motion is generally determined by (cf. equation (15.33))

$$\int \frac{\mathrm{d}r}{\sqrt{\mathrm{R}}} = \int \frac{\mathrm{d}r}{\sqrt{r\left[r^3 + (a^2 - \xi^2)r + 2M\left(a - \xi\right)^2\right]}}\,, \tag{15.47}$$

and the θ-motion is determined by equation (15.16). The above integral can be reduced to a Jacobian elliptic integral. Then the trajectory in the (r, θ)-plane is determined by

$$\frac{\operatorname{arcsech} \frac{\mu}{\mu_{\max}}}{\sqrt{a^2 - \xi^2}} = \pm \frac{\mathrm{F}(\psi, k)}{\sqrt{AB}}\,, \tag{15.48}$$

[1] see [7, page 353]

where

$$k^2 = \frac{(A+B) - r_1^2}{4AB}\,, \tag{15.49}$$

$$\cos\psi = \frac{(A-B)r + r_1 A}{(A+B)r + r_1 A}\,, \tag{15.50}$$

$$A^2 = r_1^2 + \left(a^2 - \xi^2\right)\,, \tag{15.51}$$

$$B^2 = 3r_1^2 + \left(a^2 - \xi\right)\,, \tag{15.52}$$

$$r_1 = -\sqrt{\frac{4}{3}\left(a^2 - \xi^2\right)}\sinh\vartheta \tag{15.53}$$

and

$$\sinh(3\vartheta) = \sqrt{27M^2\frac{a-\xi}{(a+\xi)^3}}\,. \tag{15.54}$$

These trajectories exist only for $\eta < a$. They terminate at the singularity (see figure 15.3 where there is an example of a trajectory derived from equation (15.48)).

15.2.3 The case $\eta < 0$

In this section the class of orbits with $\eta < 0$ are considered. These orbits extend to regions of negative r. They have very strict conditions of occurrence: $|\eta| < a^2$ and $0 < |\xi| \leq |a| - \sqrt{|\eta|}$. The result of integration is

$$\int_0^r \frac{\mathrm{d}r}{\sqrt{R}} = g[\mathrm{F}(\phi,k) + \mathrm{K}(k)]\,, \tag{15.55}$$

where

$$g = \frac{2}{A+B}\,, \tag{15.56}$$

$$\phi = \arctan\frac{r - b_1 + a_1 g_1}{a_1 + b_1 g_1 - g_1 r}\,, \tag{15.57}$$

$$g_1^2 = \frac{4a_1^2 - (A-B)^2}{(A+B)^2 - 4a_1^2}\,, \tag{15.58}$$

$$k^2 = \frac{4AB}{(A+B)^2}\,, \tag{15.59}$$

$$A^2 = (b_1 - b_2)^2 + (a_1 + a_2)^2 \,, \tag{15.60}$$

$$B^2 = (b_1 - b_2)^2 + (a_1 - a_2)^2 \,, \tag{15.61}$$

$$a_1^2 = -\frac{(u_1 - \bar{u_1})^2}{4} \,, \tag{15.62}$$

$$b_1 = \frac{u_1 + \bar{u_1}}{2} \,, \tag{15.63}$$

$$b_2 = \frac{u_3 + \bar{u_3}}{2} \,, \tag{15.64}$$

$$a_2^2 = -\frac{(u_3 - \bar{u_3})^2}{4} \,, \tag{15.65}$$

and $u_1,\ \bar{u_1},\ u_3$ and $\bar{u_3}$ are the roots of the polynomial R$= r^4 + (a^2 - \xi^2 - \eta)r^2 + 2M[\eta + (\xi - a)^2]r - a^2\eta$. The r- and the θ- motions are shown in Figure 15.4[2].

15.3 The φ-motion

In the second integral in the equation (13.18) we replace θ by $\mu = \cos\theta$ as the variable of integration (as in the section 15.1 before) and consider, instead, the integral

$$I_\mu = \int \frac{L + aE(\mu^2 - 1)}{(\mu^2 - 1)\sqrt{\Theta_\mu}} \mathrm{d}\mu \,, \tag{15.66}$$

where Θ_μ is the same as in (15.8).

15.3.1 $\eta > 0$

With Θ_μ in the form (15.9), explicit expression for the integral (15.66) can be written down:

$$\int_\mu^{\mu_+} \frac{L + aE(\mu^2 - 1)}{(\mu^2 - 1)\sqrt{\Theta_\mu}} \mathrm{d}\mu = g \left[E\,\mathrm{F}(\psi, k) - \frac{L}{a(1 - \mu^2)} \Pi\left(\psi, \alpha^2, k\right) \right] \,, \tag{15.67}$$

[2]Cf. [7, Figure 37]

where

$$g = 1/\sqrt{{\mu_+}^2 + {\mu_-}^2}\,, \tag{15.68}$$

k and ψ are the same as in (15.13), and $\mu_\pm$ are defined in equations (15.10), (15.11).

The unstable orbits of constant radius

After substituting (15.42) for R, the first integral in the equation (13.18) will have the form

$$I_{\rm R} = a\int^r \frac{(r^2+a^2)E - aL}{\Delta(r-r_s)\sqrt{r^2 - 2rr_s - a^2\eta_s/{r_s}^2}}{\rm d}r\,. \tag{15.69}$$

This integral can be reduced to three simple integrals by the method of partial fractions. After letting

$$y_\pm = r_\pm - r \qquad \text{and} \qquad y_s = r - r_s\,, \tag{15.70}$$

we can write

$$\varphi = I_\mu + a\left[\frac{({r_+}^2+a^2)E - aL}{(r_+-r_-)(r_+-r_s)}f_+ - \frac{({r_-}^2+a^2)E - aL}{(r_+-r_-)(r_--r_s)}f_- + \right.$$
$$\left. + \frac{({r_s}^2+a^2)E - aL}{(r_+-r_s)(r_--r_s)}f_s\right]\,, \tag{15.71}$$

where I_μ is given by (15.67) and

$$f_\pm = \begin{cases} -\dfrac{1}{\sqrt{c}}\ln\left|\dfrac{2\sqrt{c}}{y_\pm}\sqrt{{y_\pm}^2 + 2(r_s-r_\pm)y_\pm + c} + \dfrac{2c}{y_\pm} + 2(r_s-r_\pm)\right| & \text{for } c>0, \\ \dfrac{1}{\sqrt{-c}}\arcsin\dfrac{2[(r_s-r_\pm)y_\pm + c]}{y_\pm\sqrt{{r_s}^2 + \dfrac{a^2\eta}{{r_s}^2}}} & \text{for } c<0, \\ -\dfrac{1}{r_s-r_\pm}\sqrt{\dfrac{y_\pm + 2(r_s-r_\pm)}{y_\pm}} & \text{for } c=0, \end{cases} \tag{15.72}$$

$$f_s = \frac{r_s}{\sqrt{r_s^4 + a^2\eta}}\arccos\frac{\sqrt{r_s^4 + a^2\eta}}{r_s|y_s|}\,, \tag{15.73}$$

where

$$c = {r_\pm}^2 - \frac{a^2\eta}{{r_s}^2} - 2r_\pm r_s \,. \tag{15.74}$$

An example of a trajectory derived from equation (15.71) is illustrated in the second picture of figure 15.2. The trajectory derived from equations (15.45) and (15.71) is illustrated in figure 15.1.

15.3.2 $\eta = 0$

With Θ_μ in the form (15.14), an explicit expression for the integral (15.66) can be written down:

$$\int_\mu^{\mu_{\max}} \frac{L + aE(\mu^2-1)}{(\mu^2-1)\sqrt{\Theta_\mu}}\mathrm{d}\mu = \frac{L-aE}{\sqrt{a^2-\xi^2}} \ln\left|\frac{\mu_{\max}+\sqrt{\mu_{\max}-\mu^2}}{\mu}\right| + \\ + \frac{L}{2\xi}\left[\arcsin\frac{{\mu_{\max}}^2-\mu}{\mu_{\max}(\mu-1)} + \arcsin\frac{{\mu_{\max}}^2+\mu}{\mu_{\max}(\mu+1)}\right], \tag{15.75}$$

where $\mu_{\max}$ is defined in (15.15).

The first integral in the equation (13.18) will have the form

$$I_{\mathrm{R}} = a\int^r \frac{(r^2+a^2)E - aL}{\Delta\sqrt{r\left[r^3 + (a^2-\xi^2)r + 2M\,(a-\xi)^2\right]}}\mathrm{d}r \,. \tag{15.76}$$

This integral can be reduced, with the help of the partial fractions method, to Jacobian elliptic integrals. We can write

$$\varphi = I_\mu + aEg[\mathrm{F}(\phi,k) + \mathrm{K}(k)] + \\ + \frac{ag(B-A)}{r_+ + r_-}\left\{\left[\left(a^2+{r_+}^2\right)E - aL\right]\cdot \right. \\ \cdot\frac{\alpha_2[\mathrm{F}(\phi,k)+K(k)] + \dfrac{\alpha_+-\alpha_2}{1-\alpha_+}\left[\Pi\left(\phi,\dfrac{{\alpha_+}^2}{{\alpha_+}^2-1},k\right) + \Pi\left(\dfrac{{\alpha_+}^2}{{\alpha_+}^2-1},k\right) - 2\alpha_+ f_+\right]}{Ar_1 - r_+(A+B)} \\ \left. - \left[\left(a^2+{r_-}^2\right)E - aL\right]\cdot \right.$$

$$\left.\cdot\frac{\alpha_2[\mathrm{F}(\phi,k)+K(k)]+\dfrac{\alpha_- -\alpha_2}{1-\alpha_-}\left[\Pi\left(\phi,\dfrac{{\alpha_-}^2}{{\alpha_-}^2-1},k\right)+\Pi\left(\dfrac{{\alpha_-}^2}{{\alpha_-}^2-1},k\right)-2\alpha_- f_-\right]}{Ar_1-r_-(A+B)}\right\}, \tag{15.77}$$

where k is defined in (15.49), A in (15.51), B in (15.52), $f_\pm$ in (14.63), $r_\pm$ are the roots of Δ, and

$$g = 1/\sqrt{AB}\,, \tag{15.78}$$

$$\phi = \arccos\frac{(A-B)r-Ar_1}{(A+B)r-Ar_1} \tag{15.79}$$

$$r_1 = -\sqrt{\frac{4}{3}\left(a^2-\xi^2\right)}\sinh\frac{\vartheta}{3}\,, \tag{15.80}$$

$$\sinh\vartheta = M\sqrt{\frac{a-\xi}{(a+\xi)^3}}\,, \tag{15.81}$$

$$\alpha_\pm = \frac{Ar_1-Ar_\pm-Br_\pm}{-Ar_1+Ar-\pm_B r_\pm}\,, \tag{15.82}$$

$$\alpha_2 = \frac{B+A}{B-A}\,. \tag{15.83}$$

An example of a trajectory derived from equation (15.77) is illustrated in the figure 15.5. The trajectory derived from equations (15.48) and (15.77) is illustrated in figure 15.6.

15.3.3 $\eta < 0$

The function Θ_μ has form (15.17). Therefore

$$\int_\mu^{\mu_+}\frac{L+aE(\mu^2-1)}{(\mu^2-1)\sqrt{\Theta_\mu}}\mathrm{d}\mu = g\left[E\mathrm{F}(\psi,k)+\frac{L}{a(\mu_+^2-1)}\Pi\left(\psi,\alpha^2,k\right)\right]\,, \tag{15.84}$$

where

$$g = \frac{1}{\mu_+}\,, \tag{15.85}$$

$$\psi = \arcsin\sqrt{\frac{\mu_+^2 - \mu^2}{\mu_+^2 - \mu_-^2}}\,, \tag{15.86}$$

$$k^2 = \frac{\mu_+^2 - \mu_-^2}{\mu_+^2} \tag{15.87}$$

and

$$\alpha^2 = \frac{\mu_+^2 - \mu_-^2}{\mu_+^2 - 1}\,. \tag{15.88}$$

The first integral in (13.18) can be written in the form

$$E\int_0^r \frac{\mathrm{d}r}{\sqrt{R}} + \int_0^r \frac{(2EMr - aL)\mathrm{d}r}{\Delta\sqrt{R}}\,, \tag{15.89}$$

where R is defined in (15.2) and Δ is the horizon function (B.31). The first integral in the expression above is (15.55). An example of an orbit with negative η derived numerically is in figures 15.7 and 15.8.

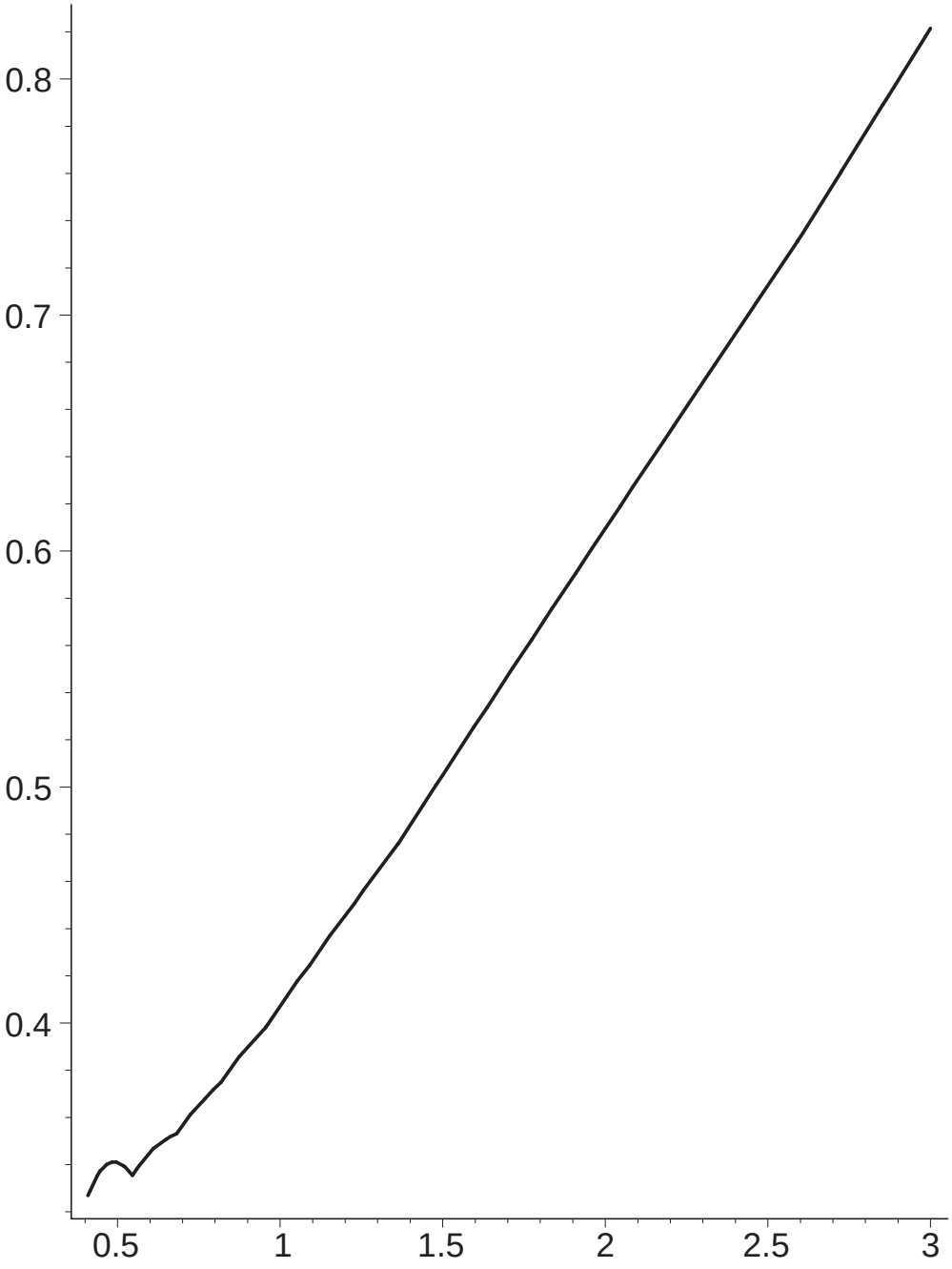

Figure 15.3: An example of a null geodesic with $\eta = 0$ in the (r, θ)-plane (projection on the plane). These are the only orbits, out of the equatorial plane, which reach the singularity. Parameters are $M = 1$, $E = 1$, $a = 0.8$ and $L = 0.4$.

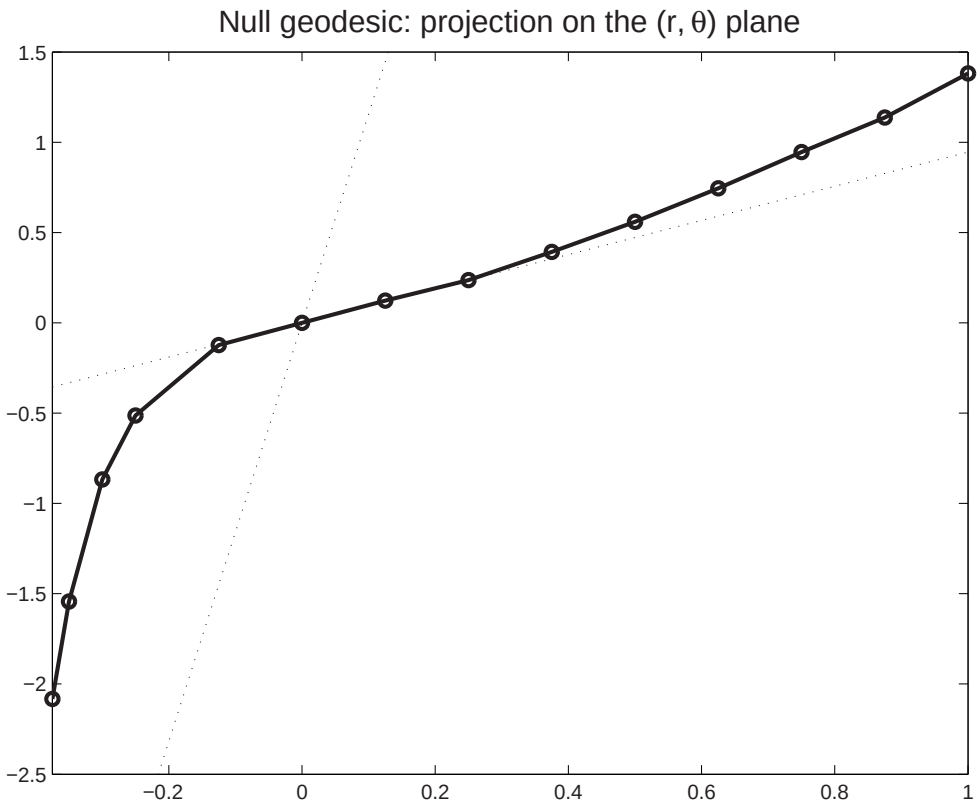

Figure 15.4: An example of a null geodesic with $\eta = -0.3$ in the (r, θ)-plane (projection on the plane). The orbit is confined between two angles. Parameters are $M = 1$, $\xi = -0.05 = 1$ and $a = 0.8$.

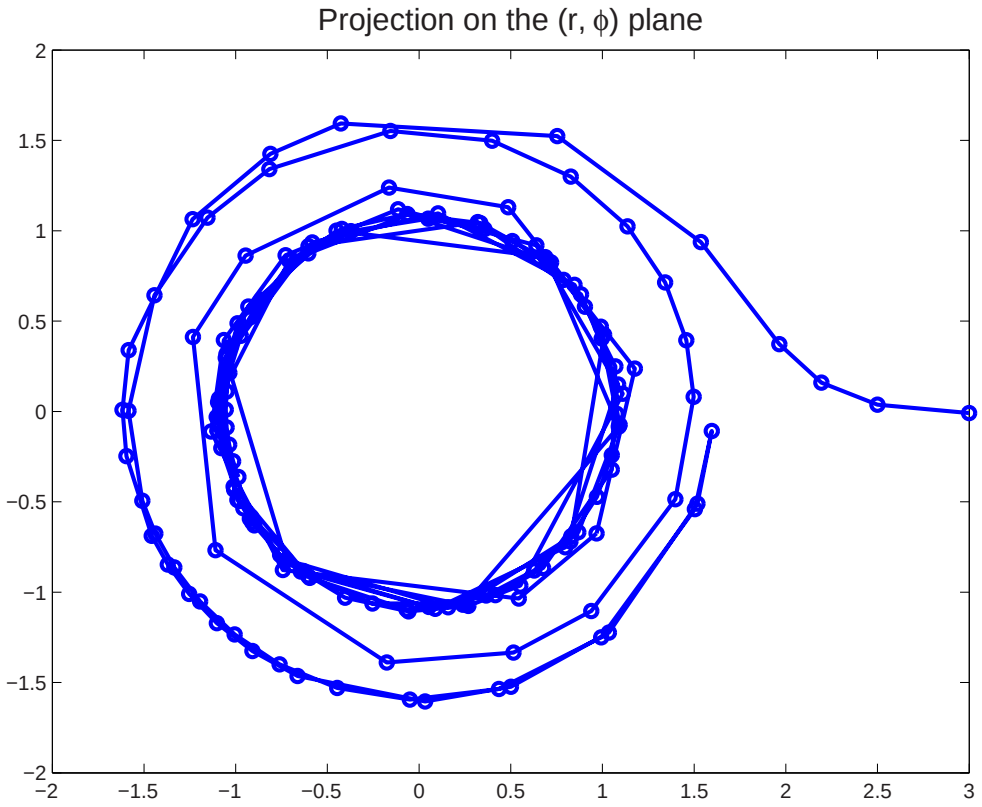

Figure 15.5: An example of a null geodesic with $\eta = 0$ in the (r, φ)-plane. The orbit spirals to the singularity. Parameters are $M = 1$, $E = 1$, $a = 0.8$ and $L = 0.4$.

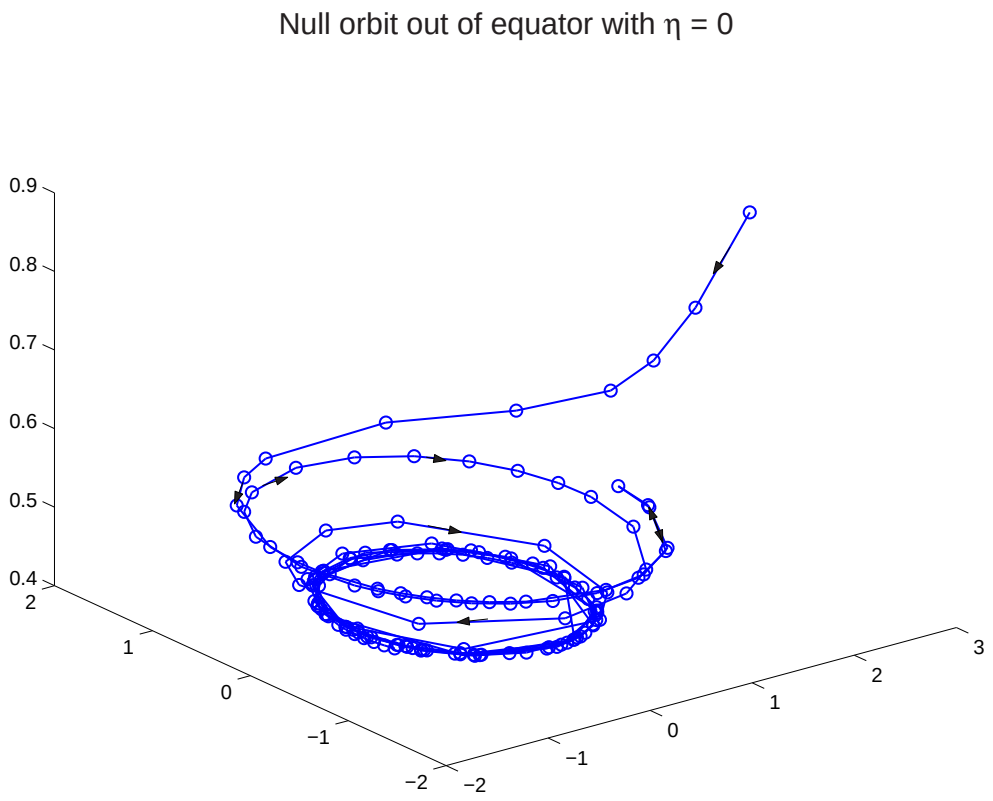

Figure 15.6: An example of a null geodesic in "spherical" coordinates with $\eta = 0$. The orbit spirals to the singularity. Parameters are $M = 1$, $E = 1$, $a = 0.8$ and $L = 0.4$.

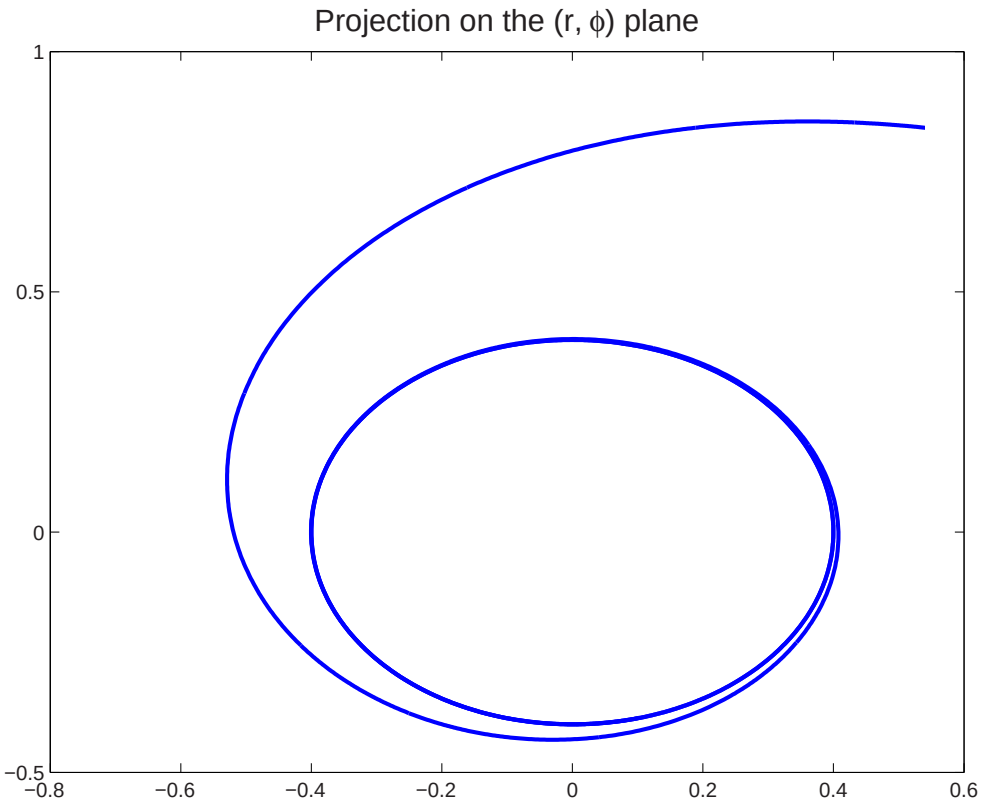

Figure 15.7: An example of a null geodesic with $\eta < 0$. Projection on the r-φ plane. Parameters are $M = 1$, $E = 1$, $a = 0.8$, $\eta = -0.3$ and $\xi = 0.4$.

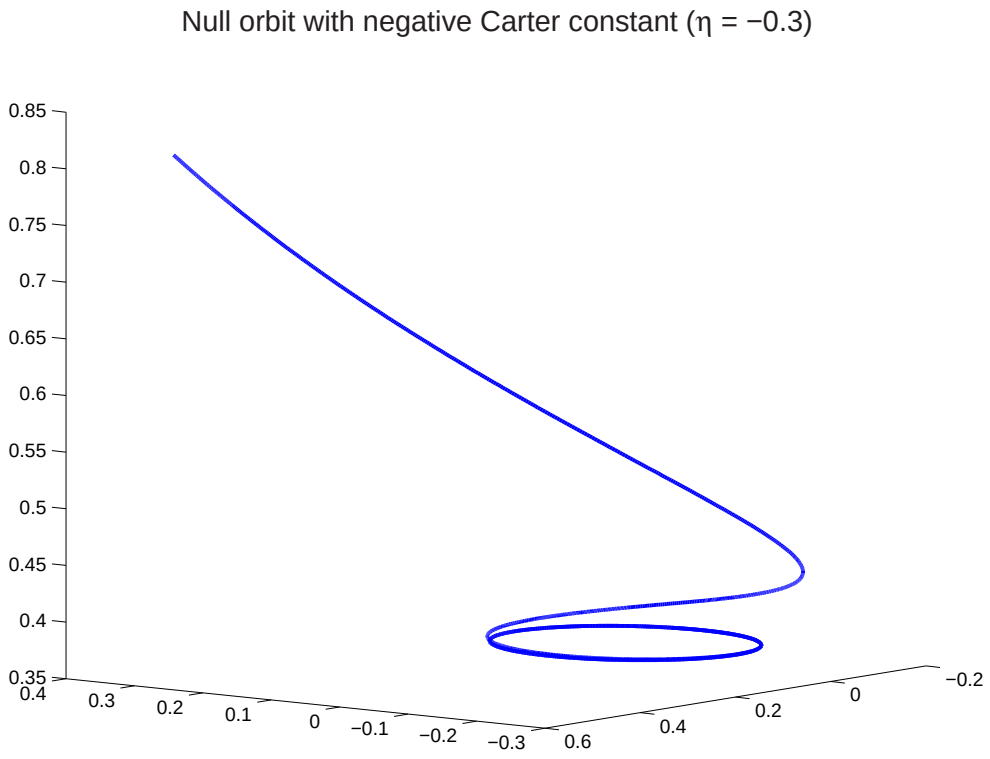

Figure 15.8: An example of a null geodesic with $\eta < 0$ in "spherical" coordinates. Parameters are $M = 1$, $E = 1$, $a = 0.8$, $\eta = -0.3$ and $\xi = 0.4$.

Chapter 16

The space-like geodesics

This chapter studies space-like geodesics in Kerr spacetime and it is our original work. As in Chapter 15 we shall write R and Θ instead of R/E^2 and Θ/E^2:

$$\mathrm{R} = r^4 + \left(a^2 - \xi^2 - \eta\right) r^2 + 2M\left[\eta + (\xi - a)^2\right] r - a^2\eta + \frac{r^2\Delta}{E^2} \tag{16.1}$$

and

$$\Theta = \eta + a^2\left(1 + \frac{1}{E^2}\right)\cos^2\theta - \xi^2\cot^2\theta\,, \tag{16.2}$$

where ξ and η are defined in (15.1).

16.1 The θ-motion

In this section the θ-motion specified by the integral over $\Theta^{-1/2}$ will be considered, and as in section 15.1, the variable of integration shall be $\mu = \cos\theta$. The integral (15.7) is considered with Θ_μ in the form

$$\Theta = \eta - \left[\xi^2 + \eta - a^2\left(1 + \frac{1}{E^2}\right)\right]\mu^2 - a^2\left(1 + \frac{1}{E^2}\right)\mu^4\,. \tag{16.3}$$

It is convenient to use substitution

$$\alpha^2 = a^2\left(1 + \frac{1}{E^2}\right)\,. \tag{16.4}$$

and write Θ_μ as

$$\Theta_\mu = \eta - \left(\xi^2 + \eta - \alpha^2\right)\mu^2 - \alpha^2\mu^4 \,. \tag{16.5}$$

Now the discussion in section 15.1 applies with the replacement of a^2 by α^2. The space-like orbits are very much like null geodesics.

16.2 The r-motion

In this section the radial motion specified by the integral over $\mathrm{R}^{-1/2}$ is investigated.

16.2.1 The unstable orbits of constant radius

These special orbits provide a basis for a classification of the orbits, and also illustrate the nature of the orbits. The conditions for the occurrence of orbits with constant radius are

$$\mathrm{R} = 0 \qquad \text{and} \qquad \frac{\partial \mathrm{R}}{\partial r} = 0 \,. \tag{16.6}$$

After following the same procedure as in section 15.2.1, only with the additional term, $+r^2\Delta/E^2$, in the definition of R, we can replace the equations (15.35) and (15.36) by

$$3r^4 + r^2a^2 - \eta\left(r^2 - a^2\right) + \frac{r^2}{E^2}\left(3r^2 - 4Mr + a^2\right) = r^2\xi^2 \tag{16.7}$$

and

$$r^4 - a^2Mr - \eta(a^2 - Mr) + \frac{r^3}{E^2}(r - M) = rM\left(\xi^2 - 2a\xi\right) \,; \tag{16.8}$$

and, as in section 15.2.1, these equations can be solved for ξ and η.

Eliminating η from the above equations yields (in place of equation (15.37))

$$a^2(r-M)\xi^2 + 2aM\left(r^2 - a^2\right)\xi + \left(r^2 + a^2\right)\left[r\left(r^2 + a^2\right) - M\left(3r^2 - a^2\right)\right] + \frac{r\Delta}{E^2} = 0 \,; \tag{16.9}$$

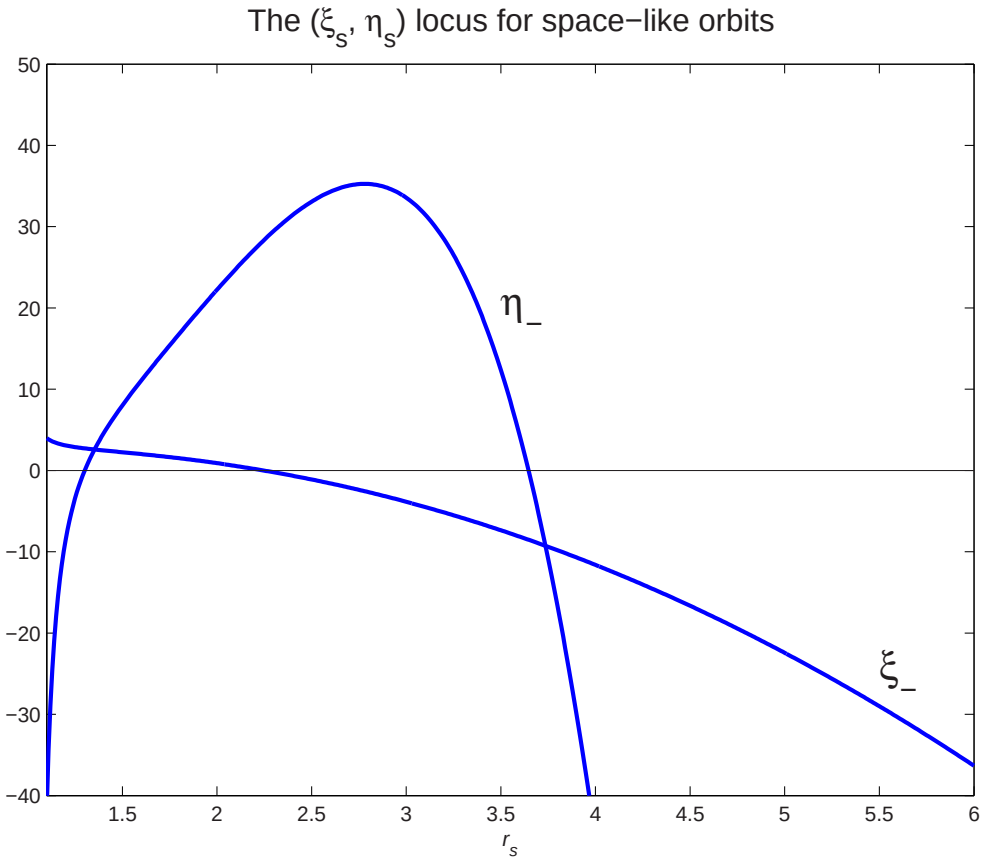

Figure 16.1: The critical locus (ξ_s, η_s) for space-like orbits with $E^2 = 1$. The chosen parameters for the black hole are $M = 1$ and $a = 0.96$.

and the solution of this equation is given by (cf. equation (15.39))

$$\xi = \frac{M(r^2 - a^2) \pm r\Delta\sqrt{1 + \frac{1}{E^2}\left(1 - \frac{M}{r}\right)}}{a(r - M)}\,; \tag{16.10}$$

and the corresponding solution for η is (cf. equation (15.41))(see Fig.16.1)

$$\eta a^2(r - M) = \frac{2r^3 M\Delta}{r - M}\left[1 \mp \sqrt{1 + \frac{1}{E^2}\left(1 - \frac{M}{r}\right)}\right] - r^4(r - M) - \frac{r^2}{E^2}\left[r\,(r - 2M)^2 - a^2 M\right]\,. \tag{16.11}$$

Now, let the constants of the motion, ξ and η, have the values ξ_s and η_s appropriate to a particle on a orbit with constant radius r_s. That means that

in equations (16.10) and (16.11) r is replaced by r_s. Then r_s is a double root of $\mathrm{R} = 0$, and R can be reduced to

$$\mathrm{R} = (r - r_s)^2 \left\{ r^2 \left(1 + \frac{1}{E^2}\right) + 2 r r_s \left[1 + \frac{1}{E^2}\left(1 - \frac{M}{r_s}\right)\right] - \frac{a^2 \eta_s}{r_s^2} \right\} . \quad (16.12)$$

After substitution (15.44) the integral is

$$\int \frac{\mathrm{d}r}{\sqrt{\mathrm{R}}} = -\int \mathrm{d}x \left\{ \left(1 + \frac{1}{E^2}\right) + \left[4 r_s \left(1 + \frac{1}{E^2}\right) - \frac{2M}{E^2}\right] x + \right.$$
$$\left. + \left[3 r_s^2 \left(1 + \frac{1}{E^2}\right) - \frac{a^2 \eta_s}{r_s^2} - \frac{2 M r_s}{E^2}\right] x^2 \right\}^{-\frac{1}{2}} . \quad (16.13)$$

With the definition

$$\mathrm{X}(x) = A x^2 + B x + C \,, \quad (16.14)$$

where A, B and C are the coefficients of the quadratic in x that appear in the integral (16.13). Therefore

$$\int \frac{\mathrm{d}r}{\sqrt{\mathrm{R}}} = \frac{\ln |2\sqrt{A\mathrm{X}} + 2Ax + B|}{\sqrt{A}} \qquad \text{for } A > 0 \,, \quad (16.15)$$

$$= -\frac{\arcsin \dfrac{2Ax + B}{\sqrt{-D}}}{\sqrt{-A}} \qquad \text{for } A < 0 \,, \quad (16.16)$$

where

$$D = -4 \left\{ \left[r_s \left(1 + \frac{1}{E^2}\right) - \frac{M}{E^2} \right]^2 + \frac{\alpha^2 \eta_s}{r_s^2} \right\} \quad (16.17)$$

is negative.

16.2.2 The case $\eta = 0$

The r-motion is determined by (cf. equation (16.1))

$$\int \frac{\mathrm{d}r}{\sqrt{\mathrm{R}}} = \int \frac{\mathrm{d}r}{\sqrt{r\left\{\left(1 + \frac{1}{E^2}\right) r^3 + \left[a^2 \left(1 + \frac{1}{E^2}\right) - \xi^2 - \frac{2Ma}{E^2}\right] r + 2M (a - \xi)^2\right\}}} \,, \quad (16.18)$$

while the θ-motion is determined by the equation (15.16). By substituting r with $u = 1/r$ as the independent variable, the above integral becomes

$$-\int \frac{\mathrm{d}u}{\sqrt{\left(1 + \frac{1}{E^2}\right) + \left[a^2 \left(1 + \frac{1}{E^2}\right) - \xi^2 - \frac{2Ma}{E^2}\right] u^2 + 2M (\xi - a)^2 u^3}} \quad (16.19)$$

and can be reduced to a Jacobian elliptic integral.

When $a^2(1+1/E^2) > (L^2+2Ma)/E^2$, there is only one real root of the cubic polynomial, u_1, and the integration gives

$$-g[\mathrm{F}(\varphi,k)+\mathrm{K}(k)]\,, \tag{16.20}$$

where

$$\varphi = \arccos\frac{A+u_1-u}{A-u_1+u} \tag{16.21}$$

and g is defined by equations (14.54) (14.58), (14.60) and (14.59), and k is as in equation (14.57).

When $a^2(1+1/E^2) < (L^2+2Ma)/E^2$, there are three real roots of the cubic polynomial, $u_1 < 0 < u_2 < u_3$, and the above solution holds for $u \le u_2$, with φ as it is in equation (14.45), k in (14.37), and g in (14.35). For $u_3 \le u < \infty$, the solution becomes

$$-g\,\mathrm{F}(\varphi,k)\,, \tag{16.22}$$

where

$$\varphi = \arcsin\sqrt{\frac{u_3-u_1}{u-u_1}}\,, \tag{16.23}$$

and k and g are defined by (14.37) and (14.35) respectively.

16.3 The φ-motion

The integral I_μ is solved in section 15.3, with the replacement of a^2 by α^2 in (15.67).

16.3.1 The unstable orbits of constant radius

Substituting (16.12) for R yields to the integral over r in (13.18) having form

$$I_{\mathrm{R}} = a\int^r \frac{(r^2+a^2)E-aL}{\Delta(r-r_s)\sqrt{r^2\left(1+\dfrac{1}{E^2}\right)+2rr_s\left[1+\dfrac{1}{E^2}\left(1-\dfrac{M}{r_s}\right)\right]-\dfrac{a^2\eta_s}{r_s^2}}}\mathrm{d}r\,. \tag{16.24}$$

Substitution (15.44) and the partial fractions method transform this integral to three integrals

$$I_x = \frac{a[aL - E(a^2 + r_s^2)]}{\Delta_s} \int \frac{\mathrm{d}x}{\sqrt{\mathrm{X}(x)}} - \frac{a(aL - 2MEr_s^2)}{\Delta_s} \int \frac{\mathrm{d}x}{[\Delta_s x^2 + 2(r_s - M)x + 1]\sqrt{\mathrm{X}(x)}} - \frac{2a[ME(a^2 - r_s^2) + aL(r_s - M)]}{\Delta_s} \int \frac{x\,\mathrm{d}x}{[\Delta_s x^2 + 2(r_s - M)x + 1]\sqrt{\mathrm{X}(x)}}, \tag{16.25}$$

where (16.14) is the definition of $\mathrm{X}(x)$ and $\Delta_s = r_s^2 - 2Mr_s + a^2$.

Chapter 17

The time-like geodesics

Finally we look at the time-like geodesics in Kerr space-time. We expand discussion of [7].

For time-like geodesics $\delta_1 = 1$. Writing R and Θ instead of R/E^2 and Θ/E^2 we have

$$R = r^4 + (a^2 - \xi^2 - \eta^2)r^2 + 2M[\eta + (\xi - a)^2] - a^2\eta - \frac{r^2\Delta}{E^2} \tag{17.1}$$

and

$$\Theta = \eta + a^2\left(1 - \frac{1}{E^2}\right)\arccos\theta - \xi^2\cot^2\theta\,. \tag{17.2}$$

17.1 The θ-motion

As in sections 15.1 and 16.1 we use $\mu = \cos\theta$ as a variable of integration. Then the right-hand side of equation (15.4) that describes the orbit on (r, θ)-plane becomes integral (15.7) where

$$\Theta_\mu = \eta - \left[\xi^2 + \eta - a^2\left(1 - \frac{1}{E^2}\right)\right]\mu^2 - a^2\left(1 - \frac{1}{E^2}\right)\mu^4\,. \tag{17.3}$$

As in the cases of time-like geodesics in Schwarzschild and Reissner-Nordström space-times we must distinguish orbits with $E^2 < 1$ (bound orbits), $E^2 = 1$ (marginally bound orbits), and $E^2 > 1$ (unbound orbits).

17.1.1 The bound orbits

It is useful to replace a^2 by

$$\alpha^2 = a^2 \left(\frac{1}{E^2} - 1 \right) > 0 \,. \tag{17.4}$$

Then Θ_μ will be written in the form

$$\Theta_\mu = \eta - \left(\xi^2 + \eta + \alpha^2 \right) \mu^2 + \alpha^2 \mu^4 \,. \tag{17.5}$$

Following [7, page 362], the solution of integral (15.7) is

$$\int_0^\mu \frac{\mathrm{d}\mu}{\sqrt{\Theta_\mu}} = \frac{\mathrm{F}(\psi, k)}{\alpha \mu_+} \,, \tag{17.6}$$

where

$$\mu_\pm^2 = \frac{(\xi^2 + \eta + \alpha^2) \pm \sqrt{(\xi^2 + \eta + \alpha^2)^2 - 4\alpha^2 \eta}}{2\alpha^2} \,, \tag{17.7}$$

$$k = \frac{\mu_-}{\mu_+} \tag{17.8}$$

and

$$\sin \psi = \frac{\mu}{\mu_-} \,, \tag{17.9}$$

with μ^2 between zero and μ_-^2 and η non-negative.

17.1.2 The marginally bound orbits

For these orbits $E^2 = 1$ and so equation (17.5) becomes

$$\Theta_\mu = \eta - (\xi^2 + \eta) \mu^2 \,. \tag{17.10}$$

Negative values of η are not allowed and the solution is [7, page 362]

$$\int^\mu \frac{\mathrm{d}\mu}{\sqrt{\Theta_\mu}} = - \frac{\arccos \left(\mu \sqrt{\dfrac{\xi^2 + \eta}{\eta}} \right)}{\sqrt{\xi^2 + \eta}} \,. \tag{17.11}$$

Both bound and marginally bound orbits cross the equatorial plane and oscillate about it.

17.1.3 The unbound orbits

For orbits with $E^2 > 1$, after replacing a^2 by

$$\alpha^2 = a^2 \left(1 - \frac{1}{E^2}\right) > 0\,, \tag{17.12}$$

the discussion in section 16.1 applies.

17.2 The r-motion

We consider two simple integrable cases.

17.2.1 The circular orbits

In this section the orbits with constant radial coordinate will be considered. They occur when equations (16.6) hold. The constraints on the constants of motion, ξ, η and E^2, can be obtained by the same procedure as in section 15.2.1, with an additional term, $-r^2\Delta/E^2$, in the definition for R. Instead of equations (15.35) and (15.36) there are now equations

$$3r^4 + r^2a^2 - \eta\left(r^2 - a^2\right) - \frac{r^2}{E^2}\left(3r^2 - 4Mr + a^2\right) = r^2\xi^2 \tag{17.13}$$

and

$$r^4 - a^2Mr + \eta(a^2 - Mr) - \frac{r^3}{E^2}(r - M) = rM\left(\xi^2 - 2a\xi\right)\,; \tag{17.14}$$

and, as in sections 15.2.1 and 16.2.1, these equations can be solved for ξ and η.

Eliminating η from above equations gives (cf. equations (15.37) and (16.9))

$$a^2(r - M)\xi^2 - 2aM\left(r^2 - a^2\right)\xi \\ - \left\{\left(r^2 + a^2\right)\left[r\left(r^2 + a^2\right) - M\left(3r^2 - a^2\right)\right] - \frac{r\Delta}{E^2}\right\} = 0\,. \tag{17.15}$$

The solution of this equation is (cf. equations (15.39) and (16.10))

$$\xi = \frac{M(r^2 - a^2) \pm r\Delta\sqrt{1 - \frac{1}{E^2}\left(1 - \frac{M}{r}\right)}}{a(r - M)}\,, \tag{17.16}$$

and the corresponding solution for η is (cf. equations (15.41) and (16.11))

$$\begin{aligned}\eta a^2(r - M) &= \frac{r^3}{r - M}[4a^2M - r\,(r - 3M)^2] + \\ &+ \frac{r^2}{E^2}\left[r\,(r - 2M)^2 - a^2M\right] - \frac{2r^3M\Delta}{r - M}\left[1 \mp \sqrt{1 + \frac{1}{E^2}\left(1 - \frac{M}{r}\right)}\right]\,. \end{aligned}\tag{17.17}$$

The particle in an orbit with constant radius, r_s, has values ξ_s and η_s given by above equations. Because r_s is a double root of the equation $R = 0$, R can be reduced to

$$\mathrm{R} = (r - r_s)^2\left\{r^2\left(1 - \frac{1}{E^2}\right) + 2rr_s\left[1 - \frac{1}{E^2}\left(1 - \frac{M}{r_s}\right)\right] - \frac{a^2\eta_s}{r_s^2}\right\}\,. \tag{17.18}$$

Substituting (15.44), the integral on the left-hand side of equation (15.4) becomes (cf. equation (16.13))

$$\begin{aligned}\int \frac{\mathrm{d}r}{\sqrt{\mathrm{R}}} = -\int \mathrm{d}x\Bigg\{&\left(1 - \frac{1}{E^2}\right) + \left[4r_s\left(1 - \frac{1}{E^2}\right) + \frac{2M}{E^2}\right]x + \\ &+ \left[3r_s^2\left(1 - \frac{1}{E^2}\right) - \frac{a^2\eta_s}{r_s^2} + \frac{2Mr_s}{E^2}\right]x^2\Bigg\}^{-\frac{1}{2}}\,. \end{aligned}\tag{17.19}$$

With the definition (16.14), the integral is

$$\int \frac{\mathrm{d}r}{\sqrt{R}} = \pm\frac{\ln(B + 2Cx + 2\sqrt{CX})}{\sqrt{C}} \qquad (C > 0)\,, \tag{17.20}$$

$$= \pm\frac{\operatorname{arcsinh}\frac{2Cx+B}{\sqrt{D}}}{\sqrt{C}} \qquad (C > 0,\ D > 0)\,, \tag{17.21}$$

$$= \mp\frac{\arcsin\frac{2CX+B}{\sqrt{-D}}}{\sqrt{-C}} \qquad (C < 0,\ D < 0), \tag{17.22}$$

where

$$D = -4\left\{\left[r_s\left(1 - \frac{1}{E^2}\right) + \frac{M}{E^2}\right]^2 + \frac{\alpha^2\eta_s}{{r_s}^2}\left(1 - \frac{1}{E^2}\right)\right\}\,. \tag{17.23}$$

Examples of orbits with constant radius are in figures 17.1 and 17.2.

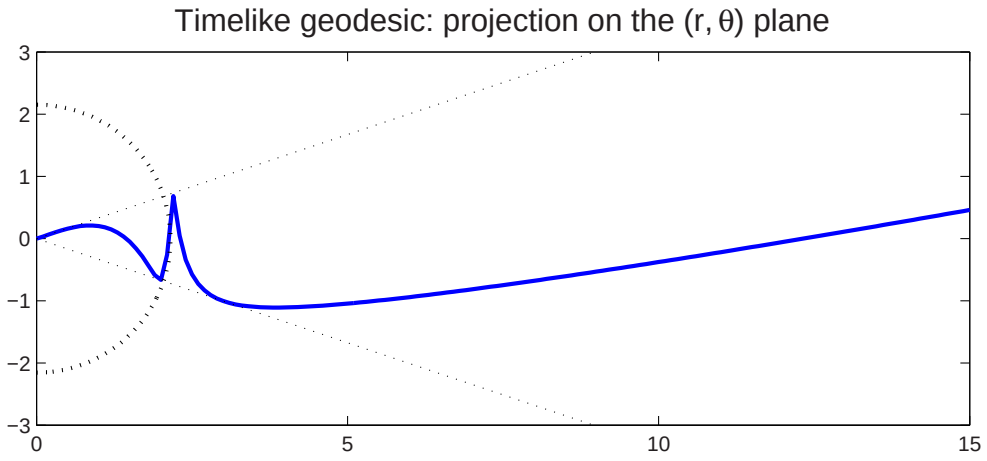

Figure 17.1: An example of a marginally bound time-like geodesic with constant radius $r_s = 2.154$. Parameters are $M = 1$, and $a = 0.8$.

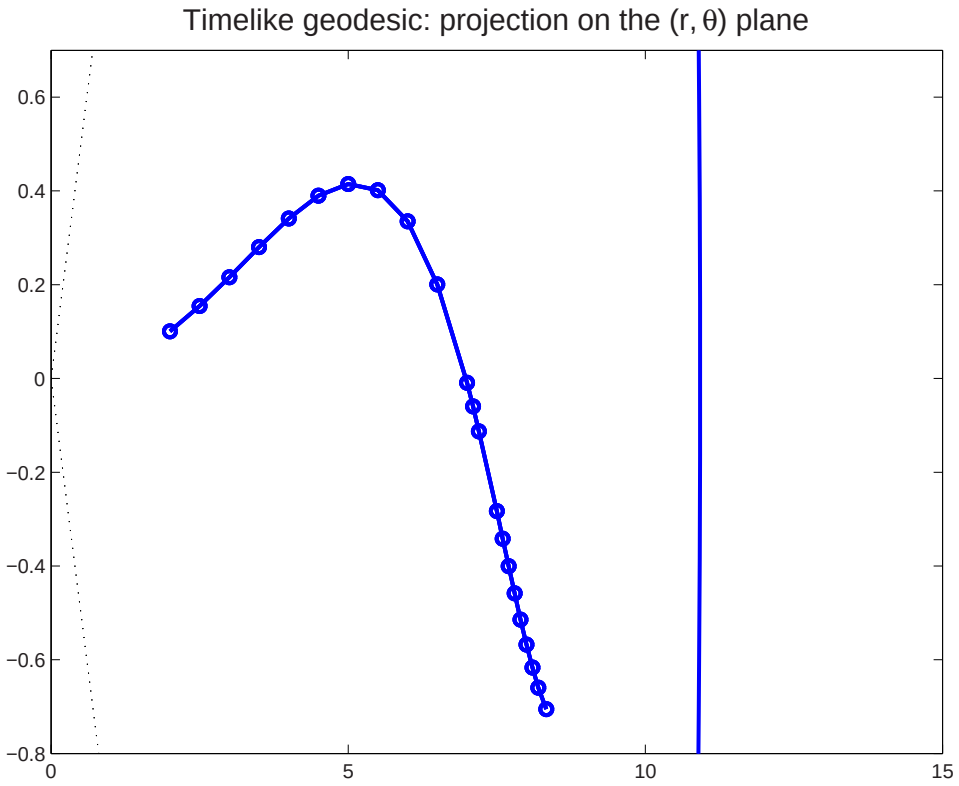

Figure 17.2: An example of a stable spherical time-like geodesic. Parameters are $M = 1$, $e = -0.08$ and $a^2 = 0.84$.

17.2.2 Orbits with negative η

Because of the conditions on parameters η, α and xi from section 17.1.3, integration of the left-hand side of equation (15.4) gives

$$\int \frac{\mathrm{d}r}{\sqrt{\mathrm{R}}} = g[\mathrm{F}(\phi), k) + \mathrm{K}(k)]\,, \tag{17.24}$$

where

$$g = \frac{1}{\sqrt{A+B}}\,, \tag{17.25}$$

$$\phi = \arccos\frac{(A-B)r + u_2 B - u_1 A}{(A+B)r - u_2 B - u_1 A}\,, \tag{17.26}$$

$$k = \frac{\sqrt{\dfrac{(A+B)^2 - (u_2-u_1)^2}{AB}}}{2}\,, \tag{17.27}$$

$$A = \sqrt{(u_2 - b_1)^2 + a_1^2}\,, \tag{17.28}$$

$$B = \sqrt{(u_1 - b_1)^2 + a_1^2}\,, \tag{17.29}$$

$$a_1 = \frac{\sqrt{-(u_3 - \bar{u_3})^2}}{2}\,, \tag{17.30}$$

and

$$b_1 = \frac{u_3 + \bar{u_3}}{2}\,, \tag{17.31}$$

where u_1, u_2, u_3 and $\bar{u_3}$ are the solutions of the equation $R = 0$. Example of this kind of orbit is in figure 17.3.

17.3 The φ-motion

17.3.1 Marginally bound orbits

We substitute $E^2 = 1$ in the equations (17.18) and (17.2), then

$$R = (r - r_s)^2 \left(2rM - \frac{a^2\eta_s}{{r_s}^2}\right) \tag{17.32}$$

$$\Theta = \eta_s - {\xi_s}^2 \cot^2\theta\,. \tag{17.33}$$

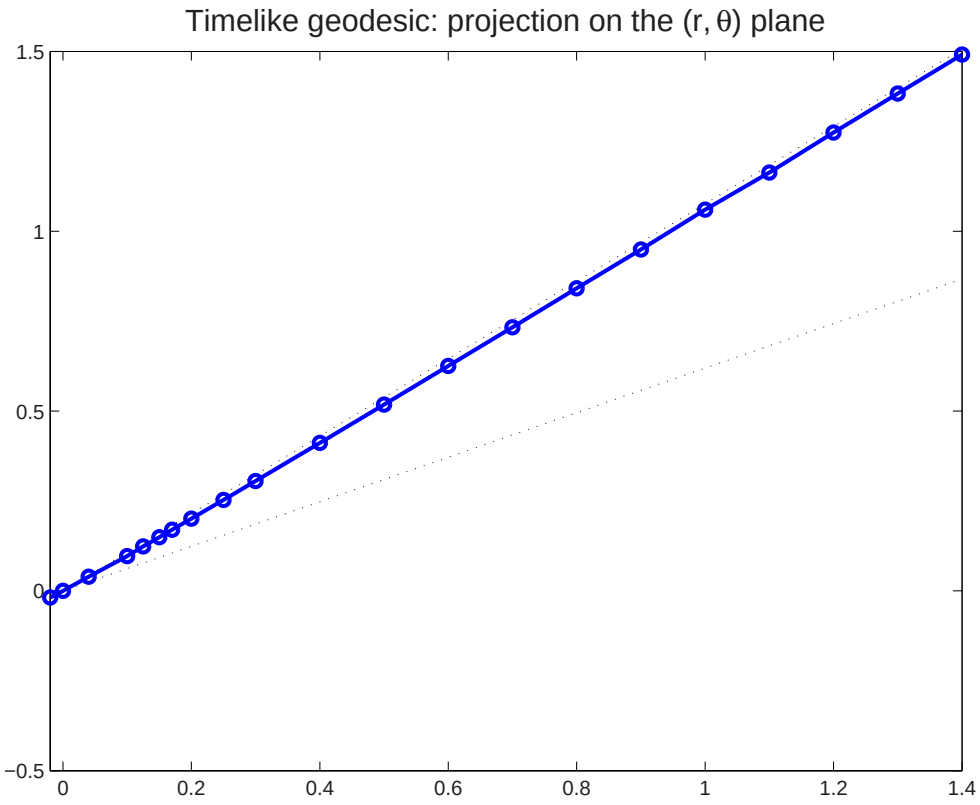

Figure 17.3: An example of a time-like orbit with negative Carter constant. Parameters are $M = 1$, $e = -0.08$, $\xi = -0.5$, $\eta = -1/9$, $E = 3$ and $a^2 = 0.84$.

The φ-motion is determined by integral

$$\varphi = a\int[(r^2+a^2)-aL]\frac{\mathrm{d}r}{\Delta\sqrt{R}} + \int(L\csc^2\theta - a)\frac{\mathrm{d}\theta}{\sqrt{\Theta}}\,. \tag{17.34}$$

Using method of partial fractions, the integral over r will become

$$I_R = -\frac{1}{\Delta_s}\int\frac{Ar+B}{\Delta\sqrt{2Mr-\dfrac{a^2\eta_s}{{r_s}^2}}}\mathrm{d}r + \frac{a^2-aL+{r_s}^2}{\Delta_s}\int\frac{\mathrm{d}r}{(r-r_s)\sqrt{2Mr-\dfrac{a^2\eta_s}{{r_s}^2}}}\,, \tag{17.35}$$

where

$$\Delta_s = r_s^2 - 2Mr_s + a^2\,, \tag{17.36}$$

$$A = 2r_sM + 2a^2 - aL \tag{17.37}$$

and

$$B = 2r_sa^2 - r_saL - 2Ma^2 + 2MaL\,. \tag{17.38}$$

The first integral can be further reduced to

$$\begin{aligned} I_1 &= 4M\int\frac{At^2+\gamma}{t^4+2t^2\alpha+\beta}\mathrm{d}t = \\ &= 4M\int\frac{At^2+\gamma}{(t^2+\alpha^2-\sqrt{\alpha^4-\beta})(t^2-\sqrt{\beta}+\sqrt{\alpha^4-\beta})}\mathrm{d}t\,, \end{aligned} \tag{17.39}$$

where

$$\alpha = \frac{a^2\eta_s}{{r_s}^2} - 2M^2\,, \tag{17.40}$$

$$\beta = \left(\frac{a^2\eta_s}{{r_s}^2}\right)^2 - 4M^2\frac{a^2\eta_s}{{r_s}^2} + 4M^2a^2 \tag{17.41}$$

and

$$\gamma = A\frac{a^2\eta_s}{{r_s}^2} + 2MB\,. \tag{17.42}$$

Using the partial fractions method again we find

$$I_1 = 4M\arctan(2t)\left(\frac{\mathrm{const}_1}{\sqrt{\alpha^2-\sqrt{\alpha^4-\beta}}} + \frac{\mathrm{const}_2}{\sqrt{\sqrt{\alpha^4-\beta}-\sqrt{\beta}}}\right)\,, \tag{17.43}$$

where

$$\begin{aligned}\text{const}_1 = &-5\gamma\beta^{3/2} - 3\gamma\alpha^2\beta + 3\gamma\alpha^6 + 4\gamma\alpha^2 * \sqrt{\beta}\sqrt{\alpha^4-\beta} + 5\gamma\sqrt{\beta}\alpha^4 \\ &+ 6\gamma\alpha^4\sqrt{\alpha^4-\beta} - 10\gamma\beta\sqrt{\alpha^4-\beta} + A\beta^{3/2}\alpha^2 - 5A\beta^{3/2}\sqrt{\alpha^4-\beta} - 13A\alpha^4\beta \\ &+ 7A\alpha^2\beta\sqrt{\alpha^4-\beta} + 3A\alpha^8 - 3A\alpha^6\sqrt{\alpha^4-\beta} \\ &+ A\alpha^4\sqrt{\beta}\sqrt{\alpha^4-\beta} - A\sqrt{\beta}\alpha^6 + 10A\beta^2 \end{aligned} \tag{17.44}$$

and

$$\begin{aligned}\text{const}_2 = &\, 5\gamma\beta^{3/2} + \\ &+ 3\gamma\alpha^2\beta - 3\gamma\alpha^6 - 4\gamma\alpha^2\sqrt{\beta}\sqrt{\alpha^4-\beta} - 5\gamma\sqrt{\beta}\alpha^4 - 6\gamma\alpha^4\sqrt{\alpha^4-\beta} + \\ &+ 10\gamma\beta\sqrt{\alpha^4-\beta} + 15A\beta^2 + \\ &+ 5A\beta^{3/2}\sqrt{\alpha^4-\beta} - A\beta^{3/2}\alpha^2 - 7A\alpha^2\beta\sqrt{\alpha^4-\beta} + A\sqrt{\beta}\alpha^6 + \\ &+ 3A\alpha^6\sqrt{\alpha^4-\beta} - 21A\alpha^4\beta - A\alpha^4\sqrt{\beta}\sqrt{\alpha^4-\beta} + 6A\alpha^8 \,. \end{aligned} \tag{17.45}$$

The second integral in (17.35) is

$$I_2 = \begin{cases} \dfrac{2\arctan\sqrt{\dfrac{2Mr - \dfrac{a^2\eta_s}{{r_s}^2}}{-D}}}{\sqrt{-D}} & \text{for } D < 0 \\ \dfrac{\ln\left|\dfrac{\sqrt{2Mr - \dfrac{a^2\eta_s}{{r_s}^2}} - \sqrt{D}}{\sqrt{2Mr - \dfrac{a^2\eta_s}{{r_s}^2}} + \sqrt{D}}\right|}{\sqrt{D}} & \text{for } D > 0., \end{cases} \tag{17.46}$$

where

$$D = 2Mr_s - \frac{a^2\eta_s}{{r_s}^2} \,. \tag{17.47}$$

We substitute $x = \sin\theta$ in the integral over θ in (17.34). Then

$$\begin{aligned} I_x &= \int \frac{L - a^2x^2}{x\sqrt{x^2(\eta_s + {\xi_s}^2) - {\xi_s}^2}}\mathrm{d}x = \\ &= \frac{\xi_s \arccos\dfrac{\xi_s}{|x|\sqrt{\eta_s + {\xi_s}^2}} - a^2\sqrt{x^2(\eta_s + {\xi_s}^2) - {\xi_s}^2}}{\eta_s + {\xi_s}^2} \,. \end{aligned} \tag{17.48}$$

Chapter 18

Summary of part III

Let us recall that while there are certain similarities between geodesics in the equator of the Kerr black holes and spherically symmetric solutions (Schwarzschild and Reissner Nordström), (for example the function f(u) is cubic, as it is in the case of the Schwarzschild black hole, so unlike in the Reissner-Nordström case, equatorial geodesics of the Kerr black hole can reach the singularity), rotation of the black hole adds a new feature, so now we have to distinguish between direct and retrograde orbits. Also the radial geodesics are "dragged" around the black hole.

Besides the three conservation laws (the energy, the angular momentum and the norm of the four-velocity), in the Kerr space-time there is the fourth conserved quantity, the Carter constant, which discovery followed from demonstrating the separability of the Hamilton-Jacobi equation. That is why it is possible to find the general solution of orbits outside the equatorial plane, (the function f(r) is quartic), although the solution is not explicit. As before, in the case of geodesics of the Schwarzschild and Reissner-Nordström black holes, only time-like geodesics can be bound.

This thesis extends previous work of [7] by giving general solutions of time-like, space-like and null orbits in equatorial plane in slow, extreme and fast

black holes, and by studying special types of non-equatorial time-like, space-like and null geodesics in complete detail. General observation about relationship between parameters and types of orbits were made in addition to work of [34].

Chapter 19

Conclusion

There is a close relationship between Killing tensors and separable systems for the geodesic Hamilton-Jacobi equation (conservation lemma). The existence of a separable system in Petrov type D space-times is a consequence of the algebraic properties of the Weyl tensor [44]. [8] demonstrated the separability of the Hamilton-Jacobi equation (which led to the discovery of Carter constant). Then the basic equations of motions can be deduced, and their analytical solutions found.

Geodesics are of three types:

- Time-like
- Null
- Space-like

Time-like and *null* geodesics in Schwarzschild space-time have been studied before, [7, 12, 31]. In this thesis space-like geodesics are studied and solutions are provided.

In this thesis geodesics of Reissner-Nordström space-time are studied and solutions for these two types are provided:

- $M^2 \geq Q_*^2$ (general solutions in terms of elliptic integrals)

- $M^2 < Q_*^2$ (both general and circular orbits)

In this thesis equatorial geodesics of Kerr space-time are studied and general solutions are provided.

Special cases of non-equatorial geodesics were also given. Doing this we have corrected errors in various places (such as [7, 34], see footnotes in the thesis).

[27] claim there exist repulsive space-like orbits in the Schwarzschild space-time and unstable, space-like, circular orbits in the Schwarzschild field for all radii in the range $0 < r < 3M$. By investigating restrictions that should be applied to parameters L, E, and M, in this thesis it is concluded that there can be neither repulsive orbits nor circular orbits with $r \leq 2M$.

[7] gives two solutions for circular null geodesics in the equator of the slow Kerr black hole. In this thesis three solutions are presented that are in agreement with [34] who claims there are three null circular orbits.

Let us recall that in classical mechanics flyby and bound orbits are hyperbolas and ellipses respectively. While these orbits are analogues of the orbits of the first kind, the associated orbits of the second kind have no Newtonian analogue. Other differences include the precession of bound orbits and dragging of the inertial frame in the case of a rotating black hole.

It is clear that there are similarities between geodesics in Schwarzschild black hole, Reissner-Nordström black hole and equator of the Kerr black hole, because of spherical symmetry of the first two and special choice of θ in the third case. To find general solutions we had to find zeros of a cubic or quartic polynomial and integrals of its square root, which is possible and leads to elliptic integrals. The integration methods used were standard and analytical solution were obtained sometimes using Maple program for symbolic mathematics.

This thesis studies all geodesics regardless of their physical significance.

However, the results of this thesis could be used for example to test whether the properties of orbits of a black hole candidate have the characteristics of black hole orbits in general relativity.

Some cases that did not fit within the scope and time frame of this PhD program, e.g. a complete analysis of non-equatorial geodesics in rotating black holes, such as qualitative analysis of geodesics with $Q < 0$ (r-L plots), solutions for general orbits and some special cases like axial and polar orbits and geodesics in horizons. Further work could also include an analysis of geodesics in the charged black holes (including a magnetic monopole) and a cosmological constant ([41] discus equatorial photons in a Kerr-Newman black hole with non-zero cosmological constant). Schwarzschild coordinates (t, r, θ, φ), which were used in this thesis, give pathological description at the horizons, so that e.g. Kruskal-Szekeres coordinates could be used instead.

Appendix A

Source code listing

Files listed in this appendix were used to generate pictures in this thesis. They are written with MATLAB, version 6.0.0.88 (R12)[1] and Maple 6[2].

A.1 MATLAB codes

A.1.1 Files that create figure 4.1

Listing of `prp_time.m`

```
function [tau] = prp_time(eta)
% Schwarzschild radial spacelike geodesic
% Proper time in Schwarzschild space-time
% for radial spacelike geodesic with initial
% condition r_i = M.
% eta is a variable.
tau = (eta+sinh(eta)) *sqrt(1^3/8);
```

[1] www.mathworks.com

[2] www.maplesoft.com

Listing of `radius.m`

```
function [r] = radius(eta, r_i)
% Schwarzschild radial spacelike geodesic
% Radius in Schwartzchild space-time
% for radial spacelike geodesic with initial
% condition r_i = M.
% eta is a variable.
r = cosh(eta/2).^2;
```

Listing of `time.m`

```
function [t] = time(eta)
% Schwarzschild radial space-like geodesic
% Time coordinate in Schwarzschild space-time for radial
% space-like geodesic with initianl condition for radius
% r_i = M (energy E = 1).
% eta is variable.
t = sqrt(1/2) *((eta+sinh(eta))/2+2*eta) ...
    -4*atanh(tanh(eta/2)/tanh(asinh(-1)));
```

Listing of `plot_rad.m`

```
subplot(211)
plot(prp_time(0:0.005:pi), radius(0:0.005:pi), 'LineWidth', 2)
title('Proper time, {\it \tau}', 'Fontsize', 15)
axis([-1 5 0 7])
set(gca, 'Box', 'off')
xlabel('\tau/M', 'FontAngle', 'italic', 'FontSize', 16, ...
    'Position', [4.8 -0.9])
ylabel('r/M', 'FontAngle', 'italic','FontSize', 16, ...
```

```
    'Position', [-1.4 6], 'Rotation', 0)
subplot(212)
plot(time(0:-0.005:2*asinh(-1)), ...
    radius(0:-0.005:2*asinh(-1)), 'LineWidth', 2)
set(line([0 -11], [2 2]), 'LineStyle', ':')
axis([-11 1 0 3])
set(gca, 'Box', 'off')
xlabel('t/M', 'FontAngle', 'italic', 'FontSize', 16, ...
    'Position', [.5 -0.4])
ylabel('r/M', 'FontAngle', 'italic', 'FontSize', 16, ...
    'Position', [-11.8 2.5], 'Rotation', 0)
title('Schwarzschild time, {\it t}', 'Fontsize', 15)
```

A.1.2 Files that create figure 4.2

Listing of `potentia.m`

```
function [V] = potentia(l, r)
% Schwarzschild space-like geodesic
% Potential V for parametr l = L/M (L denotes angular momentum
% about an axis normal to the invariant plane, M is mass)
% r is in mass units.
V = (1-2./r) .*(l^2./r.^2-1);
```

Listing of `plot_pot.m`

```
r = 0.005:0.005:5;
plot(r, potentia(0, r), 'k', ...
    r, potentia(3, r), 'k',...
    r, potentia(4.33, r), r, potentia(5, r), ...
    'k', r, potentia(10, r), 'k', r, ...
```

```
    potentia(15, r), 'k')
title('The effective potential', 'Fontsize', 15)
axis([0 5 -1 9])
set(gca, 'Box', 'off')
xlabel('{\it r/M}', 'FontSize', 16, 'Position', [5 -1.6])
ylabel('{\it V}', 'FontSize', 16, ...
    'Position', [-0.3 8.8], 'Rotation', 0)
GTEXT('a', 'FontWeight', 'bold')
GTEXT('b', 'FontWeight', 'bold')
GTEXT('c', 'FontWeight', 'bold', 'Color', 'b')
GTEXT('d', 'FontWeight', 'bold')
GTEXT('e', 'FontWeight', 'bold')
GTEXT('f', 'FontWeight', 'bold')
```

A.1.3 File that creates figure 4.3

File `implot.m` was downloaded from http://www.mathworks.com/support/ftp/graphicsv5.shtml on 13th January 2003.

Listing of `koef_mue.m`

```
f = inline('1-6*mu-2*mu*e', 'mu', 'e');
g = inline('mu*(3+e^2)-1', 'mu', 'e');
implot(g,[0 1/4 1 10])
hold on
implot(f, [0 1/4 1 10])
hold on
xlabel('\mu', 'FontAngle', 'italic','FontSize', 16, ...
    'Position', [.25 .6]);
```

```
ylabel('e', 'FontAngle', 'italic','FontSize', 16, ...
    'Position', [-0.014 9.8], 'Rotation', 0);
title('Solutions for coefficients {\it\mu} and {\it e}', ...
    'Fontsize', 15);
text(0.035, 7.2, 'A', 'FontWeight', 'bold', ...
    'HorizontalAlignment', 'right');
text(0.1, 3.3,'[1/12, 3]', 'FontWeight', 'bold')
set(gca, 'Box', 'off')
```

A.1.4 Files that create figure 4.4, figure 5.4 and figure 5.9

Listing of `radius1.m`

```
function [r1] =  radius1(chi, l, e)
% Schwarzschild spacelike geodesic
% Radius in Schwarzschild space-time
% for spacelike geodesic of the first kind
% l and e are parameters
% chi is a variable.
r1 = l./(1+e*cos(chi));
```

Listing of `radius2.m`

```
function [r2] =  radius2(xi, l, e, M)
% Schwarzschild spacelike geodesic
% Radius in Schwarzschild space-time
% for spacelike geodesic of the second kind
% l and e are parameters
% xi is a variable.
```

```
r2 = 1./(1/2/M-2/l +(1/2/M-(3+e)/l)*tan(xi/2).^2);
```

Listing of `spacelik.m`

```
function spacelik
% Schwarzchild  geodesic
% of the first and the second kind
e = 3/2;       % eccentricity 5 - space-like
               % 1/2 - bound, 3/2 unbound - time-like
M = 2/14;      % mass of the black hole
l = 4.5;       % latus rectum 4.5 - unbound,   3 - bound

mu = M/l;
%1 -mu*(3+e^2)    % > 0
%l/(e+1)
k = 2*sqrt(mu*e/(1-6*mu+2*mu*e));

chispan = [0 acos(-1/e)]; % [0 acos(-1/e)] - unbound
                          % [0 12*pi]  - bound
options = odeset('Refine',38);
[fi1, chi] = ode45(@fi1, chispan, -1, options, e, ...
    mu, k); % chi0 = 0 - unbound,  0 - bound

xispan = [0 pi];
[fi2, xi] = ode45(@fi2, xispan, 0, options, e, ...
    mu, k);

polar(fi1, radius1(chi, l, e))
hold on
```

```
%polar(-fi1, radius1(chi, l, e))     % <--- for unbound
%hold on
polar(fi2, radius2(xi, l, e, M))
title(['M = ' num2str(M) ', l = ' num2str(l), ...
        ', e = ' num2str(e)], 'Fontsize' , 15);
%-----------------------------------------------

function f1 = fi1(fi, chi, e, mu, k)
% ODE for phi coordinate for the geodesics of the first kind
% f1 is d chi / d phi
f1 = sqrt(1-6*mu+2*mu*e) *sqrt(1-k^2*cos(chi/2)^2);

function f2 = fi2(fi, xi, e, mu, k)
% ODE for phi coordinate for the geodesics of the second kind
% f2 is d xi / d phi
f2 = sqrt(1-6*mu+2*mu*e) *sqrt(1-k^2*sin(xi/2)^2);
```

A.1.5 Files that create figure 4.5

Files `radius1.m` and `radius2.m` are listed in section A.1.4.

Listing of `plottime.m`

```
function plottime
% Schwarzchild space-like geodesic
% of the first and the second kind
e = 6;     % eccentricity
M = 2/14;  % mass of the black hole
l = 4.5;   % latus rectum
```

```
mu = M/l;
k = 2*sqrt(mu*e/(1-6*mu+2*mu*e));

zac = -4.2 ;
timespan = [zac 0];
chi0 = 0;
options = [];
[pt1, pchi] = ode45(@tau1, timespan, chi0, options, e, mu, ...
    k, l);
[st1, schi] = ode45(@t1, timespan, chi0, options, e, mu, k, l);

tauspan = [zac -3.937];
xi0 = 0;
[pt2, pxi] = ode45(@tau2, tauspan, xi0, options, e, mu, k, l);
[st2, sxi] = ode45(@t2, timespan, xi0, options, e, mu, k, l);

subplot(211)
plot(pt1, radius1(pchi, l, e), pt2, radius2(pxi, l, e, M), ...
    'b', 'LineWidth', 2);
xlabel('\tau', 'FontAngle', 'italic','FontSize', 16, ...
    'Position', [-2.02 -0.4]);
ylabel('r', 'FontAngle', 'italic','FontSize', 16, ...
    'Position', [-4.61 2.8], 'Rotation', 0);
title('Proper time', 'Fontsize', 15);
text(-3.55, .6, 'first kind', 'FontWeight', 'bold');
text(-3.55, .35, 'second kind', 'FontWeight', 'bold');
axis([-4.5 -2 0 3]);
set(gca, 'Box', 'off');
```

```
subplot(212)
plot(st1, radius1(schi, l, e), st2, radius2(sxi, l, e, M), ...
    'b', 'LineWidth', 2 );
xlabel('t', 'FontAngle', 'italic','FontSize', 16, ...
    'Position', [-0.52 -0.4]);
ylabel('r', 'FontAngle', 'italic','FontSize', 16, ...
    'Position', [-4.7 2.8], 'Rotation', 0);
title('Schwarzschild time', 'Fontsize', 15);
text(-1.6, 1, 'first kind', 'FontWeight', 'bold');
text(-1.6, .75, 'second kind', 'FontWeight', 'bold');
set(line([-4.5 0], [2*M 2*M]), 'LineStyle', ':');
axis([-4.5 -0.5 0 3]);
set(gca, 'Box', 'off');
%-------------------------------------------

function f1 = tau1(tau, chi, e, mu, k, l)
% ODE for proper time for the geodesics of the first kind
% f1 is d chi / d tau
f1 = 2*mu/k/l *sqrt(e/(3*mu+mu*e^2-1)) *(1+e*cos(chi))^2 ...
    *sqrt(1-k^2*cos(chi/2)^2);

function g1 = t1(t, chi, e, mu, k, l)
% ODE for schwarzschild time for the geodesic of the first kind
% g1 is d chi / d t
g1 = 2*mu*sqrt(e) /k/l *(1-2*mu-2*mu*e*cos(chi)) ...
    *(1+e*cos(chi))^2 /sqrt(1-4*mu+4*mu^2-4*mu^2*e^2) ...
    *sqrt(1-k^2*cos(chi/2)^2);
```

```
function f2 = tau2(tau, xi, e, mu, k, l)
% ODE for proper time for the geodesics of the second kind
% f2 is d xi / d tau
f2 = sqrt(e) /2/mu/k/l ...
    *(1+4*mu+(1-6*mu-2*mu*e)*tan(xi/2)^2)^2 ...
    *sqrt(3*mu+mu*e^2-1) *sqrt(1-k^2*sin(xi/2)^2);


function g2 = t2(t, xi, e, mu, k, l)
% ODE for schwarzschild time for the geodesic of the second kind
g2 = sqrt(e-e*k^2*sin(xi/2)^2) /2/mu/k/l ...
    /sqrt(1-4*mu+4*mu^2-4*mu^2*e^2) ...
    *(1-4*mu+(1-6*mu-2*mu*e)*tan(xi/2)^2)^2 ...
    *(4*mu -(1-6*mu-2*mu*e)*tan(xi/2)^2);
```

A.1.6 Files that create figure 4.6, figure 5.7 and figure 5.10

Files `radius1.m` and `radius2.m` are listed in section A.1.4.

Listing of `spac_spc.m`

```
function spac_spc
% Schwarzchild geodesic
% of the first and the second kind
% case 2*mu*(3+e) = 1
e = 3;  % 1/2 - time--like bound     6 - space--like
          % 3/2 - time--like unbound
M = 1;   %2/14


l = 2*M*(3+e);
```

```
mu = M/l;
r = 2*(3+e)/(1+e)
%2*mu*(3+e)
chi = .01:0.0001:1.5;  % 0.1--pi time--like bound
                       % 0.01--1.5 space--like
                       % 0.01--2 time-like unbound
xi = 0.1:.0001:pi;
u = (1+e+2*e*tan(xi/2).^2)/l;


polar(-log(tan(chi/4))/sqrt(mu*e), radius1(chi, l, e))
hold on
polar(-log(tan(xi/2))/sqrt(mu*e), 1./u)
%title('Special case 2\mu(3+e) = 1', 'Fontsize', 15);
title(['Unstable space-like circular orbit with r_p = ' num2str(r), 'M'], 'Fontsi
```

A.1.7 Files that create figure 4.7 and figure 5.8

Listing of `i_radius.m`

```
function [ri] =  i_radius(xi, l, e)
% Schwarzschild spacelike geodesic
% Radius in Schwarzschild space-time
% for spacelike geodesic with immaginary eccentricity
% l and e are parameters
% xi is a variable.
ri = l./(1+e*tan(xi/2));
```

Listing of `imaginar.m`

```
function imaginar
% Schwarzchild geodesic
```

```
% with the imaginary eccentrities
e = 1;     % eccentricity
M = 2/14;  % mass of the black hole: 2/14 -- space-like

l = 1;   % latus rectum: 0.16 -- space-like
                           % 1 -- time-like
mu = M/l;                              % < .25
% Delta = sqrt((6*mu-1)^2+4*mu^2*e^2);
% k = sqrt((Delta +6*mu-1)/2/Delta) % > 1
% 1-3*mu+mu*e^2                     % > 0
% 2*ellipke(k)/sqrt(Delta)
% 2*atan(-(6*mu-1)/2/mu/e)
% 1/(1/2/M-2/l)                          % > 0

xispan = [1 5.9];
                   % [-1.57 .1] -- space-like
                   % [1 5.9] -- time-like
options = odeset('Refine',38);

[fi, xi] = ode45(@fi, xispan, 1, ...
    options, e, ...
    mu);        % init. cond: -1 -- space-like, 1 -- time-like

polar(fi, i_radius(xi, l, e))
title(['M = ' num2str(M) ', l = ' num2str(l) ...
        ', e = ' num2str(e) '\cdot i'], 'Fontsize', 15);
%-------------------------------------------
```

```
function f = fi(fi, xi, e, mu)
% ODE for phi coordinate for the geodesics
% with imaginary eccentricity
% f1 is d xi / d phi
f = sqrt(2*(6*mu -1 +2*mu*e*sin(xi) +(6*mu-1)*cos(xi)));
```

A.1.8 Files that create figure 4.8

File `i_radius.m` is listed in section A.1.7.

Listing of `pl_itime.m`

```
function pl_itime
% Schwarzchild space-like geodesic
% with immaginary eccentricity
e = 1;     % eccentricity
M = 2/14;  % mass of the black hole
l = 0.16;   % latus rectum


mu = M/l;
Delta  = sqrt((6*mu-1)^2 +4*mu^2*e^2);
k = sqrt((Delta+6*mu-1) /2/Delta);


zac = -4.1;
timespan = [zac 1.055];
xi0 = -1;
options = [];
[pt, pxi] = ode45(@tau, timespan, xi0, options, e, mu, k, l);
[st, sxi] = ode45(@t, timespan, xi0, options, e, mu, k, l);
```

```
subplot(211)
plot(pt, i_radius(pxi, l, e), 'LineWidth', 2);
xlabel('\tau', 'FontAngle', 'italic','FontSize', 16, ...
    'Position', [1.5 -0.05]);
ylabel('r', 'FontAngle', 'italic','FontSize', 16, ...
    'Position', [-5.1 .35], 'Rotation', 0);
title('Proper time', 'Fontsize', 15);
axis([-4.5 2 0 0.4]);
set(gca, 'Box', 'off');
subplot(212)
plot(st, i_radius(sxi, l, e), 'LineWidth', 2);
xlabel('t', 'FontAngle', 'italic','FontSize', 16, ...
    'Position', [1.5 0.27]);
ylabel('r', 'FontAngle', 'italic','FontSize', 16, ...
    'Position', [-5.1 .37], 'Rotation', 0);
title('Schwarzschild time', 'Fontsize', 15);
set(line([-4.5 0], [2*M 2*M]), 'LineStyle', ':');
axis([-4.5 2 0.28 .38]);
set(gca, 'Box', 'off');
%-----------------------------------------------

function f = tau(tau, xi, e, mu, k, l)
% ODE for proper time for the geodesics with immaginary
% eccentricity
% f is d xi / d tau
f = mu *sqrt(2) /(mu*(3-e^2)-1) *(1+e*tan(xi/2))^2 ...
    /sqrt(6*mu -1 +2*mu*e*sin(xi) +(6*mu-1)*cos(xi));
```

```
function g = t(t, xi, e, mu, k, l)
% ODE for schwarzschild time for the geodesic with immaginary
% eccentricity
% g is d xi / d t
g = (1+e*tan(xi/2))^2/l *(1 -2*mu*(1+e*tan(xi/2))) ...
    *sqrt(2*mu/(4*mu^2*e^2+4*mu^2-4*mu+1)) ...
    *sqrt(6*mu -1 +2*mu*e*sin(xi) +(6*mu-1)*cos(xi));
```

A.1.9 File that creates figure 5.1

Listing of `tm_prp_t.m`

```
function [tau] = tm_prp_t(eta)
% Schwarzschild radial time-like geodesic
% Proper time in Schwarzschild space-time
% for radial time-like geodesic with initial
% condition r_i = 6M. (M = 1)
% eta is a variable.
tau = (eta+sin(eta)) *3*sqrt(3);
```

Listing of `tm_rads.m`

```
function [r] = tm_rads(eta)
% Schwarzschild radial time-like geodesic
% Radius in Schwartzschild space-time
% for radial time-like geodesic with initial
% condition r_i = 6M. (M = 1)
% eta is a variable.
r = 6*cos(eta/2).^2;
```

Listing of `tm_radia.m`

```
subplot(211)
plot(tm_prp_t(0:0.005:pi), tm_rads(0:0.005:pi), 'LineWidth', 2)
title('Proper time, {\it \tau}', 'Fontsize', 15)
axis([-1 30 0 6])
set(gca, 'Box', 'off')
xlabel('\tau/M', 'FontAngle', 'italic', 'FontSize', 16, ...
    'Position', [29 -0.7])
ylabel('r/M', 'FontAngle', 'italic','FontSize', 16, ...
    'Position', [-3.5 5.3], 'Rotation', 0)
subplot(212)
plot(tm_time(0:0.005:2*asin(sqrt(2/3))), ...
    tm_rads(0:0.005:2*asin(sqrt(2/3))), 'LineWidth', 2)
set(line([0 30], [2 2]), 'LineStyle', ':')
axis([-1 30 0 6])
set(gca, 'Box', 'off')
xlabel('t/M', 'FontAngle', 'italic', 'FontSize', 16, ...
    'Position', [29 -0.7])
ylabel('r/M', 'FontAngle', 'italic', 'FontSize', 16, ...
    'Position', [-3.5 5.3], 'Rotation', 0)
title('Schwarzschild time, {\it t}', 'Fontsize', 15)
```

A.1.10 File that creates figure 5.2

Listing of `time_pot.m`

```
function [V] = time_pot(l, r)
% Schwarzschild time-like geodesic
% Potential V for parametr l = L/M (L denotes angular momentum
```

```
% about an axis normal to the invariant plane, M is mass)
% r is in mass units.
V = sqrt((1-2./r) .*(1+l^2./r.^2));
```

Listing of `pl_tpot.m`

```
r = 2:0.005:25;
plot(r, time_pot(3.464, r), ...
    r, time_pot(3.75, r), r, time_pot(4, r), ...
    r, time_pot(4.33, r), 'LineWidth', 2)
title('The effective potentials', 'Fontsize', 15)
axis([0 25 .92 1.05])
set(gca, 'Box', 'off')
xlabel('{\it r/M}', 'FontSize', 16, 'Position', [24 0.913])
ylabel('{\it V}', 'FontSize', 16, ...
    'Position', [-2 1.04], 'Rotation', 0)
GTEXT('a', 'FontWeight', 'bold')    %3.464
GTEXT('b', 'FontWeight', 'bold')    %3.75
GTEXT('c', 'FontWeight', 'bold')    %4
GTEXT('d', 'FontWeight', 'bold')    %4.33
```

A.1.11 File that creates figure 5.5

Listing of `tm_bnd_b.m`

```
e = 0;      % eccentricity
l = 3/2;    % latus rectum
M = 2/14;   % mass of the black hole


mu = M/l;
phi_0 = 0;
```

```
phi = 0:0.1:1.5*pi;
u = 1/l + (1/2/M-3/l)*sec((phi-phi_0)*sqrt(1-6*mu)/2).^2;


ezpolar('3/2')
hold on
polar(phi,1./u)
title('Special case  \it{e} = 0, \mu \neq 1/6', 'Fontsize'...
    , 15);
```

A.1.12 File that creates figure 5.6

Listing of `tm_bnd_d.m`

```
e = 0;      % eccentricity
%mu = 1/6;
M = 2/14;   % mass of the black hole


phi_0 = 0.001;
phi = 0:0.1:5*pi;
u = 1/6/M +2/M./(phi-phi_0).^2;


ezpolar('6/7')
hold on
polar(phi,1./u)
title('Special case  \it{e} = 0, \mu = 1/6', 'Fontsize'...
    , 15);
```

A.1.13 File that creates figure 3.2

Listing of `null.m`

```
function null
% Schwarzchild null geodesic
% of the first and the second kind
P = 1;
M = 2/14;  % mass of the black hole


Q = sqrt((P-2*M)*(P+6*M));
k = sqrt((Q-P+6*M)/2/Q);



chispan = [2*asin(sqrt((Q-P+2*M)/(Q-P+6*M))) 3.75];
                        %2*asin(sqrt((Q-P+2*M)/(Q-P+6*M)))
options = odeset('Refine',38);
[fi1, chi1] = ode45(@fi, chispan, 2.2, options, Q, ...
    P, k);


chispan = [0 pi];
[fi2, chi2] = ode45(@fi, chispan, 0, options, Q, ...
    P, k);


u1 = 1/P -(Q-P+6*M)/8/M/P*(1+cos(chi1));
u2 = 1/P +(Q+P-6*M)/4/M/P*sec(chi2/2).^2;


polar(fi1, 1./u1)
hold on
```

```
%polar(-fi1, 1./u1)
polar(fi2, 1./u2)
title(['M = ' num2str(M) ', P = ' num2str(P)], 'Fontsize', ...
    15);
%-----------------------------------------------


function f = fi(fi, chi, Q, P, k)
% ODE for phi coordinate for the null geodesics
% f1 is d chi / d phi
f = sqrt(Q/P) *sqrt(1-k^2*sin(chi/2)^2);
```

A.1.14 File that creates figure 3.3

Listing of `null_spc.m`

```
function tm_bnd_g
% Schwarzchild null geodesic
% critical orbit
M = 2/14;


phi = 0:0.1:15;
phi_0 =  -2*pi/3;    %2*atanh(1/sqrt(3));
u1 = -1/6/M +tanh((phi-phi_0)/2).^2/2/M;
u2 = 1/3/M + 2*exp(phi)/M./(exp(phi-1)).^2;


polar(phi, 1./u1)
hold on
polar(phi, 1./u2)
title('Special case  {\it D} = 3{\it M}3^{1/2}', 'Fontsize'...
    , 15);
```

A.1.15 File that creates figure 9.1

Listing of `slpotent.m`

```
function slpotent
% Reissner-Nordstrom space-like geodesic
% plotting of potential
% M is a mass of black hole
Q = 0.8;                 % charge of black hole


r = .005:0.005:10;


subplot 311
M = 10/14;
plot(r, potentia(M, Q, 3, r),  r, potentia(M, Q, 5, r), 'b', ...
    r, potentia(M, Q, 10, r), 'b', r, potentia(M, Q, 15, r), ...
    'b', 'LineWidth', 2)
axis([0 10 -10 40])
set(gca, 'Box', 'off')
title('Case when {\it M} = 10/14 <{\it M}_{cr}', 'Fontsize', 15)
xlabel('{\it r}', 'FontSize', 16, 'Position', [9.5 -11])
ylabel('{\it V}', 'FontSize', 16, ...
    'Position', [-1 27], 'Rotation', 0)
GTEXT('a', 'FontWeight', 'bold')
GTEXT('b', 'FontWeight', 'bold')
GTEXT('c', 'FontWeight', 'bold')
GTEXT('d', 'FontWeight', 'bold')
subplot 312;
plot(r, potentia(mass(3, Q), Q, 3, r), 'b', r, ...
```

```
    potentia(mass(5, Q), Q, 5, r), 'b', r, potentia(mass(10, ...
    Q), Q, 10, r), 'b', r, potentia(mass(15, Q), Q, 15, r), ...
    'b', 'LineWidth', 2)
axis([0 10 -5 40])
set(gca, 'Box', 'off')
title('Special case when {\it M} ={\it M}_{cr}', ...
    'Fontsize', 15)
xlabel('{\it r}', 'FontSize', 16, 'Position', [9.5 -6])
ylabel('{\it V}', 'FontSize', 16, ...
    'Position', [-1 30], 'Rotation', 0)
GTEXT('a', 'FontWeight', 'bold')
GTEXT('b', 'FontWeight', 'bold')
GTEXT('c', 'FontWeight', 'bold')
GTEXT('d', 'FontWeight', 'bold')
subplot 313
M = 12/14;
plot(r, potentia(M, Q, 3, r), 'b', r, potentia(M, Q, 5, r), ...
    'b', r, potentia(M, Q, 10, r), 'b', r, ...
    potentia(M, Q, 15, r), 'b', 'LineWidth', 2)
axis([0 10 -70 40])
set(gca, 'Box', 'off')
title('Case when {\it M} = 12/14 >{\it M}_{cr}', 'Fontsize', 15)
xlabel('{\it r}', 'FontSize', 16, 'Position', [9.5 -70])
ylabel('{\it V}', 'FontSize', 16, ...
    'Position', [-1 3.8], 'Rotation', 0)
GTEXT('a', 'FontWeight', 'bold')
GTEXT('b', 'FontWeight', 'bold')
GTEXT('c', 'FontWeight', 'bold')
```

```
GTEXT('d', 'FontWeight', 'bold')


%-------------------------------------------------------------
function [V] = potentia(M, Q, L, r)
% Potential V for parametres M, L and Q (L is angular momentum
% about an axis normal to the invariant plane, M is mass,
% Q is charge)
V = (r.^2-2*M*r+Q^2) ./r.^2 .*(L^2./r.^2-1);


function [M] = mass(L, Q)
% Mass for special case, when f(u) has an inflexion
M = sqrt(6*(-Q^4+14*Q^2*L^2-L^4) ...
    +2*sqrt(3*(3*L^2-Q^2)*(L^2+5*Q^2)^3)) /12/ L;
```

A.1.16 File that creates figure 13.1

Listing of `r_Ltimel.m`

```
% e-Q chart - the time-like geodesics
e = -1/9:.0167:1.2;     % variable for Q+
e1 = -1/9:.0167:0;      % variable for Q-
e2 = .2:.0167:1.2;      %   "
e3 = .0167:.0167:.2;    %   "
e4 = 0:.0167:1.2;       % variable for restriction for Q
Q_p = 1/2*(27*e.^2+18*e-1+sqrt((27*e.^2+18*e-1).^2+64*e))./e;
Q_m1 = 1/2*(27*e1.^2+18*e1-1-sqrt((27*e1.^2+18*e1-1).^2 ...
    +64*e1))./e1;
Q_m2 = 1/2*(27*e2.^2+18*e2-1-sqrt((27*e2.^2+18*e2-1).^2 ...
+64*e2))./e2;
Q_m3 = 1/2*(27*e3.^2+18*e3-1-sqrt((27*e3.^2+18*e3-1).^2 ...
```

```
    +64*e3))./e3;
a2e = -19*e4;           % Carter's inequality, a = sqrt(19)
plot(e, Q_p, e1, Q_m1, e2, Q_m2, e3, Q_m3, ...
    '--', e4, a2e)
text(0.3,20, 'Q_+')
text( -0.2, 24, 'Q_-')
text(0.7, -3, 'Q_-')
text(0.15, 26, 'd > 0')
text(-0.1, 8, 'd < 0')
text(0.2, -1.3, 'd > 0')
text(0.9, -6, 'd < 0')
text(0.8, -10, 'Q = -a^2e')
axis([-1 1.2 -12 32])
title('{\it e-Q} chart for the time-like geodesics', ...
    'FontWeight', 'bold', 'FontSize', 15, 'FontName', ...
    'TIMES')
set(findobj('Type', 'text'), 'FontAngle', 'italic', ...
    'FontName', 'TIMES', 'FontWeight', 'bold')
line([-1 1.2], [0 0])
text(-.97, 12, '12M^2')
text(-.97, 16, '16M^2')
xlabel('e', 'FontAngle', 'italic')
ylabel('Q', 'Rotation', 0, 'FontAngle', 'italic')
set(findobj('Type', 'line'), 'LineWidth', 2)
set(gca, 'Box', 'off')
line([-1 -.97], [12 12])
line([-1 -.97], [16 16])
set(findobj('Type', 'line'), 'Color', 'k')
```

A.1.17 File that creates figure 13.2

Listing of `r_Lnull.m`

```
% e-Q chart for the null geodesics
e = 0:.0167:1.2;        % variable for Q_null
Q_null = 27*e;          % solution for f(e, Q) = 0, where d = 0
a2e = -19*e;           % Carter's inequality, a = sqrt(19)
plot(e, Q_null, e, a2e, 'k', 'LineWidth', 2)
axis([0 1.2 -12 32])
text(1, 22, 'Q = 27eM^2')
text(0.4, 26, 'd > 0')
text(0.8, 1, 'd < 0')
text(0.8, -10, 'Q = -a^2e')
set(findobj('Type', 'text'), 'FontAngle', 'italic', ...
    'FontName', 'TIMES', 'FontWeight', 'bold')
title('{\it e-Q} chart for the null geodesics', ...
    'FontWeight', 'bold', 'FontSize', 15, 'FontName', ...
    'TIMES')
xlabel('e', 'FontAngle', 'italic')
ylabel('Q', 'Rotation', 0, 'FontAngle', 'italic')
set(gca, 'Box', 'off')
```

A.1.18 File that creates figure 13.3

Listing of `r_Lspace.m`

```
% e-Q chart for the space-like geodesics
e = 1:.001:1.2;        % variable for Q+ and Q-
Q_p = 1/2*(27*e.^2-18*e-1+sqrt((27*e.^2-18*e-1).^2-64*e))./e;
Q_m = 1/2*(27*e.^2-18*e-1-sqrt((27*e.^2-18*e-1).^2-64*e))./e;
```

```
a2e = -19*e;           % Carter's inequality, a = sqrt(19)
plot(e, Q_p, e, Q_m, 'b', e, a2e, 'k')
set(gca, 'YTick', -20:10:20, 'Box', 'off')
axis([1 1.2 -23 23])
text(1.1, 15, 'Q_+')
text(1.1, 4, 'Q_-')
text(1.12, 20, 'd > 0')
text(1.12, 6, 'd < 0')
text(1.12, -12, 'd < 0')
text(1.01, 1.3, 'd > 0')
text(1.12, -19, 'Q = -a^2e')
line([1 1.2], [0 0], 'Color', 'k')
set(findobj('Type', 'line'), 'LineWidth', 2)
set(findobj('Type', 'text'), 'FontAngle', 'italic', ...
    'FontName', 'TIMES', 'FontWeight', 'bold')
text(1, 4, '4M^2', 'HorizontalAlignment', 'Right')
line([1 1.003], [4 4], 'Color', 'k')
xlabel('e', 'FontAngle', 'italic')
ylabel('Q', 'Rotation', 0, 'FontAngle', 'italic')
title('{\it e-Q} chart for the space-like geodesics', ...
    'FontWeight', 'bold', 'FontSize', 15, 'FontName', ...
    'TIMES')
```

A.1.19 File that created figure 14.4

Data for this figure were obtained by Maple code listed in section A.2.10.

Listing of `eqnuplot.m`

```
% Kerr null euatorial geodesics
```

```
% a = .96 - angular momentum per unit mass of the black hole
% M = 1 - mass of the black hole

% D = 4 - impact parameter
y1 = [.085:.005:.305]; % 0.005:.33
phi1 = [%126.7411364 126.5615010 126.3799190 126.1962926 ...
        %126.0105220 125.8225048 125.6321363 125.4393088 ...
        %125.2439112 125.0458294 124.8449450 124.6411360 ...
        %124.4342755 124.2242321 124.0108691 123.7940442 ...
        123.5736091 123.3494088 123.1212816 122.8890576 ...
        122.6525592 122.4115999 122.1659834 121.9155030 ...
        121.6599410 121.3990672 121.1326384 120.8603968 ...
        120.5820690 120.2973646 120.0059740 119.7075676 ...
        119.4017928 119.0882726 118.7666022 118.4363466 ...
        118.0970372 117.7481678 117.3891904 117.0195100 ...
        116.6384785 116.2453882 115.8394630 115.4198500 ...
        114.9856062 114.5356864 114.0689255 113.5840184 ...
        113.0794948 112.5536876 112.0046938 111.4303230 ...
        110.8280321 110.1948384 109.5272022 108.8208666 ...
        108.0706302 107.2700177 106.4107846 105.4821379 ...
104.4694482 %103.3519685 102.0984244 100.6573680 98.93177565 ...
%96.68629120
];
y12 = [.305:.001:.325];
phi12 = [104.4694482 104.2551456 104.0364787 103.8132254 ...
        103.5851434 103.3519685 103.1134104 102.8691498 ...
        102.6188338 102.3620709 102.0984244 101.8274050 ...
        101.5484613 101.2609678 100.9642106 100.6573680 ...
```

```
        100.3394870 100.0094504 99.66593535 99.30735435 ...
        98.93177565];
y11 = .325:.0005:.335;
phi11 = [98.93177565 98.73688650 98.53680640 98.33113625 ...
        98.11942240 97.90114530 97.67570520 97.44240370 ...
        97.20041930 96.94877460 96.68629120 96.41152675 ...
        96.12268315 95.81747030 95.49289320 95.14490405 ...
    94.76779665 94.35306040 93.88695725 93.34447445 ...
    92.66943005];

y24 = .75:.001:.78;
phi24 = [86.92425115 92.24502520 97.54861850 102.8619916 ...
        108.2101802 113.6172933 119.1073442 124.7050016 ...
        130.4363306 136.3295802 142.4160892 148.7313700 ...
        155.3164873 162.2198490 169.4996380 177.2271888 ...
        185.4918364 194.4081033 204.1267621 214.8525994 ...
226.8744787 240.6195970 256.7599416 276.4458796 301.9082740 ...
338.4649726 405.7206186 499.7360435 369.4320964 323.3437426 ...
294.9208838];
y25 = .79:.01:1;
phi25 = [191.1306461 ...
    153.1361315 130.4649750 114.6096690 102.5453380 ...
    92.85921240 84.78245525 77.85243315 71.76979020 ...
    66.32957305 61.38472560 56.82523245 52.56541400 ...
    48.53569226 44.67686560 40.93574140 37.26134080 ...
    33.60098766 29.89543834 26.07165605 22.03036933 ...
    17.62154586];
y26 = 1.1:.1:2;
```

```
phi26 = [8.379873050 9.588609670 10.52606313 11.26599579 ...
        11.85721982 12.33356876 12.71935458 13.28679813 ...
   13.49258854 13.65818710];
y2 = .744:.001:.75;
phi2 = [52.38339145 58.75941665 64.77190450 70.52899420 ...
        76.10535650 81.55610685 86.92425115];
y22 = .7405:.0001:.744;
phi22 = [22.75235882 23.98768292 25.17107270 26.30909997 ...
        27.40708501 28.46940344 29.49970676 30.50107720 ...
        31.47614689 32.42718386 33.35615986 34.26480024 ...
        35.15462482 36.02698216 36.88307602 37.72398228 ...
        38.55067174 39.36402132 40.16482702 40.95381396 ...
    41.73164504 42.49892864 43.25622232 44.00404287 ...
    44.74286687 45.47313460 46.19525768 46.90961810 ...
    47.61657220 48.31645234 49.00957095 49.69622072 ...
    50.37667570 51.05119600 51.72002475 52.38339145];
y23 = .7399:.00005:.7405;
phi23 = [13.52660931 14.48556626 15.39297749 16.25659379 ...
        17.08241278 17.87518480 18.63874907 19.37625952 ...
        20.09034678 20.78323391 21.45681253 22.11271554 ...
        22.75235882];

polar(phi1, 1./y1, '-+')
hold on
polar(-phi1, 1./y1, '-+')
hold on
polar(phi11, 1./y11, '-+')
hold on
```

```
polar(-phi11, 1./y11, '-+')
hold on
polar(phi12, 1./y12, '-+')
hold on
polar(-phi12, 1./y12, '-+')
hold on
polar(phi2, 1./y2, '+')
hold on
polar(phi22, 1./y22, '+')
hold on
polar(phi23, 1./y23, '+')
hold on
polar(phi24, 1./y24, '+')
hold on
polar(phi25, 1./y25, '+')
hold on
polar(phi26, 1./y26, '+')
set(findobj(gca,'Type','line'),...
    'LineWidth',2)
title('M = 1, a = 0.96, D = 4', 'Fontsize', ...
    15);
```

A.1.20 File that created figure 14.17

Listing of `eqspacsp.m`

```
function eqspacsp
% equatorial plane of the Kerr black hole
% spacelike geodesics with L = aE
```

```
M = 1; % mass of the black hole
a = .8; % angular momentum per unit mass of the black hole
E = 2; % energy of the particle

fi = 0.001:.007:2*pi;
u = .3:.007:300;
r = 1./u; % radius
phi = -1/2*(atanh((-M^2 -M*(M^2-a^2)^(1/2) +E^2*a^2 ...
    +a^2 +u*a^2*(M^2-a^2)^(1/2)) /a^2 /E ...
    ./(a^2*u.^2-2*M*u+E^2+1).^(1/2)) -atanh((-M^2 ...
    +M*(M^2-a^2)^(1/2) +E^2*a^2 +a^2 ...
    -u*a^2*(M^2-a^2)^(1/2)) /a^2 /E ...
    ./(a^2*u.^2-2*M*u+E^2+1).^(1/2))) /E /(M^2-a^2)^(1/2);

polar(phi, r)
hold on
polar(fi, (M -sqrt(M^2-a^2)).*fi./fi, '-.k')
hold on
polar(fi, (M +sqrt(M^2-a^2)).*fi./fi, '-.k')
title('Special case L = aE', 'Fontsize', 15);
```

A.1.21 File that created figures 15.1 and 15.2

Data for this figure were obtained by Maple code listed in section A.2.12.

Listing of `nullcirc.m`

```
theta1 = [ 1.959006645  1.816103982  1.578378022 ...
        1.706286761  1.866968697  1.910804702 ...
        1.954576990  1.962037228  1.915820358 ...
```

```
        1.847886276  1.784055902  1.680305400 ...
        1.602077196  1.600545517  1.649663159 ...
        1.723995864  1.777339096  1.798573938 ...
        1.833106054  1.870594479  1.919934247];
r =      [ 1.855        1.86         1.87         1.88  ...
        1.9          1.91         1.93         1.95 ...
        2            2.05         2.1          2.2 ...
        2.3          2.4          2.5          2.7 ...
        2.9          3            3.2          3.5 ...
        4.2];
phi1 =   [-5.541341296 -5.320016908 -4.924482036 ...
        -4.327705853 -3.544342369 -3.240382475 ...
        -2.726240862 -2.396850466 -2.399627742 ...
        -2.359807195 -2.310512051 -2.233163264 ...
        -2.192546950 -2.091587306 -1.949251907 ...
        -1.753758502 -1.626961119 -1.579784075 ...
        -1.507997117 -1.440134137 -1.388536037];
%-------------------------------------------------------------
theta2 = [ 1.950206247  1.692797067  1.594889333 ...
        1.698540486 1.775954266 1.834710595  1.911654315 ...
        1.949916684  1.962465732  1.951397043 ...
        1.897375677 1.766360541  1.651451663  ...
        1.601225111  1.586579322 1.669103670  ...
        1.684244315 1.773141096 1.831029535 1.879714381 ...
        1.945814758 1.960479956  1.960712810 1.954832117 ...
        1.936159610 1.909190131 1.929546513 1.847996993 ...
        1.801473714  1.728540846  1.704772923 ...
        1.689185640  1.677302749];
```

```
phi2 =    [-5.609001073 -4.653018397 -4.308363707 ...
        -3.817095513 -3.426801711 -3.089056800 ...
        -2.495500640 -1.966177206 -1.397530535 ...
        -1.229151770 -.700154274 -.508268507 ...
        -1.072283865 -1.198786153 -1.247967614 ...
        -1.148745892 -1.127498734 -.979288603 ...
        -.848860023 -.695960167 -.276897702 ...
        .35332549e-1 .368964695 .670180716  .736756660 ...
        -.327276781  .323973264 -1.229000300 ...
        -1.665385193 -2.229559342 -2.402511389 ...
        -2.515903747 -2.602972572];
r2 =      [ 1.845        1.83         1.82         1.81 ...
        1.8          1.79         1.77         1.75 ...
        1.725        1.7         1.65        1.55 ...
        1.45         1.4          1.35         1.25 ...
        1.23        1.1         1         .9          .7 ...
        .6           .5          .45         .37 ...
        .3           .35          .2           .15 ...
        .1           .09          .085         .082];


subplot(2, 1, 1)
plot(r, r.*cos(theta1), '-ok', r2, r2.*cos(theta2), ...
    '-ok', 'LineWidth',2)
title('Projection on the (r, \theta) plane', ...
    'Fontsize', 15);
subplot(2, 1, 2)
plot(r.*cos(phi1), r.*sin(phi1), '-o', r2.*cos(phi2), ...
    r2.*sin(phi2), '-ob', 'LineWidth',2)
```

```
title('Projection on the (r, \phi) plane', ...
    'Fontsize', 15);
figure
plot3(r.*cos(phi1).*sin(theta1), ...
    r.*sin(phi1).*sin(theta1), r.*cos(theta1) ,'-o', ...
    r2.*cos(phi2).*sin(theta2), ...
    r2.*sin(phi2).*sin(theta2), r2.*cos(theta2) ,'-ob', ...
    'LineWidth',2);
title('Unstable circular null orbit (r_s = 1.85)', ...
    'Fontsize', 15);
```

A.1.22 File that creates figure 15.5 and 15.6

Data for this figure were obtained by Maple code listed in section A.2.13.

Listing of `null2.m`

```
r =     [3           2.5           2.2           2 ...
        1.8          1.7          1.65         1.64 ...
        1.63        1.62         1.617        1.615 ...
        1.612       1.611        1.61         1.609 ...
        1.608       1.607        1.605        1.604 ...
        1.603       1.602         1.6          1.598 ...
        1.597       1.596        1.595        1.594 ...
        1.593       1.592        1.591        1.59 ...
        1.589       1.588        1.585        1.58 ...
        1.575       1.57         1.56         1.55 ...
        1.54        1.53         1.52         1.51 ...
        1.5             1.48          1.45          1.43 ...
        1.4          1.35          1.3          1.28 ...
```

```
        1.25         1.23         1.2          1.18 ...
        1.17         1.15         1.14         1.135 ...
        1.13         1.125        1.12         1.115 ...
        1.11         1.109        1.108        1.107 ...
        1.106        1.105        1.104        1.103 ...
        1.102        1.101        1.1          1.0995 ...
        1.099        1.0985       1.0983       1.098 ...
        1.0977       1.0976       1.0975       1.09749 ...
        1.09748     1.09745       1.09743      1.0974 ...
        1.0973        1.09725     1.0972       1.0971 ...
        1.097        1.0968       1.0965       1.0964 ...
        1.0963       1.0962       1.0961       1.096  ...
        1.0955       1.09548      1.09545       1.09543 ...
        1.0954      1.09535      1.0953       1.0952 ...
        1.0951       1.095        1.0948       1.0947 ...
        1.0946       1.0945       1.0944       1.0943 ...
        1.094        1.0938       1.0935       1.0933 ...
        1.093        1.092        1.091        1.09 ...
        1.089        1.088        1.087        1.086 ...
        1.085        1.083        1.082        1.081 ...
        1.08         1.079        1.078        1.077 ...
        1.075        1.074        1.073        1.072 ...
        1.071        1.07         1.068        1.065 ...
        1.063        1.06        1.059        1.058 ...
        1.056        1.055        1.054        1.053 ...
        1.052        1.051        1.05];
theta = [1.294462769  1.282094207    1.271670896 ...
        1.262777690 1.251653855  1.244980096 ...
```

```
1.241299222 1.240532523 1.239755162 1.238966918 ...
1.238728288 1.238568643 1.238328333 1.238248004 ...
1.238167561 1.238087006 1.238006337 1.237925553 ...
1.237763644 1.237682518 1.237601277 1.237519921 ...
1.237356862 1.237193339 1.237111404 1.237029352 ...
1.236947183 1.236864896 1.236782493 1.236699973 ...
1.236617334 1.236534577 1.236451702 1.236368709 ...
1.236119014 1.235700462 1.235278890 1.234854263 ...
1.233995719 1.233124561 1.232240514 1.231343293 ...
1.230432607 1.229508152 1.228569621 ...
1.226649038  1.223654277  1.221577638 ...
1.218334690  1.212559669  1.206269072 ...
1.203592964  1.199391766  1.196458109 ...
1.191842991  1.188613332  1.186949903 ...
1.183520937  1.181753318  1.180855747 ...
1.179948813  1.179032370  1.178106271 ...
1.177170364 1.176224493  1.176034109 ...
1.175843319   1.175652122  1.175460516 ...
1.175268501  1.175076073  1.174883234 ...
1.174689980  1.174496311  1.174302226 ...
1.174205026  1.174107723  1.174010314 ...
1.173971321  1.173912800  1.173854242 ...
1.173834713  1.173815181  1.173813227 ...
1.173811274 1.173805413   1.173795645 ...
1.173801506 1.173776104   1.173766332 ...
1.173756559  1.173737010  1.173717457 ...
1.173678338  1.1736196    1.173600049 ...
1.173580466  1.173560879  1.173541287 ...
```

```
          1.173521692  1.173423650  1.17341972 ...
          1.173413841   1.173409917  1.173404030 ...
          1.173394218  1.173384405  1.173394218 ...
          1.173345142  1.173325503  1.173286215 ...
          1.173266565  1.173246910  1.173227251 ...
          1.173207587  1.173187919  1.173128891 ...
          1.173089517  1.173030425  1.172991008 ...
          1.172931852  1.172734386  1.172536491 ...
          1.172338166  1.172139410  1.171940220 ...
          1.171740597  1.171540537  1.171340041 ...
          1.170937730  1.170735914  1.170533655 ...
          1.170330951  1.170127802  1.169924206 ...
          1.169720161  1.169310720  1.169105320 ...
          1.168899465  1.168693156  1.168486388 ...
          1.168279161  1.167863324  1.167236089 ...
          1.166815593  1.166181312 1.165968934  ...
          1.165756079  1.165328930  1.165114633 ...
          1.164899850  1.164684583  1.164468828 ...
          1.164252585  1.164035851];
phi =    [-.30951580e-2 .149493628e-1  .724160709e-1 ...
          .1872877788 .5475707216 1.111795622 1.832518264 ...
          2.088156749 2.430127190 2.930514363 3.135780030 ...
          3.295347900 3.582549846 3.695374618 3.819426418 ...
          3.957076872 4.111550714 4.287326949 4.732889198 ...
          5.030027158 5.414594881 5.958637198 18.78207817 ...
          5.938106396 5.383563501 4.988572916 4.681022328 ...
          4.428771492 4.214677020 4.028479284 3.863611246 ...
          3.715564779 3.581124664 3.457898678 3.139491128 ...
```

```
2.722626670 2.392841803 2.117995304 1.671443132 ...
1.310772681 1.003777185  .7332400372 ...
.4888461273 .2639034517 .538062587e-1 ...
-.3343025470 -.8661201550 -1.202323916 ...
-1.696578288 -2.536792898 -3.464315936 ...
-3.880619862 -4.581036618 -5.118387695 ...
-6.084711058 -6.892355805 -7.370289796 ...
-8.556424770 -9.326746293 -9.780319319 ...
-10.29602270 -10.89352838 -11.60358584 ...
-12.47826787 -13.61689450 -13.89212769 ...
-14.18879017 -14.51054171 -14.86193896 ...
-15.24904668 -15.67986677 -16.16550080 ...
-16.72190151 -17.37326415 -18.15858054 ...
-18.62116738 -19.14739694 -19.75742601 ...
-20.03152546 -20.48313379 -20.99514252 ...
-21.18224390 -21.37881240 -21.39902281 ...
-21.41944784 -21.48105352 -21.58608803 ...
-21.52267930 -21.80517849 -21.91959072 ...
-22.03751229 -22.28479355 -22.54907825 ...
-23.13947429 -24.24031386 -24.69061593 ...
-25.20072672 -25.78900040 -26.48379829 ...
-27.33291729 -32.90671323 -32.17172098 ...
-31.27929513 -30.78354772 -30.14134122 ...
-29.26264352 -28.54849917 -27.42591530 ...
-26.55799571 -25.84995143 -24.73518318 ...
-24.27926984 -23.87170235 -23.50338764 ...
-23.16692970 -22.85769758 -22.05581185 ...
-21.60114955 -21.00608620 -20.65508959 ...
```

```
        -20.18200868 -18.92652182 -17.98078407 ...
        -17.22162588 -16.58737460 -16.04254989 ...
        -15.56498258 -15.13982821 -14.75669031 ...
        -14.08790780 -13.79217106 -13.51728942 ...
        -13.26050745 -13.01955899 -12.79258829 ...
        -12.57804762 -12.18125354 -11.99692798 ...
        -11.82084411 -11.65229524 -11.49065414 ...
        -11.33536071 -11.04192734 -10.63882916 ...
        -10.39111054 -10.04612004 -9.937419566 ...
        -9.831575142 -9.627883648 -9.529762758 ...
        -9.433964160 -9.340381530 -9.248906502 ...
        -9.159442720 -9.071900276];


plot(r.*cos(phi), r.*sin(phi), '-o', 'LineWidth',2)
title('Projection on the (r, \phi) plane', ...
    'Fontsize', 15);
figure
plot3(r.*cos(phi).*sin(theta), ...
    r.*sin(phi).*sin(theta), r.*cos(theta) ,'-o', ...
    'LineWidth',1);
title('Null orbit out of equator with \eta = 0', ...
    'Fontsize', 15);
```

A.1.23 File that creates figure 15.4

Data for this figure were obtained by Maple code listed in section A.2.14.

Listing of `null_Cart.m`

```
% Null non-equatrial geodesic in Kerr space-time
```

```
% negative eta
% data by null-Cart.mws
mu = [.9841748095 .9752419696 .9450342070 .8991332746 ...
        .7018743088 .7723506395 .7007318896 .6874398041 ...
        .7229829375 .7457523831 .7661076839 .7834342967 ...
        .7924506676 .8100588375];
r  = [-.375 -.35 -.3 -.25 -.125 0 .125 .25 .375 .5 .625 .75 ...
        .875 1];
plot(r, r.*cot(acos(mu)), '-o', 'LineWidth',2)      % the orbit
line([-0.375 1], [-0.375*cot(acos(0.9962923062)) ...
        cot(acos(.9962923062))], 'LineStyle', ':')
line([-0.375 1], [-0.375*cot(acos(0.6872011283)) ...
        cot(acos(.6872011283))], 'LineStyle', ':');
title('Null geodesic: projection on the (r, \theta) plane', ...
    'Fontsize', 15);
axis([-.375 1 -2.5 1.5])
```

A.1.24 File that creates figure 15.7 and 15.8

Listing of `nullneta.m`

```
function nullneta
% Kerr null non-equatorial geodesics
% with eta < 0
eta = -0.3;     % related to Carter constant, negative
xi = -0.05;     % related to particle's angular momentum
M = 1;          % mass of the black hole
a = .8;         % angular momentum per unit mass of black hole


tauspan = [-0.3  -.85101925];
```

```
initcond = [1 0.6265 1];
options = odeset('Refine', 38, 'Mass', @Mass, ...
    'MStateDependence', 'strong', 'MvPattern', MvPat, ...
    'MassSingular', 'no');

[tau, y] = ode15s(@nullKerr, tauspan, initcond, options, ...
    a, xi, eta, M);

plot(y(:,1).*cos(y(:,3)), y(:,1).*sin(y(:,3)))
title('Projection on the (r, \phi) plane', ...
    'Fontsize', 15);
figure
plot3(y(:,1).*cos(y(:,3)).*sin(y(:,2)), ...
    y(:,1).*sin(y(:,3)).*sin(y(:,2)), y(:,1).*cos(y(:,2)))
set(findobj('Type', 'line'), 'LineWidth', 2)
title(['Null orbit with negative Carter constant (\eta = ', ...
    num2str(eta), ')'], 'Fontsize', 15);
%-------------------------------------------------------------

function dy = nullKerr(tau, y, a, xi, eta, M)
% dy(1) is d r / d tau
% dy(2) is d theta / d tau
% dy(3) is d phi / d tau
dy = zeros(3, 1);
dy(1) = sqrt(y(1)^4 +(a^2-xi^2-eta)*y(1)^2 ...
    +2*M*(eta+(xi-a)^2)*y(1) -a^2*eta);
dy(2) = sqrt(eta +(a*cos(y(2)))^2 -(xi*cot(y(2)))^2);
dy(3) = 2*a*M*y(1) ...
```

```
    +((y(1)^2+a^2*cos(y(2)))^2-2*M*y(1))*eta*csc(y(2))^2;


function Mass = Mass(tau, y, a, xi, eta, M)
% 'mass' matrix for ODE solver r^2 + a^2 cos theta
rho = y(1)^2 +a^2*cos(y(2));
Delta = y(1)^2 -2*M*y(1) +a^2;
rho_vec = [rho^2 rho^2 rho^2*Delta];
Mass = diag(rho_vec);


function S = MvPat
% sparsity pattern
% S(i, j) = 1 if for any k, the (i, k) component of
% Mass(tau, y) depends on component j of y, and 0 otherwise
S = sparse(3, 3);
for i = 1:2
    for j = 1:3
        S(i, j) = 1;
    end
end
S(1, 1) = 1;
```

A.1.25 File that creates figure 16.1

Listing of `spacpara.m`

```
M = 1; E = 1; a = 0.96;     % parameters
r = M+0.1:.01:6;            % radius of the space-like orbit
Delta = r.^2 -2*M*r +a^2;   % horizon function
xi_plus = (M*(r.^2-a^2)+r.*Delta.*sqrt(1+(1-M./r)/E^2)) ...
    /a^2 ./(r-M);
```

```
xi_minus = (M*(r.^2-a^2)-r.*Delta.*sqrt(1+(1-M./r)/E^2)) ...
    /a^2 ./(r-M);
eta_plus = (2*r.^3*M.*Delta ...
    .*(1-sqrt(1+(1-M./r)/E^2))./(r-M) -r.^4.*(r-M) ...
    -r.^2/E^2.*(r.*(r-2*M).^2-a^2*M)) /a^2 ./(r-M);
eta_minus = (2*r.^3*M.*Delta ...
    .*(1+sqrt(1+(1-M./r)/E^2))./(r-M) -r.^4.*(r-M) ...
    -r.^2/E^2.*(r.*(r-2*M).^2-a^2*M)) /a^2 ./(r-M);
%subplot(1, 2, 1)
%plot(r, xi_plus, r, eta_plus)
%axis([M+.1 6 -00 120])
%text(5, -1520, '\eta_+')       % this parameter is negative
%text(5, -100, '\xi_+')
%subplot(1, 2, 2)
plot(r, xi_minus, r, eta_minus, 'LineWidth', 2, 'Color', 'b')
axis([M+.1 6 -40 50])
text(3.5, 20, '\eta_-')
text(5.5, -25, '\xi_-')
line([M+.1 6], [0 0], 'color', 'k')
xlabel('r_s', 'FontAngle', 'italic')
title('The (\xi_s, \eta_s) locus for space-like orbits', ...
    'Fontsize', 15)
set(findobj('Type', 'text'), 'Fontsize', 19, 'FontAngle', ...
    'italic', 'FontName', 'TIMES', 'FontWeight', 'bold')
```

A.1.26 File that creates figure 17.1

Data for this figure were obtained by Maple code listed in section A.2.15.

Listing of `tlmgcirc.m`

```
function tlmgcirc
% Kerr timelike marginally-bound (E = 1) critical orbits
a = .8;
r_s = 2.154;      % r_s = 1.85 gives negative values for eta_s
M = 1;

Delta = r_s^2 -2*M*r_s +a^2;
eta_s = r_s^2/a^2/(r_s-M) ...
    *(r_s*(4*a^2*M-r_s*(r_s-3*M)^2)/(r_s-M) ...
    +r_s*(r_s-2*M)^2 -a^2*M ...
    -2*r_s*M/(r_s-M)*Delta*(1-sqrt(M/r_s)))
xi_s = (M*(r_s^2-a^2) -r_s*Delta*sqrt(M/r_s)) /a /(r_s-M);
gama = -a^2*eta_s/r_s^2 +2*M*r_s
beta = 2*M;
mu_max = sqrt(eta_s/(xi_s^2+eta_s));

r = 0:.1:15;
x = 1./(r - r_s);
F = beta*x +gama*x.^2;
mu = sqrt(eta_s/(xi_s^2+eta_s)) ...
    *cos(log(abs(beta+2*gama*x +2*sqrt(gama*F))));
plot(r, r.*mu, 'LineWidth',2)
hold on
ezpolar(num2str(r_s), [-pi/2, pi/2])
line([0 15], [0 15*mu_max], 'LineStyle', ':', 'Color', 'k')
line([0 15], [0 -15*mu_max], 'LineStyle', ':', 'Color', 'k')
axis equal
```

```
axis([0 15 -3 3])
title(...
'Timelike geodesic: projection on the (r, \theta) plane', ...
    'Fontsize', 15);
```

A.1.27 File that creates figure 17.2

Data for this figure were obtained by Maple code listed in section A.2.16.

Listing of `tmbdcirc.m`

```
mu = [.5019766114e-1 ...
        .6174013747e-1 .7193269083e-1 .8007127001e-1 ...
    .8530484860e-1 .8663348979e-1 .8293193101e-1 ...
    .7302501022e-1 .5586301312e-1 .3088176960e-1 ... %5.5
    -.1311327065e-2 -.8412883022e-2 -.1565626878e-1 ... %7
    -.3771603241e-1 -.4495944307e-1 ...
    -.5201187035e-1 -.5877390468e-1 -.6513304053e-1 ... %7.7
-.7096287089e-1 ...
    -.7612248184e-1 -.8045621244e-1 -.8465346478e-1];
r1 = [2 2.5 3 3.5 ...
        4 4.5 5 ...
        5.5 6 6.5 ...
        7 7.1 7.2 ...
        7.5 7.6 ...
        7.7 7.8 7.9 ...
        8 ...
    8.1 8.2 8+1/3];
plot(r1, r1.*mu, '-o', 'LineWidth', 2)
hold on
```

```
ezpolar('10.92214439', [-pi/2, pi/2])
line([0 15], [0 15*.9987125027], 'LineStyle', ':', 'Color', 'k')
line([0 15], [0 -15*.9987125027], 'LineStyle', ':', ...
    'Color', 'k')
axis([0 15 -.8 .7])
title(...
'Timelike geodesic: projection on the (r, \theta) plane', ...
    'Fontsize', 15);
```

A.1.28 File that creates figure 17.3

Data for this figure were obtained by Maple code listed in section A.2.17.

Listing of `tim_Cart.m`

```
% nubmers cerated by tim_Cart.mws
mu = [.6780513813 .6864067161 .7015501632 .6944770527 ...
        .7037227809 .7056148039 .7069683485 .7087837041 ...
       .7113613559 .7135160284 .7169383936 .7195460504 ...
   .7215979572 .7232480058 .7245956435 .7257091088 ...
   .7274169134 .7266373914 .7280755002 .7286348614 ...
   .7291122111 .7295213682 .7298735311 .7301778415 .7304418066];
r      = [-.02 0 0.04 .1 .125 .15 .17 .2 .25 .3 .4 .5 .6 .7 ...
        .8 .9 1 1.1 1.2 1.3 1.4 1.5 1.6 1.7 1.8];
plot(r, r.*cot(acos(mu)), '-o',...
    'LineWidth',2)
line([-0.02 1.8], [-0.02*cot(acos(.5265412721)) ...
        1.8*cot(acos(.5265412721))], ...
'LineStyle', ':', 'Color', 'k')
line([-0.02 1.8], [-0.02*cot(acos(.7326270425)) ...
```

```
        1.8*cot(acos(.7326270425))], ...
'LineStyle', ':', 'Color', 'k');
title(...
'Timelike geodesic: projection on the (r, \theta) plane', ...
    'Fontsize', 15);
axis([-.02 1.4 -0.5 1.5])
```

A.2 Maple codes

Maple output is blue.

A.2.1 File that creates figure 8.3

Listing of `null_2.mws`

Reissner-Nordstrom solution

$Q\_^2 \leq M^2$

Null geodesics

All real roots

```
> restart:
> r := 1/y:
> f := -Q_^2*u^4+2*M*u^3-u^2+1/De^2 = 0:
> r_cr := 1.5*M*(1+sqrt(1-8*Q_^2/9/M^2)):
```

M should be $> .8 = Q\_$.

```
> evalf(12/14); Q_ := .8:  is(12/14 > Q_);
```

.8571428571

true

```
> r_c := subs(M = 12/14, r_cr);
```

$$r\_c := 1.896501668$$

should be $> r\_c$.

```
> r2 := subs(M = 18/14, r_cr); is(r2 > r_c);
```

$$r2 := 3.490425376$$

$$true$$

```
> M := 12/14:  subs(u = 1/r2, f);
```

$$-.04607972106 + \frac{1}{De^2} = 0$$

Impact parameter

```
> IP := {solve(%, De)};
```

$$IP := \{-4.658489053,\ 4.658489053\}$$

```
> subs(De = IP[2], f);
```

```
> u := solve(%, u);
```

$$-.64\,u^4 + \frac{12}{7}\,u^3 - u^2 + .04607972106 = 0$$

$$u := -.1854454261,\ .2864980317,\ .7358253611,\ 1.841693462$$

Cauchy horizon

```
> r_Ca := M- sqrt(M^2- Q_^2);
```

$$r\_Ca := .5494191538$$

Is turning point of geodesics of second kind inside the Cauchy horizon?

```
> 1/u[4]; is(1/u[4] < r_Ca);
```

$$.5429785253$$

$$true$$

The turning point of the geodesic of the first kind

```
> 1/u[2];
```

$$3.490425376$$

```
> ph1 := g*(EllipticF(arcsin(sqrt((u[4]-u[2]) *(y-u[1])
  /(u[2]-u[1]) /(u[4]-y))), k) +EllipticK(k))/Q_:
> ph2 := g*EllipticF(arcsin(sqrt((u[4]-u[2]) *(y-u[3])
  /(u[4]-u[3]) /(y-u[2]))), k)/Q_:
> g := 2/sqrt((u[4]-u[2])*(u[3]-u[1])):
```

k should be $<$ or $= 1$.

```
> k := sqrt((u[4]-u[3])*(u[2]-u[1])/(u[4]-u[2])
  /(u[3]-u[1])); is(k<= 1);
```

$$k := .6035461928$$

$$true$$

```
> with(plots):
Warning, the name changecoords has been redefined
> Fi1 := polarplot([r, ph1, y = 0..u[2]], -4..10, -10..10,
  thickness = 3, color = blue):
> Se := polarplot([r, ph2, y = u[3]..u[4]], thickness = 3,
  color = blue):
> rP := polarplot(M+ sqrt(M^2- Q_^2), color = black):
> rN := polarplot(r_Ca, color = black):
> rC := polarplot(r_cr, linestyle = 2, color = black):
> plotsetup(ps, plotoutput = `null2.eps`, plotoptions =
  `color, portrait, noborder`):
> display({Fi1, Se, rP, rN, rC}, axes = frame, scaling =
  constrained);
```

A.2.2 File that creates figures 8.5, 8.7, 8.11, 8.13 and 8.15

Listing of `nuimagin.mws`

Reissner-Nordstrom solution

Null geodesics

Complex roots

```
> restart:
> ph := g *(EllipticF(((u_4-y)*B-(y-u_1)*A)
  /((u_4-y)*B+(y-u_1)*A), k) +EllipticK(k)) /Q_:
> g := 1/sqrt(A*B):
> k := sqrt(((u_4-u_1)^2-(A-B)^2)/4/A/B):
> A := sqrt((u_4-b_1)^2+a_1^2):
> B := sqrt((u_1-b_1)^2+a_1^2):
> b_1 := (u_2-_u_2)^2/2:
> a_1 := sqrt(-(u_2-_u_2)^2/4):
> r := 1/y:
> f := -Q_^2*u^4+2*M*u^3-u^2+1/De^2 = 0:
> D_c := r_cr^2/sqrt(r_cr^2-2*M*r_cr+Q_^2):
> Q_ := 0.8:
> with(plots):
Warning, the name changecoords has been redefined
> PO := `color, portrait, noborder`:
```

$Q\_^2 \leq M^2$

```
> M := 12/14:  r_cr := 1.5*M*(1+sqrt(1-8*Q_^2/9/M^2)):
> D_c;
```

3.622947910

$De < D\_c$

```
> De := 3:
> res := solve(f, u);
```

$res := -.2711026131,\ .5402070456 - .2253128891\,I,\ .5402070456 + .2253128891\,I,\ 1.869259951$

```
> u_1 := res[1]:  _u_2 := res[2]:  u_2 := res[3]:  u_4 :=
  res[4]:
> k;
```

should be $<$ or $=$ 1.

$$.8589066470 + 0.\,I$$

```
> rI := polarplot([r, ph, y = 0..u_4], -10..2, -2..2,
  thickness = 3, colour = blue):
> rP := polarplot(M+ sqrt(M^2- Q_^2), colour = black):
> rN := polarplot(M- sqrt(M^2- Q_^2), colour = black):
> plotsetup(ps, plotoutput = `nuimagi1.eps`, plotoptions =
  PO):
> display({rI, rP, rN}, axes = frame, scaling =
  constrained);
```

$M^2 < Q\_^2 < \frac{9\,M^2}{8}$

```
> evalf(11/14);
```

$$.7857142857$$

```
> M := 11/14:
> is(9*M^2/8 > Q_^2);
```

$$true$$

```
> r_cr := 1.5*M*(1-sqrt(1-8*Q_^2/9/M^2)):
> D_c;
```

$$4.414717576$$

$D\_cs < De$

```
> De := 5:
> res := solve(f, u);
```

$res := -.1756926702,\ .2481796423,\ 1.191435085 - .1177231404\,I,\ 1.191435085 + .1177231404\,I$

```
> u_1 := res[1]:  u_4 := res[2]:  _u_2 := res[3]:  u_2 :=
  res[4]:
> k;
```

should be $<$ or $=1$

$$.8589066470 + 0.\,I$$

```
> plotsetup(ps, plotoutput = `nuimagi2.eps`, plotoptions =
  PO):
> polarplot({[r, ph, y = 0..u_4]},
  -20..6, -10..10, scaling = constrained, thickness = 3,
  axes = frame, color = blue, numpoints = 100);
```

$Q\_^2 = \frac{9\,M^2}{8}$

```
> M:= sqrt(8*Q_^2/9):  r_cr :=
  1.5*M*(1+sqrt(1-8*Q_^2/9/M^2)):
> D_c;
```

$$D\_c := 2.771281294$$

$\boldsymbol{D\_c < D}$

$D\_c < De$

```
> De := 3:
> res := solve(f, u);
```

$res := -.2754794469,\ .5566080169,\ 1.037947017 - .2343222916\,I,$
$1.037947017 + .2343222916\,I$

```
> u_1 := res[1]:  u_2 := res[4]:  _u_2 := res[3]:  u_4 :=
  res[2]:
> k;
```

should be $<$ or $=1$.

$$.7980466640 + 0.\,I$$

```
> plotsetup(ps, plotoutput = `nuimagi3_2.eps`, plotoptions =
  PO):
```

```
> polarplot({[r, ph, y = 0..u_4]},
  -10..10, -10..10, thickness = 3, axes = frame, scaling =
   constrained, color = blue);
```

$$\boldsymbol{D < D\_c}$$

$D\_c < De$

```
> De := 2:
```

```
> res := solve(f, u);
```

$res := -.3860244110,\ .6880983387 - .5165741872\,I,\ .6880983387 + .5165741872\,I,\ 1.366850338$

```
> u_1 := res[1]:  u_2 :=res[3]:  _u_2 := res[2]:  u_4 :=
res[4]:
```

```
> k;
```

should be $<$ or $=$ 1.

$$.4912118011 + 0.\,I$$

```
> plotsetup(ps, plotoutput = `nuimagi4_2.eps`, plotoptions =
PO):
> polarplot({[r, ph, y = 0..u_4]},
-10..2, -30..30, thickness = 3, axes = frame, scaling =
constrained, color = blue);
```

$\frac{9\,M^2}{8} < Q\_^2$

M should be $< \frac{\sqrt{8\,Q\_^2}}{3}$.

```
> evalf(sqrt(8*Q_^2)/3);
```

$$.7542472333$$

```
> M := .7:  De := 5:
```

```
> res := solve(f, u);
```

$res := -.1775581062,\ .2386464340,\ 1.063205836 - .5869991701\,I,\ 1.063205836 + .5869991701\,I$

```
> u_1 := res[1]:  u_2 := res[4]:  _u_2 := res[3]:  u_4 :=
  res[2]:
> k;
```

should be $<$ or $=$ 1.

$$.1444101517 + 0.\,I$$

```
> plotsetup(ps, plotoutput = `nuimagi5.eps`, plotoptions =
  PO):
> polarplot({[r, ph, y = 0..u_4], [r, -ph, y = 0..u_4]},
  -80..10, -160..160, scaling = constrained, thickness = 3,
  axes = frame, color = blue);
```

A.2.3 File that creates figure 8.8

Listing of `nulcircst2.mws`

Reissner-Nordstrom solution

Null geodesics

Double root - stable circular orbit

$M^2 < Q\_^2 < \frac{9\,M^2}{8}$

```
> restart:
> ph := arcsin((2*c*xi+b)/sqrt(4*Q_^2*c+b^2)) /sqrt(-c):
> b := 2 *(M-2*Q_^2*u_c):
> c := u_c *(3*M-4*Q_^2*u_c):
> r := 1/u:
> f := (u-u_c)^2
  *(-Q_^2*u^2+2*(M-Q_^2*u_c)*u+u_c*(M-Q_^2*u_c)):
> u_c := 1/r_cr:
> r_cr := 1.5*M*(1-sqrt(1-8*Q_^2/9/M^2)):
```

```
> M := 11/14:  Q_ := 0.8:
> u := solve(f, u);
```

$$u := 1.178725989,\ 1.178725989,\ .2941015908,\ -.1961964261$$

```
> u_2 := u[3]:
```

The turning point is

```
> 1/u[3];
```

$$3.400185620$$

```
> u := 1/xi +u_c:
> -1/u_c;
```

ξ must not exceed this

$$-.8483735909$$

```
> with(plots):
Warning, the name changecoords has been redefined
> Fi := polarplot([r, ph, xi = 1/(u_2-u_c)..-.85], -5..30,
  -10..10, color = blue):
> rC := polarplot(r_cr, color = blue):
> plotsetup(ps, plotoutput = `nullcst_2.eps`, plotoptions =
  `color, portrait, noborder`):
> display({Fi, rC}, axes = frame, scaling =
  constrained, thickness = 3);
```

A.2.4 File that creates figure 8.12

Listing of `nucirst2.mws`

Reissner-Nordstrom solution

Null geodesics

Double root - unstable circular orbit

$Q_{-}{}^{2} = \frac{9\,M^2}{8}$

```
> restart:
```

```
> ph := 2 *sqrt(b*xi-Q_^2) /b:
> b := 2 *(M-2*Q_^2*u_c):
> r := 1/u:
> u_c := 1/r_cr:
> r_cr := 1.5*M:
> Q_ := 0.8:  M:= sqrt(8*Q_^2/9):
> u := 1/xi +u_c:
> with(plots):
Warning, the name changecoords has been redefined
> -1/u_c;
```

ξ must not exceed this

$$-1.131370850$$

```
> Fi := polarplot([r, ph, xi = -30..-1.14], -2.5..1.5,
  -7..2, color = blue, thickness = 3, numpoints = 300):
> rC := polarplot(r_cr, linestyle = 2, color = black):
> plotsetup(ps, plotoutput = `nullcst2.eps`, plotoptions =
  `color, portrait, noborder`):
> display({Fi, rC}, axes = frame, scaling = constrained);
```

A.2.5 File that creates figure 10.3

Listing of `timeplot.mws`

Reissner-Nordstrom solution

Time-like geodesics

All real roots

```
> restart:
```

```
> ph1 := g *EllipticF(arcsin(sqrt((u_4-u_2) *(y-u_1)
  /(u_2-u_1) /(u_4-y))), k)/Q_:
> ph2 := g *EllipticF(arcsin(sqrt((u_4-u_2) *(y-u_3)
  /(u_4-u_3) /(y-u_2))), k)/Q_:
> g := 2/sqrt((u_4-u_2)*(u_3-u_1)):
> k := sqrt((u_4-u_3)*(u_2-u_1)/(u_4-u_2)/(u_3-u_1)):
> r := 1/y:
> f := -Q_^2*u^4+2*M*u^3-u^2*(1+Q_^2/L^2)+
  2*M/L^2*u-(1-E^2)/L^2 = 0:
> u_c := 0.2225:  Q_ := .8:  M := 1.2:  r_c := 1/u_c;
```

$$r\_c := 4.494382022$$

```
> r_r := 9*M^2/8; Q_^2; Q_^2/M;
```

$$r\_r := 1.620000000$$

$$.64$$

$$.5333333333$$

Following must hold:

```
> 1 -3*M*u_c +2*Q_^2*u_c^2 > 0;
```

$$0 < .2623680000$$

```
> E_c := (1-2*M*u_c+Q_^2*u_c^2)/ sqrt(1-3*M*u_c
  +2*Q_^2*u_c^2);
> L_c := sqrt(M-Q_^2*u_c)/ sqrt(u_c*(1-3*M*u_c
  +2*Q_^2*u_c^2));
```

$$E\_c := .9716240286$$

$$L\_c := 4.256378896$$

```
> L := 6:  E := 0.98:
> u := solve(f);
```

$$u := .02671189456, .04910213582, .4002564198, 3.273929550$$

```
> u_1 := u[1]:  u_3 := u[3]:  u_4 := u[4]:  u_2 := u[2]:
```

```
> k;
```

should be $<$ or $=$ 1.

.2311126109

```
> with(plots):
Warning, the name changecoords has been redefined

> Fi1 := polarplot([r, ph1, y = u_1..u_2], -24..38, -30..30,
  thickness = 3, color = blue):
> Fi2 := polarplot([r, -ph1, y = u_1..u_2], thickness = 3,
  color = blue):
> Se := polarplot([r, ph2, y = u_3..u_4], thickness = 3,
  color = blue):
> rC := polarplot(r_c, linestyle = 2, color = black):
> rR := polarplot(r_r, color = black):
> plotsetup(ps, plotoutput = `timeplot.eps`, plotoptions =
  `color, portrait, noborder`):
> display({Fi1, Fi2, Se, rC, rR}, axes = frame, scaling =
  constrained);
```

A.2.6 File that creates figure 11.1

Listing of `charplot.mws`

Reissner-Nordstrom solution

Charged particle

```
> restart:
> f := -Q_^2*u^4
  +2*M*u^3 -(1 +Q_^2*(1-q^2)/L^2)*u^2 +
  2/L^2*(M-q*Q_*E)*u -(1-E^2)/L^2 = 0:
> u_c := 0.2225:  Q_ := .8:  M := 1.2:  r_c := 1/u_c; q :=
  2:
```

$$r\_c := 4.494382022$$

```
> E_c := 1/2*(u_c*q*Q_*(4*M*u_c-1-3*Q_^2*u_c^2)
  -sqrt((2*M*u_c-1-Q_^2*u_c^2)^2
  *(4-12*M*u_c+8*Q_^2*u_c^2+u_c^2*Q_^2*q^2)))
  /(-2*Q_^2*u_c^2+3*M*u_c-1);
> L_c := (u_c*Q_^2-u_c*Q_^2*q^2-M+q*Q_*E_c)
  /(u_c*(-2*Q_^2*u_c^2+3*M*u_c-1));
```

$$E\_c := 1.046972868$$

$$L\_c := -.8214996932$$

```
> L := 6:  E := 1.1:
> u := solve(f);
```

$$u := -.08570880353,\ .06863713358,\ .4699066176,\ 3.297165052$$

```
> ph1 := g
  *(EllipticF(arcsin(sqrt((u[4]-u[2]) *(y-u[1])
  /(u[2]-u[1]) /(u[4]-y))), k) +EllipticK(k))/Q_:
> ph2 := g *EllipticF(arcsin(sqrt((u[4]-u[2]) *(y-u[3])
  /(u[4]-u[3]) /(y-u[2]))), k)/Q_:
> g := 2/sqrt((u[4]-u[2])*(u[3]-u[1])):
> k :=
  sqrt((u[4]-u[3])*(u[2]-u[1])/(u[4]-u[2])/(u[3]-u[1]));
> should be < or = 1.
```

$$k := .4932202926$$

```
> r := 1/y:
> with(plots):
Warning, the name changecoords has been redefined
> Fi1 := polarplot([r, ph1, y = u[1]..u[2]], -12..12,
  -30..30, thickness = 3, color = blue):
> Fi2 := polarplot([r, -ph1, y = u[1]..u[2]], thickness = 3,
  color = blue):
> Se := polarplot([r, ph2, y = u[3]..u[4]], thickness = 3,
  color = blue):
> rC := polarplot(r_c, color = blue):
```

```
> plotsetup(ps, plotoutput = `charplot.eps`, plotoptions =
  `color, portrait, noborder`):
> display({Fi1, Fi2, Se, rC}, axes = frame, scaling =
  constrained);
```

A.2.7 File that creates figures 13.4, 13.6, 13.8, 13.10, 13.12, 13.14, 13.16, 13.18 and 13.20

Listing of `orbits.mws`

Kerr space-time

First integrals and orbits

Continents configuration

Time-like geodesics

```
> restart:
> L_plus := (2*M*a*E*r +sqrt(Dr))/r/(2*M-r):
> L_minus := (2*M*a*E*r -sqrt(Dr))/r/(2*M-r):
> Dr := r*Delta*fir:
> fir := e*r^3 +2*M*delta1*r^2 -Q*r +2*M*Q:
> Delta := r^2 -2*M*r +a^2:
> solve(e = E^2 -delta1, E);
```

$$\sqrt{e+\delta 1},\ -\sqrt{e+\delta 1}$$

```
> E := %[1]:
> M := 1:  a := sqrt(.84):  e := .4:  Q := 1:  delta1 := 1:
> P1 := plot(L_plus, r = 0..2*M, L = -10..10, labelfont =
  [TIMES, ITALIC, 16]):
> P3 := plot(L_plus, r = 2*M..8*M):
```

```
> P4 := plot(L_minus, r = 0..8*M):

> popis := textplot({[4, 8, N], [4, -9, S], [.2, 1, W]},
  font = [TIMES, BOLDITALIC, 10]):

> with(plots):
Warning, the name changecoords has been redefined

> plotsetup(ps, plotoutput = `t-orbits.eps`, plotoptions =
  `portrait, noborder`):

> display(P1, P3, P4, popis, thickness = 2, title = "r-L
  plot:  Continents configuration \n The time-like
  geodesics", titlefont = [TIMES, ROMAN, 15]);
```

Null geodesics

```
> delta1 := 0:

> Q_plus := 27*M^2*e;
```

$$Q < Q\_plus$$

$$Q\_plus := 10.8$$

```
> P1 := plot(L_plus, r = 0..2*M, L = -10..10, labelfont =
  [TIMES, ITALIC, 16], color = blue):

> P3 := plot(L_plus, r = 2*M..8*M, color = blue):

> P4 := plot(L_minus, r = 0..8*M, color = blue):

> plotsetup(ps, plotoutput = `n-orbits.eps`, plotoptions =
  `portrait, noborder, color`):

> display(P1, P3, P4, popis, thickness = 2, title = "r-L
  plot:  Continents configuration \n The null geodesics",
  titlefont = [TIMES, ROMAN, 15]);
```

Space-like geodesics

```
> e := 1.04:  delta1 := -1:
> Q_plus := M^2*(27*e^2 -18*e -1 +(e -1)^(1/2)*(9*e
  -1)^(3/2))/2/e; Q_minus := M^2*(27*e^2 -18*e -1 -(e
  -1)^(1/2)*(9*e -1)^(3/2))/2/e;
```

$$Q < Q\_minus$$

$$Q\_plus := 6.883444575$$

$$Q\_minus := 2.235016962$$

```
> Q := 1:
> P1 := plot(L_plus, r = 0..2*M, L = -10..10, labelfont =
  [TIMES, ITALIC, 16], color = blue):
> P3 := plot(L_plus, r = 2*M..8*M, color = blue):
> P4 := plot(L_minus, r = 0..8*M, color = blue):
> plotsetup(ps, plotoutput = `s-orbits1.eps`, plotoptions =
  `portrait, noborder, color`):
> popis1 := textplot([1.2, .5, U], font = [TIMES,
  BOLDITALIC, 10]):
> display(P1, P3, P4, popis, popis1, thickness = 2, title =
  "r-L plot:  Continents configuration \n The space-like
  geodesics", titlefont = [TIMES, ROMAN, 15]);
> Q := 5:
```

$Q\_minus < Q < Q\_plus$

```
> P1 := plot(L_plus, r = 0..2*M, L = -10..10, labelfont =
  [TIMES, ITALIC, 16], color = blue):
> P3 := plot(L_plus, r = 2*M..8*M, color = blue):
> P4 := plot(L_minus, r = 0..8*M, color = blue):
> plotsetup(ps, plotoutput = `s-orbits.eps`, plotoptions =
  `portrait, noborder, color`):
> display(P1, P3, P4, popis, thickness = 2, title = "r-L
  plot:  Continents configuration \n The space-like
  geodesics", titlefont = [TIMES, ROMAN, 15]);
```

Barrier configuration

Time-like geodesics

```
> e := .4:  Q := 28:  delta1 := 1:
```

```
> P1 := plot(L_plus, r = 0..2*M, L = -10..10, labelfont =
  [TIMES, ITALIC, 16]):
> P3 := plot(L_plus, r = 2*M..10*M):
> P4 := plot(L_minus, r = 0..10*M):
> plotsetup(ps, plotoutput = `t-orbits2.eps`, plotoptions =
  `portrait, noborder`):
> display(P1, P3, P4, popis, thickness = 2, title = "r-L
  plot:  Barrier configuration \n The time-like geodesics",
  titlefont = [TIMES, ROMAN, 15]);
```

Null geodesics

```
> delta1 := 0:
> P1 := plot(L_plus, r = 0..2*M, L = -15..10, labelfont =
  [TIMES, ITALIC, 16], color = blue):
> P3 := plot(L_plus, r = 2*M..10*M, color = blue, numpoints
  = 5000):
> P4 := plot(L_minus, r = 0..10*M, color = blue, numpoints =
  2000):
> plotsetup(ps, plotoutput = `n-orbits2.eps`, plotoptions =
  `portrait, noborder, color`):
> display(P1, P3, P4, popis, thickness = 2, title = "r-L
  plot:  Barrier configuration \n The null geodesics",
  titlefont = [TIMES, ROMAN, 15]);
```

Space-like geodesics

```
> e := 1.04:  delta1 := -1:
> P1 := plot(L_plus, r = 0..2*M, L = -10..10, labelfont =
  [TIMES, ITALIC, 16], color = blue):
> P3 := plot(L_plus, r = 2*M..8*M, color = blue):
> P4 := plot(L_minus, r = 0..8*M, color = blue):
```

```
> plotsetup(ps, plotoutput = `s-orbits2.eps`, plotoptions =
  `portrait, noborder, color`):
> display(P1, P3, P4, popis, thickness = 2, title = "r-L
  plot:  Barrier configuration \n The space-like geodesics",
  titlefont = [TIMES, ROMAN, 15]);
```

Bay configuration

Time-like geodesics

```
> delta1 := 1:  e := -.2:  Q := 1:
> P1 := plot(L_plus, r = 0..2*M, L = -10..10, labelfont =
  [TIMES, ITALIC, 16]):
> P3 := plot(L_plus, r = 2*M..10*M):
> P4 := plot(L_minus, r = 0..10*M):
> popis := textplot({[2, -2, "R > 0"], [4, -9, "R < 0"]},
  font = [TIMES, BOLDITALIC, 10]):
> plotsetup(ps, plotoutput = `t-orbits3.eps`, plotoptions =
  `portrait, noborder`):
> display(P1, P3, P4, popis, thickness = 2, title = "r-L
  plot:  Bay configuration \n The time-like geodesics",
  titlefont = [TIMES, ROMAN, 15]);
```

Lake configuration

Time-like geodesics

```
> e := -.08:  Q := 14.2:
> P1 := plot(L_plus, r = 0..2*M, L = -10..10, labelfont =
  [TIMES, ITALIC, 16]):
> P3 := plot(L_plus, r = 2*M..20*M):
> P4 := plot(L_minus, r = 0..20*M, numpoints = 2000):
> popis1 := textplot([12, .5, "lake"], font = [TIMES, BOLD,
  10]):
```

```
> plotsetup(ps, plotoutput = `t-orbits4.eps`, plotoptions =
  `portrait, noborder`):
> display(P1, P3, P4, popis, popis1, thickness = 2, title =
  "r-L plot:  Lake configuration \n The time-like
  geodesics", titlefont = [TIMES, ROMAN, 15]);
```

A.2.8 File that creates figures 13.5, 13.7, 13.9, 13.11, 13.13, 13.15, 13.17, 13.19 and 13.21

Listing of `orbits2.mws`

Kerr space-time

First integrals and orbits

Continents configuration

Time-like geodesics

```
> restart:
> L_plus := (2*M*a*E*r +sqrt(Dr))/r/(2*M-r):
> L_minus := (2*M*a*E*r -sqrt(Dr))/r/(2*M-r):
> Dr := r*Delta*fir:
> fir := e*r^3 +2*M*delta1*r^2 -Q*r +2*M*Q:
> Delta := r^2 -2*M*r +a^2:
> solve(e = E^2 -delta1, E);
```

$$\sqrt{e+\delta 1},\ -\sqrt{e+\delta 1}$$

```
> E := %[1]:
> M := 1:  a := sqrt(19):  e := .4:  Q := 1:  delta1 := 1:
> P1 := plot(L_plus, r = 0..2*M, L = -30..30, labelfont =
  [TIMES, ITALIC, 16],  color = blue):
```

```
> P3 := plot(L_plus, r = 2*M..10*M,  color = blue):
> P4 := plot(L_minus, r = 0..10*M,  color = blue):
> popis := textplot({[4, 20, N], [4, -20, S], [.2, 5, W]},
  font = [TIMES, BOLDITALIC, 10]):
> with(plots):
Warning, the name changecoords has been redefined

> popt := `portrait, noborder, color`:
> plotsetup(ps, plotoutput = `t-orbitsf.eps`, plotoptions =
  popt):
> display(P1, P3, P4, popis, thickness = 2, title = "r-L
  plot:  Continents configuration \n The time-like
  geodesics", titlefont = [TIMES, ROMAN, 15]);
```

Null geodesics

```
> delta1 := 0:
> Q_plus := 27*M^2*e;
```

$Q < Q\_plus$

$$Q\_plus := 10.8$$

```
> P1 := plot(L_plus, r = 0..2*M, L = -30..30, labelfont =
  [TIMES, ITALIC, 16], color = blue):
> P3 := plot(L_plus, r = 2*M..8*M, color = blue):
> P4 := plot(L_minus, r = 0..8*M, color = blue):
> plotsetup(ps, plotoutput = `n-orbitsf.eps`, plotoptions =
  popt):
> display(P1, P3, P4, popis, thickness = 2, title = "r-L
  plot:  Continents configuration \n The null geodesics",
  titlefont = [TIMES, ROMAN, 15]);
```

Space-like geodesics

```
> e := 1.04:  delta1 := -1:
```

```
> Q_plus := M^2*(27*e^2 -18*e -1 +(e -1)^(1/2)*(9*e
  -1)^(3/2))/2/e; Q_minus := M^2*(27*e^2 -18*e -1 -(e
  -1)^(1/2)*(9*e -1)^(3/2))/2/e;
```

$Q < Q\_minus$

$$Q\_plus := 6.883444575$$

$$Q\_minus := 2.235016962$$

```
> Q := 1:

> P1 := plot(L_plus, r = 0..2*M, L = -30..30, labelfont =
  [TIMES, ITALIC, 16], color = blue):

> P3 := plot(L_plus, r = 2*M..8*M, color = blue):

> P4 := plot(L_minus, r = 0..8*M, color = blue):

> plotsetup(ps, plotoutput = `s-orbits1f.eps`, plotoptions =
  popt):

> display(P1, P3, P4, popis, thickness = 2, title =
  "r-L plot:  Continents configuration \n The space-like
  geodesics", titlefont = [TIMES, ROMAN, 15]);

> Q := 5:
```

$Q\_minus < Q < Q\_plus$

```
> P1 := plot(L_plus, r = 0..2*M, L = -30..30, labelfont =
  [TIMES, ITALIC, 16], color = blue):

> P3 := plot(L_plus, r = 2*M..8*M, color = blue):

> P4 := plot(L_minus, r = 0..8*M, color = blue):

> plotsetup(ps, plotoutput = `s-orbitsf.eps`, plotoptions =
  popt):

> display(P1, P3, P4, popis, thickness = 2, title = "r-L
  plot:  Continents configuration \n The space-like
  geodesics", titlefont = [TIMES, ROMAN, 15]);
```

Barrier configuration

Time-like geodesics

```
> e := .4:  Q := 28:  delta1 := 1:
> P1 := plot(L_plus, r = 0..2*M, L = -30..40, labelfont =
  [TIMES, ITALIC, 16], color = blue):
> P3 := plot(L_plus, r = 2*M..10*M, color = blue):
> P4 := plot(L_minus, r = 0..10*M, color = blue):
> plotsetup(ps, plotoutput = `t-orbits2f.eps`, plotoptions =
  popt):
> display(P1, P3, P4, popis, thickness = 2, title = "r-L
  plot:  Barrier configuration \n The time-like geodesics",
  titlefont = [TIMES, ROMAN, 15]);
```

Null geodesics

```
> delta1 := 0:
> P1 := plot(L_plus, r = 0..2*M, L = -50..50, labelfont =
  [TIMES, ITALIC, 16], color = blue):
> P3 := plot(L_plus, r = 2*M..10*M, color = blue, numpoints
  = 5000):
> P4 := plot(L_minus, r = 0..10*M, color = blue, numpoints =
  2000):
> plotsetup(ps, plotoutput = `n-orbits2f.eps`, plotoptions =
  popt):
> display(P1, P3, P4, popis, thickness = 2, title = "r-L
  plot:  Barrier configuration \n The null geodesics",
  titlefont = [TIMES, ROMAN, 15]);
```

Space-like geodesics

```
> e := 1.04:  delta1 := -1:
> P1 := plot(L_plus, r = 0..2*M, L = -50..50, labelfont =
  [TIMES, ITALIC, 16], color = blue):
> P3 := plot(L_plus, r = 2*M..8*M, color = blue):
```

```
> P4 := plot(L_minus, r = 0..8*M, color = blue):

> plotsetup(ps, plotoutput = `s-orbits2f.eps`, plotoptions =
  popt):

> display(P1, P3, P4, popis, thickness = 2, title = "r-L
  plot:  Barrier configuration \n The space-like geodesics",
  titlefont = [TIMES, ROMAN, 15]);
```

Bay configuration

Time-like geodesics

```
> delta1 := 1:  e := -.2:  Q := 1:

> P1 := plot(L_plus, r = 0..2*M, L = -10..40, labelfont =
  [TIMES, ITALIC, 16], color = blue):

> P3 := plot(L_plus, r = 2*M..15*M,  color = blue):

> P4 := plot(L_minus, r = 0..15*M, color = blue):

> popis := textplot({[.8, 39, "R > 0"], [2, -8, "R > 0"],
  [4, 9, "R < 0"]}, font = [TIMES, BOLDITALIC, 10]):

> plotsetup(ps, plotoutput = `t-orbits3f.eps`, plotoptions =
  popt):

> display(P1, P3, P4, popis, thickness = 2, title = "r-L
  plot:  Bay configuration \n The time-like geodesics",
  titlefont = [TIMES, ROMAN, 15]);
```

Lake configuration

Time-like geodesics

```
> e := -.08:  Q := 14.2:

> P1 := plot(L_plus, r = 0..2*M, L = -10..40, labelfont =
  [TIMES, ITALIC, 16], color = blue):

> P3 := plot(L_plus, r = 2*M..20*M, color = blue):
```

```
> P4 := plot(L_minus, r = 0..20*M, numpoints = 2000, color =
  blue):
> popis1 := textplot([11, -1, "lake"], font = [TIMES, BOLD,
  10]):
> plotsetup(ps, plotoutput = `t-orbits4f.eps`, plotoptions =
  popt):
> display(P1, P3, P4, popis, popis1, thickness = 2, title =
  "r-L plot:  Lake configuration \n The time-like
  geodesics", titlefont = [TIMES, ROMAN, 15]);
```

A.2.9 File that creates figures 14.1, 14.2, and 14.3

Listing of `r-Lequat.mws`

Kerr black hole

Equatorial plane

Null geodesics

```
> restart:
> D_plus := (2*M*a+r*sqrt(r^2-2*M*r+a^2)) /(2*M-r):
> D_minus := (2*M*a-r*sqrt(r^2-2*M*r+a^2)) /(2*M-r):
> popt := `portrait, noborder, color`:
```

Extreme Kerr solution

```
> a := M:
> M := 1:
> with(plots):
Warning, the name changecoords has been redefined
```

```
> plus := plot(D_plus, r = 0..7*M, D = -10..5, discont =
  true, color = blue):
> minu := plot(D_minus, r = 0..7*M, color = blue):
> popis := textplot({[2, 4, N], [4, -9, S], [.4, 1.3, W]},
  font = [TIMES, BOLDITALIC, 10]):
> crit := plot(a, r = 0..7*M, thickness = 1, linestyle = 3,
  color = black):
> popis2 := textplot([0, a, "a"], align = 'LEFT'):
> plotsetup(ps, plotoutput = `r-Leqext.eps`, plotoptions =
  popt):
> display(plus, minu, popis, thickness = 2, crit, popis2,
  title = "r-D plot in the extreme Kerr solution \n The null
  geodesics", titlefont = [TIMES, ROMAN, 15]);
```

Fast Kerr solution

```
> a := 2*.52;
```

$$a := 1.04$$

```
> plus := plot(D_plus, r = 0..7*M, D = -10..5, discont =
  true, color = blue):
> minu := plot(D_minus, r = 0..7*M, color = blue):
> popis := textplot({[2, 4, N], [4, -9, S], [.4, 1.3, W]},
  font = [TIMES, BOLDITALIC, 10]):
> plotsetup(ps, plotoutput = `r-Leqfas.eps`, plotoptions =
  popt):
> display(plus, minu, popis, thickness = 2, crit, popis2,
  title = "r-D plot in the fast Kerr solution \n The null
  geodesics", titlefont = [TIMES, ROMAN, 15]);
```

Slow Kerr solution

```
> a := 2*.48;
```

$$a := .96$$

```
> plus := plot(D_plus, r = 0..7*M, D = -10..5, discont =
  true):
> minu := plot(D_minus, r = 0..7*M):
> popis := textplot({[2, 4, N], [4, -9, S], [.4, 1.3, W]},
  font = [TIMES, BOLDITALIC, 10]):
> plotsetup(ps, plotoutput = `r-Leqslo.eps`, plotoptions =
  `portrait, noborder`):
> display(plus, minu, popis, thickness = 2, crit, popis2,
  title = "r-D plot in the slow Kerr solution \n The null
  geodesics", titlefont = [TIMES, ROMAN, 15]);
```

A.2.10 File that creates figure 14.4

Listing of `eqnuplot.mws`

Kerr black hole

Equatorial plane

Null geodesics

```
> restart:
> r := 1/y:
> f := 2*M*(a-De)^2*u^3 +(a^2-De^2)*u^2+1:
```

M should be $> a$

```
> a := .96:  M := 1:  De := 4:
> u := solve(f, u);
```

$$u := -.2277020572,\ .3356987941,\ .7077927367$$

```
> g := 2/sqrt(u[3] -u[1]):
```

k should be $<$ or $= 1$

```
> k := sqrt((u[2]-u[1]) /(u[3]-u[1])); is(k <= 1);
```

$$k := .7760470671$$

$$true$$

```
> p := 2*M*(a -De)*(M^2 -a^2) +(a^2*De -2*M^2*(a
  -De))*sqrt(M^2 -a^2):
> h := solve(a^2*x^2 -2*M*x +1, x);
```

$$h := 1.388888889, .7812500000$$

```
> u_plus := h[1]:  u_minus := h[2]:
> ph1 := g*p/2/(M^2 -a^2)*
  ((EllipticPi(sqrt((0.325-u[1])/(u[2]-u[1])),
  (u[2]-u[1])/(u_plus-u[1]), k)
  +EllipticPi((u[2]-u[1])/(u_plus-u[1]),
  k))/(u_plus-u[1])
  -EllipticPi(sqrt((0.325-u[1])/(u[2]-u[1])),
  (u[2]-u[1])/(u_minus-u[1]), k)
  +EllipticPi((u[2]-u[1])/(u_minus-u[1]),
  k)/(u_minus-u[1]));
```

$$ph1 := 98.93177565$$

```
> y := 1.19:
> ph2 := g*p/2/(M^2-a^2)
  *((EllipticPi((sqrt(u[3]-u[1])/(y-u[1])),
  (u_minus-u[1])/(u[3]-u[1]), k)
  +EllipticF((sqrt(u[3]-u[1])/(y-u[1])), k)) /(u_minus-u[1])
  -(EllipticPi((sqrt(u[3]-u[1])/(y-u[1])),
  (u_plus-u[1])/(u[3]-u[1]), k)
  +EllipticF((sqrt(u[3]-u[1])/(y-u[1])), k))
  /(u_plus-u[1]));
```

$$ph2 := 13.49258854$$

A.2.11 File that creates figures 14.5, 14.6, 14.7, 14.8, 14.9, 14.10, 14.11, 14.12, 14.13, 14.14, 14.15 and 14.16

Listing of `RLEQSPAC.mws`

Kerr black hole

Equatorial plane

Spacelike geodesics

```
> restart:
> L_plus := (2*M*a*E +sqrt(r *Delta *((E^2+1) *r -2 *M)))
  /(2 *M -r):
> L_minus := (2*M*a*E -sqrt(r *Delta *((E^2+1) *r -2 *M)))
  /(2 *M -r):
> Delta := r^2 -2*M*r +a^2:
> popt := ‘portrait, noborder, color‘:
> M := 1:
```

Slow Kerr solution

```
> a := .96:
> r_pm := solve(Delta);
```

$$r\_pm := 1.280000000, .7200000000$$

```
> r_ := PLOT(CURVES([[r_pm[2],-16],[r_pm[2],8]],
  [[r_pm[1],-16],[r_pm[1],8]]), LINESTYLE(3)):
> popis2 := textplot([[r_pm[2], 0, "r_-"], [r_pm[1], 0,
  "r_+"]], ’align = BELOW’):
> popis3 := textplot([0, 2*M, "2M"], align = ’LEFT’):
> E1 := sqrt(r_pm[1]/r_pm[2]);
```

$$E1 := 1.333333333$$

```
> E := 2: sqrt(r_plus/r_minus) < E
> minu := plot(L_minus, r = 0..5*M, color = blue, thickness
  = 2):
> plus1 := plot(L_plus, r = 0..2*M, L = 0..8*M, color =
  blue, thickness = 2):
> plus2 := plot(L_plus, r = 2*M..5*M, L = -16..0, color =
  blue, thickness = 2):
> popis := textplot({[1.7, 7, N], [4, -16, S], [.6, 2.7,
  W]}, font = [TIMES, BOLDITALIC, 10]):
> with(plots):
Warning, the name changecoords has been redefined
> plotsetup(ps, plotoutput = `rLeqsls1.eps`, plotoptions =
  popt):
> display(plus1, plus2, minu, r_, popis, popis2, popis3,
  title = "r-L plot in the slow Kerr solution:  The
  space-like geodesics\n E > sqrt(r_+/r_-)", titlefont =
  [TIMES, ROMAN, 15]);

> E := E1:
> minu := plot(L_minus, r = 0..5*M, color = blue, thickness
  = 2):
> plus1 := plot(L_plus, r = 0..2*M, L = 0..8*M, color =
  blue, thickness = 2):
> plus2 := plot(L_plus, r = 2*M..5*M, L = -16..0, color =
  blue, thickness = 2):
> bod := PLOT(POINTS([r_pm[2], 2], SYMBOL(CIRCLE)),
  COLOR(RGB, 0, 0, 1)):
> dvaM := plot(2*M, r = 0..r_pm[2], linestyle = 2, color =
  black):
> plotsetup(ps, plotoutput = `rLeqsls2.eps`, plotoptions =
  popt):
```

```
> display(plus1, plus2, minu, bod, r_, dvaM, title = "r-L
  plot in the slow Kerr solution:  The space-like
  geodesics\n E = sqrt(r_+/r_-)", titlefont = [TIMES, ROMAN,
  15], popis, popis2, popis3);

> E2 := sqrt(r_pm[2]/r_pm[1]);
```

$$E2 := .7500000000$$

```
> E := 1: E2 < E < E1
> minu := plot(L_minus, r = 0..5*M, color = black, thickness
  = 2):
> plus1 := plot(L_plus, r = 0..2*M, L = 0..8*M, color =
  black, thickness = 2):
> plus2 := plot(L_plus, r = 2*M..5*M, L = -16..0, color =
  black, thickness = 2):
> popis := textplot({[2.5, 6, N], [3.5, -13, S], [.85, 2,
  W]}, font = [TIMES, BOLDITALIC, 10]):
> plotsetup(ps, plotoutput = `rLeqsls3.eps`, plotoptions =
  popt):
> display(plus1, plus2, minu, r_, title = "r-L plot in the
  slow Kerr solution:  The space-like geodesics\n
  sqrt(r_-/r_+) < E < sqrt(r_+/r_-)", titlefont = [TIMES,
  ROMAN, 15], popis, popis2, popis3);

> E := E2:
> minu := plot(L_minus, r = 0..5*M, color = black, thickness
  = 2):
> plus1 := plot(L_plus, r = 0..2*M, L = 0..8*M, color =
  black, thickness = 2):
> plus2 := plot(L_plus, r = 2*M..5*M, L = -16..0, color =
  black, thickness = 2):
> dvaM := plot(2*M, r = 0..r_pm[1], linestyle = 2, color =
  black):
```

```
> popis := textplot({[2.4, 6, N], [3.5, -12, S], [1, 1.5,
  W]}, font = [TIMES, BOLDITALIC, 10]):
> plotsetup(ps, plotoutput = `rLeqsls4.eps`, plotoptions =
  popt):
> display(plus1, plus2, minu, r_, dvaM, title = "r-L plot in
  the slow Kerr solution:  The space-like geodesics\n E =
  sqrt(r_-/r_+)", titlefont = [TIMES, ROMAN, 15], popis,
  popis2, popis3);
```

```
> E := .6: 0 < E < E2
```

```
> minu := plot(L_minus, r = 0..5*M, color = black, thickness
  = 2):
> plus1 := plot(L_plus, r = 0..2*M, L = 0..8*M, color =
  black, thickness = 2):
> plus2 := plot(L_plus, r = 2*M..5*M, L = -16..0, color =
  black, thickness = 2):
> plotsetup(ps, plotoutput = `rLeqsls5.eps`, plotoptions =
  popt):
> display(plus1, plus2, minu, r_, title = "r-L plot in the
  slow Kerr solution:  The space-like geodesics\n 0 < E <
  sqrt(r_-/r_+)", titlefont = [TIMES, ROMAN, 15], popis,
  popis2, popis3);
```

```
> E := 0:
> minu := plot(L_minus, r = 0..5*M, color = black, thickness
  = 2):
> plus1 := plot(L_plus, r = 0..2*M, L = 0..8*M, color =
  black, thickness = 2):
> plus2 := plot(L_plus, r = 2*M..5*M, L = -16..0, color =
  black, thickness = 2):
> popis := textplot({[3, 6, N], [3.4, -12, S], [1, 0, W]},
  font = [TIMES, BOLDITALIC, 10]):
```

```
> plotsetup(ps, plotoutput = `rLeqsls6.eps`, plotoptions =
  popt):

> display(plus1, plus2, minu, r_, title = "r-L plot in the
  slow Kerr solution:  The space-like geodesics\n E = 0",
  titlefont = [TIMES, ROMAN, 15], popis, popis2, popis3);
```

Extreme Kerr solution

```
> a := M:

> r_pm := solve(Delta);
```

$$r\_pm := 1, 1$$

```
> popis2 := textplot([[r_pm[2], 0, "r_+/-"]], 'align =
  BELOW'):

> minu := plot(L_minus, r = 0..5*M, color = blue, thickness
  = 2):

> plus1 := plot(L_plus, r = 0..2*M, L = 0..8*M, color =
  blue, thickness = 2):

> plus2 := plot(L_plus, r = 2*M..5*M, L = -16..0, color =
  blue, thickness = 2):

> popis := textplot({[3, 6, N], [3.4, -12, S], [.9, 0.5,
  W]}, font = [TIMES, BOLDITALIC, 10]):

> bod := PLOT(POINTS([r_pm[2], 0], SYMBOL(CIRCLE)),
  COLOR(RGB, 0, 0, 1)):

> r_ := PLOT(CURVES([[r_pm[2],-16],[r_pm[2],8]],
  [[r_pm[1],-16],[r_pm[1],8]]), LINESTYLE(3)):

> plotsetup(ps, plotoutput = `rLeqexs1.eps`, plotoptions =
  popt):

> display(plus1, plus2, minu, r_, bod, title = "r-L plot in
  the extreme Kerr solution\n The space-like geodesics with
  E = 0", titlefont = [TIMES, ROMAN, 15], popis, popis2,
  popis3);
```

```
> E := .6: 0 < E < 1
> minu := plot(L_minus, r = 0..5*M, color = blue, thickness
  = 2):
> plus1 := plot(L_plus, r = 0..2*M, L = 0..8*M, color =
  blue, thickness = 2):
> plus2 := plot(L_plus, r = 2*M..5*M, L = -16..0, color =
  blue, thickness = 2):
> bod := PLOT(POINTS([r_pm[2], 2*M*E], SYMBOL(CIRCLE)),
  COLOR(RGB, 0, 0, 1)):
> dvaME := plot(2*M*E, r = 0..r_pm[2], linestyle = 2, color
  = black):
> popis4 := textplot([0, 2*M*E, "2ME"], align = 'LEFT'):
> plotsetup(ps, plotoutput = `rLeqexs2.eps`, plotoptions =
  popt):
> display(plus1, plus2, minu, r_, bod, dvaME, title = "r-L
  plot in the extreme Kerr solution\n The space-like
  geodesics with 0 < E < 1", titlefont = [TIMES, ROMAN, 15],
  popis, popis2, popis3, popis4

> E := 1:
> minu := plot(L_minus, r = 0..5*M, color = blue, thickness
  = 2):
> plus1 := plot(L_plus, r = 0..2*M, L = 0..8*M, color =
  blue, thickness = 2):
> plus2 := plot(L_plus, r = 2*M..5*M, L = -16..0, color =
  blue, thickness = 2):
> popis := textplot({[3, 6, N], [3.4, -12, S]}, font =
  [TIMES, BOLDITALIC, 10]):
> dvaM := plot(2*M, r = 0..r_pm[2], linestyle = 2, color =
  black):
> plotsetup(ps, plotoutput = `rLeqexs3.eps`, plotoptions =
  popt):
```

```
> display(plus1, plus2, minu, r_, dvaM, title = "r-L plot in
  the extreme Kerr solution\n The space-like geodesics with
  E = 1", titlefont = [TIMES, ROMAN, 15], popis, popis2,
  popis3);

> E := 2:  1 < E
> minu := plot(L_minus, r = 0..5*M, color = blue, thickness
  = 2):
> plus1 := plot(L_plus, r = 0..2*M, L = 0..8*M, color =
  blue, thickness = 2):
> plus2 := plot(L_plus, r = 2*M..5*M, L = -16..0, color =
  blue, thickness = 2):
> dvaME := plot(2*M*E, r = 0..r_pm[2], linestyle = 2, color
  = black):
> popis4 := textplot([0, 2*M*E, "2ME"], align = 'LEFT'):
> popis := textplot({[1.6, 7, N], [3.6, -16, S], [.6, 3,
  W]}, font = [TIMES, BOLDITALIC, 10]):
> plotsetup(ps, plotoutput = `rLeqexs4.eps`, plotoptions =
  popt):
> display(plus1, plus2, minu, r_, dvaME, title = "r-L plot
  in the extreme Kerr solution\n The space-like geodesics
  with E > 1", titlefont = [TIMES, ROMAN, 15], popis,
  popis2, popis3, popis4);
```

Fast Kerr solution

```
> a := 1.04:
> minu := plot(L_minus, r = 0..5*M, color = blue, thickness
  = 2):
> plus1 := plot(L_plus, r = 0..2*M, L = 0..8*M, color =
  blue, thickness = 2):
> plus2 := plot(L_plus, r = 2*M..5*M, L = -16..0, color =
  blue, thickness = 2):
> popis := textplot({[1.6, 7, N], [4, -16, S]}, font =
  [TIMES, BOLDITALIC, 10]):
```

```
> plotsetup(ps, plotoutput = ‘rLeqfas1.eps‘, plotoptions =
  popt):
> display(plus1, plus2, minu, title = "r-L plot in the fast
  Kerr solution\n The space-like geodesics with E > 0",
  titlefont = [TIMES, ROMAN, 15], popis, popis3);

> E := 0:
> minu := plot(L_minus, r = 0..5*M, color = blue, thickness
  = 2):
> plus1 := plot(L_plus, r = 0..2*M, L = 0..8*M, color =
  blue, thickness = 2):
> plus2 := plot(L_plus, r = 2*M..5*M, L = -16..0, color =
  blue, thickness = 2):
> popis := textplot({[3, 5, N], [3, -10, S]}, font = [TIMES,
  BOLDITALIC, 10]):
> plotsetup(ps, plotoutput = ‘rLeqfas2.eps‘, plotoptions =
  popt):
> display(plus1, plus2, minu, title = "r-L plot in the fast
  Kerr solution\n The space-like geodesics with E = 0",
  titlefont = [TIMES, ROMAN, 15], popis, popis3);
```

A.2.12 File that creates figures 15.1 and 15.2

Listing of `nullcirc.mws`

Kerr black hole

Null geodesics

η positive

Unstable orbits with constant radius

```
> restart:
```

```
> res := EllipticF(sin(ps),k)/a/sqrt(mu_plus^2 + mu_minus^2)
  = ln(abs(2*sqrt(c*(1 + 4*r_s*x + c*x^2)) + 2*c*x + 4*r_s))
  / sqrt(c):
> ph := E *EllipticF(sin(ps), k) /sqrt(mu_plus^2+mu_minus^2)
  -Lz/a /sqrt(mu_plus^2+mu_minus^2)/(1-mu^2)
  *EllipticPi(sin(ps), alpha^2, k)
  +a*(((r_p^2+a^2)*E-a*Lz)/(r_p-r_m)/(r_p-r_s)*f_p
  -((r_m^2+a^2)*E-a*Lz)/(r_p-r_m)/(r_m-r_s)*f_m
  -((r_s^2+a^2)*E-a*Lz) /(r_p-r_s) /(r_m-r_s) /sqrt(c)
  *ln(abs(2*sqrt(c)*sqrt(y_s^2+4*r_s*y_s+c)/y_s +2*c/y_s
  +4*r_s*y_s))):
> c := 3*r_s^2 - a^2*eta_s/r_s^2:
> x := 1/(r - r_s):
> Lz := E/a/(r_s-M)
  *(M*(r_s^2-a^2)-r_s*(r_s^2-2*M*r_s+a^2)):
> alpha := mu_plus/sqrt(mu_plus^2-1):
> r_p := M +sqrt(M^2-a^2):  r_m := M -sqrt(M^2-a^2):
> k := mu_plus/sqrt(mu_plus^2 + mu_minus^2):
> ps := arccos(mu/mu_plus):
> mu := cos(theta):
> mu_plus := sqrt((sqrt((xi^2+eta_s-a^2)^2+4*a^2*eta_s)
  -(xi^2+eta_s-a^2)) /a^2/2):
> mu_minus :=sqrt((sqrt((xi^2+eta_s-a^2)^2+4*a^2*eta_s)
  +(xi^2+eta_s-a^2)) /a^2/2):
> y_p := r_p -r:  y_m := r_m -r:  y_s := r -r_s:
> xi := Lz/E: eta_s := r_s^3/a^2/(r_s-M)^2*
  (4*M*(r_s^2-2*M*r_s+a^2)-r_s*(r_s-M)^2):
> a := .8:  r_s := 1.85:  E := 1:
> subs(M = 1, r_p^2 -a^2 *eta_s/r_s^2 +2*r_p*r_s);
```

above is positive so

```
> f_p := -1/sqrt(r_p^2 -a^2 *eta_s/r_s^2 +2*r_p*r_s)
*ln(abs(2 *sqrt(r_p^2 -a^2 *eta_s/r_s^2 +2*r_p*r_s)
*sqrt(y_p^2+(-2*r_s-2*r_p)*y_p +r_p^2 -a^2 *eta_s/r_s^2
+2*r_p*r_s) /y_p +2 *sqrt(r_p^2 -a^2 *eta_s/r_s^2 +2*r_p*r_s)
/y_p -2(r_p+r_s))):
```

```
> subs(M = 1, r_m^2 -a^2 *eta_s/r_s^2 +2*r_m*r_s);
```

$$1.349697232$$

above is positive so

```
> f_m := -1/sqrt(r_m^2 -a^2 *eta_s/r_s^2 +2*r_m*r_s)
  *ln(abs(2 *sqrt(r_m^2 -a^2 *eta_s/r_s^2 +2*r_m*r_s)
  *sqrt(y_m^2+(-2*r_s-2*r_m)*y_m +r_m^2 -a^2 *eta_s/r_s^2
  +2*r_m*r_s) /y_m +2 *sqrt(r_m^2 -a^2 *eta_s/r_s^2
  +2*r_m*r_s) /y_m -2(r_m+r_s))):
```

```
> r := 3.2:
```

```
> res1 := subs(M = 1, res):
```

```
> teta := solve(res1,theta);
```

$$teta := 1.833106054,\ 1.308486600$$

```
> evalf(subs({M = 1, theta = teta[1]}, ph));
```

$$-1.507997117$$

A.2.13 File that creates figures 15.3, 15.5 and 15.6

Listing of `null2.mws`

Kerr black hole

Null geodesics

$\eta = 0$

```
> restart:
> fii := a*E*g*(EllipticF(sin(ph), k)+EllipticK(k))
  +a*g*(B-A)/(r_p+r_m)*
  (((a^2+r_p^2)*E-a*L)*(alfa_2*(EllipticF(sin(ph),
  k)+EllipticK(k))
  +(alfa_p-alfa_2)/(1-alfa_p)*(EllipticPi(sin(ph),
  alfa_p^2/(alfa_p^2-1),
  k)+EllipticCPi(alfa_p^2/(alfa_p^2-1),
  k)-2*alfa_p*f_p))/(A*r1-(A+B)*r_p)
  -((a^2+r_m^2)*E-a*L)*(alfa_2*(EllipticF(sin(ph),
  k)+EllipticK(k))
  +(alfa_m-alfa_2)/(1-alfa_m)*(EllipticPi(sin(ph),
  alfa_m^2/(alfa_m^2-1),
  k)+EllipticCPi(alfa_m^2/(alfa_m^2-1),
  k)-2*alfa_m*f_m))/(A*r1-(A+B)*r_m))
  +(L-a*E)/sqrt(a^2-xi^2)
  *ln(abs((sqrt(1-xi^2/a^2)+sqrt(1-xi^2/a^2-mu^2))/mu))
  +L/2/xi
  *arcsin((1-mu-xi^2/a^2)/(mu-1)/sqrt(1-xi^2/a^2))
  +L/2/xi *arcsin((mu+1-xi^2/a^2)/(mu+1)/sqrt(1-xi^2/a^2)):

> k_ := sqrt(1-k^2):

> r_p := M +sqrt(M^2-a^2):  r_m := M -sqrt(M^2-a^2):

> alfa_2 := (B+A)/(B-A):

> alfa_p := (A*r1-A*r_p-B*r_p)/(-A*r1+A*r_p-B*r_p):

> alfa_m := (A*r1-A*r_m-B*r_m)/(-A*r1+A*r_m-B*r_m):

> g := 1/sqrt(A*B):

> ph := arccos(((A-B)*r-A*r1)/((A+B)*r-A*r1)):

> r1 := -sqrt(4*(a^2-xi^2)/3)*sinh(mateta/3):

> mateta := arcsinh(M*sqrt((a-xi)/(a+xi)^3)):
```

```
> psi := arccos((r*A-r*B+r_1*A)/(r*A+r*B+r_1*A)):

> k := 1/2*sqrt(-A*B*(-A^2-2*A*B-B^2+r_1^2))/A/B:

> B := sqrt(3*r_1^2+a^2-xi^2):

> A := sqrt(r_1^2+a^2-xi^2):

> r_1 := -sqrt(4*(a^2-xi^2)/3)*sinh(teta):

> teta := 1/3*arcsinh(3*(M^2*(a-xi)/((a+xi)^3))^(1/3)):

> mu := cos(theta):  mu_max := sqrt(1-xi^2/a^2):  xi := L/E:

> E:=1:  a:=.8:  L:=.4:

> evalf(subs(M = 1, alfa_p^2/(alfa_p^2-1) -k^2));
```

.0418448815

because above is positive

```
> f_p := sqrt((alfa_p^2-1)/(alfa_p^2*k_^2+k^2)) /2
  *ln(abs((sqrt(k^2+k_^2*alfa_p^2)*JacobiDN(sin(ph),
  k)+sqrt(alfa_p^2-1)*JacobiSN(sin(ph),
  k))/(sqrt(k^2+k_^2*alfa_p^2)*JacobiDN(sin(ph),
  k)-sqrt(alfa_p^2-1)*JacobiSN(sin(ph), k)))):

> evalf(subs(M = 1, alfa_m^2/(alfa_m^2-1) -k^2));
```

.0402442245

because above is positive

```
> f_m := sqrt((alfa_m^2-1)/(alfa_m^2*k_^2+k^2)) /2
  *ln(abs((sqrt(k^2+k_^2*alfa_m^2)*JacobiDN(sin(ph),
  k)+sqrt(alfa_m^2-1)*JacobiSN(sin(ph),
  k))/(sqrt(k^2+k_^2*alfa_m^2)*JacobiDN(sin(ph),
  k)-sqrt(alfa_m^2-1)*JacobiSN(sin(ph), k)))):

> vysl := subs(M = 1, arcsech(mu/mu_max)/sqrt(a^2-xi^2) =
  EllipticF(sin(psi), k)/sqrt(A*B)):

> with(plots):

> addcoords(rtheta,[e1,e2],[e1,e1*cos(e2)]):

Warning, the name changecoords has been redefined
```

```
> plotsetup(ps, plotoutput = `null1.eps`, plotoptions =
  `portrait, noborder`):
> obr := implicitplot(vysl, r = 0..3, theta=0..Pi/2,
  numpoints=500, color = black, thickness = 3):
> changecoords(obr, rtheta);
> r := 1.107:
> theta_fin := solve(vysl, theta);
> evalf(subs({M = 1, theta = theta_fin}, fii));
```

$$theta\_fin := 1.175652122$$

$$-14.51054171$$

A.2.14 File that creates figure 15.4

Listing of `null-Cart.mws`

Kerr space-time

Non-equatorial geodesics

Null geodesics

$\eta < 0$

```
> restart:
> res := 1/a/mu_plus *EllipticF(sqrt(mu_plus^2
  *(mu^2-mu_minus^2)/mu^2/(mu_plus^2-mu_minus^2)), k_theta)
  = g*(EllipticF(sin(ph), k_r) +EllipticK(k_r)):
> k_theta := sqrt(mu_plus^2 - mu_minus^2)/mu_plus:
> mu := cos(teta):
> mu_plus := sqrt((abs(eta)+a^2-xi^2
  +sqrt((abs(eta)+a^2-xi^2)^2-4*a^2*abs(eta))) /a^2/2):
```

```
> mu_minus := sqrt((abs(eta)+a^2-xi^2
  -sqrt((abs(eta)+a^2-xi^2)^2-4*a^2*abs(eta))) /a^2/2):

> g:= 2/(A+B):

> ph := arctan((r-b1+a1*g1)/(a1+b1*g1-g1*r)):

> g1 := sqrt((4*a1^2-(A-B)^2)/((A+B)^2-4*a1^2)):

> k_r := sqrt(4*A*B/(A+B)^2):

> A := sqrt((b1-b2)^2+(a1+a2)^2):

> B := sqrt((b1-b2)^2+(a1-a2)^2):

> a1 := sqrt(-(u1-u1bar)^2/4):  b1 := (u1+u1bar)/2:

> b2 := (u3+u3bar)/2:  a2 := sqrt(-(u3-u3bar)^2/4):

> R := r^4 +(a^2-xi^2-eta)*r^2 +2*M*(eta+(xi-a)^2)*r
  -a^2*eta:

> M:=1:  a:= .8:  xi:= -.05:  eta:= -.3:

> is(abs(eta) < a^2); is(abs(xi) < abs(a)-sqrt(abs(eta)));
  is(a^2 > xi^2); is(sqrt(abs(eta)) < abs(a-xi));
```

true

true

true

true

```
> res_r := solve(R);
```

$$res\_r := -.3616054637 - .1237265849\,I,$$
$$-.3616054637 + .1237265849\,I,\ .3616054637 - 1.087983803\,I,$$
$$.3616054637 + 1.087983803\,I$$

```
> u1 := res_r[1]:  u1bar := res_r[2]:  u3 := res_r[3]:
  u3bar := res_r[4]:

> evalf(k_theta); k_r;
```

$$.7240394697$$

$$.9969020174 + 0.\,I$$

```
> r := 0.825:  res_mu := solve(res, mu);
```

$res\_mu := -.7924506676, .7924506676$

```
> evalf(arccos(mu_plus)*360/2/Pi);  # minimum angle
```

4.935416764

```
> evalf(arccos(mu_minus)*360/2/Pi); # maximum angle
```

46.59103978

```
> evalf(mu_plus); evalf(mu_minus);
```

.9962923063

.6872011280

A.2.15 File that creates figure 17.1

Listing of `tlmgcirc.mws`

Kerr black hole

Timelike geodesics

Unstable orbits with constant radius

```
> restart:
> eta_s := r_s^2/a^2/(r_s-M)
  *(r_s*(4*a^2*M-r_s*(r_s-3*M)^2)/(r_s-M)
  +(r_s*(r_s-2*M)^2 -a^2*M)/E^2
  -2*r_s*M/(r_s-M)*Delta*(1-sqrt(1-(1-M/r_s)/E^2))):

> Delta := r_s^2 -2*M*r_s +a^2:
> a := sqrt(.84):  r_s := 2.154:
> r_s = 1.85 gives negative values for eta_s
  M := 1:  E := sqrt(1-.02):
> eta_s;
> should be positive
```

5.551938391

```
> Q := eta_s*E^2;
```

$Q := 5.440899624$

```
> gama := -a^2*eta_s/r_s^2 +2*M*r_s;
```

$$gama := 4.208591961$$

```
> alpha := 1-1/E^2:
> De := -4*((r_s*(1-1/E^2)+M/E^2)^2
  +alpha^2*eta_s/r_s^2*(1-1/E^2));
```

$$De := -3.813805160$$

```
> res := EllipticF(sin(psi),k)/alpha/mu_plus =
  ln(abs(2*sqrt(gama*F)+2*gama*x+beta))/sqrt(gama):
> F := beta*x +gama*x^2:
> beta := 4*r_s*(1-1/E^2) +2*M/E^2:
> x := 1/(r - r_s):
> k := mu_minus/mu_plus:  psi := arcsin(mu/mu_minus):
  mu_plus := (xi_s^2+eta_s+alpha^2
  +sqrt((xi_s^2+eta_s+alpha^2)^2-4*alpha^2*eta_s))
  /2/alpha:
> mu_minus := (xi_s^2+eta_s+alpha^2
  -sqrt((xi_s^2+eta_s+alpha^2)^2-4*alpha^2*eta_s)) /2/alpha:
> mu := cos(theta):
> xi_s := (M*(r_s^2-a^2)
  -r_s*Delta*sqrt(1-(1-M/r_s)/E^2)) /a /(r_s-M);
```

$$xi\_s := 2.805967772$$

```
> lim := solve(eta_s -(xi_s^2+eta_s+alpha^2)*mu^2
  +alpha^2*mu^4 = 0, mu); mu_max := lim[4]:
```

$$lim := -143.6502598,\ 143.6502598,\ -.2895717129,\ .2895717129$$

```
> solve(subs(r, res), r);
```

$$2.154000000,\ .1030562634$$

A.2.16 File that creates figure 17.2

Listing of `tmbdcirc.mws`

Kerr black hole

Timelike geodesics

η positive

Stable orbits with constant radius

```
> restart:
> rov1 := M*r^2 -Q*r +3*M*Q = 0:
> rov2 := e*r^2 -M*(3*e-1)*r -4*M^2 =0:
> M :=1:  a := sqrt(.84):  e := -.08:  E := sqrt(e+1);
```

$$E := .9591663047$$

```
> aa := solve({rov1, rov2}, {r, Q});
```

$$aa := \{r = 4.577855615,\ Q = 13.28179957\},\ \{Q = 15.05820043,\ r = 10.92214439\}$$

```
> r_s := 10.92214439:  Q_minus := 15.05820043:  Lz :=
  2*M*a*E/(2*M-r_s):  eta_s := Q_minus/E^2;
```

$$eta\_s := 16.36760916$$

```
> gama := -a^2*eta_s/r_s^2 +2*M*r_s;
```

$$gama := 21.72903672$$

```
> alpha := 1-1/E^2:
> De := -4*((r_s*(1-1/E^2)+M/E^2)^2
  +alpha^2*eta_s/r_s^2*(1-1/E^2));
```

$$De := -.07493980729$$

```
> res := EllipticF(sin(psi),k)/alpha/mu_plus =
  ln(abs(2*sqrt(gama*F)+2*gama*x+beta))/sqrt(gama):
> F := 1-1/E^2+beta*x +gama*x^2:
> beta := 4*r_s*(1-1/E^2) +2*M/E^2:
```

```
> x := 1/(r - r_s):

> xi_s := Lz/E:
> k := mu_minus/mu_plus:  psi := arcsin(mu/mu_minus):
  mu_plus := (xi_s^2+eta_s+alpha^2
  +sqrt((xi_s^2+eta_s+alpha^2)^2-4*alpha^2*eta_s))
  /2/alpha;
```

$$mu\_plus := -188.7131272$$

```
> mu_minus := (xi_s^2+eta_s+alpha^2
  -sqrt((xi_s^2+eta_s+alpha^2)^2-4*alpha^2*eta_s)) /2/alpha;
```

$$mu\_minus := -.08673276975$$

```
> lim := solve(eta_s -(xi_s^2+eta_s+alpha^2)*mu^2
  +alpha^2*mu^4 = 0, mu);
```

$$lim := -46.58541571,\ 46.58541571,\ -.9987125027,\ .9987125027$$

```
> solve(subs(r = 8+1/3, res), mu);
```

$$-.08465346478$$

```
> 2*M/3/abs(e);
```

$$8.333333333$$

A.2.17 File that creates figure 17.3

Listing of `tim_Cart.mws`

Kerr space-time

Non-equatorial geodesics

Timelike geodesics

$\eta < 0$

```
> restart:
```

```
> res := 1/alpha/mu_plus
  *EllipticF(sqrt(mu_plus^2*(mu^2-mu_minus^2)/mu^2
  /(mu_plus^2-mu_minus^2)), k_theta) =
  g*(EllipticF(sin(ph), k_r) +EllipticK(k_r)):

> k_theta := sqrt(mu_plus^2 - mu_minus^2)/mu_plus:

> mu := cos(teta):
> mu_plus := sqrt((abs(eta)+alpha^2-xi^2
  +sqrt((abs(eta)+alpha^2-xi^2)^2-4*alpha^2
  *abs(eta))) /alpha^2/2):
> mu_minus := sqrt((abs(eta)+alpha^2-xi^2
  -sqrt((abs(eta)+alpha^2-xi^2)^2-4*alpha^2
  *abs(eta))) /alpha^2/2):

> g:= 1/sqrt(A+B):

> ph := arccos(((A-B)*r+u2*B-u1*A)/((A+B)*r-u2*B-u1*A)):

> k_r := sqrt(((A+B)^2-(u2-u1)^2)/A/B)/2:

> A := sqrt((u2-b1)^2+a1^2):

> B := sqrt((u1-b1)^2+a1^2):

> a1 := sqrt(-(u3-u3bar)^2)/2:  b1 := (u3+u3bar)/2:
> R := r^4 +(a^2-xi^2-eta)*r^2 +2*M*(eta+(xi-a)^2)*r
  -a^2*eta -r^2*Delta/E^2:

> alpha := a*sqrt(1-E^(-2)):  Delta := r^2-2*M*r+a^2:

> M:=1:  a:= sqrt(.84):  xi:= -.5:  eta:= -1/9:  E:=3:
> is(abs(eta) < alpha^2); is(abs(xi) <
  abs(alpha)-sqrt(abs(eta))); is(a^2 > xi^2);
  is(sqrt(abs(eta)) < abs(a-xi));
```

true

true

true

true

```
> res_r := solve(R);
```

$$res\_r := -1.551956533,\ -.02471812107,\ .6633373271 - 1.515620811\,I,\ .6633373271 + 1.515620811\,I$$

```
> u1 := res_r[1]:  u2 := res_r[2]:  u3 := res_r[3]:
  u3bar := res_r[4]:
```

```
> evalf(k_theta); k_r;
```

$$.6953171656$$

$$.9631517120 + 0.\,I$$

```
> r_p := M+sqrt(M^2-a^2); r_m := M-sqrt(M^2-a^2);
```

$$r\_p := 1.400000000$$

$$r\_m := .6000000000$$

```
> r := 1.8:  res_mu := solve(res, mu);
```

$$res\_mu := -.7304418066,\ .7304418066$$

```
> evalf(mu_plus); evalf(mu_minus);
```

$$.7326270425$$

$$.5265412721$$

Appendix B

Derivation of the metrics

The general Theory of Relativity (GTR) was developed by Einstein in order to discuss gravitation. He postulated the *principle of covariance*, which asserts that the laws of physics must be independent of the space-time coordinates. Einstein also introduced the *principle of equivalence*, which states that in an arbitrary gravitational field no local experiment can distinguish a freely falling nonrotating system (local inertial system) from a uniformly moving system in the absence of a gravitational field.

The metric field depends on the gravitating masses and energies which are present. This is expressed quantitatively in *Einstein's field equations*,

$$R_{ij} = \frac{8\pi G}{c^4}\left(T_{ij} - \frac{1}{2}g_{ij}T\right) \qquad (T = g^{ij}T_{ij}) \tag{B.1}$$

where T_{ij} denotes the *energy-momentum tensor* of the matter and of the field (other than gravitational) which may be present and G is the constant of gravitation (which, like c, we shall set equal to 1). They are the core of GTR. Einstein discovered these after a long and difficult search, and announced them in November 1915. He was also able to show that this theory reduces to the Newtonian one, in lowest order, for the case of weak field and slow motions of the masses which serve as sources of the gravitational field.

Today we know that objects having extremely strong gravitational field

exist in the Universe. Not even the most repulsive nuclear forces can always prevent the final collapse to a black hole. For such dramatic events GTR must be used.

B.1 Derivation of the spherically symmetric Schwarzschild solution

The Schwarzschild metric is a spherically symmetric solution of Einstein's equation for the vacuum. A metric of the form

$$\mathrm{d}s^2 = \mathrm{e}^{2\nu}\,(\mathrm{d}t)^2 - \mathrm{e}^{2\mu_2}\,(\mathrm{d}r)^2 - r^2[(\mathrm{d}\theta)^2 + (\mathrm{d}\varphi)^2\sin^2\theta]\,, \tag{B.2}$$

where ν and μ_2 are functions of t ($= x^0 = -\mathrm{i}x^4$) and r, is spherically symmetrical.

We must now insert the ansatz (B.2) into the field equations. For this, it is necessary to compute the Ricci tensor (or the Einstein tensor) corresponding to the metric (B.2), which can be accomplished with the help of the Cartan calculus [7, 40] (the traditional computation using the Christoffel symbols can be found in [36]). The only non-vanishing components of the Riemann tensor are

$$\begin{aligned}
-R_{1212} &= -R_{2323} = +\frac{\mathrm{e}^{-2\mu_2}}{r}\mu_{2,r}\,,\\
-R_{1414} &= -R_{3434} = -\frac{\mathrm{e}^{-2\mu_2}}{r}\nu_{,r}\,,\\
-R_{2334} &= +R_{1214} = -\frac{\mathrm{e}^{-\nu-\mu_2}}{r}\mu_{2,4}\,,\\
-R_{1313} &= r^{-2}\left(1-\mathrm{e}^{-2\mu_2}\right)\,,
\end{aligned} \tag{B.3}$$

and

$$-R_{2424} = -\mathrm{e}^{-\mu_2-\nu}\left[\left(\mathrm{e}^{\mu_2-\nu}\mu_{2,4}\right)_{,4} + \left(\mathrm{e}^{\nu-\mu_2}\nu_{,r}\right)_{,r}\right]\,.$$

The field equations now follow from setting the various components of the Ricci tensor equal to zero. Therefore

$$\mu_2 \equiv \mu_2(r) \tag{B.4}$$

and

$$\nu = -\mu_2 \,. \tag{B.5}$$

The solution can now be completed by considering the equation

$$R_{33} = R_{1313} + R_{2323} + R_{4343} = 0 \,. \tag{B.6}$$

Hence

$$-2\mu_{2,r}\frac{\mathrm{e}^{-2\mu_2}}{r} = \frac{1}{r}\left(1 - \mathrm{e}^{-2\mu_2}\right) \,. \tag{B.7}$$

The solution of this equation is

$$\mathrm{e}^{-2\mu_2} = 1 - 2M/r \,, \tag{B.8}$$

where M is a constant, and it can be identified physically with the rest mass of the gravitating particle by comparison with Newtonian limit at large distances. We thus obtain the *Schwarzschild solution* in the most familiar form (and also in the form in which Schwarzschild originally wrote it)

$$\mathrm{d}s^2 = \left(1 - \frac{2M}{r}\right)(\mathrm{d}t)^2 - \frac{(\mathrm{d}r)^2}{1 - 2M/r} - r^2\left[(\mathrm{d}\theta)^2 + (\mathrm{d}\varphi)^2\sin^2\theta\right] \,. \tag{B.9}$$

It consists of an event horizon (at $r = 2M$) and a singularity at the center. Since the metric coefficients are explicitly independent of time and there is no dragging of the inertial frame the space-time is *static* as experienced by an observer external to the horizon. The radial coordinate r is a 'luminosity distance' in the sense that the surface area of a sphere of 'radius' r is $4\pi r^2$, t is a measure of proper time for an observer at rest at infinity.

If a signal is emitted from inside the horizon, it will not reach a distant observer. The stellar matter is cut off from the outside world. The horizon is the boundary of the region which is causally connected to a distant observer. Thus it acts like a one way membrane through which energy and information can pass to the interior, but not to the exterior. The singularity has no causal connection to an external observer; he cannot "see" it.

An external observer far away from the collapsing star will see it reach the horizon only after an infinitely long time as a result of the gravitational time dilatation. However, in practice, the star will become invisible, since the red shift will start to increase, and luminosity decreases. Afterwards, we are dealing with a "black hole".

B.2 Reissner–Nordström solution

A spherically symmetric solution of the coupled equations of Einstein and of Maxwell represents a black hole with mass and charge. We can, as in section B.1, write the line element

$$\mathrm{d}s^2 = \mathrm{e}^{2\mu_2}\left[\left(\mathrm{d}x^0\right)^2 - \left(\mathrm{d}x^2\right)^2\right] - \mathrm{e}^{2\mu_3}\left[(\mathrm{d}\theta)^2 + (\mathrm{d}\varphi)^2\sin^2\theta\right], \tag{B.10}$$

where μ_2 and μ_3 are functions only of x^0 and x^2. As we are now considering a space-time, in which an electromagnetic field is present, we cannot set the Ricci tensor to zero, as we did in B.1. Instead we must set $R_{ab} = -2\left(\eta^{cd}F_{ac}F_{bd} - \frac{1}{4}\eta_{ab}F_{ef}F^{ef}\right)$, where F_{ab} denotes the tetrad components of the Maxwell tensor and η_{ab} denotes the Minkowskian metric of the chosen ortho-normal tetrad-frame.

B.2.1 The solution of Maxwell equations

The axial components of the Maxwell tensor must vanish. As none of the components of the Maxwell tensor can depend on θ, the only non-vanishing component of the Maxwell tensor is F_{02} which must have the form

$$F_{02} = -Q_*\mathrm{e}^{-2\mu_3}, \tag{B.11}$$

where Q_* is a constant.

With $F_{03} = F_{23} = 0$ and F_{02} given by equation (B.11), we find that

$$-R_{44} = R_{00} = R_{11} = -R_{22} = R_{33} = Q_*^2\mathrm{e}^{-4\mu_3}, \text{ and } R_{42} = 0. \tag{B.12}$$

B.2.2 Derivation of the Reissner–Nordström metric

A similar derivation to one for the Schwarzschild metric in section B.1, can be given. Hence, with a metric of the form (B.2), we have the same expressions (B.3) for the non-vanishing components of the Riemann tensor. And with (B.12), the conclusions expressed in (B.4) and (B.6) continue to hold. But in place of (B.7) there is now (see (B.12))

$$2\mu_{2,r}\frac{\mathrm{e}_{-2\mu_2}}{r}+\frac{1}{r^2}\left(1-\mathrm{e}^{-2\mu_2}\right)=R_{33}=\frac{Q_*}{r^4}\,. \tag{B.13}$$

The solution of this equation is

$$\mathrm{e}^{-2\mu_2}=1-\frac{2M}{r}+\frac{Q_*^2}{r^2}\quad\left(=\mathrm{e}^{2\nu}=\frac{\Delta}{r^2}\right)\,; \tag{B.14}$$

and we have the solution in its standard form

$$\mathrm{d}s^2=\frac{\Delta}{r^2}\left(\mathrm{d}t\right)^2-\frac{r^2}{\Delta}\left(\mathrm{d}r\right)^2-r^2\left[\left(\mathrm{d}\theta\right)^2+\left(\mathrm{d}\varphi\right)^2\sin^2\theta\right]\,. \tag{B.15}$$

Asymptotically the electric field is radial and the corresponding Gaussian flux integral is $4\pi Q_*$. This shows that Q_* is the *charge* of the black hole.

B.3 Axisymmetric space-time – The Kerr Solution

A metric appropriate to stationary axisymmetric space-times can be written as

$$\mathrm{d}s^2=\mathrm{e}^{2\nu}\left(\mathrm{d}t\right)^2-\mathrm{e}^{2\psi}\left(\mathrm{d}\varphi-\omega\mathrm{d}t\right)^2-\mathrm{e}^{2\mu_2}\left(\mathrm{d}x^2\right)^2-\mathrm{e}^{2\mu_3}\left(\mathrm{d}x^3\right)^2\,, \tag{B.16}$$

where ν,ψ,ω, and μ_3 are functions of x^2 and x^3 with the freedom to impose coordinate conditions on μ_2 and μ_3.

The vanishing and the non-vanishing components of the Riemann tensor can be found (see [7]).

The components of the Ricci (R_{ab}) and the Einstein (G_{ab}) tensors are given by linear combinations of the components of the Riemann tensor [7]. By setting them equal to zero, the equations governing stationary axisymmetric vacuum space-times can be obtained. It will be sufficient to consider only the following equations:

$$\begin{aligned} &\mathrm{e}^{-2\mu_2}\left[\nu_{,2,2}+\nu_2\left(\psi+\nu-\mu_2+\mu_3\right)_{,2}\right]+\\ &+\mathrm{e}^{-2\mu_3}\left[\nu_{,3,3}+\nu_{,3}\left(\psi+\nu+\mu_2-\mu_3\right)_{,3}\right]= \\ &=+\frac{1}{2}\,\mathrm{e}^{2\psi-2\nu}\left(\mathrm{e}^{-2\mu_2}{\omega_{,2}}^2+\mathrm{e}^{-2\mu_3}{\omega_{,3}}^2\right)\qquad (R_{00}=0)\ , \end{aligned} \tag{B.17}$$

$$\begin{aligned} &\mathrm{e}^{-2\mu_2}\left[\psi_{,2,2}+\psi_{,2}\left(\psi+\nu-\mu_2+\mu_3\right)_{,2}\right]\\ &+\mathrm{e}^{-2\mu_3}\left[\psi_{,3,3}+\psi_{,3}\left(\psi+\nu+\mu_2-\mu_3\right)_{,3}\right]= \\ &=-\frac{1}{2}\,\mathrm{e}^{2\psi-2\nu}\left(\mathrm{e}^{-2\mu_2}{\omega_{,2}}^2+\mathrm{e}^{-2\mu_3}{\omega_{,3}}^2\right)\qquad (R_{11}=0)\ , \end{aligned} \tag{B.18}$$

$$\left(\mathrm{e}^{3\psi-\nu-\mu_2+\mu_3}\omega_{,2}\right)_{,2}+\left(\mathrm{e}^{3\psi-\nu+\mu_2-\mu_3}\omega_{,3}\right)_{,3}=0\qquad (R_{00}=0)\ , \tag{B.19}$$

$$\begin{aligned} &\left(\psi+\nu\right)_{,2,3}-\left(\psi+\nu\right)_{,2}\mu_{2,3}-\left(\psi+\nu\right)_{,3}\mu_{3,2}+\psi_{,2}\psi_{,3}+\nu_{,2}\nu_{,3}= \\ &=\frac{1}{2}\,\mathrm{e}^{2\psi-2\nu}\omega_{,2}\omega_{,3}\qquad (R_{23}=0)\,, \end{aligned} \tag{B.20}$$

$$\begin{aligned} &\mathrm{e}^{-2\mu_3}\left[\left(\psi+\nu\right)_{,3,3}+\left(\psi+\nu\right)_{,3}\left(\nu-\mu_3\right)_{,3}+\psi_{,3}\psi_{,3}\right]\\ &+\mathrm{e}^{-2\mu_2}\left[\nu_{,2}\left(\psi+\mu_3\right)_{,2}+\psi_{,2}\mu_{3,2}\right]= \\ &=-\frac{1}{4}\,\mathrm{e}^{2\psi-2\nu}\left(\mathrm{e}^{-2\mu_2}{\omega_{,2}}^2-\mathrm{e}^{-2\mu_3}{\omega_{,3}}^2\right)\qquad (G_{22}=0)\ , \end{aligned} \tag{B.21}$$

$$\begin{aligned} &\mathrm{e}^{-2\mu_2}\left[\left(\psi+\nu\right)_{,2,2}+\left(\psi+\nu\right)_{,2}\left(\nu-\mu_2\right)_{,2}+\psi_{,2}\psi_{,2}\right]\\ &+\mathrm{e}^{-2\mu_3}\left[\nu_{,3}\left(\psi+\mu_2\right)_{,3}+\psi_{,3}\mu_{2,3}\right]= \\ &=+\frac{1}{4}\,\mathrm{e}^{2\psi-2\nu}\left(\mathrm{e}^{-2\mu_2}{\omega_{,2}}^2-\mathrm{e}^{-2\mu_3}{\omega_{,3}}^2\right)\qquad (G_{33}=0)\ . \end{aligned} \tag{B.22}$$

The sum and the difference of equations (B.17) and (B.18) give

$$\left(\mathrm{e}^{\mu_3-\mu_2}\mathrm{e}^{\beta}{}_{,2}\right)_{,2}+\left(\mathrm{e}^{\mu_2-\mu_3}\mathrm{e}^{\beta}{}_{,3}\right)_{,3}=0\,, \tag{B.23}$$

$$\begin{aligned} &\left[\mathrm{e}^{\beta+\mu_3-\mu_2}\left(\psi-\nu\right)_{,2}\right]_{,2}+\left[\mathrm{e}^{\beta+\mu_2-\mu_3}\left(\psi-\nu\right)_{,3}\right]_{,3}= \\ &=-\mathrm{e}^{3\psi-\nu}\left(\mathrm{e}^{\mu_3-\mu_2}{\omega_{,2}}^2+\mathrm{e}^{\mu_2-\mu_3}{\omega_{,3}}^2\right)\ , \end{aligned} \tag{B.24}$$

where $\beta = \psi + \nu$.

The addition of equations (B.21) and (B.22) gives the same equation (B.23), while subtracting them gives

$$\begin{aligned} &4\mathrm{e}^{\mu_3-\mu_2}\left(\beta_{,2}\mu_{3,2}+\psi_{,2}\nu_{,2}\right)-4\mathrm{e}^{\mu_2-\mu_3}\left(\beta_{,3}\mu_{2,3}+\psi_{,3}\nu_{,3}\right)= \\ &=2\mathrm{e}^{-\beta}\left[\left(\mathrm{e}^{\mu_3-\mu_2}\mathrm{e}^{\beta}{}_{,2}\right)_{,2}-\left(\mathrm{e}^{\mu_2-\mu_3}\mathrm{e}^{\beta}{}_{,3}\right)_{,3}\right]-\mathrm{e}^{2\psi-2\nu}\left(\mathrm{e}^{\mu_3-\mu_2}{\omega_{,2}}^2-\mathrm{e}^{\mu_2-\mu_3}{\omega_{,3}}^2\right)\,. \end{aligned} \tag{B.25}$$

Exercising the gauge-freedom, we have to impose coordinate condition on μ_2 and μ_3 in some convenient manner. The metric (B.16) we now write in the form

$$\mathrm{d}s^2=\mathrm{e}^{\beta}\left[\chi\left(\mathrm{d}t\right)^2-\frac{1}{\chi}\left(\mathrm{d}\varphi-\omega\mathrm{d}t\right)^2\right]-\frac{\mathrm{e}^{\mu_2+\mu_3}}{\sqrt{\Delta}}\left[\left(\mathrm{d}x^2\right)^2+\Delta\left(\mathrm{d}x^3\right)^2\right]\,, \tag{B.26}$$

where

$$\chi=\mathrm{e}^{-\psi+\nu}\,. \tag{B.27}$$

B.3.1 The choice of gauge

It is useful to choose the polar angle θ (with respect to the axis of symmetry) as the spacial coordinate x^3. We shall suppose that the metric allows an *event horizon*, which we shall define as a smooth two–dimensional, null surface, which is spanned by the Killing vectors $\partial/\partial t$ and $\partial/\partial\varphi$.

With the stationarity and axisymmetry of the space-time, the equation of the event horizon is $N\left(x^2,x^3\right)=0$. The condition to be null is $g^{ij}N_{,i}N_{,j}=0$. For the chosen form of metric this equation gives

$$\mathrm{e}^{2(\mu_3-\mu_2)}{N_{,r}}^2+{N_{,\theta}}^2=0\,, \tag{B.28}$$

where $x^2=r$. Because of the gauge freedom we can suppose that

$$\mathrm{e}^{2(\mu_3-\mu_2)}=\Delta(r)\,, \tag{B.29}$$

where $\Delta(r)$ is some function of r. We shall assume that e^{β} is separable in the variables r and θ,

$$e^{\beta} = \Delta^{1/2} f(\theta)\,, \tag{B.30}$$

where $f(\theta)$ is some function of θ which is regular on the axis $\theta = 0$.

With $e^{\mu_3-\mu_2}$ and e^{β} given by equations (B.29) and (B.30), a solution of equation (B.23), compatible with the requirements of regularity on the axis and convexity of the horizon, is determined by $\Delta_{,r,r} = 2$ and $f = \sin\theta$; and the appropriate solution for Δ is

$$\Delta = r^2 - 2Mr + a^2\,, \tag{B.31}$$

where M and a are constants.

Choice of gauge consistent with the existence of an event horizon gives the solution $e^{\mu_3-\mu_2} = \Delta^{1/2}$ and $e^{\beta} = \Delta^{1/2}\sin\theta$, where Δ is given by equation (B.31).

With the solutions for $e^{\mu_3-\mu_2}$ and e^{β} and by using $\mu = \cos\theta$ instead of θ as the variable indicated by index '3', the equations (B.24) and (B.19), respectively become

$$\left[\Delta\left(\psi-\nu\right)_{,2}\right]_{,2} + \left[\delta\left(\psi-\nu\right)_{,3}\right]_{,3} = -e^{2(\psi-\nu)}\left(\Delta{\omega_{,2}}^2 + \delta{\omega_{,3}}^2\right)\,, \tag{B.32}$$

and

$$\left[\Delta e^{2(\psi-\nu)}\omega_{,2}\right]_{,2} + \left[\delta e^{2(\psi-\nu)}\omega_{,3}\right]_{,3} = 0\,, \tag{B.33}$$

where $\delta = 1-\mu^2 = \sin^2\theta$. Using the equation (B.27), the equations (B.32) and (B.33) will have the forms

$$\left(\frac{\Delta}{\chi}\chi_{,2}\right)_{,2} + \left(\frac{\delta}{\chi}\chi_{,3}\right)_{,3} = \frac{1}{\chi^2}\left(\Delta{\omega_{,2}}^2 + \delta{\omega_{,3}}^2\right)\,, \tag{B.34}$$

$$\left(\frac{\Delta}{\chi^2}\omega_{,2}\right)_{,2} + \left(\frac{\delta}{\chi^2}\omega_{,3}\right)_{,3} = 0\,. \tag{B.35}$$

Letting $X = \chi+\omega$ and $Y = \chi-\omega$, we obtain the pair of symmetric equations.

Equations (B.20) and (B.25) become

$$-\frac{\mu}{\delta}\left(\mu_3+\mu_2\right)_{,2}+\frac{r-M}{\Delta}\left(\mu_3+\mu_2\right)_{,3}=\frac{2}{\left(X+Y\right)^2}\left(X_{,2}Y_{,3}+Y_{,2}X_{,3}\right) \quad \text{(B.36)}$$

and

$$2(r-M)\left(\mu_3+\mu_2\right)_{,3}+\frac{r-M}{\Delta}\left(\mu_3+\mu_2\right)_{,3}= \\ =\frac{4}{\left(X+Y\right)^2}\left(\Delta X_{,2}Y_{,2}-\delta X_{,3}Y_{,3}\right)-3\frac{(r-M)^2-\Delta}{\Delta}+\frac{\mu^2-\delta}{\delta}\,. \quad \text{(B.37)}$$

The Ernst equation

Additional form of the basic equations that is related to the finding of all stationary axisymmetric solutions of Einstein's equations for the vacuum is due to Ernst.

The potential Φ is governed by the equation

$$\left(\frac{\chi^2}{\delta}\Psi_{,2}\right)_{,2}+\left(\frac{\chi^2}{\Delta}\Psi_{,3}\right)_{,3}\,; \quad \text{(B.38)}$$

and equation (B.34) in terms of Φ becomes

$$\left[\Delta\left(\ln\chi\right)_{,2}\right]_{,2}+\left[\delta\left(\ln\chi\right)_{,3}\right]_{,3}=\frac{\chi^2}{\Delta}{\Phi_{,3}}^2+\frac{\chi^2}{\delta}{\Phi_{,2}}^2\,. \quad \text{(B.39)}$$

Letting $\Psi=\sqrt{\Delta\delta}/\chi$, equations (B.38) and (B.39) can be reduced to ([7])

$$\Psi\left[\left(\Delta\Psi_{,2}\right)_{,2}+\left(\delta\Psi_{,3}\right)_{,3}\right]=\Delta\left({\Psi_{,2}}^2-{\Psi_2}^2\right)+\delta\left({\Psi_{,3}}^2-{\Psi_{,3}}^2\right)\,, \quad \text{(B.40)}$$

$$\Psi[\left(\Delta\Phi_{,2}\right)_{,2}+\left(\delta\Phi_{,3}\right)_{,3}]=2\Delta\Psi_{,2}\Phi_{,2}+2\delta\Psi_{,3}\Phi_{,3}\,. \quad \text{(B.41)}$$

Now expressing Ψ and Φ as the real and imaginary parts of a complex function Z, equations (B.40) and (B.41) can be combined into the single equation

$$\left[\left(\Delta Z_{,2}\right)_{,2}+\left(\delta Z_{,3}\right)_{,3}\right]\mathrm{Re}\,Z=\Delta{Z_{,2}}^2+\delta{Z_{,3}}^2\,. \quad \text{(B.42)}$$

Using the transformation,

$$Z\;=-\frac{1+E}{1-E}\,, \quad \text{(B.43)}$$

(see [7]), equation (B.42) becomes

$$(1 - EE^*)\left[(\Delta E_{,2})_{,2} + (\delta E_{,3})_{,3}\right] = -2E^*\left(\Delta {E_{,2}}^2 + \delta {E_{,3}}^2\right) . \tag{B.44}$$

This is Ernst's equation.

Associated with a solution (χ, ω), we have the conjugate solution $(\tilde{\chi}, \tilde{\omega})$. (analysis in [7]). Accordingly, a conjugate Ernst-equation may be derived. Thus by defining

$$\tilde{\Psi} = \frac{\sqrt{\Delta\delta}}{\tilde{\chi}} = \mathrm{e}^{\psi+\nu}\frac{\chi^2 - \omega^2}{\chi} = \mathrm{e}^{2\nu} - \omega\,\mathrm{e}^{2\psi}\,; \tag{B.45}$$

$$\tilde{\Phi}_{,2} = \frac{\delta}{\tilde{\chi}^2}\tilde{\omega}_{,3}\,;\ \tilde{\Phi}_{,3} = -\frac{\Delta}{\tilde{\chi}^2}\tilde{\omega}_{,2} = -\frac{\tilde{\Psi}^2}{\delta}\tilde{\omega}_{,2}\,; \tag{B.46}$$

and chaning back to the variables η and μ, we have

$$\left(1 - \tilde{E}\tilde{E}^*\right)\left\{\left[\left(\eta^2 - 1\right)\tilde{E}_{,\eta}\right]_{,\eta} + \left[\left(1 - \mu^2\right)\tilde{E}_{,\mu}\right]_{,\mu}\right\} = \\ = -2\tilde{E}^*\left[\left(\eta^2 - 1\right)\left(\tilde{E}_{,\eta}\right)^2 + \left(1 - \mu^2\right)\left(\tilde{E}_{,\mu}\right)^2\right] . \tag{B.47}$$

B.3.2 The derivation of the Kerr metric

Ernst's equation (B.47) allows an elementary solution. The solutions for $\tilde{\Psi}$ and $\tilde{\Phi}$ ca be found by separating the real and imaginary parts of the corresponding solution for $\tilde{Z}$, and reverting to the variable r (see [7, p. 286]). Then with equations (B.46) and (B.45) and with the knowledge of $\mathrm{e}^{2\beta}(= \Delta\delta)$, the solutions for ω and $\mathrm{e}^{2\psi}$ take simple forms because of the identities

$$\left[\left(r^2 + a^2\right) \mp a\sqrt{\Delta\delta}\right]\left(\sqrt{\Delta} \pm a\sqrt{\delta}\right) = \rho^2\sqrt{\Delta} \pm 2aMr\sqrt{\delta}\,, \tag{B.48}$$

and

$$\Sigma^2\left(\Delta - a^2\delta\right) = \rho^4\Delta - 4a^2M^2r^2\delta\,, \tag{B.49}$$

where

$$\Sigma^2 = \left(r^2 + a^2\right)^2 - a^2\Delta\delta\,. \tag{B.50}$$

Therefore, using the identity (B.49),

$$\mathrm{e}^{2\psi} = \frac{\delta \Sigma^2}{\rho^2}\,, \tag{B.51}$$

and

$$\omega = \frac{2aMr}{\Sigma^2}\,. \tag{B.52}$$

Further,

$$\mathrm{e}^{2\nu} = \mathrm{e}^{2\beta - 2\psi} = \frac{\rho^2 \Delta}{\Sigma^2}\,. \tag{B.53}$$

and

$$\chi = \mathrm{e}^{-\psi+\nu} = \frac{\rho^2}{\Sigma^2}\sqrt{\frac{\Delta}{\delta}}\,. \tag{B.54}$$

To complete the solution, using the formulae that give the derivatives of X and Y,equations (B.36) and (B.37) can be reduced. Their solution is given by (see [7, p. 288])

$$\mathrm{e}^{\mu_3+\mu_2} = \frac{\rho^2}{\Delta}\,; \tag{B.55}$$

and because $\mathrm{e}^{\mu_3-\mu_2} = \sqrt{\Delta}$, the solutions for e^{μ_3} and e^{μ_2}, separately, are

$$\mathrm{e}^{2\mu_2} = \rho^2/\Delta \qquad \text{and} \qquad \mathrm{e}^{2\mu_2} = \rho^2\,. \tag{B.56}$$

The solution for all metric coefficients are completed; and the final metric is

$$\mathrm{d}s = \rho^2 \frac{\Delta}{\Sigma^2}\left(\mathrm{d}t\right)^2 - \frac{\Sigma^2}{\rho^2}\left(\mathrm{d}\varphi - \frac{2aMr}{\Sigma^2}\mathrm{d}t\right)^2 \sin^2\theta - \frac{\rho^2}{\Delta}\left(\mathrm{d}r\right)^2 - \rho^2\left(\mathrm{d}\theta\right)^2\,. \tag{B.57}$$

From the asymptotical behavior we conclude that the parameter M is to be identified with the mass of the black hole, and a is to be interpreted as the angular momentum per unit of black hole.

References

[1] Akhiezer, N. I. Elements of the theory of elliptic functions (transated form the Russian by McFaden, H. H., ed. Silver, B., Translations of mathematical monographs, vol. 79) Providence: American Mathematical society (1990).

[2] Bardeen, J. M. "Timelike and null geodesics in the Kerr mertic." In: Black holes, 215–289. (eds. DeWitt, C. & DeWitt, B. S.) New York, London, Paris: Gordon and Breach science publishers(1973).

[3] Boyer, R. H., and Lindquist, R. W., "Maximal analytic extension of the Kerr metric." *Journal of mathematical physics* 8(2): 265–281 (1967).

[4] Byrd, F. P., and Friedman, M. D. Handbook of elliptic integrals for engineers and scientists (2nd ed.) Berlin: Springer-Verlag (1971).

[5] Calvani, M., de Felice, F. "Vortical null orbits, repulsive barriers, energy confinement in Kerr metric." *General Relativity and Graviation* 9(10): 889–902 (1977).

[6] Calvani, M., de Felice, F., Muchotrzeb, B., and Salmistraro, F.. "Time machine and geodesic motion in Kerr metric." *General Relativity and Garvitation* 9(2): 155–163 (1978).

[7] Chandrasekhar, S. The mathematical theory of black holes. Oxford: Clarendon Press. (Oxford Classics Series) (1998).

[8] Carter, B. A. "Hamilton-Jacobi and Schrodinger separable solurions of Einstein's equations." *Commun. math. Phys.* 10(1968): 280–310 (1968).

[9] Connors, P. A., and Stark, R. F. "Observable gravitational effects on polarised radiation coming from near a black hole." *Nature* 269: 128, 129 (1977).

[10] Connors, P. A., Piran, T., and Stark, R. F. "Polarization features of X-ray radiation emitted near black holes." *The Astrophysical Journal* 235: 224–244 (1979).

[11] Cramer, C. R. "Using the uncharged Kerr black hole as a gravitational mirror." *General Relativity and Gravitation* 26(4): 445–454 (1996).

[12] Dawin, C. "The gravity field of a particle." *Proc. R. Soc. London A* 248: 180–194 (1958).

[13] Done, C. "Accretion flows in X-ray binaries." *arXiv: astro-ph/0203246 v1* (2002). Retrieved March 2004 from http://au.arXiv.org

[14] Dokuchaev, V. I., and Eroshenko, Yu. N. "Origin of Correlations between Central Black Holes Masses and Galactic Bulge Velocity Dispersions." *arXiv: astro-ph/0209324 v1* (2002). Retrieved March 2004 from http://au.arXiv.org

[15] Science Expo webpage. Copyright 1995, The Board of Trustees of the University of Illinois. Visited 26/3/2004. http://archive.ncsa.uiuc.edu/Cyberia/NumRel/BlackHoleHistory.html

[16] Falomo, R. "The host galaxy - AGN connection at low and high redshift." *arXiv: astro-ph/0212164 v1* (2002). Retrieved March 2004 from http://au.arXiv.org

[17] Fayngold, M. Special relativity and motions faster than light. Wiley-VCH Verlag GmbH, Weinheim (2002).

[18] de Felice, F. "Repulsive phenomena and energy emission in the field of a naked singularity." *Astron. & Asrophys.* 34: 15–19 (1974).

[19] de Felice, F. "Classical instabilty of a naked singularity." *Nature* 273: 429–431 (1978).

[20] Gursky, H. "Observations of galactic X-ray sources." In: Black holes, 292–341. (eds. DeWitt, C. & DeWitt, B. S.) New York, London, Paris: Gordon and Breach science publishers (1973).

[21] Gültekin, K., Miller, C. M., and Hamilton, D. P. "Three-body encounters of black holes in glubular clusters." *arXiv: astro- ph/0306204 v2* (2003). Retrieved March 2004 from http://au.arXiv.org

[22] Hagihara, Y. "Theory of the relativistic trajectories in a Gravitational Field of Schwarzschild." *Japanese journal of astronomy and geophysics* Vol. 8: 67–176 (1931).

[23] Hancock, H. Lectures on the theory of elliptic functions (Vol. I Analysis) New York: Dover publications (1958).

[24] Helliwell, T. M., and Mallinckrodt, A. J. "Null geodesics in the extended Kerr manifold." *Physical Review D* 12(10): 2993–3003 (1975).

[25] Heusler, M. Black hole uniqueness theorems. Cambridge, New York : Cambridge University Press (1996).

[26] Ho, L. C. "Black hole demography from nearby active galactic nuclei." In: Carnegie Observatories Astrophysics Series. (Vol. 1: Coevolution of Black Holes and Galaxies, ed. Ho, L. C.). Cambridge: Cambridge Univ. Press (2004).

[27] Honig, E., Lake, K., and Roeder, R. C. "Behavior of spacelike geodesics in the extended Schwarzchild manifold." *Physical Review D* 10(10): 3155–3161 (1974).

[28] Liang, E. P. T. "Equatorial circular orbits of some static gravitational fields with naked singularities." *Physical Review D* 9(12): 3257–3262 (1974).

[29] Kaaret, P., Corbel, S., Prestwich, A., and Zezas, A. "Radio emission from an ultraluminous X-ray Source." *arXiv: astro-ph/ 0302182 v1* (2003). Retrieved March 2004 from http://au.arXiv.org

[30] Kerr, R. P. "Gravitational field of a spinning mass as an example of algebraically special metrics." *Phys. Rev. Lett. II* 273–278.

[31] Misner, Ch. W., Thorne, K. S., and Wheeler, J. A. Gravitation. San Francisco: W. H. Freeman Company (1973).

[32] Marconi, A. "Black Holes in Galactic Nuclei: the Promise and the Facts." *arXiv: astro-ph/0201504 v1* (2002). Retrieved March 2004 from http://au.arXiv.org

[33] McLure, R. J. "Supermassive black holes in radio-loud AGN." *arXiv: astro-ph/0302455 v1* (2003). Retrieved March 2004 from http://au.arXiv.org

[34] O'Neill, B. The geometry of Kerr black holes. Wellesley, Massachusetts: A K Peters (1995).

[35] Schmidt, M., 1040*Nature* 197 (1963).

[36] Spain, B. Tensor calculus (3rd ed.). Edinburgh: Oliver and Boyd (1960).

[37] Sharp, N. A. "Geodesics in black hole space-times." *General Relativity and Graviatation* 10(8): 659–670 (1978).

[38] Stark, R. F. and Connors, P. A. "Observational test for he existence of a rotating black hole in Cyg X-1." *Nature* 266: 429, 430 (1977).

[39] Steward, J., and Walker, M. Black holes: The outside story. Berlin: Springer. (Springer Tracts in Modern Physics, Vol. 69) (1973).

[40] Straumann, N. General relativity and relativistic astrophysics. Berlin: Springer-Verlag (1984).

[41] Stuchlík, Z., and Hledík, S. "Equatorial photon motion in the Kerr-Newman spacetimes with a non-zero cosmological constant." *Class. Quantum Grav.* 17: 4541–4576 (2000).

[42] Townsend, P. K. Black holes (1997). Retrieved November 1997 from http://xxx.lanl.gov/abs/gr-qc/9707012/

[43] Wilkins, D. C. "Bound geodesics in the Kerr meric." *Physical Review D* 5(4): 814–822 (1972).

[44] Woodhouse, N. M. J. "Killing tensors and the separation of the Hamilton-Jacobi equation." *Commun. math. Phys.* 44(1975): 9–38 (1975).

[45] Zhen-guo, M. "Geodesics of boundd particles around a Kerr black hole." *Chinese Astronomy and Astrophysics* 24(2000): 135–144 (2000).